PROCESSING AND CHARACTERIZATION OF SINGLE POLYMER COMPOSITES USING ELECTROSPUN NANOFIBRES

by

KGABO PHILLEMON MATABOLA

Submitted in accordance with the requirements for the degree

PHILOSOPHIAE DOCTOR (PhD)

Department of Chemistry

Faculty of Natural and Agricultural Sciences

at the

UNIVERITY OF THE FREE STATE (QWAQWA CAMPUS)

SUPERVISOR: DR A.R. DE VRIES (DST)
CO-SUPERVISOR: PROF A.S LUYT (UFS)

MAY 2011

DECLARATION

I declare that the thesis hereby submitted for the PhD degree at the University of the Free State is my own independent work and has not previously been submitted by me at another university/faculty. I furthermore cede copyright of the thesis in favour of the University of the Free State.

_____ _____

K.P. Matabola Prof A.S. Luyt

DEDICATION

This research work is dedicated to the following special people:

- My son, Manthibu John Teffo;
- My parents, Mabotse Raynett Matabola (Mother) and Manthibu John Matabola (Father), for their unwavering support;
- My siblings: Enny, Frans, Mashao, Rivonia, Jerry and Phillistus Matabola; and
- To the memory of my Grandmother, Makwena Pauline Seroka, who supported me throughout my studies. May your soul rest in peace.

ACKNOWLEDGEMENTS

- I am heartily thankful to my supervisor and promoter, Dr Andrew Robert de Vries, whose encouragement, constructive guidance and support from the inception of this work to the final level enabled me to develop an understanding of the subject.
- I am also grateful to my co-supervisor, Prof A.S. Luyt, for his continued encouragement, invaluable advice and helpful discussions.
- I am grateful to the CSIR for awarding me the PhD studentship, for general assistance and for doing the work on their premises.
- Mr Osei Ofosu and Dr Rakesh Kumar for respectively ensuring that all the instruments were working properly and for proof-reading my work.
- Mrs Valencia Jacobs for doing the SEM analysis of my PMMA nanofibres and the PMMA composite materials.
- Haydon Whitebooi for providing me with the moulds required for my experiments and for fixing the compression moulder when not responding appropriately. Without your assistance, I would not have made it.
- Dr Sean Moolman and the entire Polymers and Composites group for providing a conducive working environment and for constructive criticism and helpful inputs in my work.
- My uncles, Kgabo David Seroka and Koena Alfred Seroka for affording me the opportunity to have a taste of higher education. Thank you for all the sacrifices, moral support and financial support over the years. Without you I would not have made it this far.
- My family for believing in me and giving me the moral support and love throughout my studies.
- My friends for being by my side: Ben, Maropeng, Lackson, Tumelo, Monyai, Thabang, Tebogo, Elias, Andy, Mpho Ngoepe and others.
- Lastly, God for giving me the strength to bring this task to successful completion.

PUBLICATIONS FROM THIS WORK

1. K.P. Matabola, A.R. De Vries, A.S. Luyt, R. Kumar. Studies on single polymer composites of poly(methyl methacrylate) reinforced with electrospun nanofibers with a focus on their dynamic mechanical properties. eXPRESS Polymer Letters 2011; 5:635-642
   DOI:10.3144/expresspolymlett.2011.61

2. K.P. Matabola, A.R. De Vries, F.S. Moolman, A.S. Luyt. Single polymer composites. A review. Journal of Materials Science 2009; 44:6213-6222
   DOI:10.1007/s10853-009-3792-1

ABSTRACT

This study describes the preparation and characterization of single polymer composites of poly(methyl methacrylate) (PMMA) reinforced with electrospun nanofibres. These single polymer composites, which refer to composites in which both the matrix and reinforcement are from the same polymer, have specific economic and ecological advantages and can be recycled. The nanofibres used as reinforcements in this study were produced by an electrospinning process. The interest in the nanofibres over traditional fibres was motivated by the large specific surface area to volume ratio, the smaller diameter and superior mechanical properties.

The effect of the electrospinning parameters on the morphology and diameters of the electrospun high molecular weight PMMA ($PMMA_{high}$) was investigated in order to obtain suitable diameters for the reinforcing fibres. The electrospinning parameters investigated were the polymer solution concentration, applied voltage and spinning distance. The results showed that the polymer solution concentration influences the diameter of the electrospun nanofibres more than the spinning voltage and the spinning distance. Furthermore, SEM analysis of the $PMMA_{high}$ nanofibres showed that the fibres had a smooth regular and cylindrical morphology with no beads and junctions.

Effects of the processing temperature on the preparation of the single polymer composites of PMMA *via* a film stacking method were investigated. $PMMA_{high}$ nanofibres, with diameters ranging from 400-650 nm, were used as the reinforcement and a low molecular weight PMMA ($PMMA_{low}$) as the matrix. The results indicated that a processing temperature of 150 °C yielded the best composite with distinguishable physical phases and adequate melting of the matrix material.

The effects of the different nanofibre diameters, fibre loading and processing temperature on the thermo-mechanical properties of the PMMA SPCs were investigated. Dynamic mechanical analysis showed a pronounced improvement in the storage moduli, loss moduli and tan δ of the composites compared to the matrix. This behaviour is the result of a positive reinforcing effect of the $PMMA_{high}$ nanofibres. The possibility of using the $PMMA_{high}$ nanofibres to improve the thermal stability of the PMMA SPCs was also investigated. The

results indicated that the thermal stability of the neat $PMMA_{low}$ matrix is unaffected by the composites formation. This is probably the result of the lower thermal stability of the $PMMA_{high}$ nanofibres.

Characterization of the mechanical properties of the PMMA single polymer composites revealed that the flexural and impact properties improved upon composite formation whilst the tensile properties remained unchanged.

LIST OF ABBREVIATIONS

All-PP	All-polypropylene
AFM	Atomic force microscopy
ATR-FTIR	Attenuated total reflectance Fourier-transform infrared spectroscopy
BET	Branauer-Emmett-Teller
T_c	Crystallization temperature
DSC	Differential scanning calorimetry
DMF	Dimethyl formamide
DMA	Dynamic mechanical analysis
FESEM	Field emission scanning electron microscopy
FTIR `	Fourier-transform infrared spectroscopy
GMT	Glass mat reinforced thermoplastic
T_g	Glass transition temperature
HDPE	High-density polyethylene
ISO	International Organization for Standardization
iPP	Isotactic polypropylene
LDPE	Lower-density polyethylene
T_m	Melting temperature
NMT	Natural fibre mat reinforced thermoplastic
NMR	Nuclear magnetic resonance spectroscopy
% RH	Percentage relative humidity
PAA	Poly(acrylic acid)
PAN	Poly(acrylonitrile)
PA6	Polyamide-6
PBI	Polybenzimidazole
PE	Polyethylene
PEN	Poly(ethylene naphthalate)
PEO	Poly(ethylene oxide)
PET	Poly(ethylene terephthalate)
PMMA	Poly(methyl methacrylate)
PLLA	Poly(L-lactic acid)
PLA	Poly(lactic acid)

PLGA	Poly(lactic acid-co-glycolic acid)
PCL	Polycaprolactone
PPTA	Poly(p-phenylene terephthalamide)
PP	Polypropylene
PU	Poly(urethane)
PVC	Poly(vinyl chloride)
KH_2PO_4	Potassium dihydrogen phosphate
PPE	Propylene-ethylene
SEM	Scanning electron microscopy
SPCs	Single polymer composites
SAXS	Small-angle x-ray scattering
SBS	Styrene-butadiene-styrene
THF	Tetrahydrofuran
TGA	Thermogravimetric analysis
TEM	Transmission electron microscopy
UHMWPE	Ultrahigh molecular weight polyethylene
M_w	Weight average molecular weight
WAXD	Wide-angle x-ray diffraction
XPS	X-ray photoelectron spectroscopy

TABLE OF CONTENTS

LIST OF TABLES

LIST OF FIGURES

Chapter 1

Introduction

1.1 Single polymer composites

The demand for sustainable materials has risen worldwide. This has further triggered the development of environmentally friendly materials due to the increasing global environmental concerns and unsustainable high rate of the depletion of natural resources [1]. Currently, the manufacturers of materials and end-products are being pressured by the environmental legislation and waste management regulations to carefully consider the environmental impact of their products at all stages of its cycle including recycling and ultimate disposal. The legislation was introduced in 2002 to regulate the use of recyclable materials, particularly in the automotive industry, aiming to increase the recyclable content to at least 95 percent on average weight by the year 2015 [2].

This development naturally also involves composite materials, which is widely applied in various fields [3]. The elements of polymer composites, namely matrix and fibres, are areas of concern as the primary resources from which polymers (excluding biopolymers) are produced are crude oil and natural gas. The most commonly used fibre reinforcements in these composite materials are glass and carbon [4]. The concerns originate from the high rate of consumption of natural resources and the environmental concerns as it relates to the end of life disposal of glass fibres through thermal or mechanical recycling [2]. Although both polymers and glass are perfectly recyclable individually, when combined they are not easy to recycle as each has a very different recycling requirement [5]. The non-renewable and non-recyclable nature of these materials limits their potential as sustainable materials, hence there is a need to develop material systems consisting of a minimum of different, compatible polymers [4]. This in practice means mono-component systems or in other words single polymer composites (SPCs) [6].

Single polymer composites are composites in which both the polymer and fibre originate from the same polymer family, thereby supporting the ease of recyclability; hence they

represent the right alternative to traditional composites materials [7]. The concept was developed by Capiati and Porter three decades ago showing its feasibility on high-density polyethylene-based systems [8]. Since the 1990s, subsequent to Capiati and Porter's pioneering work, the interest in single polymer composites increased significantly on a wide range of polymers. Different methods have been reported for their production, which utilise the melting temperature difference between the matrix and the fibre [9,10]. Moreover, the small temperature difference between the fibre and the matrix poses a challenge during the fabrication [10].

The preparation of recyclable single polymer composites requires high modulus polymer fibres. Such fibres have been produced by a variety of production routes and subsequent orientation by drawing that has led to good mechanical properties of the fibres [11]. A high degree of chain extension in combination with a high molar mass is needed for high-performance fibres. Due to the finiteness of the molecular chains, chain overlap is needed for load transfer through the system, which in practice means the use of high molecular weight polymers [6].

In addition to recyclability, the use of polymer fibres has a number of ecological and technological advantages compared to glass fibres. They are non-abrasive to processing equipment and can be thermally recycled at the end of their lifetime for energy recovery. They also have a very low density, which can potentially lead to lightweight parts, lowering fuel consumption and gas emissions. Another advantage of using a more flexible and ductile fibre is the improvement of crash behaviour. Single polymer composites (e.g. all-polypropylene composites) will not splinter, but will fail in a more ductile manner [5].

1.2 Considerations of single polymer composites

Most of the reported work on single polymer composites available in the literature utilised micro-size fibres such as yarns, melt spun fibres, and tapes as reinforcements. Currently not much work has been published on single polymer composites using electrospun nanofibres, hence the focus of this study. The electrospinning process was used to produce nanofibres using electrostatic forces. The interest in the process was brought about by the simplicity of the electrospinning set-up, the very large specific surface area to volume ratio, the smaller

diameter and superior mechanical properties (e.g. stiffness and tensile strength) of the fibres [12]. With these outstanding properties, it is hypothesized that improved structural properties of the electrospun nanofibre reinforced composites can be expected. As for the matrix, a lower molecular weight amorphous poly(methyl methacrylate) (PMMA) was adopted on the basis of being readily available and at low cost.

Unlike the single polymer composites involving semi-crystalline polymers, our PMMA single polymer composites are unique in the sense that they were fabricated from amorphous PMMA with sufficient amount of molecular orientation.

Despite the recyclable and lightweight character of the single polymer composites, a strong interfacial adhesion is anticipated since the matrix and the fibre are of identical chemistry [13].

1.3 Aim and objectives

1.3.1 Aim

The main aim of this project is the preparation and characterisation of single polymer composites (SPCs) of PMMA reinforced with electrospun nanofibres. PMMA nanofibres of different diameters were produced by the electrospinning technique and were used as reinforcements in PMMA single polymer composites. The composites were manufactured by a film stacking technique applying a two-component approach and the properties of the composites were assessed.

1.3.2 Objectives

This study had three primary objectives:

1. The investigation of suitable electrospinning conditions for the production of nanofibres from a high molecular weight PMMA. The parameters that were investigated included polymer solution concentration, spinning voltage and distance. Different fibre diameters were targeted.

2. The development of a large enough processing window for the SPCs. A suitable processing temperature needed to be found that allows the matrix to melt and the reinforcement to stay intact.
3. The investigation of the effect of different fibre diameters, fibre loadings and processing temperatures on the thermo-mechanical and mechanical properties of the PMMA composites. The idea was to investigate if the electropun nanofibres, as opposed to conventional fillers, can adequately reinforce the polymer matrix. The high specific surface to volume ratio of the nanofibres might significantly increase the interaction between the fibres and the matrix, leading to better reinforcement than conventional fibres.

1.4 Overview of the thesis

Chapter 1 (the present chapter) gives a summary of the study. In **Chapter 2,** the electrospinning of polymers, ranging from the historical background to potential applications of the nanofibres, are discussed. A literature review on single polymer composites is presented in **Chapter 3**. The reported work on single polymer composites and the fabrication methods used are discussed. **Chapter 4** presents the experimental conditions of the study, and **Chapter 5** deals with the electrospinning of high molecular weight PMMA. The effect of various electrospinning parameters on the morphology and diameters of the electrospun nanofibres are discussed. The electrospun nanofibres were characterized by various techniques and the results are presented and discussed. **Chapter 6** deals with the preparation and thermal properties of single polymer composites of poly(methyl methacrylate). The effect of fibre loading, fibre diameter and processing temperature was investigated. The mechanical characterization of the PMMA single polymer composites are presented in **Chapter 7.** The effect of fibre loading, fibre diameter and processing temperature on the mechanical properties of the composites was investigated. **Chapter 8** gives the overall conclusions and recommendations of the study.

1.5 References

[1] A.N. Netravali, S. Chabba. Composites turn greener. MaterialsToday 2003; 22-29.

[2] N. Cabrera, B. Alcock, J. Loos, T. Peijs. Processing of all-polypropylene composites for ultimate recyclability. Proceedings of the Institution of Mechanical Engineers Par L: Journal of Materials: Design and Applications 2004; 218:145-155.

[3] A. Pegoretti. Editorial corner – A personal view. Trends in composites materials: The challenge of single-polymer composites. eXPRESS Polymer Letters 2007; 1:710-710. DOI: 10.3144/expresspolymlett.2007.97

[4] L.S. Lee, R. Jain. The role of FRP composites in a sustainable world. Clean Technologies Environmental Policy 2009; 11:247-249. DOI: 10.1007/s10098-009-0253-0

[5] T. Peijs. Composites for recyclability. MaterialsToday 2003; 30-35.

[6] N.-M. Barkoula, T. Peijs. Processing of single polymer composites using the concept of constrained fibres. Polymer Composites 2005; 26:114-120. DOI 10.1002/pc.20082

[7] T. Abraham, S. Siengchin, J. Karger-Kocksis. Dymanic mechanical thermal analysis of all-propylene composites based on β and α polymorphic forms. Journal of Materials Science 2008; 43:3697-3703. DOI 10.1007/s10853-008-2593-2

[8] D. Yao, R. Li, P. Nagarajan. Single-polymer composites based on slowly crystallizing polymers. Polymer Engineering and Science 2006; 46:1223-1230. DOI 10.1002/pen.20583

[9] R. Li, D. Yao. Preparation of single poly(lactic acid) composites. Journal of Applied Polymer Science 2008; 107:2909-2916. DOI 10.1002/app.27406

[10] N.J. Capiati, R.S. Porter. The concept of one polymer composites modelled with high density polyethylene. Journal of Materials Science 1975; 10:1671-1677. DOI: 10.1007/BF00554928

[11] B. Alcock, N.O. Cabrera, N.-M. Barkoula, J. Loos, T. Peijs. The mechanical properties of unidirectional all-polypropylene composites. Composites: Part A 2006; 37:716-726. DOI:10.1016/j.compositesa.2005.07.002

[12] Z.-M. Huang, Y.-Z. Zhang, M. Kotaki, S. Ramakrishna. A review on polymer nanofibres by electrospinning and their applications in nanocomposites. Composites Science and Technology 2003; 63:2223-2353. DOI:10.1016/S0266-3538(03)00178-7

[13] Y. Gong, G. Yang. Manufacturing and physical properties of all-polyamide composites. Journal of Materials Science 2009; 44:4639-4644.
DOI 10.1007/s10853-009-3708-0

Chapter 2

Electrospinning of polymers – Literature review

2.1 Introduction

The discovery of polymers has significantly revolutionized the lives of humankind. These polymers are being used in different forms and for a wide range of applications. Noticeable among these are the synthetic and regenerated polymers that have found applications in not only the textile and apparel sector, but also in numerous industrial usages like tyre rods, reinforcing and structural agents, barrier films, food and packaging industry, automotive parts, etc [1,2]. The fibres from polymers have been prepared and used in a wide variety of industrial fields. The common methods of polymer fibre production include melt spinning, dry spinning, wet spinning and gel spinning. These techniques rely upon pressure-driven extrusion of a viscous polymer fluid through a spinneret and subsequent drawing of the resultant filament as they solidify or coagulate. The fibre diameters produced by these methods are in the range of 10-50 μm [3,4,5].

The recent awareness on nanotechnology, development of materials at nano-levels, has spurred interest in researchers. Many of the science and engineering domains are currently harnessing the potential of the nanotechnology initiative, hence nanotechnology became the prioritized area of interest in all countries. Polymer nanofibres happen to be one of the mostly researched areas in nanotechnology. These nanofibres are produced by a simple, straight forward process called electrospinning, which generates fibres with submicron diameters. The interesting properties like nanoscale diameter and large specific surface-to-volume ratio of the nanofibres are beneficial in a wide variety of applications. Proposed uses of the electrospun nanofibres include nanocatalysis, tissue scaffolds, protective clothing, filtration, optical electronics and fibre-based sensors [6].

A comprehensive review by Huang *et al.* [7] shows a phenomenal increase in the number of publications in recent years. Since electrospun fibres find applications in both nanotechnology and biotechnology, this certainly can be seen as a driving force behind the recent interest in a technique that has been known since the 1930's [8,9]. This electrospinning

approach has been used successfully to spin a number of synthetic and natural polymers into fibres many kilometres in length [10-16].

This review looks at the history of electrospinning, the fundamentals and the process of electrospinning, features of electrospun nanofibres, the relationship between the processing parameters and morphology, characterisation and potential applications of the nanofibres.

2.2 History of electrospinning

Electrospinning is an old technique which has its basis in early studies [17,18]. The study of the effects of electricity on liquids has been of interest for many years. In the early 1700s, Gray studied the behaviour of water under the influence of electrostatics [19]. The aerosols generated by the application of high electric potentials to drops of liquids were described by Bose in 1745 [20]. Lord Rayleigh investigated the question of how many charges are needed to overcome the surface tension of a drop [21] before a jet is created. Later in 1898, electrodynamics was used to explain the excitation of dielectric liquid under the influence of an electric charge [22]. Cooley and Morton patented the first devices to spray liquids through the application of an electrical charge and this led to the invention of electrospinning to produce fibres [23-25]. Hagiwaba *et al.* described the fabrication of artificial silk through the use of electrical charge [26]. The breakthrough in the electrospinning of plastics was patented for the first time by Formhals in the 1930s and the work was considered as the first significant study in electrospinning. The first patent appeared in 1934 wherein the process and apparatus for producing fibres through electric charges was described. The apparatus consisted of a movable thread-collecting device for collecting aligned fibres. The cellulose acetate fibres were spun using acetone as the solvent. The shorter distance between the capillary tip and the collector presented a challenge as the solvent could not completely evaporate, hence the fibres sticked to the collector and to one another making removal difficult [8].

In 1939, Formhals produced another patent in which the distance between the capillary tip and the collector was increased to give the solvent more time to evaporate. Furthermore, the patent also described the use of multiple nozzles for the simultaneous spinning of a number of fibres from the same polymer solution as well as a means to direct the fibre jets toward the

collector [27]. Another patent was published in 1940 in which a polymer solution was directly electrospun onto a moving base thread to generate composite fibres [28].

Streams of highly electrified uniform droplets of about 0.1 mm in diameter were successfully produced by Vonnegut and Neubauer in 1952 [29]. They invented a simple apparatus for electrical atomization. A glass tube was drawn down to a capillary having a diameter in the order of a few tenths of a millimetre. The tube was filled with water or some other liquid and a high voltage electric wire (varying from 5-10 kV) was introduced into the liquid. The dispersion of a series of liquids into aerosols under high electric potentials was investigated by Drozin in 1955 [30]. He used a glass tube ending in a fine capillary similar to the one used by Vonnegut and Neubauer. It was found that for certain liquids, and under proper conditions, the liquid was issued from the capillary as a highly dispersed aerosol consisting of droplets with a relatively uniform size. Different stages of the dispersion were also captured. An electrical spinning apparatus for the production of light-weight ultra-thin non-woven fabric with different patterns was patented by Simons in 1966 [31]. The positive electrode was immersed into the polymer solution and the collector was grounded. It was found that the fibres from the low viscosity solutions tended to be shorter and finer whereas those from the more viscous solutions were relatively continuous.

In 1969, Taylor initiated studies on the jet forming process, and the idea was to examine how the polymer droplet at the capillary tip behaves when an electric field is applied [32]. He found that the pendant droplet develops into a cone (called Taylor's cone) when the surface tension is balanced by electrostatic forces. He also found that the jet is emitted from the apex of the cone, which is one of the reasons why electrospinning can be used to generate fibres with diameters significantly smaller than the diameter of the capillary from which they are ejected. Taylor subsequently determined that an angle of 49.3 degrees is required to balance the surface tension of the polymer with the electric forces. Subsequent to Taylor's work, focus shifted from a fundamental understanding of the electrospinning process to a deeper understanding of the relationship between individual processing parameters and the structural properties of nanofibres. Wide-angle x-ray diffraction (WAXD), SEM, TEM, DSC and TGA have been used by researchers to characterize electrospun nanofibres [33]. In 1971 Baumgarten reported the effect of varying certain solution and processing parameters (solution viscosity, flow rate, applied voltage, etc.) on the structural properties of electrospun

fibres [34]. In his research a poly(acrylonitrile)/dimethyl formamide (PAN/DMF) solution was used. It was deduced that fibre diameter had a direct dependence on solution viscosity, with higher viscosities giving larger fibre diameters. In addition, Baumgarten found that the fibre diameter does not monotonically decrease with increasing applied electric field, but that it rather initially decreases with an increase in applied field reaching a minimum and then increases when the applied field is further increased. By varying the solution and processing parameters, he was able to electrospin fibres with diameters ranging from 500 to 1100 nm.

Simm *et al.* [35] obtained very thin, relatively short and highly charged fibre fleece in large numbers for filtering purposes, when the fibre material was sprayed electrostatically. The polymers used were polystyrene, cellulose esters or polycarbonates. The non-combustible solvents considered were methylene chloride, chloroform and carbon tetrachloride. The solution was sprayed and they dried along their way to the precipitation electrodes, the collecting device that was placed equidistant from the ring electrode. The fibre filters produced by this process thus consisted of a fibre fleece, which has been electrostatically sprayed from the liquid state on to a conductive support. The resultant fibre fleece covered with permeable cellulose fleece was thick, dry and porous and was used as an air filter.

The research on the electrospinning of the nanofibres increased due to the increased knowledge on the application potential of nanofibres in high efficiency filter media, protective clothing, catalyst substrates, adsorbent materials, etc. Furthermore, research on nanofibres gained momentum due to the work of Doshi and Reneker [36]. They studied the characteristics of polyethylene oxide (PEO) nanofibres by varying the solution concentration and applied electrical potential. Jet diameters were measured as a function of distance from the apex of the cone and they observed that the jet diameter decreases with an increase in distance. They found that a PEO solution with viscosity less than 800 centipoise (cP) was too dilute to form a stable jet, and that solutions with a viscosity of more than 4000 cP were too thick to form fibres.

Many researchers became interested in the technique after the work of Doshi and Reneker. Srinivasan [37,38] spun poly(p-phenylene terephthalamide) (PPTA) by the electrospining process. PPTA fibres (Kevlar 49®) were dissolved in sulphuric acid to form an isotropic

solution. The results showed meridional and equatorial reflections showing the orderliness in the material. Bright and dark field electron microscopy revealed aspects of the morphology and arrangement of crystallites in the fibre. Atomic force microscope images were used to extract roughness parameters. The produced fibres were in the order of a few hundred nanometers in diameter and were thermally stable.

Chun [39,40] developed a new process to describe the electrsopinning process, which showed the relationship between applied voltage, electrical charge, fibre geometry, fibre velocity, mass flow rate and electrical current. He concluded experiments on solutions of poly(ethylene terephthalate), poly(amic acid) and poly(acrylonitrile). The obtained fibres had diameters of less than 1 micron. Charaterization of these fibres involved studying the effects of applied potentials, flow rate and the spinning velocity. Structural and morphological studies included analysis of electrospun fibres with the aid of optical, scanning electron, transmission electron and atomic force microscopes. Experiments were carried out on poly(ethylene terephthalate) and poly(ethylene) melts using the electrospinning process in air and poly(ethylene terephthalate) melts in vacuum. The fibres were successfully electrospun under these conditions and the fibres were around 15 microns in diameter.

Fong *et al.* [41] spun electrospun fibres using poly(ethylene oxide). Fibre diameter was calculated using scanning electron microscopy. SEM images showed bead formation and this was also investigated and reported that the beads are formed because of variation in solution viscosity, net charge density, charges on the fibre and surface tension. Bergshoef *et al.* [42] carried out experiments on solutions of nylon-4,6 in formic acid to produce ultra thin fibres of nylon-4,6 with a semi-finite length. The produced fibres had diameters in the range of 30 to 200 nm when observed under scanning electron and transmission electron microscopes. The fibres were assessed for mechanical performance and also investigated for pattern of the structure by wide angle x-ray scattering and degree of crystallinity by differential scanning calorimetry.

Kim *et al*. [43] spun electrospun fibres of aromatic heterocyclic polybenzimidazole (PBI). The solution was prepared by dissolving PBI with a little lithium chloride in N,N-dimethylacetamide under nitrogen gas. Scanning electron, transmission electron and atomic

force microscopy showed that the fibres were round and smooth with diameters of around 300 nm. The sheet under a polarizing microscope showed that the fibres were birefringent, indicating the molecules were aligned. Norris *et al.* [44] produced a non-woven mat using an electrospinning process by blending the conducting polymer polyaniline and poly(ethylene oxide) in chloroform. The morphology showed that these blended fibres had diameters less than 2 microns.

Electropinning was done on solutions of poly(acrylonitrile) and poly(ethylene oxide) by Buer *et al.* [45]. The velocity of the jet at various distances from the apex was obtained from laser Doppler velocimetry. It was found that the electrospinning process partially orients the molecules in the fibres. The strength of the fibres was calculated and the fibre diameter obtained from SEM micrographs. Deitzel *et al.* [46] showed that an increase in the applied voltage changes the shape of the surface from which the jet originates and the shape change has been correlated to the increase in bead defects.

Since the 1980s and particularly in recent years, the electrospinning process has regained more attention probably due to a surging interest in nanotechnology, as ultrafine fibres or fibrous structures of various polymers with diameters down to submicrons or nanometers can be easily fabricated with this process [7,17,18]. The combination of both fundamental and application-oriented research from different science and engineering disciplines has also been of interest [17]. It has been noted that over 200 universities and research institutes worldwide are studying various aspects of the electrospinning process and the fibre it produces. In addition, the number of patents for applications based on electrospinning has grown in recent years [18].

2.3 Electrospinning of poly(methyl methacrylate)

Poly(methyl methacrylate) (PMMA) nanofibres have already been produced through electrospinning and the effect of some parameters has been reported. Liu *et al.* [47] investigated the effect of polymer solution concentration and different solvents on the morphology of PMMA nanofibres. It was observed that different morphologies and diameters resulted using different solvents and concentrations. The effect of the needle diameter on the diameter of the electrospun PMMA nanofibres has been explored by Macossay *et al.* [48].

They found that the nanofibre diameter is not being influenced by the needle diameter. The effect of different solvents on the morphology of electrospun PMMA nanofibres has been investigated by Qian *et al.* [49]. It was observed that each solvent behaved differently upon electrospinning and different morphologies were obtained for each solvent. Wang *et al.* [29] fabricated PMMA nanofibres varying the effect of polymer concentration, voltage, spinning distance and feed rate. They found that the electrospinning parameters influence the morphology of the nanofibres. Srikar *et al.* [51] prepared PMMA nanofibres for spray cooling of hot surfaces in micro- and optoelectronic and radiological devices. Uyar *et al.* [52] investigated the effect of cyclodextrine nanoparticles in the electrospun PMMA nanofibres. They observed that the addition of the nanoparticles in the electrospun PMMA solutions led to bead-free uniform nanofibres for filtration purposes. Megelski *et al.* [53] investigated the influence of various solvents on the morphologies of the PMMA nanofibres. They observed that the properties of the solvents explain the different morphologies of the nanofibres. Piperno *et al.* [54] investigated the influence of polymer concentration on the morphology of the PMMA nanofibre. They observed that an increase in PMMA concentration increases the homogeneity of the diameter of the nanofibres. The thermal and mechanical properties of elecrospun PMMA nanofibres were studied by Carrizales *et al.* [55]. It was observed that the thermal stability of the nanofibres improved as compared to the powdered PMMA while modest mechanical properties (Young's modulus, peak stress, stress at break and energy at break) were reported. All the authors used a PMMA of molecular weight ranging from 95,000 to 540,000 g mol^{-1}, but Srikar *et al.* [51] used a higher molecular weight of 996,000 g mol^{-1}.

2.4 Electrospinning fundamentals / basic setup

Electrospinning is a unique and novel approach using electrostatic forces to produce fine fibres. The formation of nanofibres is based on the uniaxial stretching of a viscoelastic solution. Electrostatic precipitates and pesticide sprayers work similarly to the electrospinning technique. An interest in the electrospinning process is its potential to form fine fibres of small pore size and high surface area. The principles of electrospinning and the different parameters that affect the process have to be taken into account in order to understand the formation of nanofibres [56].

A schematic of the electrospinning process is shown in Figure 2.1. The typical electrospinning set-up consists of a syringe pump, a high voltage source and a collector. In electrospinning, the spinning of fibres is achieved primarily by the tensile forces created in the axial direction of the flow of the polymer by the induced charges in the presence of an electric field [10]. During the electrospinning process, a polymer solution is held at a needle tip by surface tension. The electric field is induced into the polymer solution through the electrode, resulting in charge repulsion within the solution. The electrostatic forces oppose the surface tension. As the electric field strength is increased further, a point will be reached at which the electrostatic forces balance out the surface tension of the liquid leading to the development of a Taylor cone. A further increase in applied voltage will result in the ejection of the fibre jet from the apex of the cone and acceleration toward the grounded collector. When the fibre jet travels through the atmosphere to the collector, it undergoes a stretching chaotic bending instability leading to the formation of long and thin threads. The bending instability, as suggested by Yarin *et al.* [57] is due to the repulsive forces originating from the charged ions within the electrospinning jet. As the jet is continually elongated and the solvent is evaporated, its diameter can be greatly reduced. The charged jet is then field directed towards the oppositely charged collector, which can be a flat surface or a rotating drum to collect the fibres. As the jet travels, the solvent evaporates. In conventional spinning techniques, the fibre is subjected to a group of tensile, gravitational, aerodynamic, rheological and inertial forces. This approach has been used successfully to spin a number of synthetic and natural polymers into fibres many kilometres in length [11-16]. Figure 2.2 shows SEM and TEM images of electrospun polymer nanofibres [17].

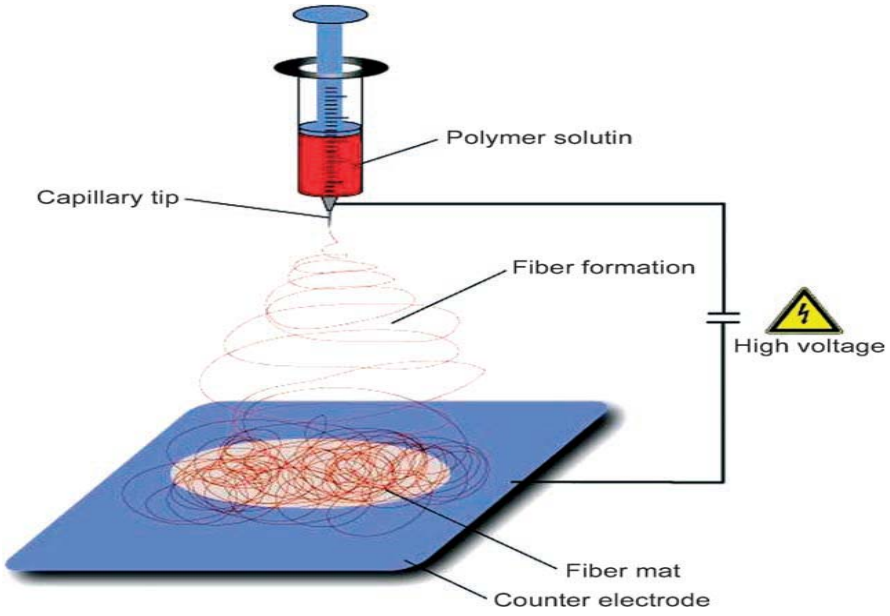

Figure 2.1 An electrospinning setup

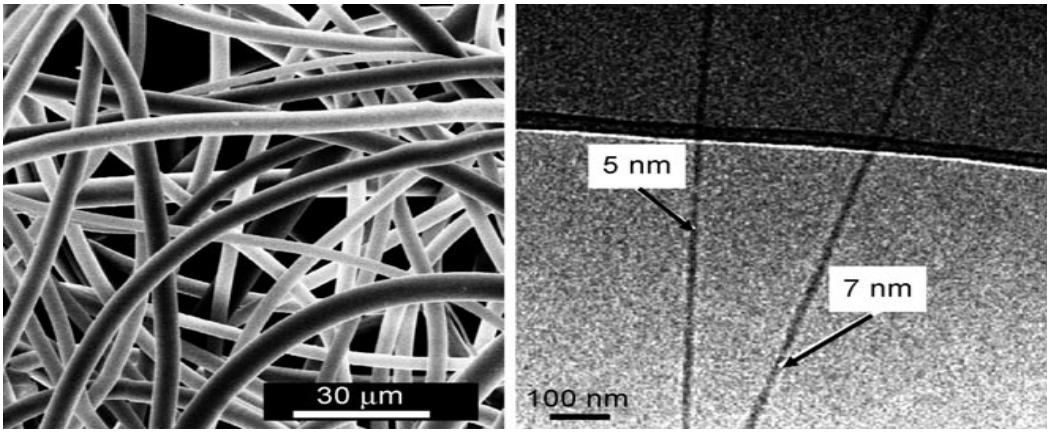

Figure 2.2 SEM (left) and TEM (right) images of electrospun nanofibre (4)

2.5 Electrospinning process

The setup for the electrospinning process as shown in Figure 2.1 is very simple. However, the spinning mechanism is somewhat difficult to understand [58]. There is a complex electro-fluid mechanical issue in electrospinning, as in electrospraying. It was believed (before 1999) that the repulsion between surface charges was causing the splitting or splaying of the electrified jet during the formation of the nanofibres [39]. The recent findings show that the thinning of the jet during electrospinning is attributed to the bending instability associated with the electrified jet [59-62] as shown in Figure 3A [58,62]. The figure shows that the jet was initially a straight line and then became unstable. The cone-shaped, instability region appears to be composed of multiple jets. However, a closer examination using high-speed photography (Figure 2.3B) established that the conical shape contained only a single, rapidly bending or whipping thread. Splaying of the electrified jet might also be observed in some cases, though it was never a dominant process during spinning [61,62]. Due to the high frequency of the whipping, conventional photography cannot properly resolve it and it was believed that the original liquid jet splits into multiple branches as it moves toward the collector. Shin *et al.* [62] and Warmer *et al.* [63] have also used high-speed photography to confirm that the unstable region of the jet, which appears as an inverse cone suggesting multiple splitting, is in reality a single rapidly whipping jet. These suggest that the whipping phenomena occur so fast that the jet appears to be splitting into smaller fibre jets, resulting in ultra fine fibres.

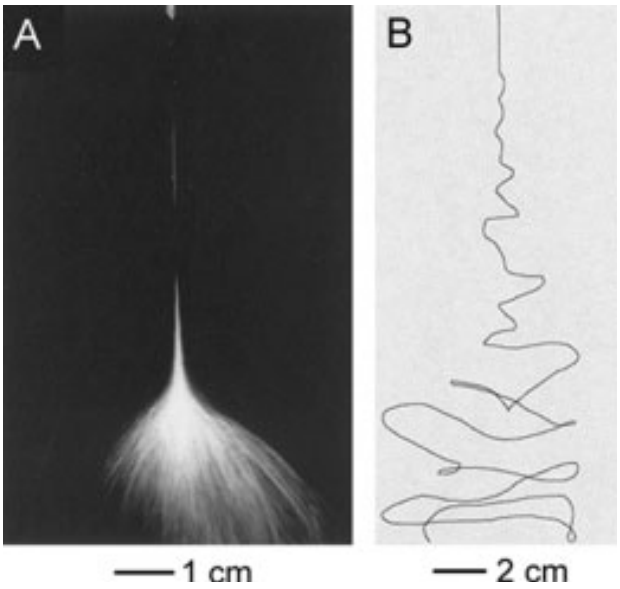

Figure 2.3 Instability region of the poly(ethylene oxide) (PEO) liquid jet at (A) 1/250 s, and (B) 18 ns

The electrospinning process was further investigated using mathematical models based on experimental observations and electrohydrodynamic theories. Various researchers were involved in this task to better understand the electrospining process. Reneker and co-workers treated the charged liquid jets as a system of connected, viscoelastic dumbbells and provided a good interpretation for the formation of bending instability [59,61]. They also calculated the three-dimensional trajectory for the jet using a linear Maxwell equation and the computed results were in agreement with the experimental data. The jet was considered as a long, slender object by Rutledge and co-workers and they therefore developed a different model to account for the electrospinning phenomenon [62,64-66]. Their experimental and theoretical studies clearly showed that the spinning process only involves whipping (rather than splaying) of a liquid jet. The whipping instability is mainly caused by the electrostatic interactions between the external electric field and the surface charges on the jet. The stretching and accelaration of the fluid filament in the instability region led to the formation of fine diameter fibres. The same group further showed that the model could be extended to predict the saturation of whipping amplitude as well as the diameter of the resultant fibres [66]. Feng proposed another model to describe the motion of a highly charged liquid jet in an electric field, and the role of non-linear rheology in the stretching of an electrified jet was also examined [67,68]. Spivat *et al.* [69] developed a steady state model of the jets using non-

linear power law constitutive equations (Oswald-de Waele model) [70,71]. Shin *et al.* [60] in their attempt to model the instability behaviour of electrically forced jets stressed the competition between different types of instabilities that could occur due to the interactions between the charged ions and the electric field. These instabilities were shown to vary along the path depending upon the fluid parameters and the operating conditions. The work showcased the possibility of three types of instabilities: (1) the classical Rayleigh mode (axisymmetric) instability; (2) electric field induced axisymmetric conducting mode; and (3) whipping conducting mode instabilities. Shin *et al.* [62] presented an approach to model the stability of the jets as a function of fluid properties like viscosity and conductivity and process variables like applied electric field and flow rate. They observed that the whipping mode instability is dominant with high charge density in the jets, while the axisymmetric instability dominates at lower charge density. The physical mechanisms of the instability and the development of asymptotic approximations for modelling the instability behaviour were discussed in detail elsewhere [64,65]. Fridrikh *et al.* [66] earlier re-examined the equations of motion derived for creating a model to derive the ultimate diameter of the jets by accounting for the non-linear instability of the jets at the final stage of whipping [64,65]. Their model assumes the charged fluid jet as a Newtonian fluid, and they derived an empirical model of the terminal diameter of the whipping jet as a function of flow rate, electric current, and surface tension of the fluid. The model predicted $10^{2/3}$ fold variations in fibre diameter for varying flow rate and this $^{2}/_{3}$-scaling was experimentally verified for mechanisms responsible for the electrostatic spinning process. These models provide a better understanding of the electropinning process that could assist researchers to design new setups that may provide a better control over the diameter and structure of electrospun nanofibres.

2.6 Remarkable features of electrospun nanofibres

Nanofibres possess features that distinguish themselves from 1D nanostructures produced from other techniques. This has made the electrospinning process popular for the fabrication of nanostructures. For instance, an electrospun nanofibre is highly charged following ejection from the capillary tip, and hence its trajectory is controlled electrostatically by applying an external electric field. Some of the exceptional features of the nanofibres are discussed below.

2.6.1 Extremely long length

Electrospun nanofibres are extremely long as compared with 1D nanostructures [10]. The fibres could be as long as several kilometres as a result of the continuous nature of the electrospinning process. Their length scale is comparable to that of fibres manufactured by conventional drawing or spinning techniques. The electrospun nanofibres can be assembled into a three-dimensional, non-woven mat as a result of bending instability of the spinning jet. Such a porous mat can be immediately used for various applications. Pawlowski *et al.* [72] demonstrated that lightweight wing skins for a micro-air vehicle could be directly formed by electrospinning polymer nanofibres on a wing frame. In addition to nonwoven mats, Xia and Li recently demonstrated that individual fibres with several millimetres to centimetres long could be manipulated individually using a collector containing a void gap (e.g., metallic tweezers) [73]. They showed that the position and spatial orientation of an individual fibre can be easily controlled by moving the collector around. Since the collector is a macroscopic object, the manipulation of individual nanofibres could be achieved even without the assistance of a microscope.

2.6.2 High surface area and complex pore structure

The electrospun nanofibres, as compared to the fibres fabricated using a conventional mechanical extrusion or spinning process, are much smaller in diameter and thus higher in surface-to-volume ratio. The entanglement of nanofibres also results in a high density of pores. Kim and co-workers found that the Branauer-Emmett-Teller (BET) surface areas of electrospun Nylon-6-nanofibres were between 9 and 51 $m^2 g^{-1}$, while the porosity varied from 25 % to 80 % and the pore size was in the range of 2.737 to 0.167 μm [74].

2.6.3 Alignment on the molecular level

The electrospinning process involves the rapid stretching of an electrified jet and rapid evaporation of the solvent. The polymer chains are expected to experience an extremely strong shear force during the electrospinning process. This shear force and rapid solidification may prevent polymer chains from relaxing back to their equilibrium conformations. As a result, the chain conformation and crystallinity of the resultant polymer

nanofibres should be different from products obtained by solution-casting or a conventional spinning process. Vansco *et al.* [75] investigated the structures of electrospun PEO nanofibres by optical and atomic force microscopy and concluded that the fibres possessed a surface layer, at least, of highly ordered polymer chains. Pedicini and Farris [76] characterized the stress-strain behaviour of electrospun mats of poly(urethane) (PU) fibres and found that the mats exhibited a fundamentally different stress-strain response curve in uniaxial tensile tests. This difference was believed to arise from the orientation of chains in the electrospun fibres.

2.7 Structure and morphology of polymeric nanofibres

Nanofibres have recently attracted the attention of researchers due to their pronounced micro and nanostructural characteristics that enable the development of advanced materials that have sophisticated applications. More importantly, large surface area, small pore size, and the possibility of producing three-dimensional structures have increased the interest in nanofibres. The electrospun nanofibres are formed through the action of electrostatic forces and many parameters influence the transition from polymer solution to polymer nanofibres. This section describes the influence of electrospinning parameters that affect the structure and morphology of nanofibres.

2.7.1 Influence of process parameters

2.7.1.1 Applied voltage

The electrospinning process produces the nanofibre through the action of the applied voltage, hence it is a crucial parameter [18]. It was proved that the instability modes that occur during the electrospinning process are attributed to the electrostatic field and the material properties of a polymer. The onset of different modes of instabilities in the electrospinning process depends on the shape of the jet initiating surface and the degree of instability, which effectively produces changes in the fibre morphology [46]. In electrospinning, the applied voltage increases the charge transport due to the flow of the polymer jet towards the collector. Deitzel *et al.* [46] have inferred that an increase in applied voltage causes a change in the shape of the jet initiating point and hence the structure and morphology of fibres. The PEO system showed that the morphology changed from a defect free fibre at a low voltage (5.5

kV) to a highly beaded structure at a higher voltage (9.0 kV). The occurrence of beaded morphology has been correlated to an increase in the applied voltage. It has been observed that an increase in the applied voltage increases the deposition rate due to higher mass flow from the needle tip. At low voltages or field strength, a drop is typically suspended at the needle tip and a jet will originate from the Taylor cone producing bead-free spinning (assuming that the force of the electric field is sufficient to overcome the surface tension). As the voltage is increased, the volume of the drop at the tip decreases, causing the Taylor cone to recede. The jet originates from the liquid surface within the tip and more beading is seen. As the voltage is increased further, the jet eventually moves around the edge of the tip with no visible Taylor cone. At these conditions, the presence of many beads can be observed [46,77].

It has been observed that the increase in voltage leads to the formation of several jets, producing fibres with larger diameters [78]. The presence of beads and junctions at high voltages was found when solutions of PEO, PDLA, bisphenol-A polysulfone, chitosan and gelatine were electrospun [11,12,46,77,79,80]. The correlation between fibre diameter and voltage was ambiguous. For PDLA and PVA, higher voltages yielded larger fibre diameters, however, when spinning silk-like polymer with fibronectin functionality and bisphenol-A polysulfone, the fibre diameter tended to decrease with increasing applied voltage [80-82].

2.7.1.2 Nozzle-collector distance

The variation of distance has been examined as another approach of controlling the fibre diameter and morphology. This is due to the dependence of electrospun fibres on the deposition time, evaporation rate and whipping or instability interval. Buchko *et al.* [82] showed that regardless of the concentration of the solution, smaller nozzle-collector distances produce wet fibres and beaded structures. The study also showed that aqueous polymer solutions require more distance for dry fibre formation than systems that use highly organic solvents. They also found that the morphology changed from a round to a flat shape with a decrease in the distance from 2.0 cm to 0.5 cm. Doshi *et al.* [45] found that the fibre diameter decreased with increasing distances from the Taylor cone. However, for the spinning of gelatine, chitosan, PVA and poly(vinylidene fluoride), no significant effect of the distance between the tip and collector on the fibre size and morphology was observed [11,12,81,83].

2.7.1.3 Polymer flow rate

The polymer flow rate from the syringe influences the jet velocity and the material transfer rate. A lower feed rate is more desirable as the solvent will get sufficient time for evaporation. It was observed that the fibre diameter and the pore diameter increased with an increase in the polymer flow rate, and lower flow rates yielded smaller fibre diameters [77,84]. In addition, at high flow rates a significant amount of bead defects were noticeable due to the inability of the fibres to dry completely before reaching the collector. This resulted in the formation of ribbon-like (or flattened) fibres as compared to fibres with a circular cross section [84].

2.7.2 Influence of solution parameters

2.7.2.1 Solution concentration

The solution concentration determines the spinability of a solution, whether a fibre forms or not due to variations in the viscosity and surface tension [46]. If the solution concentration is too low, the polymer fibre will break up into droplets before reaching the collector due to the effects of surface tension. However, if the solution is too concentrated then fibres cannot be formed due to the high viscosity, which makes it difficult to control the solution flow rate through the capillary. It was also observed that at low polymer concentrations, defects in the form of beading and droplets have been observed. The process under these conditions was characteristic of electrospraying rather than spinning [78]. The presence of junctions and bundles indicated that the fibres were still wet when reaching the collector [84]. Increasing the solution viscosity by increasing the polymer concentration yielded uniform fibres with few beads and junctions [11,14]. It has also been found that the fibre diameter increases with increasing polymer concentration (Figure 2.4) [85].

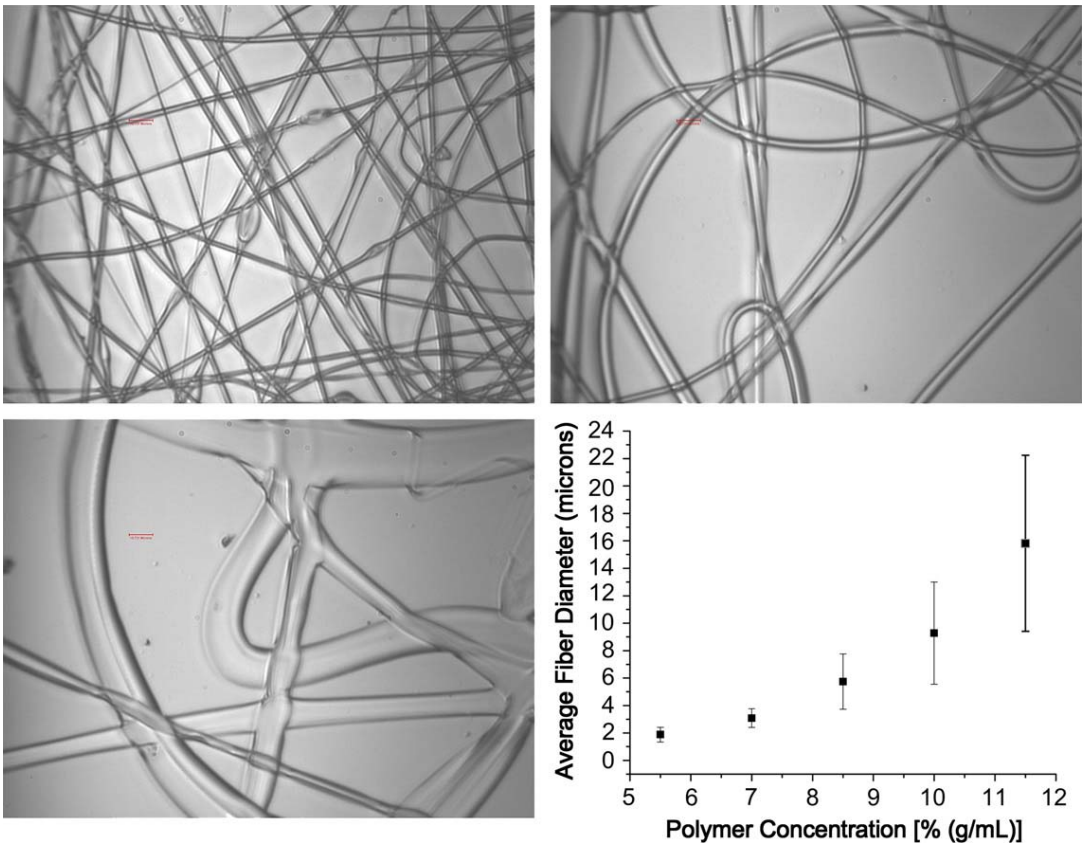

Figure 2.4 Effect of polymer solution concentration on fibre diameter [85]

2.7.2.2 Molecular weight

A polymer's molecular weight has a significant effect on rheological and electrical properties such as viscosity, surface tension, conductivity and dielectric strength [86]. High molecular weight polymer solutions provide the desired viscosity for the fibre generation, hence the uniform morphology of the electrsopun fibres. It was also found that lower molecular weight polymer solutions form in beads, while higher molecular weight solutions yield fibres with larger average diameters. The molecular weight of a polymer gives an indication of the chain entanglements, thus solution viscosity. Even when the polymer concentration is low, the high molecular weight of a polymer can maintain enough entanglements of the polymer chains, thus ensuring a sufficient level of solution viscosity to produce a uniform jet during electrospinning and restrain the effect of surface tension, which plays a significant role in bead formation on electrospun nanofibres [2]. Gupta *et al.* [87] studied the effects of polymer

weight and found that an increase in molecular weight resulted in a decrease in beads and droplets.

2.7.2.2 Viscosity

The size and morphology of the electrospun fibres are determined by the solution viscosity. It was found that a very low viscosity results is no continuous fibre formation while for very high viscosities there is difficulty in the ejection of jets from the polymer solution. Thus, there is a requirement of an optimal viscosity for electrospinning. Previous researchers reported maximum spinning viscocities ranging from 1 to 125 poise [34,36,82,88]. Fong *et al.* [82] studied the electrospinning of polyethylene (PEO) nanofibre formation in different viscosities and found that a range of viscosities between 1 and 20 poise is suitable for the production of uniform nanofibres by electrospining. Viscosity, polymer concentration and the molecular weight of a polymer are correlated to each other. The solution viscosity has been strongly related to the concentration and the relationship between the polymer viscosity and concentration. Fibres obtained from electrospinning has been studied in a number of systems, including poly(lactic-co-glycolic acid) (PLGA) [89], poly(ethylene oxide) (PEO) [14,90], poly(vinyl alcohol) (PVA) [81,91-93], poly(methyl methacrylate) (PMMA) [87], polystyrene [94], poly(L-lactic acid) (PLLA) [95], gelatine [96] and dextran [97]. At very high viscosity polymer solutions usually exhibit longer stress relaxation times, which could prevent the fracturing of the ejected jets during electrospinning. An increase in solution viscosity or concentration gives rise to a larger and more uniform fibre diameter. In electrospinning, the viscosity of a solution plays an important role in determining the range of concentrations from which continuous fibres can be obtained. For low viscosity solutions, surface tension is the dominant factor and beaded fibres are formed while above a critical concentration, a continuous fibrous structure is obtained and its morphology is affected by the concentration of the solution. These show that there exist polymer-specific, optimal viscosity values for electrospinning and this property has a remarkable influence on the morphology of the fibres.

2.7.2.3 Surface tension

Surface tension also plays a crucial role in the electrospinning process and by reducing the surface tension of a polymer solution, fibres without beads can be obtained. Different

solvents may contribute different surface tensions. Generally, the high surface tension of a solution inhibits the electrospinning process because of the instability of the jets and the generation of sprayed droplets [64]. The formation of droplets, beads and fibres depend on the surface tension of a solution. A lower surface tension of the spinning solution helps electrospinning to occur at a lower electric field [86]. However, the lower surface tension of a solvent will not necessarily always be more suitable for electrospinning. Basically, surface tension determines the upper and lower boundaries of the electrospinning window if all other variables are held constant [81,98,99].

2.7.2.4 Volatility of the solvent

The evaporation rate and the drying time are determined by the solvent vapour pressure as electrospinning involves rapid solvent evaporation and phase separations due to jet thinning. Solvent volatility plays a major role in the formation of nanostructures by influencing the phase separation process. Bognitzki *et al.* [100] found that the use of highly volatile solvents like dichloromethane yielded PLLA fibres with pore sizes of 100 nm in width and 250 nm in length along the fibre axis. The effect of the volume ratio of the solvents on the fibre diameter and morphology of electrospun PVC fibres was evaluated by Lee *et al.* [101]. The average fibre diameter decreased with an increase in the amount of DMF in the THF/DMF mixed solvent. They found that the electrolytic nature of the solvent is an important parameter in electrospinning. Megelski *et al.* [84] examined the structural properties of polystyrene fibres electrospun from solutions containing various ratios of DMF and THF. Solutions electrospun from 100% THF (more volatile) demonstrated a high density of pores, which increased the surface area of the fibre as much a 20–40% depending on the fibre diameter. Solutions electrospun from 100% DMF (less volatile) demonstrated almost a complete loss of microstructure with the formation of smooth fibres. Between these two experiments it was observed that pore size increased with decreased pore depth, thus decreasing pore density as the solvent volatility decreased.

2.7.2.5 Solution conductivity

Charged ions in the polymers are highly influential in jet formation. Solution conductivity is mainly determined by the polymer type, solvents used and the presence of ionisable salts.

More conductive solutions will have a greater charge carrying capacity than solutions with low conductivity. Thus the fibre jet of highly conductive solutions will be subjected to a greater tensile force in the presence of an electric field than that of solutions with a low conductivity [16]. Hayati *et al.* [102] showed that highly conductive solutions are extremely unstable in the presence of strong electric fields, which results in dramatic bending instability as well as a broad diameter distribution. Generally, electrospun nanofibres with the smallest fibre diameters can be obtained with the highest electrical conductivity, and it was found that a drop in the size of the fibres is due to increased electrical conductivity. Natural polymers (e.g. gelatin) are generally polyelectrolytic in nature. The ions increase the charge carrying capacity of the jet, thereby subjecting it to higher tension with the applied electric field. Zong *et al.* [103] demonstrated the effect of ions, by adding ionic salt, on the morphology and diameter of electrospun fibres. They found that with the addition of ionic salts like KH_2PO_4, NaH_2PO_4 and NaCl, beadless fibres with relatively smaller diameters ranging from 200 to 1000 nm are produced. This approach of increasing the solution conductivity by the addition of salt has also been used for other polymers such as PEO [79], collagen type I-PEO [14], PLA [81], polyacrylic acid (PAA) [104], and polyamide-6 [105]. With the use of salts, the uniformity of fibres increasesa and there is a decrease in beads generation.

2.7.3 Ambient parameters

The effects of ambient parameters (i.e. temperature and humidity) on the electrospinning process have been examined. Mit-Uppatham *et al.* [105] studied the effect of temperature on the electrospinning of polyamide-6 fibres ranging from 25 to 60 °C. It was found that an increase in temperature yielded fibres with decreased fibre diameter and the decrease was as a result of the decrease in viscosity of the polymer solutions at increased temperatures. The variation in humidity while spinning polystyrene solutions was studied and shows that by increasing humidity there is an appearance of small circular pores on the surface of the fibres, and further increase in humidity led to the pores coalescing [106]. It has been found that at very low humidity, a volatile may evaporate rapidly and this would create a problem with electrospinning. As a result, the electrospinning process may only be carried out for a few minutes before the needle tip is clogged [34]. It has also been suggested that a high humidity can help the discharge of the electrospun fibres [58,107]. Hence, apart from solution and processing parameters, ambient parameters also affect the electrospinning process.

2.8 Characterisation of the nanofibres

As discussed in section 2.7 the interest in research on nanofibres has increased due to its high surface area and nanostructure surface morphologies that enable a large number of advanced applications. There is only little information in the literature on the characterization of nanofibres, although this is important for potential nanofibre applications. However, more researchers are starting to realize the potential of the electrospinning technology and more publications are likely to come out in future.

2.8.1 Geometrical characterization

Geometric properties of nanofibres such as fibre diameter, diameter distribution, fibre orientation and fibre morphology (e.g., cross-section shape and surface roughness) can be characterized using scanning electron microscopy (SEM), field emission scanning electron microscopy (FESEM), transmission electron microscopy (TEM) and atomic force microscopy (AFM) [37,78,84,108]. Figure 2.5 shows the nanofibre structures observed through SEM, TEM and AFM.

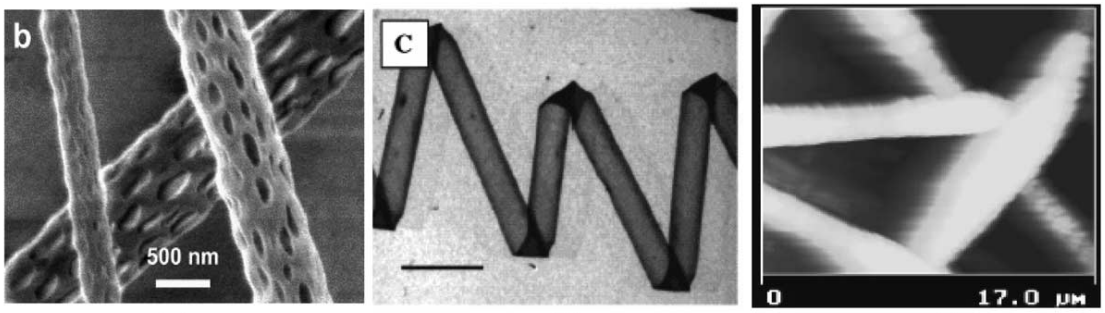

Figure 2.5 (a) SEM of PLLA nanofibres, (b) TEM of elastin-mimetic peptide fibres and (c) AFM of polyurethane nanofibres [109]

SEM has been used by many researchers to observe the morphology and diameters of the fibres produced, however the resolution is less at extreme magnifications. Samples need to be electrically conductive for SEM, and a gold or platinum coating must be applied that may

alter the diameter readings at higher magnifications. A very small sample size is required. Transmission electron microscopy (TEM) is also used for obtaining fibre diameters for extremely small fibres (< 300 nm). Another technique is atomic force microscopy (AFM), which is used to determine fibre diameter, but the process of obtaining an accurate measurement becomes more difficult due to tip convolution. Nevertheless, this technique is the best to observe any type of surface morphology and exact descriptions of the fibre surface. For precise measurement, two fibres crossing each other on the surface are generally chosen [37]. A laser light diffraction method has been used by Doshi and Reneker [36] to observe the decrease in fibre diameter on the electrospinning jet until the jet diameter became smaller than the frequency of visible light. Information regarding the crystallinity of the samples can be obtained from polarized light microscopy, which is perhaps the easiest method and determination is done by the amount of birefringence produced [36]. Polarized light microscopy is a very cost-effective and quick test that can be performed on the collected fibres. Various research groups [79,82,110,111] used many of the alternative methods to determine the crystallinity of the produced nanofibres with varying levels of success, because these methods need a reference of known crystallinity to measure against. These methods include x-ray diffraction, both wide angle and small angle (WAXS and SAXS), and differential scanning calorimetry (DSC). Other techniques such as x-ray photoelectron spectroscopy (XPS), contact angle measurements and attenuated total reflectance Fourier-transform infrared spectroscopy (ATR-FTIR) are also used to determine the surface chemistry of electrospun nanofibres.

Another geometric parameter is porosity. The porosity and pore size of nanofibre membranes are important for applications of filtration, tissue template, protective clothing, etc. [108,112]. The pore size measurement can be conducted by, for example, capillary flow porosimetry or mercury porosimetry [110,111,113]. Researchers reported a highly porous structure of electrospun nanofibrous scaffolds with 91.63 % porosity, a total pore volume of 9.69 mL g^{-1}, a total pore area of 23.54 m^2 g^{-1}, and a pore diameter ranging broadly from 2 to 465 μm with the utilization of these methods [108,113,114]. There is always a problem of small pore size with electrospun fibres, which is not very suitable for the cellular filtration/migration. Lee *et al.* [115] used a modified approach to overcome the problem. The approach include combining electrospinning technology and salt leaching/gas foaming methods for the fabrication of an electrospun fibrous scaffold with dual-sized pores that results in intrinsic

pores formed between nanofibres and also micro-sized pores created by salt particles that are distributed in the scaffolds.

2.8.2 Physical and chemical properties

The molecular structure of a nanofibre can be characterized by Fourier transform infrared spectroscopy (FTIR) and nuclear magnetic resonance spectroscopy (NMR) techniques [109]. If two materials were blended together for nanofibre fabrication, not only can the structure of the two materials be detected, the inter-molecular reaction can also be characterized. In the case of a collagen and poly(ethylene oxide) blend used for electrospinning of nanofibres, the NMR spectrum showed a new phase structure that was caused by the hydrogen bond formation between the ether oxygen of poly(ethylene oxide) and the protons of the amino and hydroxyl groups in collagen [39].

The configuration of the macromolecules in a nanofibre can be characterized by optical birefringence, wide angle x-ray diffraction (WAXD), small-angle x-ray scattering (SAXS) and differential scanning calorimetry (DSC) [82,113,116,117]. Fong and Reneker [79] studied the birefringence of the styrene-butadiene-styrene (SBS) triblock copolymer nanofibres with diameters around 100 nm under an optical microscope [79]. The occurrence of birefringence was reported and related to the molecular orientation.

2.8.3 Thermal properties

There are currently few published reports on the thermal properties of nanostructured materials. Thermal analysis has been performed on a number of electrospun polymeric materials to understand the relationship between nanostructure and thermal properties. DSC studies showed that electrospun PLLA fibres have lower crystallinity, glass transition temperature (T_g) and melting temperature (T_m) than the semicrystalline PLLA polymer [77]. Zong *et al.* [77] attributed the decrease in the T_g to the large surface to volume ratio of nanofibres with air as the plasticizer. The high evaporation rate followed by rapid solidification at the final stages of electrospinning is expected to be the reason for the low crystallinity. The T_g and peak crystallization temperature (T_c) of the electrospun poly(ethylene terephthalate) (PET) and poly(ethylene naphthalate) (PEN) decreased

significantly, while the heat of crystalline melting increased [118]. The decrease in T_g and T_m, and the increase in the heat of melting were attributed to the increase in the segmental mobility. The melting temperature of the PET and PEN electrospun fibres remained almost constant, without any significant variations compared to that of regular fibre forms. PEO nanofibres have shown a lower melting temperature and heat of fusion than the PEO powder, which is attributed to the poor crystallinity of the electrospun fibres [77]. The crystallinity of the PLLA fibres was retarded by electrospinning, and the WAXD patterns of the electrospun PLLA fibres confirmed highly oriented fibres. This decrease in crystallinity has been shown to be a general phenomenon and has been observed in poly(meta-phenylene isophthalamide), polyglycolide and polyacrylomide. Deitzel *et al.* [46] inferred that PEO nanofibres retained the same crystal structure as PEO powders, while there is a clear indication of reduced crystalline order in the nanofibres.

2.8.4 Mechanical properties

Conventional testing techniques can be used for the mechanical tests of nanofibrous non-woven membranes [101,108,119]. No anisotropy in the in-plane tensile behaviour has been reported when the membrane is collected on a static collector screen. Lee *et al.* [101,119] discovered that electrospun non-woven mats had different properties in different directions when the membranes were obtained from a rotating drum. The fibre orientation depended on the linear velocity of the drum surface and other electrospinning parameters.

Due to their very small dimensions, the mechanical characterization of nanofibre mats and individual nanofibres are a challenge for the existing test techniques. The established methods and standards for determining the mechanical behaviour of conventional fibres are inadequate in the case of testing of nanofibres. This is probably one of the main reasons why articles addressing the mechanical tests of single nanofibres are rare in the literature. Young's modulus, tensile strength and the strain at break were also determined by performing tensile tests with single polymer fibres. A conventional nano-tensile testing system has been used to conduct the tensile testing for the evaluation of mechanical properties of single ultrafine polymeric fibres of polycaprolactone (PCL) [120]. Inai *et al.* [121] carried out tensile tests of single electrospun poly(L-lactic acid) (PLLA) nanofibres collected from a rotating disc at different collection speeds. Tension tests for determining mechanical strength of electrospun

nanofibres simply follows the macroscale standards and involves the least number of assumptions necessary to extract material properties. This method is useful for fibres with diameters approaching towards 1 μm and allows for fibre testing until failure [122]. Chew *et al.* [123] conducted tensile tests on single electrospun nanofibres by mounting the fibres onto a cardboard mount with double-sided tape. The gauge length of the fibre specimen was set at 20 mm.

Another instrument that measures the elastic properties of electrospun membranes is AFM, which consists of a cantilever and tip assembly that is used for scanning of the surface of a sample. Atomic resolution can be obtained with very slight contact by AFM. This is achieved by measuring the deflection of the cantilever due to the repulsion of contacting atomic shells of the tip and the sample [124]. AFM phase imaging is an extension of the tapping mode, which allows detection of variations in composition and hardness [125]. The bending and shear moduli of the electrospun collagen fibres have been determined by AFM by performing microstructural bending tests with native and glutaraldehyde cross-linked single electrospun fibres [126]. Cuenot *et al.* [127,128] used resonant contact AFM approaches for measuring the elastic modulus of the nanofibres. In this method, there is a requirement of nanofibres attachment to a cantilever tip [129]. A three-point nanoscale bending test with an AFM tip was also employed to determine the elastic modulus of nanofibres [130,131]. The researchers reported an increase in the elastic modulus with a decrease in the fibre diameter.

Yuga *et al.* [129] described a microcantilever-based, vibrational method for determining Young's modulus of a single electrospun nanofibre. This technique basically relies on the conventional beam dynamics for which an analytical relation between fibre stiffness and the resonant frequencies is obtained for specific geometries. This method is mostly used with metallic nanofibres, but not very common with polymeric fibres, because of the limited bending rigidity of the fibres that results in a whipping motion under lateral excitation [132].

2.9 Applications of electrospun nanofibres

As already mentioned in the above sections, electrospinning has surfaced as a powerful technique for the fabrication of nanofibres. The potential applications of the nanofibres result

from the simplicity of the technique and the interesting properties of the nanofibres. Some of the applications are described below.

2.9.1 Composite applications

Polymers are typically reinforced with traditional (micro-range) fibres, such as carbon, glass and Kevlar fibres, for potential applications in automotive, aerospace, etc [133]. The final composite materials have superior structural properties such as high modulus and strength to weight ratios, which generally cannot be achieved by other engineered monolithic materials alone. Electrospun nanofibres will also eventually find applications in making nanocomposites due to their large specific surface-to-volume ratio [42].

The rules established for reinforcement by macroscopic fibres should also apply for reinforcement by nanofibres [134]. However, nanofibres have several advantages over macroscopic fibres. Since the reinforcement effect is determined by the aspect ratio of the fibres, nanofibres with diameters of 10-100 nm can be 100-1000 times shorter than fibres with diameters of 10-100 μm. Nanofibres cause little diffraction of light, because of their small diameters. Therefore, transparent matrices reinforced by nanofibres stay transparent, even if the refraction indices of the matrix and the fibres do not match [42]. Furthermore, it is predicted that smaller loadings of nanofibres in the matrix are required to achieve the same reinforcement effect as macroscopic fibres. Thus, material can be saved and the brittleness of the matrix reduced. The large specific surface area between the nanofibres and the matrix promotes relaxation processes, which improves the impact strength of the reinforced matrix.

Research on nanofibres as composites reinforcements is still in its infancy. However, some researchers have successfully reinforced polymer matrices with electrospun nanofibres. There are currently unresolved challenges such as the dispersion and the control of the nanofibre orientation in the polymer matrix. Epoxide matrices were reinforced with polyamide 4,6 nanofibres of about 30 nm in diameter by Bergshoef and Vansco [42]. An increase in the Young's modulus by a factor of 35 and of the breaking load by a factor of four was reported for the composites. Reneker and Kim [135] demonstrated that the mechanical strength of a rubber film could be significantly improved by reinforcing with nanofibres electrospun from poly(benzimidazole). The Young's modulus measured for the composite film was an order of

magnitude greater and the tear strength was twice as large as those of the pristine rubber material.

2.9.2 Filtration applications

The filtration market is increasing notably in the engineering fields [136]. Fibrous materials used for filter media provide advantages of high filtration efficiency and low air resistance [137]. Filtration efficiency, which is closely associated with the fibre fineness, has been realised as the most important concern for the filter performance. In the industry, coalescing filter media are studied to produce clean compressed air. These media are required to capture oil droplets as small as 0.3 micron. It is realised that electrospinning is rising to the challenge of providing solutions for the removal of unfriendly particles in the submicron range. Since the channels and structural elements of a filter must be matched to the scale of the particles or droplets that are to be captured in the filter, one direct way of developing efficient and effective filter media is by using nanometer sized fibres in the filter structure [138]. In general, due to the very high surface area to volume ratio and resulting high surface cohesion, tiny particles of the order of < 0.5 μm can be easily trapped in the electrospun nanofibrous structured filters and hence the filtration efficiency can be improved.

2.9.3 Sensor applications

The performance of sensors is affected by parameters like sensitivity, selectivity, response time, reproducibility and ageing, all of which are dependent directly on the property of the sensing membrane used. There is a strong need for detection of gases and biological substances at low concentration. Therefore, sensitivity in particular plays a very critical role. Modern biomedical sensors with advanced micro-fabrication and signal-processing techniques are becoming more and more accurate and inexpensive [139]. The main focus is on the miniaturization of bulky instrumentation and development of portable sensors in order to avoid the burden of accuracy and reliability and also in the development of various specific target molecules for different analytes that have exhausted all possibilities. Electrospun nanofibrous membranes have received much attention for their sensor applications because of their unique large surface area, which is the most desirable property for improving the sensitivity of conductometric sensors as a larger surface area will absorb more of a gas

analyte and change the sensor's conductivity more significantly. Silk fibroin membrane-based biosensors have been extensively used for analysing various substances such as glucose, hydrogen peroxide and uric acid [140,141]. Apart from this, the literature shows the involvement of other electrospun polymers as sensing interfaces, such as polyaniline, polypyrrole, polyamic acid, nylon-6 and poly(pyrene methanol) [142,143]. Efforts have been made recently to produce nanofibres for electrochemical sensors. Nanofibres that have a large surface area would be ideal for electrochemical biosensors. Optical sensors are relatively new and not much work has been carried out in this field. Recent progress in biomedical technology has mainly focused on the development of novel sensor products with new applications.

2.9.4 Energy generation applications

Polymeric conductive membranes also have potential for applications such as electrostatic dissipation, corrosion protection, electromagnetic interference shielding, photovoltaic devices, fabrication of tiny electronic devices or machines such as Schottky junctions, sensors and actuators, as the rate of electrochemical reactions is proportional to the surface area of the electrode [44,144]. Conductive nanofibrous membranes are also quite suitable for use as porous electrodes in developing high performance batteries and polymer electrolyte membrane fuel cells due to its high porosity and inherent large total surface area. Polymer batteries have been developed for cellular phones to replace conventional, bulky lithium batteries. The components of polymer batteries are a carbon anode, a lithium cobalt oxide cathode, and a polymer gel electrolyte. Conductive nanofibres offer noteworthy properties of polymer batteries, for example, less electrolyte leakage, and high energy density per weight [138]. However, there is still a need to improve energy density per weight of polymer batteries to increase their market share.

2.9.5 Textile applications

Non-wovens composed of nanofibres can be used in combination with conventional textiles to modify the properties of the textiles. The aim is to increase the wind resistance, to regulate the water-vapour permeability, to optimize the thermal insulation behaviour, or to give the textile a specific functionality (such as the lotus effect, aerosol filtering or protection against

chemical or biological hazards). The change from microfibre to nanofibre non-wovens leads to significant change in the transport processes of the material as a result of the reduction in the pore dimensions and the large increase in the inner surface area. For instance, in the case of gas diffusion, which is important with respect to chemical insulation, there is a transition from the normal diffusion regime (in which the diffusion path is determined by impacts between the gas particles) to the Knudsen regime (in which the diffusion path is mainly determined by impacts between the gas particles and the fibres). Gas transport properties are of great importance for textile applications [112,145,146]. Experimental findings have shown that the air flow (wind) resistance of nanofibre non-wovens is increased by up to three orders of magnitude in comparison to conventional textiles, which leads to a significant thermal effect.

The thermal insulation of non-wovens is mainly a result of the limited diffusion of air molecules in the materials. The thermal insulation increases significantly with decreasing pore size if the pore diameter of the non-woven is 10-100 times smaller than the mean free path of the gas molecules (about 70 nm for air at normal pressure). The aerosol-filtering properties of nanofibre non-wovens have also been investigated. The filter efficiency of a textile increases significantly with increasing coverage by a nanofibre non-woven. An efficiency of 100% can be achieved at a coverage of only 1 g m^{-2}. The use of nanofibre non-wovens for protection against chemical and biological hazards has also been discussed. This application is based on the functionalization of the non-woven with a catalyst (for example, an enzyme) that can decompose harmful substances [112,146,147]. The large inner surface area that is available for these catalytic processes is a great advantage of nanofibre non-wovens.

2.9.6 Wound dressing applications

Polymer nanofibres can also be used for the treatment of wounds or burns of a human skin as well as designed for haemostatic devices with some unique characteristics. Fibres of biodegradable polymers can be directly spun onto the injured location or skin to form a fibrous mat dressing. Thus, the wound would be able to heal by the formation of normal skin growth and the elimination of the scar tissue which would occur in a traditional treatment [148,149]. The non-woven mats for wound dressing usually have pore sizes ranging from 500

nm to 1 μm, so as to protect the wound from bacterial penetration. A high surface area of 5-100 m^2 g^{-1} is important for fluid absorption and dermal delivery. A non-woven nanofibre mat would thus be able to perform that function.

2.10 Concluding remarks

Researchers all over the world are now shifting their focus to nanoscience. This drive in nanoscience is motivated by the interest in the nanometer scale with advanced properties. The field looks promising as the number of publications has increased notably since its inception. Governments and other stakeholders are now supporting the initiative as most of the industries (science, medicine, etc.) are now harnessing the potential of the technology. One of the recently recognized fields of nanoscience is electrospinning. This is currently the only technique available for the fabrication of continuous nanofibres. The increased interest in the electrospinning domain is as a result of the simplicity, adaptability, ability to fabricate fibres with diameters in the nanometer size, a wide range of applications of the nanofibres and the large surface area of the electrospun nanofibres.

This review highlighted the fundamentals of electrospinning, processing parameters, nanostructure formation, features of electrospun nanofibres, characterisation and potential applications of the nanofibres. There are still a few challenges that need to be resolved. One of them is the uniformity of the fibre diameters, as fibre diameters are seldom uniform. The second one is the few reports or no information on the mechanical properties of the nanofibres. The difficulty in getting a single fibre off the fibre mat and mounting it on a tensile tester is one of the things that contribute to this. This information is needed in all the applications of nanofibres, particularly composite reinforcements. A focus on scaling up of nanofibre technology is also important for the growth and development of the field.

The electrospinning process was earlier attached to researchers with polymer, fibre and textile backgrounds. With more scientists and engineers collaborating, the field will become interdisciplinary in the near future and many applications will be realized. The number of publications will rise dramatically if more materials can be processed into nanofibres other than organic polymers.

2.11 References

[1] A.K. Haghi. Effects of some systematic parameters on formation of electrospun polyacrilonitrile (PAN) nanofibres. In: L. Liu, G.E. Zaikov. (Ed.). Chemistry as Music. Nova Science Publishers: USA (2007).

[2] S.H. Tan, R. Inai. Systematic parameters study for ultra-fibre fabrication via electrospinning process. Polymer 2005; 46:6128- 6134.
DOI:10.1016/j.polymer.2005.05.068

[3] A. Ziabicki. Fundamentals of fibre formation. In: The Science of Fibre Spinning and Drawing. Wiley-Interscience: New York (1976).

[4] W.W. Edwards. US Patent no. 3179614 (1965).

[5] R.S. Irwin. US Patent no. 3415782 (1968).

[6] A.G. MacDiarmid, J.W.E. Jones, I.D. Norris, J. Gao, A.-T. Johnson, N.J. Pinto, J. Hone, B. Han, F.K. Ko, M. Okuzaki, H. Liaguno. Electrostatically-generated nanofibres of electronic polymers. Synthetic Metals 2001; 119:27-30.

[7] Z.-M. Huang, Y.Z. Zhang, M. Kotaki, S. Ramakrishna. A review on polymer nanofibres by electrospinning and their applications in nanocomposites. Composites Science and Technology 2003; 63:2223-2253.
DOI:10.1016/S0266-3538(03)00178-7

[8] A. Formhals. US Patent no. 1975504 (1934).

[9] E. Smit, U. Buttner, R.D. Sanderson. Continuous yarns from electrospun fibres. Polymer 2005; 46:2419-2423.
DOI:10.1016/j.polymer.2005.02.002

[10] D.H. Reneker, I. Chun. Nanometer diameter fibres of polymer produced by electropsinning. Nanotechnology 1996; 7:216-223.
DOI: 10.1088/0957-4484/7/3/009

[11] C.-S. Ki, D.H. Baek, K.D. Gang, K.H. Lee, I.C. Um, Y.H. Park. Chararcterization of gelatine nanofibre prepared from gelatine-formic acid solution. Polymer 2005; 46:5094-5102.
DOI:10.1016/j.polymer.2005.04.040

[12] X.Y. Geng, O.H. Kuon, J.H. Jang. Electrospinning of chitosan dissolved in concentrated acetic acid solution. Biomaterials 2005; 26:5427-5432.
DOI:10.1016/j.biomaterials.2005.01.066

[13] H.L. Jiang, D.F. Fang, B.S. Hsiao, B. Chu, W.L. Chen. Optimization and characterization of dextran membranes prepared by electrospinning. Biomacromolecules 2004; 5(2):326-333.
DOI: 10.1021/bm034345w

[14] L. Huang, K. Nagapudi, R.P. Apkarian, E.L. Chaikof. Engineered collagen-PEO nanofibres and fabrics. Journal of Biomaterials Science Polymer Edition 2001; 12:979-993.
DOI**:** 10.1163/156856201753252516

[15] J.A. Matthews, G.E. Wnek, D.G. Simpson, G.L. Bowlin. Electrospinning of collagen nanofibres. Biomacromolecules 2002; 3:232-238.
DOI**:** 10.1021/bm015533u

[16] A. Frenot, I.S. Chronakis. Polymer nanofibres assembled by electrospinning. Current Opinion in Colloid and Interface Science 2003; 8:64-75.
DOI:10.1016/S1359-0294Ž03.00004-9

[17] A. Greiner, J.A. Wendorff. Electrospinning: A fascinating method for the preparation of ultrafine fibres. Nanotechnology. Angewandte Chemie International Edition 2007; 46:5670-5703.
DOI: 10.1002/anie.200604646

[18] N. Bhardwaj, S.C. Kundu. Electrospinning: A fascinating fibre fabrication technique. Biotechnology Advances 2010; 28:325-347.
DOI:10.1016/j.biotechadv.2010.01.004

[19] S. Gray. A letter concerning the electricity of water, from Mr. Stephen Gray to Cromwell Mortimer, M.D. Secr. R.S. Philosophical Transactions. The Royal Society 1731-1732; 37:227-260.

[20] G.M. Bose, Recherches scur la cause et sur la veritable theorie de l'electricite. Wittenberg (1745).

[21] R. Lord. On the equilibrium of liquid conducting masses charged with electricity. Philosophical Magazine Series 1882; 87:184-186.
DOI:10.1080/14786448208628425

[22] J. Lamor. Note on the complete scheme of electrodynamic equations of a moving material medium and on electrostriction. Proceedings of the Royal Society 1898; 63:365-372.
DOI: 10.1098/rspl.1898.0043

[23] J.F. Cooley. US Patent no. 692631 (1902).

[24] W.J. Morton. US Patent no. 705691 (1902).

[25] J.F. Cooley. US Patent no. 745276 (1903).

[26] K. Hagiwaba, O. Oji-Machi, K. Ku. Japan Patent no. 1699615 (1929).

[27] A. Formhals. US Patent no. 2160962 (1939).

[28] A. Formhlas. US Patent no. 2187306 (1940).

[29] B. Vonnegut, R.L. Neubauer. Production of monodisperse liquid particles by electrical atomization. Journal of Colloid Science 1952; 7:616-622.
DOI:10.1016/0095-8522(52)90043-3

[30] V.G. Drozin. The electrical dispersion of liquids as aerosols. Journal of Colloid Science 1955; 10:158-164.
DOI:10.1016/0095-8522(55)90022-2

[31] H.L. Simons. US Patent no. 3280229 (1966).

[32] G. Taylor. Electrically driven jets. Proceedings of the Royal Society of London. Series A 1969; 313:453-475.

[33] T. Subbiah, G.S. Bhat, R.W. Tock, S. Parameswaran, S.S. Ramkumar. Electrospinning of nanofibres. Journal of Applied Polymer Science 2005; 96:557-569.
DOI 10.1002/app.21481

[34] P.K. Baumgarten. Electrostatic spinning of acrylic microfibres. Journal of Colloid and Interface Science 1971; 36:71-79.
DOI:10.1016/0021-9797(71)90241-4

[35] W. Simm, C. Gosling, R. Bonart, B. Von Falkai. US Patent no. 4143196 (1979).

[36] J. Doshi, D.H. Reneker. Electrospinning process and applications of electrospun fibres. Journal of Electrostatics 1995; 35:151-160.
DOI:10.1016/0304-3886(95)00041-8

[37] G. Srinivasan, D.H. Reneker. Structure and morphology of small diameter electrospun aramid fibres. Polymer International 1995; 36:195-201.
DOI: 10.1002/pi.1995.210360210

[38] G. Srinivasan. Structure and morphology of electrospun polymer fibres. Doctoral Dissertation, The University of Akron (1994).

[39] D.H. Reneker, I. Chun. Nanometer diameter fibres of polymer produced by electrospinning. Nanotechnology 1996; 7:216-223.

[40] I. Chun. Fine fibres spun by electrospinning process from polymer solutions and melts in air and vacuum: Characterization of structure and morphology on electrtospun fibres and developing a new process model. Doctoral Dissertation, The University of Akron (1995).

[41] H. Fong. The study of electrospinning and the physical properties of electrospun nanofibres. Doctoral Dissertation. University of Akron (1999).

[42] M.M. Bergshoef, G.J. Vansco. Transparent nanocomposites with ultrathin electrospun nylon-4,6 fibre reinforcement. Advanced Materials 1999; 11(16):1362-1365.

[43] J.S. Kim, D.H. Reneker. Polybenzimidazole nanofibres produced by electrospinning. Polymer Engineering and Science 1999; 39(5):849-854.
DOI: 10.1002/pen.11473

[44] I.D. Norris, M.M. Shaker, F.K. Ko, A.G. MacDiarmid. Electrostatic fabrication of ultrafine conducting fibres: Polyaniline/polyethylene oxide blends. Synthetic Metals 2000; 114:109-114.
DOI:10.1016/S0379-6779(00)00217-4

[45] A. Buer, S.C. Ugbolue, S.B. Warmer. Electrospinning and properties of some nanofibres. Textile Research Journal 2001; 71(4):323-328.
DOI: 10.1177/004051750107100408

[46] J.M. Deitzel, J.D. Kleinmeyer, D. Harris, N.C. BeckTan. The effect of processing variables on the morphology of electrospun nanofibres and textiles. Polymer 2001; 42:261-272.
DOI:10.1016/S0032-3861(00)00250-0

[47] J. Liu, S. Kumar. Microscopic polymer cups by electrospinning. Polymer 2005; 46:3211-3214.
Doi:10.1016/j.polymer.2004.11.116

[48] J. Macossay, A. Marruffo, R. Eincon, T. Eubanks, A. Kuang. Effects of needle diameter on nanofibre diameter and thermal properties of electrospun poly(methyl methacrylate). Polymers for Advanced Technologies 2007; 18:180-183.
DOI: 10.1002/pat.844

[49] Y.F. Qian, Y. Su, X.-Q. Li, H.-S. Wang, C.-L. He. Electropsinning of polymethyl methacrylate nanofibres in different solvents. Iranian Polymer Journal 2010; 19(2):123-129.

[50] H. Wang, Q. Li, Q. Yang, Y. Li, W. Wang, L. Sun, C. Zhang, Y. Li. Electrospun poly(methyl methacrylate) nanofibres and microparticles. Journal of Materials Science 2010; 45:1032-1038.
DOI 10.1007/s10853-009-4035-1

[51] R. Srikar, T. Gambaryan-Roisman, C. Steffes, P. Stephen, C. Tropea, A.L. Yarin. Nanofibre coating of surfaces for intensification of drop or spray impact cooling. International Journal of Heat and Mass Transfer 2009; 52:5814-5826.
DOI:10.1016/j.ijheatmasstransfer.2009.07.021

[52] T. Ugar, A. Balan, L. Toppare, F. Besenbacher. Electrospinning of cyclodextrin functionalized poly(methyl methacrylate). Polymer 2009; 50:475-480.
DOI:10.1016/j.polymer.2008.11.021

[53] S. Megelski, J.S. Stephens, D.B. Chase, J.F. Rabolt. Micro- and nanostructured surface morphology on electrospun polymer fibres. Macromolecules 2002, 35:8456-8466.
DOI**:** 10.1021/ma020444a

[54] S. Piperno, L. Lozzi, R. Rastelli, M. Passacantando, S. Santucci. PMMA nanofibres production by electrospinning. Applied Surface Sience 2006; 252:5583-5586.
DOI:10.1016/j.apsusc.2005.12.142

[55] C. Carrizales, S. Pelfrey, R. Rincon, T.M. Eubanks, A. Kuang, M.J. McClure, G.L. Brown, J. Macossay. Thermal and mechanical properties of electrospun PMMA, PVC, Nylon 6 and Nylon 6,6. Polymers for Advanced Technologies 2008; 19:124-130.
DOI: 10.1002/pat.981

[56] J.M. Deitzel, N.C. BeckTan, J.D. Kleinmeyer, J. Rehrmann, D. Tevault. Generation of polymer nanofibres through electrospinning. Army Research Laboratory Technical Report (ARTL-TR-1989) 1999; 1-33.

[57] A.L. Yarin, S. Koombhongse, D.H. Reneker. Bending instability in electrospinning of nanofibres. Journal of Applied Physics 2001; 89:3018-3026.
DOI:10.1063/1.1333035

[58] D. Li, Y. Xia. Electrospinning of nanofibres: Reinventing the wheel. Advanced Materials 2004; 16:1151-1170.
DOI: 10.1002/adma.200400719

[59] D.H. Reneker, A.L. Yarin, H. Fong, S.J. Koombhongse. Bending instability of electrically charged liquid jets of polymer solutions in electrospinning. Applied Physics 2000; 87:4531-4537.

DOI: 10.1063/1.373532

[60] Y.M. Shin, M.M. Hohman, M.P. Brener, G.C. Rutledge. Electrospinning: A whipping fluid jet generates submicron polymer fibres. Applied Physics Letters 2001; 78:1149-1151.
DOI:10.1063/1.1345798

[61] A.L. Yarin, S. Koomhangse, D.H. Reneker. Taylor cone and jetting from liquid droplets in electrospinning of nanofibres. Journal of Applied Physics 2001; 90:4836-4846.
DOI: 10.1063/1.1408260

[62] Y.M. Shin, M.M. Hohman, M.P. Brener, G.C. Rutledge. Experimental characterization of electrospinning: The electrically forced jet and instabilities. Polymer 2001; 42:9955-9967.
DOI:10.1016/S0032-3861(01)00540-7

[63] S.B. Warmer, A. Buer, M. Grimler, S.C. Ugbolue, S.C. Rutledge, M.Y. Shin. A fundamental investigation of the formation and properties of electrospun fibres. National Tetile Center Annual Report 1998; 83:1-9.

[64] M.M. Hohman, M. Shin, G.C. Rutledge, M.P. Brenner. Electrospinning and electrically forced jets: I. Stability theory. Physics Fluidics 2001; 13:2201.
DOI: 10.1063/1.1383791

[65] M.M. Hohman, M. Shin, G.C. Rutledge, M.P. Brenner. Electrospinning and electrically forced jets: II. Applications. Physics Fluidics 2001; 13:2221.
DOI: 10.1063/1.1384013

[66] S.V. Fridrikh, J.H. Yu, M.P. Brenner, G.C. Rutledge. Controlling the fibre diameter during electrospinning. Physical Reviews Letters 2003; 90:144 502.
DOI: 10.1103/PhysRevLett.90.144502

[67] J.J. Feng. The stretching of an electrified non-Newtonian jet: A model for electrospinning. Physics of Fluids 2002; 14:3912.
DOI: 10.1063/1.1510664

[68] J.J. Feng. Stretching of a straight electrically charged viscoelastic jet. Journal of Non-Newtonian Fluid Mechanics 2003; 116:55-70.
DOI**:** 10.1016/S0377-0257(03)00173-3

[69] A.F. Spivak, Y.A. Dzenis, D.H. Reneker. A model of steady state jet in the electrospinning process. Mechanics Research Communications 2001; 27:37-42.

[70] R. Darby. Viscoelastic Fluids: An introduction to their properties and behaviour. Marcel Dekker: New York (1976).

[71] A.L. Yarin. Free Liquid Jets and Films: Hydrodymanics and Rheology. Longman Publishing Group: New York (1993).

[72] K.J. Pawlowski, H.L. Belvin, D.L. Raney, J. Su, J.S. Harrison, E.J. Siochi. Electrospinning of a micro-air vehicle wing skin. Polymer 2003; 44:1309-1314. DOI:10.1016/S0032-3861(02)00859-5

[73] D. Li, Y. Wang, Y. Xia. Electrospinning of polymeric and ceramic nanofibres as uniaxially aligned arrays. Nano Letters 2003; 3:1167-1171. DOI: 10.1021/nl0344256

[74] Y.J. Ryu, H.Y. Kim, K.H. Lee, H.C. Park, D.R. Lee. Transport properties of electrospun nylon 6 nonwoven mats. European Polymer Journal 2003; 39:1883-1889. DOI:10.1016/S0014-3057(03)00096-X

[75] R. Jaeger, H. Schonherr, G.J. Vancso. Chain packing in electro-spun poly(ethylene oxide) visualized by atomic force microscopy. Macromolecules 1996; 29:7634-7636. DOI: 10.1021/ma9610673

[76] A. Pedicini, R.J. Farris. Mechanical behaviour of electrospun polyurethane. Polymer 2003; 44:6857-6862. DOI:10.1016/j.polymer.2003.08.040

[77] X.H. Zong, K. Kim, D.F. Fang, S.F. Ran, B.S. Hsiao, B. Chu. Structure and process relationship of electrospun bioabsorbable nanofibre membranes. Polymer 2002; 43:4403-4412. DOI:10.1016/S0032-3861(02)00275-6

[78] M.M. Demir, I. Yilgor, E. Yilgor, B. Erman. Electrospinning of polyurethane fibres. Polymer 2002; 43:3303-3309. DOI:10.1016/S0032-3861(02)00136-2

[79] H. Fong, I. Chun, D.H. Reneker. Beaded nanofibres formed during electrospinning. Polymer 1999; 40:4585-4592. DOI:10.1016/S0032-3861(99)00068-3

[80] X.Y. Yuang, Y.Y. Zhang, S.H. Dong, J. Shang. Morphology of ultrafine polysulfone fibres prepared by electrospinning. Polymer International 2004; 53:1704-1710. DOI**:** 10.1002/pi.1538

[81] C.X. Zhang, X.Y. Yuan, L.L. Wu, Y. Han, J. Sheng. Study on morphology of electrospun poly(vinyl alcohol) mats. European Polymer Journal 2005; 41:423-432. DOI:10.1016/j.eurpolymj.2004.10.027

[82] C.J. Buchko, L.C. Chen, Y. Shen, D.C. Martin. Processing and microstructural characterization of porous biocompatible protein polymer thin films. Polymer 1999; 40:7397-7407. DOI:10.1016/S0032-3861(98)00866-0

[83] Z.Z. Zhao, J.Q. Li, X.Y. Yuan, X. Li, Y.Y. Zhang, J. Sheng. Preparation and properties of electrospun poly(vinyllinedene fluoride) membranes. Journal of Applied Polymer Science 2005; 97:466-474. DOI: 10.1002/app.21762

[84] S. Megelski, J.S. Stephens, D.B. Chase, J.F. Rabolt. Micro- and nanostructured surface morphology on electrospun polymer fibres. Macromolecules 2002; 35:8456-8466. DOI: 10.1021/ma020444a

[85] T.J. Sill, H.A. Von Recum. Electrospinning: Applications in drug delivery and tissue engineering (Review). Biomaterials 2008; 29:1989-2006. DOI:10.1016/j.biomaterials.2008.01.011

[86] A.K. Haghi, M. Akbari. Trends in electrospinning of natural nanofibres. Physica Status Solidi 2007; 204:1830:1834. DOI: 10.1002/pssa.200675301

[87] P. Gupta, C. Elkins, T.E. Long, G.L. Wilkes. Electrospinning of linear homopolymers of poly(methylmethacrylate): Exploring relationships between fibre formation, viscosity, molecular weight and concentration in a good solvent. Polymer 2005; 46:4799-47810. DOI:10.1016/j.polymer.2005.04.021

[88] J.M. Deitzel, W. Kosik, S.H. McKnight, N.C.B. Ten, J.M. Desimone, S. Crette. Electrospinning of polymer nanofibres with specific surface chemistry. Polymer 2002; 43:1025-1029. DOI:10.1016/S0032-3861(01)00594-8

[89] K.H. Kim, L. Jeong, H.N. Park, S.Y. Shin, W.H. Park, S.C. Lee et al. Biological efficacy of silk fibroin nanofibre membranes for guided bone regeneration. Journal of Biotechnology 2005; 120:327-339. DOI:10.1016/j.jbiotec.2005.06.033

[90] W.K. Son, J.H. Youk, T.S. Lee, W.H. Park. The effects of solution properties and polyelectrolyte on electrospinning of ultimate poly(ethylene oxide) fibres. Polymer 2004; 45:2959-2966.
DOI:10.1016/j.polymer.2004.03.006

[91] B. Ding, H.Y. Kim, S.C. Lee, C.L. Shao, D.R. Lee, S.J. Park et al. Preparation and characterization of a nanoscale poly(vinyl alcohol) fibre aggregate produced by an electrospinning method. Journal of Polymer Science. Part B: Polymer Physics 2002; 40:1261-1268.
DOI: 10.1002/polb.10191

[92] A. Koski, K. Yim, S. Shivkumar. Effect of molecular weight on fibrous PVA produced by electrospinning. Materials Letters 2004; 58:493-497.
DOI:10.1016/S0167-577X(03)00532-9

[93] J.S. Lee, K.H. Choi, H.D. Ghim, S.S. Kim, D.H. Chun, H.Y. Kim *et al.* Role of molecular weight of atactic poly(vinyl alcohol) (PVA) in the structure and properties of PVA nanofabric prepared by electrospinning. Journal of Applied Polymer Science 2004; 93:1638-1646.
DOI 10.1002/app.20602

[94] T. Jarusuwannapoom, W. Hongroijanawiwat, S. Jitjaicham, L. Wannatoong, M. Nithitanakul, C. Pattamaprom *et al.* Effect of solvents on electro-spinnablity of polystyrene solutions and morphological appearance of resulting electrospun polystyrene fibres. European Polymer Journal 2005; 41:409-421.
DOI:10.1016/j.eurpolymj.2004.10.010

[95] Z. Jun, H. Hou, A. Schaper, J.H. Wendorff, A. Greiner. Poly-L-lactide nanofibres by electrospinning: Influence of solution viscosity and electrical conductivity on fibre diameter and fibre morphology. e-Polymer 2003; 9:1-9.

[96] C.S. Ki, D.H. Baek, K.D. Gang, K.H. Lee, I.C. Um, Y.H. Park. Characterization of gelatine nanofibre prepared from gelatine-formic acid solution. Polymer 2005; 46:5094-5102.
DOI:10.1016/j.polymer.2005.04.040

[97] H.L. Jiang, D.F. Fang, B.S. Hsiao, B. Chu, W.L. Chen. Optimization and characterization of dextran membranes prepared by electrospinning. Biomacromolecules 2004; 5:326-333.
DOI: 10.1021/bm034345w

[98] H. Fong, D.H. Reneker. Elastomeric nanofibres of styrene-butadiene-styrene tri-block copolymers. Journal of Polymer Science Part B: Polymer Physics 1999; 37:3488-3493. DOI: 10.1002/(SICI)1099-0488(19991215) 37:24<3488::AID-POLB9>3.0.CO;2-M

[99] Q.P. Pham, U. Sharma, A.G. Mikos. Electrospun poly(ε-caprolactone) microfibre and multilayer nanofibre/microfibre scaffolds: Characterization of scaffolds and measurement of cellular infiltration. Biomacromolecules 2006; 7:2796-2805. DOI**:** 10.1021/bm060680j

[100] M. Bognitzki, W. Czado, T. Frese, A. Schaper, M. Hellwig, M. Steinhart, A. Greiner, H. Wendorff. Nanostructured fibres via electrospinning. Advanced Materials 2001; 13:70-72. DOI: 10.1002/1521-4095(200101) 13:1<70::AID-ADMA70>3.0.CO;2-H

[101] K.H. Lee, H.Y. Kim, Y.M. La, D.R. Lee, N.H. Suang. Influence of a mixing solvent with tetrahydrofuran and N,N-dimethylformamide on electrospun poly(vinyl chloride) nonwoven mats. Journal of Polymer Science: Part B: Polymer Physics 2002; 40:2259-2268. DOI: 10.1002/polb.10293

[102] I. Hayati, A.I. Bailey, T.F. Tadros. Investigations into the mechanisms of electrohydrodynamic spraying of liquids: I. Effect of electric filed and the environment on pendant drops and factors affecting the formation of stable jets and atomization. Journal of Colloid and Interface Science 1987; 117:205-221. DOI:10.1016/0021-9797(87)90185-8

[103] X. Zong, K. Kim, D. Fang, S. Ran, B.S. Hsiao, B. Chu. Structure and process relationship of electropsun bioabsorbable nanofibre membrane. Polymer 2001; 43:4403-4412. DOI:10.1016/S0032-3861(02)00275-6

[104] B. Kim, H. Park, S.H. Lee, W.M. Sigmund. Poly(acrylic acid) nanofibres by electrospinning. Materials Letters 2005; 59:829-832. DOI:10.1016/j.matlet.2004.11.032

[105] C. Mit-uppathan, M. Nithitanakul, P. Supaphol. Ultrafine electropsun polyamide-6 fibres: Effect of solution conditions on morphology and average diameter. Macromolecular Chemistry and Physics 2004; 205:2327-2338. DOI: 10.1002/macp.200400225

[106] C.L. Casper, J.S. Stephens, N.G. Tassi, D.B. Chase, J.F. Rabolt. Controlling surface morphology of electrospun polystyrene fibres: Effect of humidity and molecular weight in the electrospinning process. Macromolecules 2004; 37:573-578.
DOI**:** 10.1021/ma0351975

[107] M. Li, M.J. Mondrinos, M.R. Gandhi, F.K. Ko, A.S. Weiss, P.I. Lelkes. Electrsopun protein fibres as matrices for tissue engineering. Biomaterials 2005; 26:5999-6008.
DOI:10.1016/j.biomaterials.2005.03.030

[108] W.J. Li, C.T. Laurencin, E.J. Caterson, R.S. Tuan, F.K. Ko. Electrospun nanofibrous structure: A novel scaffold for tissue engineering. Journal of Biomedical Materials Research 2002; 60:613-621.

[109] T.V. How. US Patent no. 4552707 (1985).

[110] L. Larrondo, R.S.J. Manley. Electrostatic fibre spinning from polymer melts. 1. Experimental observations on fibre formation and properties. Journal of Polymer Science: Polymer Physics Edition 1981; 19:909-920.
DOI: 10.1002/pol.1981.180190601

[111] L. Larrondo, R.S.J. Manley. Electrostatic fibre spinning from polymer melts. 2. Examination of the flow field in an electrically driven jet. Journal of Polymer Science: Polymer Physics Edition 1981; 19:921-932.
DOI: 10.1002/pol.1981.180190602

[112] H.C. Schreuder-Gibson, P. Gibson, K. Senecal, M. Sennett, J. Walker, W. Yomans *et al.* Protective textile materials based on electrospun nanofibres. Journal of Advanced Materials 2002; 34:44-45.

[113] E. Zussmann, A.L. Yarin, D. Weihs. A micro-aerodynamic decelerator based on permeable surfaces of nanofibre mats. Experiments in Fluids 2002; 33:315-320.
DOI: 10.1007/s00348-002-0435-6

[114] C.R. Stillwell. Characterization of pore structure in filter cartridges. Advances in Filtration and Separation Technology 1996; 10:151-160.

[115] Y.H. Lee, J.H. Lee, I.G. An, C. Kim, D.S. Lee, Y.K. Lee *et al.* Electrospun dual-porosity structure and biodegradable morphology of montmorillonite reinforced PLLA nanocomposite scaffolds. Biomaterials 2005; 26:3165-3172.
DOI:10.1016/j.biomaterials.2004.08.018

[116] Z.H. Chen, M.D. Foster, W.S. Zhou, H. Fong, D.H. Reneker, R. Resendes *et al.* Structure of poly(ferrocenyldimethylsilane) in electrospun nanofibres. Macromolecules 2001; 34:6156-6158.

[117] G.J. Liu, J.F. Ding, L.J. Qiao, A. Guo, B.P. Dymov, J.T. Gleesen *et al.* Polystyrene-block-poly(2-cinnamoytethyl methacrylate) nanofibres – preparation, characterization and liquid crystalline properties. Chemistry – A European Journal 1999; 5:2740-2749.

[118] J. Kim, D.S. Lee. Thermal properties of electrospun polyesters. Polymer Journal 2000; 32:616-618.

[119] S.H. Lee, B.C. Ku, X. Wang, L.A. Samuelson, J. Kumar. Design, synthesis and electrospinning of a novel fluorescent polymer for optical sensor applications. Materials Research Society Symposium Proceedings 2002; 708:403-408.

[120] E.P.S. Tan, S.Y. Ng, C.T. Lim. Tensile testing of a single ultrafine polymeric fibre. Biomaterials 2005; 26:1453-1456.
DOI:10.1016/j.biomaterials.2004.05.021

[121] R. Inai, M. Kotaki, S. Ramakrishna. Structure and properties of electropsun PLLA single nanofibres. Nanotechnology 2005; 16:208-213.
DOI: 10.1088/0957-4484/16/2/005

[122] M.A. Haque, M.T.A. Saif. A review of MEMS-based microscale and nanoscale tensile and bending testing. Experimetal Mechanics 2003; 43:248-255
DOI: 10.1007/BF02410523

[123] S.Y. Chew, T.C. Hufnagel, C.T. Lim, K.W. Leong. Mechanical properties of single electrospun drug-encapsulated nanofibres. Nanotechnology 2006; 17:3880-3891.
DOI: 10.1088/0957-4484/17/15/045

[124] N.J. DiNardo. Nanoscale characterization of surfaces and Interfaces. P. Gregory, D. Hollis, U. Anton. VCH Verlagsgesellschaft: Weinheim (Federal Republic of Germany) and VSH Publishers: New York (1994).

[125] K. Ramanathan, M.A. Bangar, M. Yun, W. Chen, N.V. Myung, A. Mulchandani. Bioaffinity sensing using biologically functionalised conducting-polymer nanowire. Journal of American Chemical Society 2005; 127:496-497.
DOI**:** 10.1021/ja044486l

[126] L. Yang, C.F.C. Fitie, K.O.V. Werf, M.L. Bennink, P.J. Dijkstra, J. Feijen. Mechanical properties of single electrospun collagen type I fibres. Biomaterials 2008; 29:955-9662.
DOI:10.1016/j.biomaterials.2007.10.058

[127] S. Cuenot, S. Demoustier-champagne, B. Nysten. Elastic modulus of polypyrrole nanotubes. Physical Review Letters 2000; 85:1690-1693.
DOI:10.1103/PhysRevLett.85.1690

[128] S. Cuenot, C. Fretigny, S. Demooustier-champagne, B. Nysten. Measurement of elastic modulus of nanotubes by resonant constant atomic force microscopy. Journal of Applied Physics 2003; 93:5650-5655.
DOI:10.1063/1.1565675

[129] P.A. Yuga, Y. Wen, J.A. Turner, Y.A. Dzenis, Z. Li. Determination of Young's modulus of individual electrospun nanofibres by microcantilever vibration method. Applied Physics Letters 2007; 90:111909-111911.
DOI:10.1063/1.2713128

[130] M.K. Shin, S.I. Kim, S.K. Kim, H. Lee, G.M. Spinks. Size-dependent elastic modulus of single electroactive polymer nanofibres. Applied Physics Letters 2006; 89:231929-231933.
DOI:10.1063/1.2402941

[131] L. Sun, R.P.S. Han, J. Wang, C.T. Lim. Modeling the size-dependent elastic properties of polymeric nanofibres. Nanotechnology 2008; 19:1-8.
DOI: 10.1088/0957-4484/19/45/455706

[132] M. Nagaghi, I. Chasiotis, H. Kahn, Y. Wen, Y. Dzenis. Novel method for mechanical characterization of polymeric nanofibres. Review of Scientific Instruments 2007; 78:1-7.
DOI:10.1063/1.2771092

[133] S. Chand. Review: Carbon fibres for composites. Journal of Materials Science 2000; 35:1303-1313.
DOI: 10.1023/A:1004780301489

[134] S.J.V. Frankland, D.W. Brenner. Molecular dynamics simulations of polymer-nanotube composites. Materials Research Society Symposium Proceedings 2000; 593:199-204.

[135] J.S. Kim, D.H. Reneker. Mechanical properties of composites using ultrafine electrospun fibres. Polymer Composites 1999; 20:124-131.
DOI: 10.1002/pc.10340

[136] A. Suthat, G. Chase. Nanofibres in filter media. Chemical Engineer 2001, 726:26-28.

[137] P.P. Tsai, H. Screuder-Gibson, P. Gibson. Different electrostatic methods for making electric filters. Journal of Electrostatics 2002; 54:333-341.

DOI:10.1016/S0304-3886(01)00160-7

[138] S.W. Choi, S.M. Jo, W.S. Lee, Y.R. Kim. An electrospun poly(vinylidene fluoride) nanofibrous membrane and its battery applications. Advanced Materials 2003; 15:2027-2032.
DOI: 10.1002/adma.200304617

[139] D. Figeys, D. Pintos. Lab-on-a-chip: A revolution in biological and medical sciences – a look at some of the basic concepts and novel components used to construct prototype devices. Analytical Chemistry 2000; 72:330A-335A.
DOI**:** 10.1021/ac002800y

[140] Y. Liu, H. Liu, J. Qian, J. Deng, T. Yu. Feature of an amperomatric ferrocynanide-mediating H_2O_2 sensor for organic-phase assay based on regenerated silk fibroin as immobilization matrix for peroxidise. Electrochimica Acta 1996; 41:77-82.
DOI:10.1016/0013-4686(95)00280-R

[141] Y.Q. Zhang. Natural silk fibroin as a support for enzyme immobilization. Biotechnology Advances 1998; 16:961-971.
DOI:10.1016/S0734-9750(98)00012-3

[142] X. Wang, C. Drew, S.H. Lee, K.J. Senecal, J. Kumar, L.A. Samuelson. Electrospun nanofibrous membranes for highly sensitive optical sensors. Nano Letters 2002; 2:1273-1275.
DOI**:** 10.1021/nl020216u

[143] N.L. Lala, R. Ramaseshan, L. Bojun, S. Sundarrajan, R.S. Barhate, Y.J. Liu *et al.* Fabrication of nanofibres with antimicrobial functionality used as filters: Protection against bacterial contaminats. Biotechnology Bioengineering 2007; 97:1357-1365.
DOI: 10.1002/bit.21351

[144] K.J. Senecal, D.P. Ziegler, J. He, R. Mosurkal, H. Schreuder-Gibson, L.A. Samuelson. Photoelectric response from nanofibrous membranes. Materials Research Society Symposium Proceedings 2002; 708:285-289.

[145] P.P. Tsai, H. Schreuder-Gibson, P. Gibson. Different electrostatic methods for making electret filters. Journal of Electrostatics 2002; 54:333-341.
DOI:10.1016/S0304-3886(01)00160-7

[146] P. Gibson, H. Schreuder-Gibson, D. Rivin. Transport properties of porous membranes based on electrospun nanofibres. Colloids and Surfaces A: Physicochemical and Engineering Aspects A 2001; 187:469-481.

DOI:10.1016/S0927-7757(01)00616-1

[147] R. Ramaseshan, S. Sundarrajan, Y. Liu, R.S. Barhate, N.L. Lala, S. Ramakrishna. Functionalized polymer nanofibre membranes for protection from chemical warfare stimulants. Nanotechnology 2006; 17:2947-2953.
DOI:10.1088/0957-4484/17/12/021

[148] R.A. Coffee. PCT/GB97/01968 (1998).

[149] H.J. Jin, S. Fridrikh, G.C. Rutledge, D. Kaplan. Electrospinning Bombyx mori silk with poly(ethylene oxide). Biomacromolecules 2002; 3:1233-1239.
DOI: 10.1021/bm025581u

Chapter 3

Single polymer composites: A review

3.1 Introduction

In the last few decades the interest in the use of polymers as replacements for other materials such as metals, wood and ceramics has increased significantly [1]. This is due to the advantages that polymers offer over conventional materials, including ease of processing, productivity and cost reduction [2]. The polymeric materials have to be reinforced in order to meet the high demands on strength and stiffness for many applications in aerospace, automotive, electrical, microelectronics, infrastructure and construction, medical and chemical industries [1,3]. The use of conventional fillers such as glass or carbon fibres has received much academic and commercial attention in the past. Although excellent mechanical properties have been achieved in this way, life cycle assessment does not yield favourable results for traditionally reinforced composites due to limited recyclability [4] and high energy requirements of their end-of-life processes.

Glass fibres are the main component in many plastic products that still cause environmental problems, both in mechanical recycling and end-of-life disposal through incineration (thermal recycling) [5-8]. Current trends towards environmentally-friendly composite systems focus on the use of natural fibres as alternatives to glass fibres. Although these fibres do have some ecological advantages over glass fibres (since they are renewable and can be incinerated), natural fibre-based composites are generally not mechanically recyclable. In fact, next to mechanical degradation, the relatively poor thermal stability of these lignocellulosic fibres may lead to severe additional thermal degradation during subsequent recycling or reprocessing steps [9-12].

The heterogeneous composites pose a recycling challenge [10,13]. Furthermore, heterogeneous composites often have poor matrix-fibre adhesion due to chemical incompatibility of the components [1,5,14]. One promising approach to composites recycling is a single polymer composite [15] which is an emerging class of materials [16] that has specific economic and ecological advantages [10]. However, the concept of single polymer

composites (SPC) is not new. Single polymer composites were first introduced by Capiati and Porter [1] about three decades ago. The method used the noticeable difference in melting temperature between the high density polyethylene (HDPE – crystallized conventionally) matrix and HDPE reinforcement (containing aligned and extended molecular chains) to fabricate an HDPE homocomposite. These materials are often described as one-polymer composites, homocomposites, all-(the same) polymer composites, self-reinforced or homogeneous composites [17]. Such composites represent the right alternative to traditional fibre reinforced composites, because both reinforcement and matrix are from the same polymer, therefore recyclability is enhanced [18-20]. Besides recyclability, the interest in the concept of single polymer composites is based upon the premise that interfacial bonding should improve if matrix and reinforcement are made from the same polymer [1,5,12,15,21-26].

The growing interest in the recycling of materials is brought about by the desire to preserve the environment as there is limited landfill space due to the large amount of waste that is being dumped [17]. Furthermore, current environmental legislation and waste management regulations aim to encourage manufacturers of materials and end-products to consider the environmental impact of their products at all stages of their life cycle inclusive of recycling and ultimate disposal [9]. Global warming is also of concern due to the incinerator emissions. These negative impacts can be reduced by recycling the products that would otherwise go into landfills [27-30]. In addition, a strong need to reduce the energy requirements of the recycling process also exists. This has stimulated interest in the development of environmentally friendly materials, including single polymer composite materials [15,31].

This chapter gives an overview of the current status in the research and development of single polymer composites (SPCs). Firstly, polymer fibres and their production methods are reviewed. This is followed by a review of the reported work on single polymer composites and their fabrication methods. Finally, the main challenge relating to the development of single polymer composites is highlighted.

3.2 Polymer fibres

High performance polymeric fibres are one of the essential components of single polymer composites. In this section we briefly review some of the polymer fibres that have been used in SPCs and their most commonly used production methods.

The development of high stiffness and strength polymeric fibres are required to impart good mechanical properties on the resulting single polymer composites. These fibres provide some specific features, such as recyclability, ease of production, low cost, low density and good interfacial bonding without any surface treatment [32]. Improvement in the mechanical properties of the fibres can be achieved *via* molecular orientation during spinning and drawing [13]. However, the main difficulty of combining fibres and matrices of similar polymers to create single polymer composites is to retain the properties of the oriented polymer molecules in the final composite, since molecular relaxation of highly oriented fibres readily occurs during heating [13]. Table 3.1 shows the mechanical properties of polymer fibres compared with carbon and glass fibres, that are popular reinforcements for polymers. As can be seen from Table 3.1, the density of the polymer fibres is less than that of the glass and carbon fibres. The good mechanical properties of the fibres induced during drawing are their major advantages in applications where a high strength-to-weight ratio is required.

Table 3.1 Types and mechanical properties of polymer fibres

Fibres	Density (g cm^{-3})	Tensile strength (MPa)	Tensile modulus (GPa)	Elongation at break (%)	Strain to failure (%)	Elastic modulus (GPa)	Specific strength (GPa g^{-1} cm^{-3})	Specific Modulus (GPa g^{-1} cm^{-3})	References
UHMWPE[a]	0.96	2800	172	4	-	100	-	-	[12, 29, 33-35]
Polyethylene (PE)	0.96	1000-1500	40-70	4-18	-	-	1-1.5	42-73	[36]
Polypropylene (PP)	0.9	650	5-20	-	-	-	1.7	6-22	[9, 10, 12]
All-PP tapes	0.732	450	15	-	7	-	-	-	[4, 13, 19, 37, 38]
Vectran M	1.396	-	83.7	-	-	-	-	-	[39]
Vectran HS	1.403	-	88.8	-	-	-	-	-	[39]
Glass	2.54	3000	75	2.5	-	-	1.2	30	[10, 36, 38]
Carbon	1.80	3600	250	1.5	-	-	2.0	139	[36]

[a]Ultra high molecular weight polyethylene

Three methods are commonly used for the production of polymer fibres. These are solution/gel spinning, melt spinning and electrospinning [13,14,40].

The **solution/gel spinning method** is a special process used to obtain high strength fibres. The polymer is not in a true liquid state during extrusion. The process can also be described as dry-wet-spinning, since the filaments first pass through air and are then cooled further in a liquid bath [41-45]. UHMWPE fibres have been produced by this method [25,30].

In **melt spinning** the polymer melt is extruded through small orifices in the spinneret and drawn into thin fibres by a uniaxial drawing process. The spinneret is submerged in the liquid coagulation bath and the emerging filaments are coagulated in a precipitating bath or a series of baths of increasing precipitant concentration [46,47]. Barkoula *et al*. [3] produced polypropylene (PP), polyamides 6 (PA6) and poly(ethtlene terephthalate) (PET) fibres by the melt spinning method. Li *et al*. [15] and Loos *et al*. [5] produced poly(lactic acid) (PLA) and isotactic polypropylene fibres, respectively. Melt spinning is the most commonly used commercial process for production of synthetic polymeric fibres.

In **electrospinning** the polymer is deposited from a solution as fibrous material by charging the polymer solution and ejecting it through a nozzle onto an oppositely charged grounded target. The fibres can be spun into non-woven structures which are porous (in the instance where highly volatile solvents are used), but mainly non-porous with sub-micron diameters and high surface areas. This is where electrospinning offers advantages over other conventional processes [48]. Various polymers [e.g. polyethylene, polypropylene, poly(ethylene terephthalate), poly(methyl methacrylate), poly(ethylene oxide), poly(lactic acid)] have been successfully electrospun into fibres of different diameters [49].

3.3 Fabrication methods for single polymer composites

The main challenge in producing a SPC system is to combine fibre and matrix into one composite, as in most instances both constituents will have basically the same chemical structure and hence melting temperature. The main processing routes for single polymer composites are described below.

The traditional **melt (solution) or powder impregnation route** entails the impregnation of fibre bundles with a highly viscous polymer resin. Such a process would be very similar to the ones used for manufacturing continuous glass fibre reinforced PP composites. Impregnation of fibre bundles with highly viscous resins is however one of the main bottlenecks in the cost-effective manufacturing of thermoplastic composites [13]. Low molecular weight polymer grades are often used to enhance the impregnation process. The process is relatively slow and costly, because the polymer needs to flow within the fibre bundles in order to fully wet the individual filaments. In addition to the above drawbacks, the reinforcing fibres could also lose their mechanical properties because of partial dissolution or melting during impregnation [9]. The method was used for the development of PE and PP homocomposites [35,50-53].

In the **hot compaction process**, which is a one-constituent method, oriented polymer fibres are compacted to an oriented polymer sheet under suitable conditions of temperature and pressure. This occurs via partial melting of the fibres so that the molten outer surface of the fibres becomes the matrix after cooling, but the residual fibres continue to fulfil the role of the reinforcement [54-61]. The result is a fully recyclable, self-reinforced polymer material. The challenge in this process is the small processing window, typically about 5 ºC or below, between the feasible processing temperature and the melting temperature of the fibre. Within this small temperature window, it is difficult to process the SPC under normal processing conditions without significantly annealing the fibres. Excessive heating results in relaxation and hence a loss of molecular orientation, while insufficient heating leads to a poor interfacial bonding between the fibres/tapes. This small temperature processing window reduces the versatility of the processing route. However, the processing window of hot compaction can be enlarged by using fibres produced of the same material, but with different drawing ratios [62]. The main distinction from other processing routes is that the two phases (matrix and reinforcement) of the SPCs are formed from only a single polymer material, assemblies of oriented polymer fibres/tapes [9,13,15,16,19,39]. Hot compaction was used to prepare SPCs consisting of liquid crystalline polymer fibres [39], polypropylene [63-67], polyethylene [65,67-72], poly(ethylene naphthalate) [73], nylon 6,6 [74] and poly(methyl methacrylate) [75].

With the **overheating method**, the polymer fibres could effectively be overheated above their melting temperature when they are constrained, thereby shrinkage can also be prevented. The oriented polymer fibres are embedded, using this method, in a molten polymer matrix of the same

grade. The constraining of the fibre results in the melting temperature shifting to higher values, hence offering a large enough temperature window for the processing of the SPCs [3,76].

In the **film stacking method**, the reinforcing textile structure is sandwiched between the matrix films and the composite material is produced by hot pressing. The method has been applied for aramid/nylon [77], PP [12,18,78-80], PE [33,81], UHMWPE [30,34,82-85], PLA [15] and isotactic polypropylene fibres [5]. The advantages of the film-stacking method include a wide processing window, freedom of the material selection and no expensive pre-production.

Co-extrusion technology uses the co-extrusion of two types of polymer tapes (e.g. random PP copolymer/PP homopolymer) of different melting temperatures, cold drawing of the tapes to increase the mechanical properties and finally consolidation of the tapes. The oriented polymer tapes can be constrained by the moulding pressure during consolidation to increase the melting temperature of the oriented core material, and further extend the processing window. The advantages of this process is an enlarged processing window of about 20-40 ºC, a high volume fraction of reinforcement (greater than 90%) and an excellent bonding between the tapes due to the co-extrusion process. All-PP composites consisting of highly oriented polypropylene tapes have been prepared by this method by various researchers [4,9,10,13,19,20,37,38,86-88].

3.4 Reported work on single polymer composites

Recognizing that the compatibility between reinforcement and matrix is a critical factor that primarily impacts on the mechanical properties of a composite, Capiati and Porter [1] introduced the first example of a single polymer composite of polyethylene (PE). Since then a number of researchers have looked at single polymer composites of polyethylene and various other polymers. In this section we give a summary of some of the literature available on polyethylene composites with ultra high molecular weight polyethylene (UHMWPE) fibres as reinforcement and UHMWPE, high density polyethylene (HDPE) and low density polyethylene (LDPE) as matrices, respectively. We also give an overview of some reported research on single polymer composites of polypropylene (PP), poly(ethylene terephthalate) (PET), poly(lactic acid) (PLA) and poly(methyl methacrylate) (PMMA).

3.4.1 PE/PE composites

Cohen *et al*. [34] demonstrated a first-of-its-kind fabrication of a homocomposite consisting of UHMWPE fibre and UHMWPE matrix with very good fibre-matrix adhesion without the use of any chemical treatment. The formation of the composite is entirely based on physical interactions between the UHMWPE fibres and matrix. The shear strength (20-25 MPa) and tensile strength (longitudinal: 1.3-1.5 GPa, transversal: 21-25 MPa) of the novel composite material improved as compared to the known fibre composites like UHMWPE fibre/epoxy matrix composites and UHMWPE fibre/HDPE matrix composites. Furthermore, the tensile strength of the UHMWPE fibre/UHMWPE matrix composite is reported to be similar to that of kevlar fibre/epoxy matrix composites. The improved mechanical properties are attributed to good adhesion between fibres and matrix.

At around the same time as Cohen *et al*., Deng and Shalaby reported on the physical properties of UHMWPE fibres/UHMWPE matrix composites [30]. These composites were prepared from UHMWPE fibres sandwiched between UHMWPE sheets. It was shown that the tensile properties, creep resistance and impact strength of the self-reinforced UHMWPE composites increased as opposed to the plain UHMWPE. The tensile strength increased as the fibre content increased, a maximum of 70 MPa was reached. The impact strength reached approximately 116 kJ m^{-2}. Mosleh *et al*. [25] also studied homocomposites of an UHMWPE matrix and an UHMWPE reinforcing phase. The primary aim was to develop a homocomposite that demonstrates less wear for applications in joint prostheses. The mechanical properties of this composite, such as elastic modulus, tensile strength and hardness were improved in a direction parallel to the fibre orientation.

Ogawa *et al*. [33] studied the mechanical properties of UHMWPE fibres/HDPE composites. An increase in the tensile strength and elastic modulus of the composite compared to the HDPE film was observed for a fibre weight fraction of 0.74. The composites' tensile strength and elastic modulus increased up to 600 MPa and 20 GPa, respectively, almost independent of the molding time. Lacroix et al [50] reported on the morphology and crystallisation behaviour of UHMWPE fibres/HDPE composites. Low voltage scanning electron microscopy revealed a transcrystalline layer at the UHMWPE fibre/HDPE interface (Figure 3.1). The presence of a transcrystalline layer gives rise to good interfacial bonding between the matrix and reinforcement, which translates into an improvement in mechanical properties.

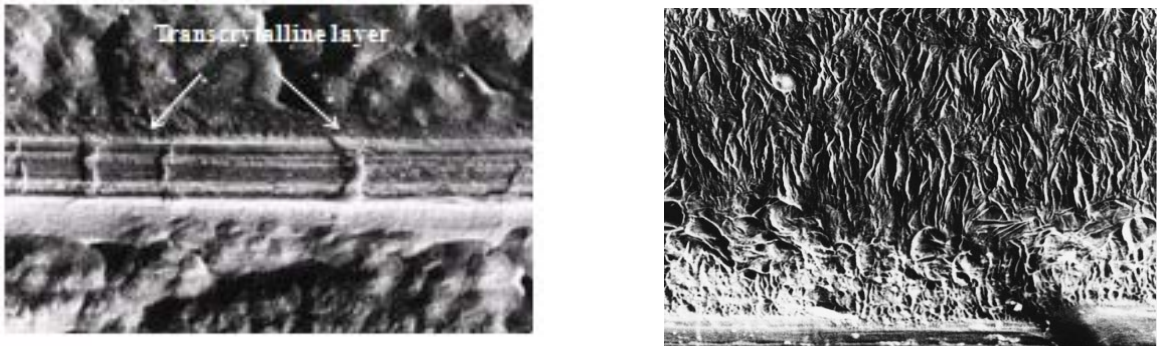

(a) **(b)**

Figure 3.1 Low voltage SEM images of (a) UHMWPE fibre/HDPE composite showing the presence of a transcrystalline layer, and (b) a close-up of the transcrystalline layer illustrating the presence of lamellae twisting. Used with permission [50].

A denser and more compact transcrystalline layer was observed by Vaisman et al [89] when brominated UHMWPE fibres was used as a reinforcement as compared to untreated UHMWPE fibres in a HDPE matrix. The more pronounced transcrystalline layer is ascribed to an increase in the nucleation density of the HDPE matrix on the fibre surface. Lacroix *et al*. [50] further reported on an alternative way of processing an UHMWPE fibre/HDPE composite by wet powder impregnation as an intermediate step. A HDPE powder in propanol suspension was used for this purpose. This method was suggested as another option to solution and dry powder impregnation. The Young's moduli and tensile strengths of the composites were reported to be high in the fibre direction, whereas the compressive strengths were low. The mechanical properties were generally poor perpendicular to the fibre direction. Pegoretti *et al*. [90] used the filament-winding process to manufacture UHMWPE fibre/HDPE composites with untreated HDPE and temperature treated HDPE as matrices. The influence of the winding angle of the fibres on the dynamic properties (storage and loss moduli) of the composites was investigated. A decrease in the storage modulus with increasing winding angle was observed for both the untreated and treated HDPE, with the untreated HDPE showing a steeper decrease in the storage modulus. A similar trend was observed for the loss modulus, but with no significant difference between the untreated and treated HDPE.

Hinrichsen *et al*. [35] prepared UHMWPE fibre/LDPE composites by aqueous powder and dry powder impregnation. The mechanical properties of UHMWPE fibre/LDPE composites were studied. Good mechanical properties with increasing fibre content were reported (tensile strength:

460-1100 MPa, elastic modulus: 11-22 GPa and elongation at break: 4.9-8.3 %). Lacroix et al. introduced the novel solution impregnation method as an intermediate process in the preparation of single polymer composites of UHMWPE fibres/LDPE matrix [51]. The process entailed the immersion of the UHMWPE fibres in a LDPE/xylene solution. The influence of immersion time on the impregnation of the fibres and the effect of the processing temperature on the mechanical properties of the composites were investigated. A high Young's modulus and tensile strength were reported, but an increase in processing temperature resulted in a decrease in these properties. This was ascribed to fibre shrinkage and damage at the higher processing temperatures. Ogawa *et al*. [33] reported on the morphology, thermal behaviour and mechanical properties of UHMWPE fibre/LDPE matrix single polymer composites. Minor voids were observed in the composites and significant fibre agglomeration was absent. Furthermore, a maximum tensile strength and elastic modulus of 660 MPa and 14 GPa, respectively, were observed for the LDPE composites. These results compare well with that obtained by Hinrichsen *et al*. The increased fibre-matrix adhesion was reported to be responsible for the improvement in the mechanical properties, especially the tensile strength. More recently, the use of chemically modified UHMWPE fibres as reinforcement in a LDPE matrix have been reported by Maity *et al*. [91,92]. The surface of the UHMWPE fibres was modified by direct fluorination. SEM images of the unmodified and modified fibres illustrate the difference in the surface roughness of the fibres (Figure 3.2). Composites were prepared with the modified and unmodified fibres. The modified fibre composites showed an improvement in mechanical properties and thermal stability compared to that of the unmodified fibre composites. Better adhesion between the modified UHMWPE fibre and the LDPE matrix is cited as one of the main reasons for the improved properties. In addition, surface energy analysis showed an increase in the surface energy for the fluorinated samples.

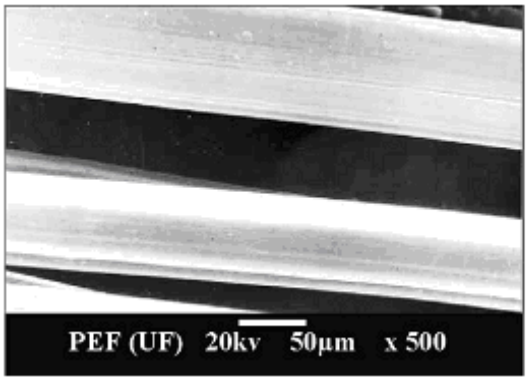

(a)

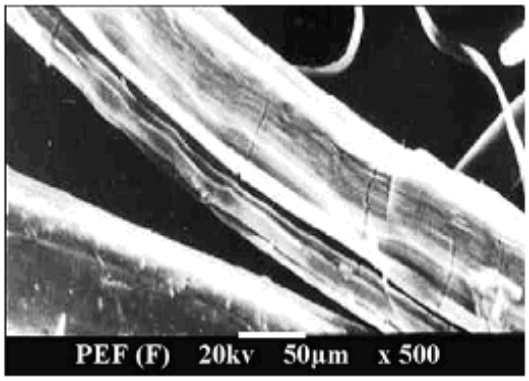

(b)

Figure 3.2 SEM micrographs of (a) unmodified and (b) modified UHMWPE fibres. Used with permission [92].

3.4.2 All-PP composites

Initial studies on the hot compaction of polypropylene fibres to form an all-PP composite was undertaken by Abo El Maaty *et al* [93]. Selective melting of the fibres was not achieved and hence good bonding between the fibres was absent, which resulted in a weak composite. Hine and Ward [94] extended the initial PP hot compaction work to woven polypropylene tapes. The effect of the compaction temperature on the properties of the PP single polymer composites was investigated. The PP sheet obtained at an optimum compaction temperature of 182 °C was reported to be homogeneous and well bonded. A significant amount of annealing was observed at the optimum compaction temperature (as much as a 20% increase in crystallinity). The good mechanical properties obtained were attributed to the formation of a transcrystalline layer between the PP tapes and tape bundles. Furthermore, Hine et al. [54] also investigated the parameters that influences the hot compaction behaviour of woven oriented PP fibres and tapes. It was reported that the molecular weight and the crystallinity of the base polymer and the geometry and weave style of the reinforcement significantly affects the mechanical properties of the final composite. Loos *et al*. [5] studied the morphology of a single polymer composite consisting of highly drawn and constrained isotactic PP (iPP) fibres embedded in an iPP matrix. Once again, the formation of transcrystalline layers showed an improvement in the interfacial adhesion between the matrix and reinforcing material.

A few studies on single polymer composites of PP, where the matrix consisted of a propylene-ethylene copolymer, have been reported. Houshyar *et al*. [12,53,95-98] successfully prepared a single polymer composite consisting of a propylene-ethylene (PPE) random copolymer matrix reinforced with PP fibres. The effect of PP fibres with different fibre diameters on the structure, as well as thermal and mechanical behaviour of thermoplastic composites based on PP was studied. Figure 3.3 illustrates the effect of the different fibre diameters on the various moduli. Incorporation of the fibres resulted in an increase in the static and storage moduli. However, only for the static modulus was a significant difference observed for the different fibre diameters. In addition, Houshyar *et al*. [32] studied the effect of fibre concentration on the mechanical and thermal

properties of fibre reinforced polypropylene composites, consisting of PP fibres in a PPE random copolymer matrix. The increase of the fibre concentration resulted in an increase in the tensile, flexural and storage moduli. Kitayama *et al*. [99] studied the interfacial properties of PPE/PP composites consisting of isotactic PP fibres and a PPE random copolymer matrix. The formation of a transcrystalline layer was found to increase the interfacial strength.

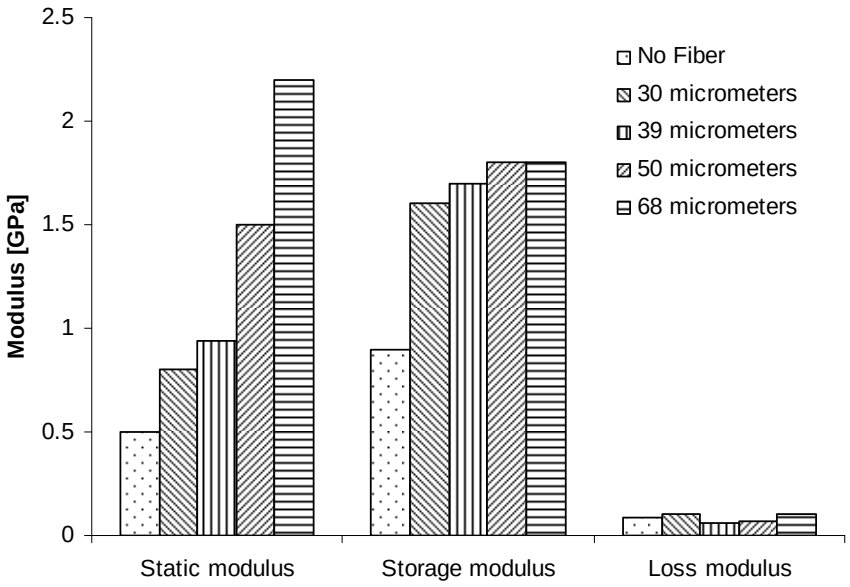

Figure 3.3 Effect of different fibre diameters on the moduli of the PPE matrix/PP fibres composites

All-polypropylene tapes, i.e. two types of polypropylene tapes (PP homopolymer – core; random PP copolymer – skin), coextruded into tapes of different melting temperatures has been described by Cabrera *et al*. [9]. It was found that the all-PP composites can compete with or even out-perform glass mat reinforced thermoplastics (GMT) or natural fibre mat reinforced thermoplastics (NMT) for structural and impact applications, owing to their good mechanical properties combined with a low density. Alcock *et al.* [13,19,20,37,38] prepared all-PP composites from highly oriented PP tapes, and the response of these composites to mechanical loading at a range of temperatures and strain rates, the impact performance, as well as the interfacial and mechanical properties, were investigated. These composites exhibited excellent resistance to falling weight penetration, and the excellent mechanical properties of the oriented tapes were retained in the resulting composites, despite the high temperatures involved in the compaction process. The specific mechanical properties were comparable to those reported for a commercial unidirectional glass fibre reinforced

PP. The compaction conditions were found to influence the interfacial properties of the composite materials.

Barany *et al*. prepared and characterized self-reinforced PP composites. A film-stacking method was used. They studied the correlation between the consolidation temperature and holding time and the mechanical and morphological properties. In their studies, random PP copolymer [85, 100] and beta polymorph of PP [18,79,101] were used as matrix material and carded mat [18,79,85,100] and woven fabric [101] of the alpha polymorph of PP as reinforcement. The increase in the processing temperature gave rise to an increase in the tensile properties, but a decrease in the perforation impact energy. An increase in the holding time did not cause any large change in tensile properties, whereas the perforation energy slightly improved.

3.4.3 PET homocomposites

One of the first successfully prepared homocomposites of poly(ethylene terephthalate) (PET) was reported by Rasburn et al. [102] using the hot compaction technique. The mechanical properties and the structure of the compacted samples were studied. They found that a high percentage of the original properties of the fibres were retained under suitable conditions. The concept of constraining of fibres for the manufacturing of single polymer composites was investigated by Barkoula *et al*. [3]. Poly(ethylene terephthalate) was one of the polar polymers that was studied. It was shown that a difference of about 10.0 °C in the crystalline melting point could be obtained between the constrained and unconstrained PET fibres (Figure 3.4). This small difference in the crystalline melting points is ascribed to the limited drawability of the PET. Post-drawing processes were recommended for further small increases in the crystalline melting point.

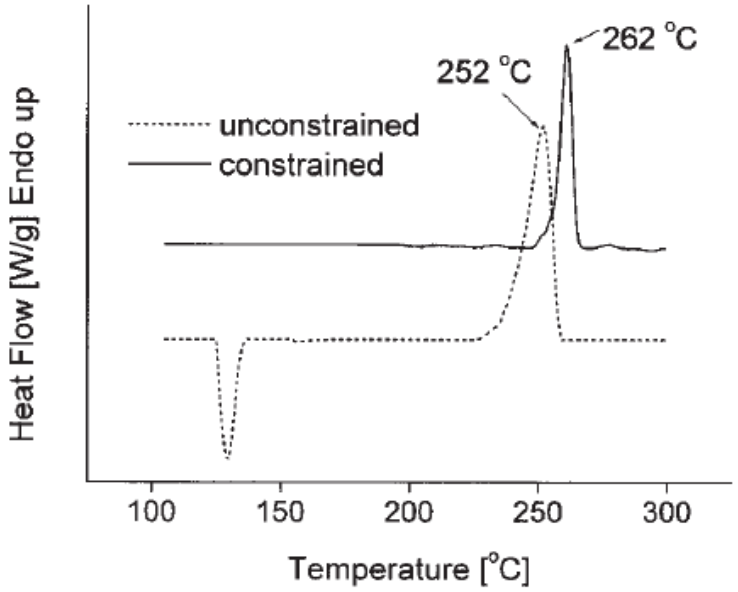

Figure 3.4 DSC curves showing the effect of constraining on the crystalline melting point of a PET fibre [3].

Rojanapitayakorn *et al*. [103] studied the effect of various hot compaction temperatures on the crystallinity and molecular orientation of PET single polymer composites. The PET single polymer composites were prepared using a simplified one-step hot compaction process. Furthermore, the influence of the processing conditions on the mechanical properties of the composites, such as flexural strength, flexural modulus and impact strength, were assessed. The most significant improvement was observed in the impact strength of the composites compared to the isotropic PET samples, as much as 5-7 times higher. Nagarajan *et al*. [104] prepared PET homocomposites consisting of PET woven fabric, meshes and an amorphous film. A reliance of the interfacial adhesion on temperature and pressure in the PET homocomposite was observed. A significant increase in the strength of the fabric reinforced PET homocomposite compared to the non-reinforced PET was reported. Yao *et al*. [105] successfully prepared a PET single polymer composite consisting of an amorphous PET film and highly crystalline PET fabrics. A substantial improvement in the mechanical properties compared to non-reinforced PET was reported. The consolidation conditions (heating temperature, heating rate and the holding time) influenced the mechanical properties of the PET single polymer composites.

3.4.4 PMMA single polymer composites

Some work on poly(methyl methacrylate) (PMMA) single polymer composites has been reported by Wright-Charlesworth *et al*. [75,106-108]. For example, a self-reinforced poly(methyl methacrylate) composite consisting of high strength PMMA fibres and PMMA matrix was described by Wright-Charlesworth *et al*. [106]. It was observed that the ultimate stress (MPa), elastic modulus (GPa) and percentage elongation (%) were 68.50, 2.51 and 8.55, respectively. Furthermore, Wright-Charlesworth *et al*. [107] undertook a systematic study of a hot compacted PMMA single polymer composite. The influence of processing temperature and time on the fracture toughness and morphology and the thermal properties of the composite were investigated. It was found that the consolidation of the composite, the fracture mechanism and the orientation of the fibres are influenced by the processing parameters. In addition, the exothermic and endothermic events of the PMMA single polymer composite as measured by DSC was shown to be affected by the processing temperature and time.

3.4.5 PLA single polymer composites

PLA single polymer composites consisting of amorphous sheets as matrix and highly crystalline fibres, yarns and fabrics were prepared by Li and Yao. [15]. A significant improvement in tensile strength to 58.6 MPa and a Young's modulus of 3.7 GPa have been reported.

3.4.6 Single polymer composites based on liquid-crystalline fibres

Pegoretti *et al*. [39] prepared single polymer composites based on liquid-crystalline fibres (Vectran M and Vectran HS). The fibres have the same chemical composition, but different physical properties. It was shown that the consolidation temperature is the key variable in the production of single-polymer liquid-crystalline composites. A decrease in tensile strength from 920 to 480 MPa was observed as the consolidation temperature increased.

The reported work on single polymer composites is summarized in Table 3.2.

Table 3.2 A summary of reported work on single polymer composites

Fibre	Matrix	References
HDPE	HDPE	[1]
UHMWPE	HDPE	[33,50-52,89,90]
UHMWPE	UHMWPE	[25,30,34,65,67-72]
UHMWPE	LDPE	[33,35,51,91,92]
PP	PP	[5,12,18,37,38,54,63-67, 79,80,93,94,101]
PP	Propylene-ethylene random copolymer	[4,9,10,12,13,19,20,32,37, 38,53,79,80,85-88,95-100]
PET	PET	[3,102-105]
PMMA	PMMA	[75,106-108]
PLA	PLA	[15]
Poly(ethylene naphthalate)	Poly(ethylene naphthalate)	[73]
Nylon 6,6	Nylon 6,6	[74]
Vectran HS	Vectran M	[39]

3.5 Main challenge in the development of single polymer composites: Proximity in melting temperatures of matrix and reinforcement

In spite of the advantages of SPCs over traditionally reinforced composites in terms of chemical compatibility and recyclability, the small difference in melting temperature between the fibres and the matrix poses a big challenge during fabrication, as both constituents have basically the same chemical structure and hence melting temperatures [104,105]. The major challenge is to find a processing window that is large enough to maintain the integrity of the fibres after consolidation [10]. A clear difference in the melting temperatures of the fibres and the matrix is required for manufacturing single polymer composites [1,3]. For instance, the melting temperature for a HDPE matrix and fibres reported by Mead *et al*. [25] were 132 and 139 ºC, respectively. With this small temperature window, it is difficult to process the resultant homocomposites under normal processing

conditions without annealing the fibres. In the case of UHMWPE, the difference in melting temperature between the fibres and matrix is in the range of 5-9 ºC. It is known that polyethylene fibres, annealed at a temperature close to its melting temperature, have a much reduced modulus compared to the modulus of 1 GPa of bulk HDPE [25,104,105].

The processing window is enlarged by using polymers with the same chemical composition, but with different chemical structures [15,51,81,104,109,110]. Examples are a HDPE matrix reinforced by UHMWPE fibres [51,81] and an LDPE matrix reinforced by HDPE fibres [25]. In both cases a processing window of about 20 °C exists. When LDPE is reinforced by UHMWPE fibres, the processing window can be further enlarged to about 40 °C [109]. Apart from different molecular weights, HDPE, LDPE and UHMWPE also have different chain configurations. The compatibility and miscibility of different grades of polyethylene are affected by the difference in chain configurations (e.g., the length of the branched chains) [111].

Tsuji *et a*l. [112] electrospun poly(lactic acid) stereocomplex nanofibres and found that the stereocomplex resulted in an increase in melting temperature to about 220 °C as compared to 178 °C for the pure polylactides of PLLA and PDLA. A 40 °C higher melting temperature was observed for the PLA blend. The PLA stereocomplex can thus be used to increase the processing window. However, the fibre form of the PLLA/PDLA blend has not yet been reported as reinforcement in a PDLLA matrix for the preparation of a single polymer composite.

Barany and co-workers successfully exploited the polymorphism of polypropylene as a possibility for enlarging the processing window in all-polypropylene composites [18,79,101]. A temperature difference of up to 25 °C between the α-PP and the β-PP has been reported with the α-PP having the higher melting point. These composites were primarily prepared by the film-stacking method. Abraham *et al.* [113] reported on the dynamic mechanical properties of all-PP composites where the β and α polymorphic forms of PP were used in the preparation of the composites. Alpha-PP tapes served as the reinforcement in a β-PP matrix.

3.6 Concluding remarks

Single polymer composites are recyclable materials first prepared and reported in 1975 by Capiati and Porter. These materials are being developed with a view to reducing growing global environmental problems such as limited landfill space, littering, and disposal problems. There is increasing interest in single polymer composites due to the need for environmentally friendly composite materials. The future of single polymer composites looks promising due to continuing improvement in their preparation and properties, their market growth and their recyclability.

3.7 References

[1] N.J. Capiati, R.S. Porter. The concept of one polymer composites modelled with high density polyethylene. Journal of Materials Science 1975; 10:1671-1677.
DOI: 10.1007/BF00554928

[2] D.N. Saheb, J.P Jog. Natural fibre polymer composites. Advances in Polymer Technology 1999; 18:351-363.
DOI: 10.1002/(SICI)1098-2329(199924)18:4<351::AID-ADV6>3.0.CO;2-X

[3] N.M. Barkoula, T. Peijs, T. Schimanski, J. Loos. Processing of single polymer composites using the concept of constrained fibres. Polymer Composites 2005; 26:114-120.
DOI: 10.1002/pc.20082

[4] K. Banik, T.N. Abraham, J. Karger-Kocsis. Flexural creep behaviour of unidirectional and cross-ply all-poly(propylene) (PURE) composites. Macromolecular Materials and Engineering 2007; 292:1280-1288.
DOI: 10.1002/mame.200700180

[5] J. Loos, T. Schimanski, J. Hofman, T. Peijs, P.J. Lemstra. Morphological investigations of polypropylene single-fibre reinforced polypropylene model composites. Polymer 2001; 42:3827-3834.
DOI: 10.1016/S0032-3861(00)00660-1

[6] Z. Xiadong, L. Qunfang, D. Gance. Studies on mechanical properties of discontinuous glass fibre/continuous glass mat/polypropylene composite. Polymers and Polymer Composites 2002; 10:299-306.

[7] V.G. Reyes, W.J. Cantwell. The mechanical properties of fibre-metal laminates based on glass fibre reinforced polypropylene. Composites Science and Technolology 2000; 60:1085-1094. DOI: 10.1016/S0266-3538(00)00002-6

[8] J.L. Thomason. Micromechanical parameters from macromechanical measurements on glass reinforced polypropylene. Composites Science and Technology 2002; 62:1455-1468. DOI: 10.1016/S0266-3538(02)00097-0

[9] N. Cabrera, B. Alcock, J. Loos, T. Peijs. Processing of all-polypropylene composites for ultimate recyclability. Proceedings of the Institution of Mechanical Engineers, Part L: Journal of Materials: Design and Applications 2004; 218:145-155.

[10] T. Peijs. Composites for recyclability. MaterialsToday 2003; 30-35.

[11] A.N. Netravali, S. Chabba. Composites get greener. MaterialsToday 2003; 22-29.

[12] S. Houshyar, R.A. Shanks. Morphology, thermal and mechanical properties of poly(polypropylene) fibre-matrix composites. Macromolecular Materials and Engineering 2003; 288:599-606. DOI: 10.1002/mame.200300023

[13] B. Alcock, N.O. Cabrera, N.M. Barkoula, J. Loos, T. Peijs. The mechanical properties of unidirectional all-polpropylene composites. Composites Part A: Applied Science and Manufacturing 2006; 37:716-726. DOI: 10.1016/j.compositesa.2005.07.002

[14] T. Stern, A. Teishev, G. Marom. Composites of polyethylene reinforced with chopped polyethylene fibres: Effect of transcrystalline interphase. Composites Science and Technology 1997; 57:1009-1015. DOI: 10.1016/S0266-3538(96)00128-5

[15] R. Li, D. Yao. Preparation of Single poly(lactic acid) composites. Journal of Applied Polymer Science 2008; 107:2909-2916. DOI: 10.1002/app.27406

[16] P. Hine, I. Ward. Holding its own. MaterialsWorld 2007; 37-39.

[17] A. Pegoretti. Editorial corner – A personal view. Trends in composites materials: The challenge of single-polymer composites. eXPRESS Polymer Letters 2007; 1:710. DOI: 10.3144/expresspolymlett.2007.97

[18] T. Barany, J. Karger-Kocsis, T. Czigany. Development and characterization of self-reinforced polypropylene composites. Proceedings of the 8th Polymers for Advanced Technologies International Symposium 2005; 1: 1-3.

[19] B. Alcock, N.O. Cabrera, N.M. Barkoula, A.B. Spoelstra, J. Loos, T. Peijs. The mechanical properties of woven tape all-polypropylene composites. Composites Part A: Applied Science and Manufacturing 2007; 38:147-161.
DOI: 10.1016/j.compositesa.2006.01.003

[20] B. Alcock, N.O. Cabrera, N.M. Barkoula, J. Loos, T. Peijs. Interfacial properties of highly oriented coextruded polypropylene tapes for the creation of recyclable all-polypropylene composites. Journal of Applied Polymer Science 2007; 104:118-129.
DOI: 10.1002/app.24588

[21] W.T Mead, R.S. Porter. The preparation and tensile properties of polyethylene composites. Journal of Applied Polymer Science 1978; 22:3249-3265.
DOI: 10.1002/app.1978.070221119

[22] T. Kitayama, K. Ishikura, T. Fukui, H. Hamada. Interfacial properties of PP/PP composites. Science and Engineering of Composite Materials 2000; 9:67-73.

[23] T.N. Abraham, S.D. Wanjale, T. Barany, J. Karger-Kocsis. Tensile mechanical and perforation impact behaviour of all-PP composites containing random PP copolymer as matrix and stretched PP homopolymer as reinforcement: Effect of β nucleation of the matrx. Composites: Part A 2009; 40:662-668.
DOI: 10.1016/j.compositesa.2009.03.001

[24] W. Wenig, T. Schoeller. Transfer of load from matrix to fibre in self-reinforced polymer composites. Colloid and Polymer Science 1991; 269:1212-1223.
DOI: 10.1007/BF00652530

[25] M. Mosleh, N.P. Suh, J. Arinez. Manufacture and properties of a polyethylene homocomposites. Coposites Part A 1998; 29:611-617.
DOI: 10.1016/S1359-835X(97)00122-X

[26] M. Deng, S.W. Shalaby. Properties of self-reinforced ultra-high-molecular-weight polyethylene composites. Biomaterials 1997; 18:645-655.
DOI: 10.1016/S0142-9612(96)00194-9

[27] G.S. Bhat, P. Gulgunje, K. Desai. Development of structure and properties during thermal calendering of polylactic acid (PLA) fibre webs. eXPRESS Polymer Letters 2008; 2:49-56.
DOI: 10.3144/expresspolymlett.2008.7

[28] J.G. Poulakis, P.C. Varelidis, C.D. Papaspyrides. Recycling of polypropylene-based composites. Advances in Polymer Technology 1997; 16:313-322.
DOI: 10.1002/(SICI)1098-2329(199711)16:4<313::AID-ADV5>3.0.CO;2-Y

[29] R.J. Ehrig. Plastics Recycling: Products and Processes. Hanser Publishers: Munich and New York (1992).

[30] K. Goda, Y. Cao. Research and development of fully green composites reinforced with natural fibres. Journal of Solid Mechanics and Materials Engineering 2007; 1:1073-1084.
DOI: 10.1299/JMMP.1.1073

[32] L. Yu, K. Dean, L. Li. Polymer blends and composites from renewable resources. Progress in Polymer Science 2006; 31:576-602.
DOI: 10.1016/j.progpolymsci.2006.03.002

[33] S. Houshyar, R.A. Shanks, A. Hodzic. The effect of fibre concentration on mechanical and thermal properties of fibre-reinforced polypropylene composites. Journal of Applied Polymer Science 2005; 96:2260-2272.
DOI: 10.1002/app.20874

[34] T. Ogawa, H. Mukai, S. Osawa. Mechanical properties of ultrahigh-molecular-weight polyethylene fibre-reinforced PE composites. Journal of Applied Polymer Science 1998; 68:1431-1439.
DOI: 10.1002/(SICI)1097-4628(19980531)68:9<1431::AID-APP7>3.0.CO;2-C

[35] Y. Cohem, D.M. Rein, L. Vaykhansky. A novel composite based on ultra-high-molecular-weight polyethylene. Composites Science and Technology 1997; 57:1149-1154.
DOI: 10.1016/S0266-3538(96)00149-2

[36] G. Hinrichsen, S. Kreuzberger, Q. Pan, M. Rath. Production of UHMWPE fibres/LDPE composites. Mechanics of Composite Materials 1966; 32:497-503.
DOI: 10.1007/BF02280631

[37] I.M. Ward, N.H. Ladizesky. Ultra high modulus polyethylene composites. Pure and Applied Chemistry 1985; 57:1641-1649.
DOI: 10.1351/pac198557111641

[38] B. Alcock, N.O. Cabrera, N.M. Barkoula, C.T. Reynolds, L.E. Govaert, T. Peijs. The effect of temperature and strain rate on the mechanical properties of highly oriented polypropylene tapes and all-polypropylene composites. Composites Science and Technology 2007; 67:2061-2070.
DOI: 10.1016/j.compscitech.2006.11.012

[39] B. Alcock, N.O. Babrera, N.M. Barkoula, T. Peijs. Low velocity impact performance of recyclable all-polypropylene composites. Composites Science and Technology 2006; 66:1724-1737.
DOI: 10.1016/j.compscitech.2005.11.010

[40] A. Pegoretti, C. Zanolli, C. Migliaresi. Preparation and tensile mechanical properties of unidirectional liquid crystalline single polymer composites. Composites Science and Technology 2006; 66:1970-1979.
DOI: 10.1016/j.compscitech.2006.01.012

[41] W.H. Carothes, J.W. Hill. Studies of polymerization and ring formation XV. Artificial fibres from synthetic linear condensation super polymer. Journal of the Americal Chemical Society 1932; 54:1579-1587.

[42] http://www.fibresource.com/f-tutor/techpag.htm (Accessed 02 Nov 2007)

[43] P.J. Lemstra, R. Kirchbaum. Speciality products based on commodity polymers. Polymer 1985; 26:1372-1384.
DOI: 10.1016/0032-3861(85)90315-5

[44] M. Kristiensen, T. Tervoort, P. Smith. Synergistic gelation of solutions of isotactic polypropylene and bis-(3,4-dimethyl benzylidene) sorbitol and its use in gel-processing. Polymer 2004; 44:5885-5891.
DOI: 10.1016/S0032-3861(03)00538-X

[45] P. Smith, P.J. Lemstra. Ultra-high strength polyethylene filaments by solution spinning/drawing. 3. Influence of drawing temperature. Polymer 1980; 21:1341-1343.
DOI: 10.1016/0032-3861(80)90205-0

[46] C.G. Cannon. Orientation processes in the drawing of dry gel films of polyethylene and polypropylene. Polymer 1982; 23:1123-1128.
DOI: 10.1016/0032-3861(82)90365-2

[47] M. Takayanagi, K. Imada, T. Kajiyama. Mechanical properties and fine structure of drawn polymers. Journal of Polymer Science Part C: Polymer Symposia 1966; 15:263-281.
DOI: 10.1002/polc.5070150118

[48] A. Peterlin. Molecular model of drawing polyethylene and polypropylene. Journal of Materials Science 1971; 6:490-508.
DOI: 10.1007/BF00550305

[49] B. Gupta, N. Revagade, J. Hilbron. Poly(lactic acid) fibre: An overview. Progress in Polymer Science 2007; 32:455-482.
DOI: 10.1016/j.progpolymsci.2007.01.005

[50] Z.M. Huang, Y.Z. Zhang, M. Kotaki, S. Ramakrishna. A review on polymer nanofibres by electrospinning and their applications in nanocomposites. Composites Science and Techynology 2003; 63:2223-2253.

DOI: 10.1016/S0266-3538(03)00178-7

[51] F.V. Lacroix, H. Lu, K. Schulte. Wet powder impregnation for polyethylene composites: Preparation and mechanical properties. Composites Part A: Applied Science and Manufacturing 1999; 30:369-373.
DOI:10.1016/S1359-835X(98)00085-2

[52] F.V. Lacroix, M. Werwer, K. Schulte. Solution impregnation of polyethylene fibre/polyethylene matrix composites. Composites Part A: Applied Science and Manufacturing 1998; 29:371-376.
DOI: 10.1016/S1359-835X(97)00101-2

[53] N. Chand, S. Kreuzberg, G. Hinrichsen. Influence of processing conditions on the tensile properties of unidirectional UHMWPE fibre/LDPE composites. Composites 1994; 25:878-880.
DOI: 10.1016/0010-4361(94)90029-9

[54] S. Houshyar, R.A. Shanks. Mechanical and thermal properties of flexible polypropylene composites. Macromolecular Materials and Engineering 2006; 291:59-67.
DOI: 10.1002/mame.200500306

[55] P.J. Hine, I.M. Ward, N.D. Jordan, R. Olley, D.C. Bassett. The hot compaction behaviour of woven oriented polypropylene fibres and tapes. I. Mechanical properties. Polymer 2003; 44:1117-1131.
DOI: 10.1016/S0032-3861(02)00809-1

[56] P.J. Hine, I.M. Ward, R.H. Olley, D.C. Basset. The hot compaction of high modulus melt-spun polyethylene fibres. Journal of Materials Science 1993; 28:316-324.
DOI: 10.1007/BF00357801

[57] I.M. Ward, P.J. Hine. The science and technology of hot compaction. Polymer 2004; 45:1413-1427.
DOI: 10.1016/j.polymer.2003.11.050

[58] M.A. Kabeel, D.C. Bassett, R.H. Olley, P.J. Hine, I.M. Ward. Comapction of high-modulus melt-spun polyethylene fibres at temperatures above and below the optimum. Journal of Materials Science 1994; 29:4694-4699.
DOI: 10.1007/BF00356511

[59] P.J. Hine, I.M. Ward, N.D. Jordan, R.A. Olley, D.C. Bassett. A comparison of the hot-compaction behaviour of oriented, high-modulus, polyethylene fibres and tapes. Journal of Macromolecular Science: Part B 2001; 40:959-989.
DOI: 10.1081/MB-100107570

[60] P.J. Hine, I.M. Ward. Hot compaction of woven poly(ethylene terphthalate). Journal of Applied Polymer Science 2004; 91:2223-2233.
DOI: 10.1002/app.13343

[61] I.M. Ward, P.J. Hine. Novel composites by hot compaction of fibres. Polymer Engineering and Science 1997; 37:1809-1814.
DOI: 10.1002/pen.11830

[62] I.M. Ward. Development in oriented polymers. Plastics, Rubber and Composites – Macromolecular Engineering 2004; 33:189-194.
DOI: 10.1179/174328904X4864

[63] A. Izer, T. Barany. Hot consolidated all-PP composites from textiles fabrics composed of isotactic PP filaments with different degrees of orientation. eXPRESS Polymer Letters 2007; 1:790-796.
DOI: 10.3144/expresspolymlett.2007.109

[64] P.J. Hine, M. Bonner, B. Brew, I.M. Ward. Hot compacted polypropylene sheet. Plastics, Rubber and Composites Processing and Applications 1998; 27:167-171.

[65] J. Teckoe, R.H. Olley, D.C. Bassett, P.J. Hine, I.M. Ward. The morphology of woven polypropylene tapes compacted at temperatures above and below optimum. Journal of Materials Science 1999; 34:2065-2073.
DOI: 10.1023/A:1004555608836

[66] Y. Le Bozec, S. Kaang, P.J. Hine, I.M. Ward. The thermal-expansion behaviour of hot-compacted polypropylene and polyethylene composites. Composites Science and Technology 2000; 60:333-344.
DOI: 10.1016/S0266-3538(99)00129-

[67] D.N. Jordan, C.D. Basset, H.R. Olley, P.J. Hine, I.M. Ward. The hot compaction behaviour of woven oriented polypropylene fibres and tapes. II. Morphology of cloths before and after compaction. Polymer 2003; 44:1133-1143.
DOI: 10.1016/S0032-3861(02)00810-8

[68] P.J. Hine, H.R. Olley, I.M. Ward. The use of interleaved films for optimising the production and properties of hot compacted, self-reinforced polymer composites. Composites Science and Technology 2008; 68:1413-1421.
DOI: 10.1016/j.compscitech.2007.11.003

[69] R.H. Olley, D.C. Bassett, P.J. Hine, I.M. Ward. Morphology of compacted polyethylene fibres. Journal of Materials Science 1993; 28:1107-1112.

DOI: 10.1007/BF00400899

[70] S.S. Moreye, P.J. Hine, A.R. Duckett, J.D. Carr, I.M. Ward. Modelling of the energy absorption by polymer composites upon ballistic impact. Composites Science and Technology 2000; 60:2631-2642.
DOI: 10.1016/S0266-3538(00)00139-1

[71] P.J. Hine, I.M. Ward. The hot compaction of 2-dimensional woven melt spun high modulus polyethylene fibres. Journal of Materials Science 2000; 35:5091-5099.
DOI: 10.1023/A:1004835816735

[72] D.N. Jordan, H.R. Olley, C.D. Basset, J.P. Hine, I.M. Ward. The development of morphology during hot compaction of tensylon high-modulus polyethylene tapes and woven cloths. Polymer 2002; 43:3397-3404.
DOI: 10.1016/S0032-3861(02)00104-0

[73] L. Shavit-Hadar, R.L. Khalfin, Y. Cohen, D.M. Rein. Harnessing the melting peculiarities of ultra-high molecular weight polyethylene fibres for the processing of compacted fibre composites. Macromolecular Materials and Engineering 2005; 290:653-656.
DOI: 10.1002/mame.200500045

[74] P.J. Hine, A. Astruc, I.M. Ward. Hot compaction of polyethylene naphthalate. Journal of Applied Polymer Science 2004; 93:796-802.
DOI: 10.1002/app.20517

[75] P.J. Hine, I.M. Ward. Hot compaction of woven 6,6 multifilaments. Journal of Applied Polymer Science 2006; 101:991-997.
DOI: 10.1002/app.22771

[76] D.D. Wright-Charlesworth, P.E. Lautenschlager, L.J. Gilbert. Hot compaction of poly(methyl methacrylate) composites based on fibre shrinkage results. Journal of Materials Science in Medicine 2005; 16:967-975.
DOI: 10.1007/s10856-005-4431-2

[77] C.W.M. Bastiaansen, P.J. Lemstra. Melting behaviour of gel-spun/drawn polyolefins. Macromolecular Symposia 1989; 28:73-84.

[78] O.A. Khondker, T. Fukui, M. Inoda, A. Nakai, H. Hamada. Fabrication and mechanical properties of aramid/nylon plain knitted composites. Composites Part A: Applied Science and Manufacturing 2004; 35:1195-1205.
DOI: 10.1016/j.compositesa.2004.03.004

[79] S. McKown, W.J. Cantwell. Investigation of strain-rate effects in self-reinforced polypropylene composites. Journal of Composite Materials 2007; 41:2457-2470.
DOI: 10.1177/0021998307084173

[80] T. Barany, J. Karger-Kocsis, T. Czigany. Development and characterization of self-reinforced poly(propylene): Carded mat reinforcement. Polymers for Advanced Technologies 2006; 17:818-824.
DOI: 10.1002/pat.813

[81] T. Barany, A. Izer, T. Czigany. High performance self-reinforced polypropylene composites. Materials Science Forum 2007; 537-538:121-128.
DOI: 10.4028/www.scientific.net/MSF.537-538.121

[82] F.V. Lacroix, J. Loos, K. Schulte. Morphological investigations of polyethylene fibre reinforced polyethylene. Polymer 1999; 40:843-847.
DOI: 10.1016/S0032-3861(98)00309-7

[83] A. Teishev, S.D. Incardona, C. Migliaresi, G. Marom. Polyethylene fibres-polyethylene matrix composites: Preparation and physical properties. Journal of Applied Polymer Science 1993; 50:503-512.
DOI: 10.1002/app.1993.070500314

[84] C. Marais, P. Feillard. Manufacturing and mechanical characterization of unidirectional polyethylene fibre/polyethylene matrix composites. Composites Science and Technology 1992; 45:247-254.
DOI: 10.1016/0266-3538(92)90086-I

[85] T. He, R.S. Porter. Melt crystallization of polyethylene on high modulus polyethylene fibres. Journal of Applied Polymer Science 1988; 35:1945-1953.
DOI: 10.1002/app.1988.070350720

[86] M. Kazanci, D. Cohn, M. Marom, C. Migliaresi, A. Pegoretti. Fatigue characterization of polyethylene fibre reinforced polyolefin biomedical composites. Composites Part A: Applied Science and Manufacturing 2002; 33:453-458.
DOI: 10.1016/S1359-835X(02)00002-7

[87] T.N. Abraham, K. Banik, J. Karger-Kocsis. All-PP composites (PURE) with unidirectional and cross-ply lay-ups: Dynamic mechanical thermal analysis. eXPRESS Polymer Letters 2007; 1:519-526.
DOI: 10.3144/expresspolymlett.2007.74

[88] K. Banik, T.N. Abraham, J. Karger-Kocsis. Flexural creep behaviour of unidirectional and cross-ply all-poly(propylene) (PURE) composites. Macromolecular Materials and Engineering 2007; 292:1280-1288.
DOI: 10.1002/mame.200700180

[89] K. Banik, J. Karger-Kocsis, T.N. Abraham. Flexural creep of all-polypropylene composites: Model analysis. Polymer Engineering and Science 2008; 48:941-948.
DOI: 10.1002/pen.21041

[90] L. Vaisman, M. F. González, G. Marom. Transcrystallinity in brominated UHMWPE fibre reinforced HDPE composites: Morphology and dielectric properties. Polymer 2003; 44:1229-1235.
DOI: 10.1016/S0032-3861(02)00848-0

[91] A. Pegoretti, M. Ashkar, C. Migliaresi, G. Marom. Relaxation processes in polyethylene fibre-reinforced polyethylene composites. Composites Science and Technology 2000; 60:1181-1189.
DOI: 10.1016/S0266-3538(00)00024-5

[92] J. Maity, C. Jacob, C.K. Das, S. Alam, R.P. Singh. Direct fluorination of UHMWPE fibre and preparation of fluorinated and non-fluorinated fibre composites with LDPE matrix. Polymer Testing 2008; 27:581-590.
DOI: 10.1016/j.polymertesting.2008.03.001

[93] J. Maity, C. Jacob, C.K. Das, S. Alam, R.P. Singh. Homocomposites of chopped fluorinated polyethylene fibre with low-density polyethylene matrix. Materials Science and Engineering 2008; A479:125-135.
DOI: 10.1016/j.msea.2007.06.045

[94] E.I. Abo, M.I. Maaty, D.C. Bassett, R.H. Olley, P.J. Hine, I.M. Ward The hot compaction of polypropylene fibres. Journal of Materials Science 1996; 31:1157-1163.
DOI: 10.1007/BF00353094

[95] P.J. Hine, I.M. Ward, J. Teckoe. The hot compaction of woven polypropylene tapes. Journal of Materials Science 1998; 33:2725-2733.
DOI: 10.1023/A:1017540530295

[96] S. Houshyar, R.A. Shanks. Tensile properties and creep response of polypropylene fibre composites with variation of fibre diameter. Polymer International 2004; 53:1752-1759.
DOI: 10.1002/pi.1569

[97] S. Houshyar, R.A. Shanks, A. Hodzic. Influence of different woven geometry in poly(propylene) woven composites. Macromolecular Materials and Engineering 2005; 290:45-52.
DOI: 10.1002/mame.200400158

[98] S. Houshyar, R.A. Shanks, A. Hodzic. Tensile creep behaviour of polypropylene fibre reinforced polypropylene composites. Polymer Testing 2005; 24:257-264.
DOI: 10.1016/j.polymertesting.2004.07.003

[99] S. Houshyar, R.A. Shanks. Mechanical and thermal properties of toughened polypropylene composites. Journal of Applied Polymer Science 2007; 105:390-397.
DOI: 10.1002/app.25034

[100] T. Kitayama, S. Utsumi, H. Hamada, T. Nishino, H. Kikutani, H. Ito. Interfacial properties of PP/PP composites. Journal Applied Polymer Science 2003; 88:2875-2883.
DOI: 10.1002/app.11805

[101] T. Barany, A. Izer, T. Czigany. On consolidation of self-reinforced polypropylene composites. Plastics, Rubber and Composites 2006; 35:375-379.
DOI**:** 10.1179/174328906X128234

[102] T. Barany, A. Izer, J. Karger-Kocsis. Impact testing of all-polypropylene composites composed of alpha and beta modifications. Polymer Testing 2009; 28:176-182.
DOI: 10.1016/j.polymertesting.2008.11.011

[103] J. Rasburn, P.J. Hine, I.M. Ward, R.H. Olley, D.C. Bassett, M.A. Kabeel. The hot compaction of polyethylene terephthalate. Journal of Materials Science 1995; 30:615-622.
DOI: 10.1007/BF00356319

[104] P. Rojanapitayakorn, P.T. Mather, A.J. Goldberg, R.A. Weiss. Optically transparent self-reinforced poly(ethylene terephthalate) composites: Molecular orientation and mechanical properties. Polymer 2005; 46:761-773.
DOI: 10.1016/j.polymer.2004.11.032

[105] P. Nagarajan, D. Yao. Homocomposites of poly(ethylene terephthalate). Antec 2005; 1559-1563.

[106] D. Yao, R. Li, P. Nagarajan. Single polymer composites based on slowly crystallizing polymers. Polymer Engineering and Science 2006; 1223-1230.
DOI: 10.1002/pen.20583

[107] J.L. Gilbert, D.S. Ney, E.P. Lautenschlager. Self-reinforced composite poly(methyl methacrylate): static and fatique properties. Biomaterials 1995; 16:1043-1055.

DOI: 10.1016/0142-9612(95)98900-Y

[108] D.D. Wright-Charlesworth, E.P. Lautenschlager, J.L. Gilbert. Bending and fracture toughness of woven self-reinforced composite poly(methyl methacrylate). Journal of Biomedical Research 1997; 36:441-453.
DOI: 10.1002/(SICI)1097-4636(19970915)36:4<441::AID-JBM2>3.0.CO;2-E

[109] D.D. Wright-Charlesworth, J.L. Gilbert, E.P. Lautenschlager. The effect of processing temperature and time on the structure and fracture characteristics of self-reinforced composite poly(methyl methacrylate). Journal of Materials Science: Materials in Medicine 1999; 10:503-512.
DOI: 10.1023/A:1008909311523

[110] E. Devaux, C. Caze. Composites of ultra-high-molecular-weight polyethylene fibres in a low-density polyethylene matrix: II. Fibre/matrix adhesion. Composites Science and Technology 1999; 59:879-882.
DOI: 10.1016/S0266-3538(98)00126-2

[111] A. Teishev, G. Marom. The effect of transcrystallinity on the transverse mechanical properties of single polymer polyethylene composites. Journal of Polymer Science 1995; 56:959-966.
DOI: 10.1002/app.1995.070560809

[112] T. Hameed, I.A. Hussein. Effect of short chain branching of LDPE on its miscibility with linear HDPE. Macromolecular Materials and Engineering 2004; 289:198-203.
DOI: 10.1002/mame.200300173

[113] H. Tsuji, M. Nakomo, M. Hashimoto, K. Takashima, S. Katsura, A. Mizano. Electrospinning of poly(lactic acid) stereocomplex nanofibres. Biomacromolecules 2006; 7:3316-3320.
DOI**:** 10.1021/bm060786e

[114] T.N. Abraham, S. Siengchin, J. Karger-Kocsis. Dynamic mechanical thermal analysis of all-PP composites based on β and α polymorphic forms. Journal of Materials Science 2008; 43:3697-3703.
DOI: 10.1007/s10853-008-2593-2

Chapter 4

Experimental

4.1 Electrospinning of PMMA nanofibres

4.1.1 Materials

High molecular weight PMMA ($PMMA_{high}$, M_w = 996,000 g mol^{-1}) was purchased from Sigma Aldrich (Schenelldorf, Germany). N,N-dimethylformamide (DMF) and tetrahydrofuran (THF) were obtained from Sigma Aldrich (Schenelldorf, Germany) and Labscan Analytical Sciences (Gliwice, Poland), respectively, and used without any further purification. Polymer solutions for the electrospinning of $PMMA_{high}$ were prepared by dissolving 4, 5 and 6 wt% PMMA in a 1:1 THF:DMF solvent mixture.

4.1.2 Electrospinning process

In the electrospinning process, $PMMA_{high}$ solutions were placed in a 5 mL syringe and gravity-fed through the tip. A copper wire was inserted into the polymer solution to act as a positive electrode. A high voltage supply, manufactured at the University of Stellenbosch, Stellenbosch, South Africa, was used to charge the polymer solution, which resulted in an accelerated fluid jet towards a grounded aluminium collector. The electrospinning voltages used were 10, 15, 20 and 25 kV at spinning distances of 10 and 15 cm. The electrospinning process was performed in horizontal mode in a fume hood at room temperature.

4.2 Preparation of single polymer composites of PMMA

4.2.1 Materials

The electrospun $PMMA_{high}$ nanofibres were used as the reinforcing phase and a low molecular weight PMMA ($PMMA_{low}$, 90 000 g mol^{-1}, Altuglass V825-TL grade) purchased

from Advanced Polymers (Altuglass International, Rho (MI), Italy) was used as the matrix material.

4.2.2 Composite preparation

The $PMMA_{low}$ pellets were dried in an oven at 60 °C for 12 h before use. They were compression moulded to a film (layer thickness of 0.80 mm) on a CSIR (Port Elizabeth, South Africa) in-house compression moulding machine at a temperature of 200 °C and a pressure of 2.5 bar. Two layers of nanofibre mats were sandwiched in-between four layers of PMMA film. The sandwich material was then placed between two plates separated by two teflon sheets and compression moulded for 10 min at a low pressure (0.5 bar) and for 5 min at a higher pressure (2.5 bar). The processing temperatures used were respectively 140, 150 and 160 °C, at a constant pressure and holding time. After compression moulding, the samples were water-cooled under pressure for 7 min.

4.3 Characterization techniques

4.3.1 Scanning electron microscopy

The morphology and diameter of the resulting $PMMA_{high}$ nanofibres was characterised by scanning electron microscopy (SEM). A Gemini LEO 1525 FE-SEM (Carl Zeiss NTS GmbH, Germany) at an accelerating voltage of 5 or 10 kV using an In-lens detector was used. Before the observation, the fibres were coated with a 20 nm layer of evaporated carbon using an Emitech K950X evaporator (Quorum Technologies, Kent, UK). SEM analysis was also used to determine the intactness of the nanofibres on the cross-sectional area of the PMMA single polymer composites and on the surface of the peeled-off sheet structure. The samples were prepared by fracturing under 3-point bending.

4.3.2 Differential scanning calorimetry

Differential scanning calorimetry (DSC) was carried out with a Perkin Elmer DSC 7 (Life and Analytical Science, Shelton, USA) under nitrogen atmosphere. About 5 mg of sample

was hermetically sealed in an aluminium pan for the measurements. The DSC samples were heated from 25 to 330 °C at a heating rate of 10 °C min^{-1}.

4.3.3 Thermogravimetric analysis

Thermogravimetric analysis (TGA) was done using a Perkin Elmer TGA7 (Quorum Technologies, Kent, UK) under nitrogen with a flow rate of 20 mL min^{-1}. The samples (powdered PMMA, electrospun $PMMA_{high}$ nanofibres, the PMMA matrix and the PMMA single polymer composites) were heated from 25 °C to 500 °C at a scanning rate of 10 °C min^{-1} using platinum pans.

4.3.4 Raman analysis

The Raman spectra were acquired with a Jobin-Yvon T64000 Raman spectrometer operated in single spectrograph mode. The 514.5 nm line of an argon ion laser was used as the excitation source. The laser beam was directed onto the sample using the 20x LWD objective of the Olympus microscope attachment. The backscattered light was dispersed via a 600 lines mm^{-1} grating onto a liquid-nitrogen cooled CCD detector. The laser power at the sample was kept low (1.1 mW) to prevent laser damage of the sample.

4.3.5 Dynamic mechanical analysis

The dynamic mechanical properties of the composite samples were determined using a Perkin Elmer DMA 8000 (Life and Analytical Science, Shelton, USA) in a dual cantilever bending mode at a frequency of 1 Hz and a scan rate of 2 °C min^{-1}. The temperature was varied from room temperature to 160 °C. The sample dimensions were 50 mm x 9 mm x 4 mm.

4.3.6 Mechanical analysis

The **flexural properties** were determined on rectangular specimens of 80x10x4 mm using an Instron 3369 machine according to standard ISO 178.1975 at a cross-head speed of 2 mm min^{-1}. All the tests were performed at ambient temperature and humidity (50 % RH). Each test was repeated five times to obtain the average.

The **tensile properties** were determined on machined dumbbell specimens using an Instron 3369 universal tester according to standard D638-03 Type IV at a cross-head speed of 2 mm min^{-1}. The span length and the width were 45 and 13 mm, respectively. All the tests were performed at ambient temperature and humidity (50 % RH). Each test was repeated four times to obtain the average.

The **Charpy impact tests** were done on notched rectangular type 1 specimens using a Resil Impactor Junior (CEAST) according to standard ISO 179.1982. The 7.5 J hammer was used at an impact velocity of 3.8 m s^{-1}. At least five specimens were tested for each sample and the average is reported.

Chapter 5

Electrospinning of high molecular weight poly(methyl methacrylate)

The influence of polymer solution concentration, applied voltage and spinning distance on the morphology and diameters of the electrospun $PMMA_{high}$ nanofibres were investigated in order to obtain nanofibres of different diameters. This is important for studying the effect of the fibre diameter on the properties of the single polymer composites of PMMA. Effects of various parameters on the morphology and diameter of the electrospun fibres are discussed.

5.1 Effect of PMMA concentration

The polymer solution concentration determines the spinability of a solution [1]. The results for the concentration effects described in this study were obtained from non-woven fibre mats electrospun at a voltage of 15 kV onto an electrically grounded electrode positioned 10 cm from the syringe tip. The concentrations examined in this study were 4, 5 and 6 wt% $PMMA_{high}$ in a DMF/THF solvent mixture. The average fibre diameters were determined from measuring the diameters of 40 individual fibres. Figure 5.1 shows that the average diameter of the fibres spun from 4, 5 and 6 wt% $PMMA_{high}$ solution was 287, 624 and 824 nm, respectively.

It can be seen from Figure 5.1 that the fibre diameter increases with an increase in polymer solution concentration. The smaller diameter of the nanofibres from the lower concentrations is the result of the solution being stretched easily during electrospinning. The larger nanofibre diameters at high concentrations are attributed to the viscosity of the solution that was high enough to lower the bending instability of the jet. The solution becomes resistant to stretching by the electrical charges on the electrospinning jet [2].

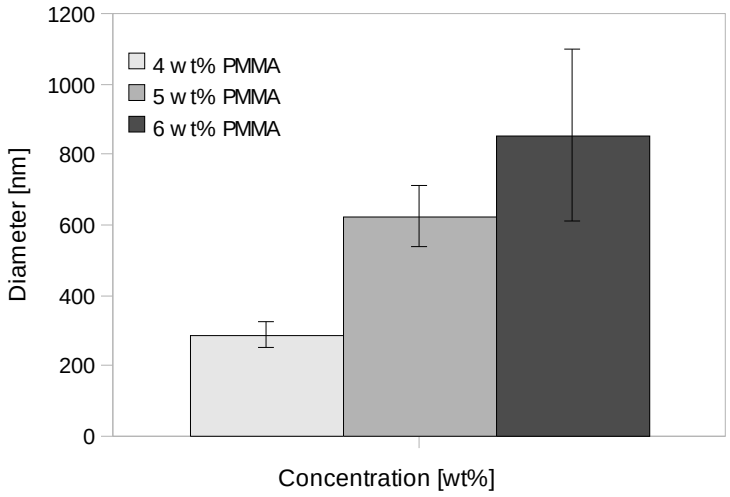

Figure 5.1 The effect of $PMMA_{high}$ solution concentration on the diameter of the electrospun fibres. Electrospinning conditions: spinning voltage = 15 kV and spinning distance = 10 cm.

Figure 5.2 shows the electron micrographs of the non-woven fibre mats electrospun from 4, 5 and 6 wt% $PMMA_{high}$ solutions. The SEM images show the presence of fibres in the 200 to 900 nm range. The electron micrographs of the $PMMA_{high}$ fibres spun from all of the $PMMA_{high}$ solutions show that the fibres have a smooth, regular and cylindrical morphology with no beads and junctions. This indicates that the nanofibres have dried completely before reaching the collector. Furthermore, the very high molecular weight of ~1 000 000 g mol^{-1} of the $PMMA_{high}$ could be the reason for the relatively uniform morphology obtained in all instances. Sufficient entanglement of the polymer chains may have been the reason for the stability of the electrospinning jet.

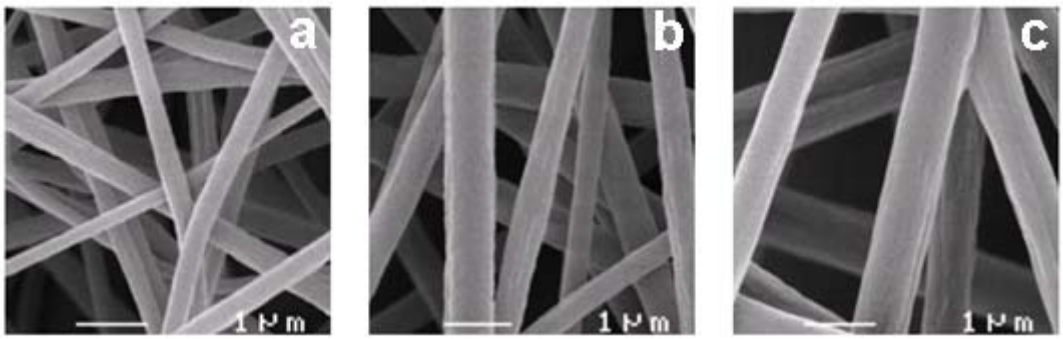

Figure 5.2 SEM images of (a) 200-400 nm, (b) 400-650 nm and (c) 600-900 nm electrospun $PMMA_{high}$ fibres.

5.2 Effect of applied voltage

The nanofibres in electrospinning are produced through the action of the applied voltage imposed on the polymer solution. The applied voltage influences the shape of the Taylor cone at the tip of the spinneret, the velocity of the fibre jet and the structural morphology of the resulting fibres [1,2]. Previous studies have shown that an increase in the applied voltage did not influence the diameter and morphology of the nanofibres for certain polymers [3-5]. This is possibly as a result of the ejection of the multi-jets that produce non-uniform fibre diameters. Other researchers observed irregular morphology (beaded nanofibre structure) and larger diameters upon an increase in the applied voltage [6]. It must be pointed out that the effect of the electrospinning parameters on the morphology and diameters of the fibres is largely polymer, and in some instances polymer molecular weight, specific.

In this study no effects of the applied voltage on the morphology of the $PMMA_{high}$ nanofibres were observed. The fibres were electrospun from a 4, 5 and 6 wt% $PMMA_{high}$ solution using a spinning distance of 10 cm. The applied voltage was varied from 10 to 25 kV. At 10 kV, a droplet of polymer remains suspended at the tip of the capillary tip and the electrospinning jet originates from a stable cone at the bottom of the droplet. At 15 kV, the volume of the droplet at the capillary tip decreased and the density increased. This increase in voltage caused the solution to be removed from the capillary tip quicker than it was supplied. The droplet at the capillary tip disappeared completely with an increase in the applied voltage to 20 and 25 kV. At these higher voltages the jet initiated directly from inside the tip and the electrospinning process became complex as multiple jets were ejected from the tip. The velocity of the jets increased even further. It can be seen from the SEM images in Figure 5.3 that the applied voltage had no significant effect on the morphology of the fibres. In all instances beadless and uniform fibres were obtained. Furthermore, no obvious variation of the diameter along the fibre length was observed with a change in the applied voltage. However, a decrease in fibre diameter was observed at higher voltages in some instances.

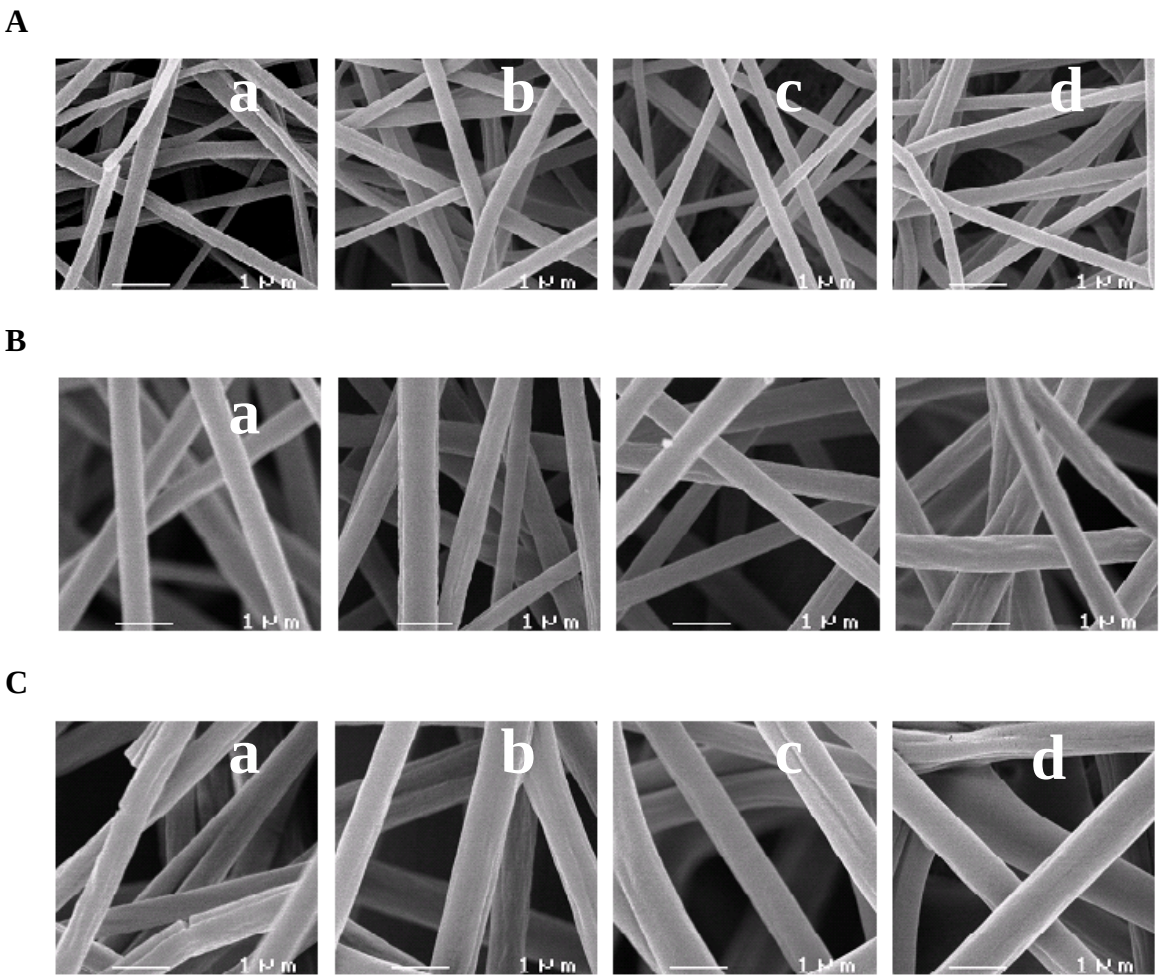

Figure 5.3 SEM images of $PMMA_{high}$ fibres electrospun at a spinning distance of 10 cm from a 4 wt% (A), 5 wt% (B) and 6 wt% (C) $PMMA_{high}$ solution at (a) 10 kV, (b) 15 kV, (c) 20 kV and (d) 25 kV.

Figure 5.4 and Table 5.1 show the correlation between the fibre diameter and the applied voltage of the $PMMA_{high}$ fibres electrospun at spinning distances of 10 and 15 cm. It can be seen from Figure 5.4 that an increase in the applied voltage resulted in a decrease in the fibre diameter for the more concentrated $PMMA_{high}$ solution (6 wt% $PMMA_{high}$) at a shorter spinning distance (10 cm). No significant changes in the diameters of the less concentrated solutions were observed, however, decreased fibre diameters were observed particularly at higher voltages. The decrease in fibre diameter with an increase in the spinning voltage became more noticeable at an increased spinning distance. The effect was observed for the more concentrated polymer solutions (5 and 6 wt% $PMMA_{high}$). It is possible that the combination of the more concentrated solutions and the increased spinning distance allows

the polymer jet to undergo more stretching due to the viscosity of the solution and the increased electrostatic forces induced on the electrospinning jet, resulting in the decreased diameters at higher spinning voltages [7,8]. An increase in applied voltage therefore favours the formation of smaller fibre diameters in the case of the more concentrated polymer solutions.

(A)

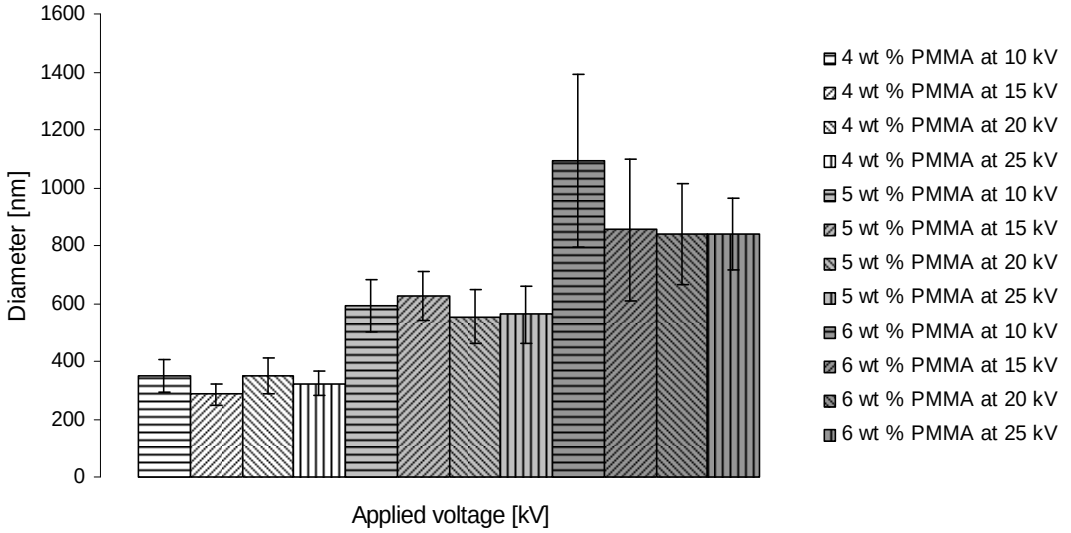

(B)

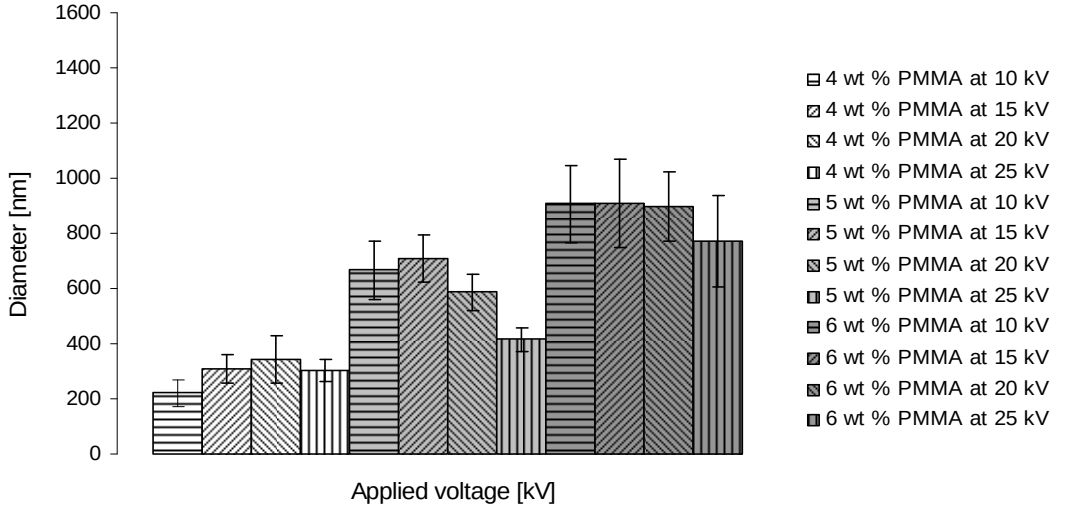

Figure 5.4 Effect of applied voltage on the diameter of $PMMA_{high}$ fibres electrospun at a spinning distance of 10 cm (A) and 15 cm (B) from a 4, 5 and 6 wt% $PMMA_{high}$ solution.

Table 5.1 Effect of different electrospinning parameters on the diameters of PMMA fibres obtained from $PMMA_{high}$ polymer solution.

Applied voltage (kV)	**4 wt %**		**5 wt %**		**6 wt %**	
	Average diameter (nm) of PMMA nanofibres at two different spinning distances					
	10 cm	**15 cm**	**10 cm**	**15 cm**	**10 cm**	**15 cm**
10	348±57	220±46	589±89	665±103	1091±297	906±141
15	286±36	307±50	624±86	708±87	854±244	909±159
20	348±62	344±85	553±93	586±65	838±175	897±125
25	323±42	304±39	561±98	415±44	839±121	772±164

5.3 Effect of spinning distance

A series of experiments were done in this study in which the spinning distance was varied from 10 to 15 cm as shown in Table 5.1. For the less concentrated solution (4 wt %), a decrease and an increase in fibre diameter were observed at 10 and 15 kV, respectively. A slight decrease in fibre diameter was observed at higher voltages (20 and 25 kV). An increase in fibre diameter was observed in the 5 wt % solution at lower voltages (10-20 kV) and a decrease in fibre diameter was observed at the highest voltage (25 kV). For the 6 wt %, there was a decrease in fibre diameter at 10 kV upon increasing the distance and an increase in fibre diameter at 20 kV. A decreased fibre diameter is observed at 25 kV. The smaller fibre diameters at higher voltages are the result of the higher electrostatic forces induced on the jet. An increase in the spinning distance to 15 cm generally did not have an adverse effect on the morphology of the fibres (Figure 5.5)

It can be seen from Figure 5.4 that an increase in the spinning distance generally seemed to favour the production of nanofibres with slightly reduced diameters in this instance, depending on the spinning voltage. Some researchers mentioned that an increase in spinning distance resulted in a significant reduction in the diameter of the fibres for different polymers, including PMMA of a significantly lower molecular weight [7]. This indicates that different polymers and different molecular weights of the same polymer behave differently towards changing of the electrospinning parameters.

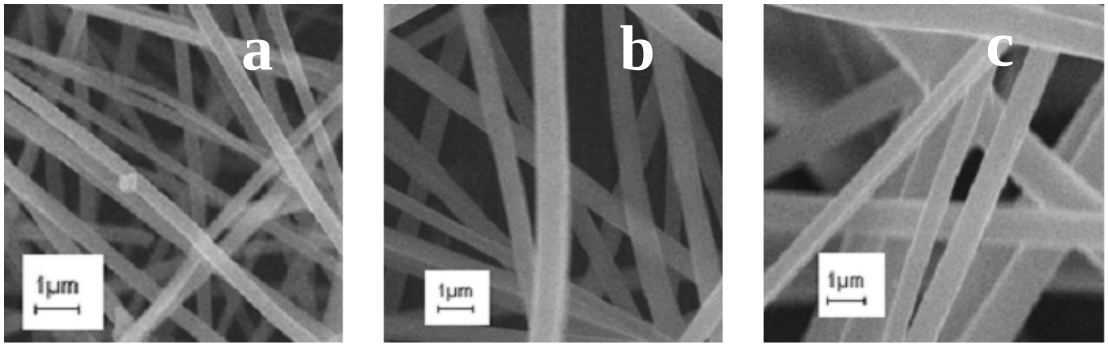

Figure 5.5 SEM images of (a) 200-400 nm, (b) 400-650 nm and (c) 600-900 nm $PMMA_{high}$ fibres electrospun at 15 kV and a spinning distance of 15 cm.

5.4 Thermal analysis of electrospun $PMMA_{high}$ nanofibres

Differential scanning calorimetry (DSC) and thermogravimetric analysis (TGA) were done on the electrospun $PMMA_{high}$ nanofibres in order to determine the thermal behaviour of the nanofibres. The results are presented in Figures 5.6 and 5.7. It can be seen from Figure 5.6 that no difference in the glass transitions of the $PMMA_{high}$ nanofibres compared to the powder was observed. However, both the DSC and TGA results indicate that the nanofibres are thermally more stable than the as-received high molecular weight PMMA powder. It can be seen from Figure 5.7 that the rate of degradation of the nanofibres is generally slower than that of the PMMA powder. Raman spectroscopy was used to investigate the possibility that the increased thermal stability of the PMMA nanofibres compared to the powder is attributed to a conformational change that the polymer side-chains undergo during the electrospinning process, resulting in a thermally more stable polymer chain conformation.

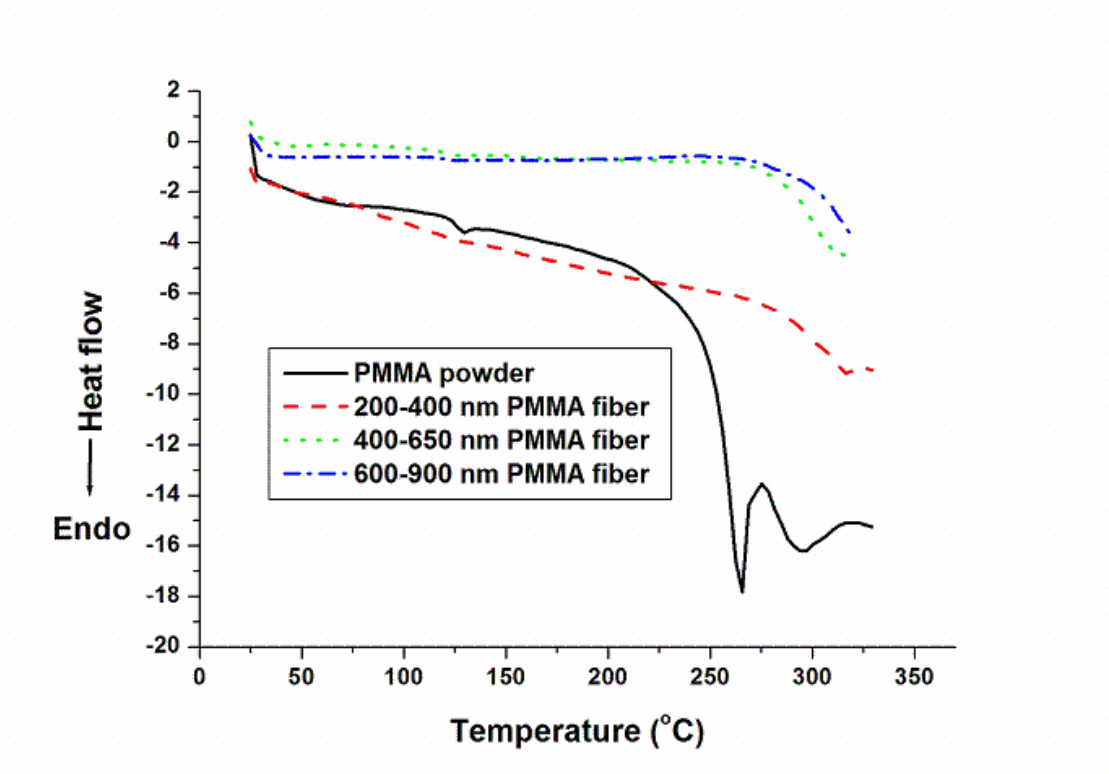

Figure 5.6 DSC results of $PMMA_{high}$ powder and $PMMA_{high}$ nanofibres.

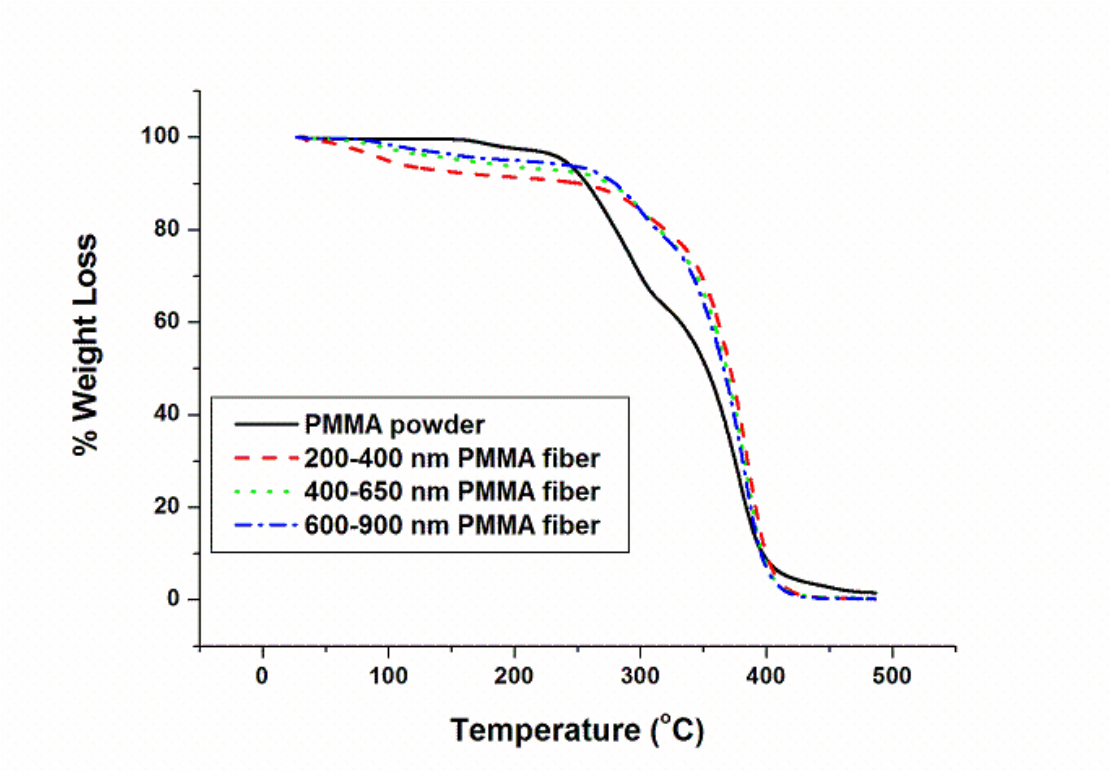

Figure 5.7 TGA results of $PMMA_{high}$ powder and $PMMA_{high}$ nanofibres.

5.5 Raman analysis of $PMMA_{high}$ nanofibres

The Raman spectroscopy results of the as-received $PMMA_{high}$ and the electrospun $PMMA_{high}$ nanofibres of diameters ranging from 200-900 nm are presented in Figure 5.8. The Raman bands and their respective assignments are given in Table 5.2 [9-11].

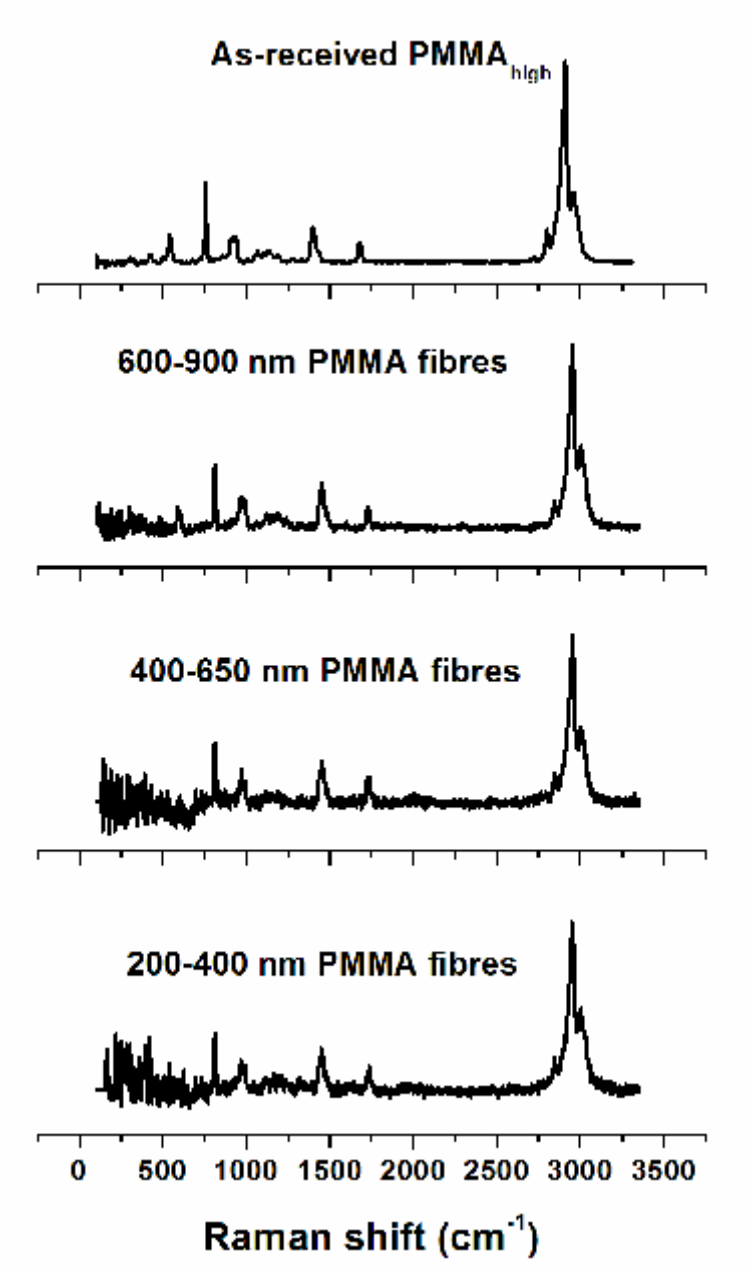

Figure 5.8 Raman spectra of the as-received $PMMA_{high}$ and the electrospun $PMMA_{high}$ nanofibres

Table 5.2 Raman bands in PMMA and their assignments.

Raman band (cm^{-1})	**Assignments**
602	ν(C-COO), ν_s(C-C-O)
853	$\nu(CH_2)$
925	$\nu(CH_2)$
999	O-CH_3 rock
1081	ν(C-C) skeletal mode
1264	ν(C-O), ν(C-COO)
1460	δ_a(C-H) of α-CH_3, δ_a(C-H) of O-CH_3
1648	Combination band involving ν(C=C) and ν(C-COO)
1736	ν(C=O) and (C-COO)
2848	Combination band involving O-CH_3
2957	ν_s(C-H) of O-CH_3 with ν_s(C-H) of α-CH_3 and $\nu_a(CH_2)$
3001	ν_a(C-H) of O-CH_3, ν_a(C-H) of α-CH_3

Stephens *et al*. [12] have studied the effect of electrospinning on the chain conformation in Nylon-6 and Nylon-12. They observed that a chain conformation occurred in Nylon-6 as a result of the polymorphic nature of the polymer, while in Nylon-12 there was no change in chain conformation due to one preferred crystalline structure. The Raman spectra of the as-received $PMMA_{high}$ and electrospun $PMMA_{high}$ nanofibres are the same, which shows that no change in chain conformation occurred during the electrospinning process. The identical chain conformation in the Raman spectra of the as-received PMMA and the electrospun nanofibres is likely a result of the higher molecular weight of the PMMA, which resisted the stresses applied during the electrospinning process.

The reason for the increased thermal stability of the nanofibres compared to the as-received $PMMA_{high}$ is not clear at this stage and will require further investigation, which is outside the scope of this study.

5.6 Conclusions

In this study, the effects of processing parameters on the diameters and morphology of electrospun $PMMA_{high}$ fibres have been investigated. $PMMA_{high}$ nanofibres with diameters ranging from 200-900 nm were prepared under various conditions. The SEM analysis of the $PMMA_{high}$ nanofibres showed that the fibres had a smooth, regular and cylindrical morphology with no beads and junctions. The spinning voltage and the spinning distance, in general, did not have a significant influence on the morphology and diameters of the fibres. However, an increase in polymer solution concentration resulted in a significant increase in fibre diameter. Furthermore, increased thermal stability of the electrospun nanofibres was observed as compared to the powdered $PMMA_{high}$. The reason for this is not certain at this stage.

5.7 References

[1] T.J. Sill, H.A. von Recum. Electrospining: Applications in drug delivery and tissue engineering. Biomaterials 2008; 29:1989-2006. DOI:10.1016/j.biomaterials.2008.01.011

[2] V. Jacobs, R.D. Anandjiwala, M. Maaza. The influence of electrospinning parameters on the structural morphology and diameter of electrospun nanofibres. Journal of Applied Polymer Science 2010; 115:3130-3136. DOI:10.1002/app.31396

[3] S.H. Tan, R. Inai, M. Kotaki, S. Ramakrishna. Systematic parameter study for ultra-fine fibre fabrication via electrospinning process. Polymer 2005; 46:6128-6134. DOI:10.1016/j.polymer.2005.05.068

[4] M.M. Demir, I. Yilgor, E. Yilgor, B. Erman. Electrospinning of polyurethane fibres. Polymer 2002; 43:3303-3309. DOI:10.1016/S0032-3861(02)00136-2

[5] X.M. Mo, C.Y. Xu, M. Kotaki, S. Ramkrishan. Electrospun P(LLA-CL) nanofibre: A biomimetic extracellular matrix for smooth muscle cell and endothelial cell proliferation. Biomaterials 2004; 25:1883-1890. DOI:10.1016/j.biomaterials.2003.08.042

[6] X. Zong, K. Kim, D. Fang, S. Ran, B.S. Hsiao, B. Chu. Structure and process relationship of electrospun bioabsorbable nanofibre membranes. Polymer 2002; 43:4403-4412.
DOI:10.1016/S0032-3861(02)00275-6

[7] J. Doshi, D.H. Reneker. Electrospinning process and applications of electrospun fibres. Journal of Electrostatics 1995; 35:151-160.
DOI:10.1016/0304-3886(95)00041-8

[8] P.J. Hine, R.H. Olley, I.M. Ward. The use of interleaved films for optimising the production and properties of hot compacted self reinforced polymer composites. Composites Science and Technology 2008; 68:1413-1421.
DOI:10.1016/j.compscitech.2007.11.003

[9] H.A. Willis, V.J.I. Zichy, P.J. Hendra. The laser- Raman and infra-red spectra of polymethyl methacrylate. Polymer 1969; 10:737-746.
DOI:10.1016/0032-3861(69)90101-3

[10] X. Xu, H. Ming, Q. Zhang, Y. Zhang. Properties of raman spectra and laser-induced birefringence in polymethyl methacrylate optical fibres. Journal of Optics A: Pure and Applied Optics 2002; 4:237-242.
DOI:10.1088/1464-4258/4/3/303

[11] K.J. Thomas, M. Sheeba, V.P.N. Nampoori, C.P.G. Vallabhan, P. Radhakrishnan. Raman spectra of poly(methyl methacrylate) optical fibres excited by a 532 nm diode pumped solid state laser. Journal of Optics A: Pure and Applied Optics 2008; 10:1-5.
DOI:10.1088/1464-4258/10/5/055303

[12] J.S. Stephens, D.B. Chase, J.F. Rabolt. Effect of electrospinning process on polymer crystallization chain conformation in Nylon-6 and Nylon-12. Macromolecules 2004; 37:877-881.
DOI**:**10.1021/ma0351569

Chapter 6

Thermal properties of single polymer composites of poly(methyl methacrylate)

In this chapter, $PMMA_{high}$ nanofibres of different diameters were produced by an electrospinning technique according to the conditions described in Chapter 4, and were used as reinforcements in PMMA single polymer composites. Suitable processing conditions for the preparation of the single polymer composites of PMMA reinforced with the nanofibres were investigated. Furthermore, single polymer composites of PMMA were manufactured by compression moulding using the film stacking technique and applying a two-component approach. Thermal analysis (DMA and TGA) of the prepared composites were performed and the results are discussed.

6.1 Investigation of processing conditions for single polymer composites of PMMA

The effect of the processing temperature on the morphology of the composites was investigated. The aim was to find a suitable processing temperature for the preparation of a quality PMMA single polymer composite. Since $PMMA_{high}$ is amorphous, the amount of orientation (although not determined in this study) in the electrospun nanofibres will determine the processing window. SEM analysis of the cross-sections of the PMMA composites was used to check the intactness of the nanofibres and the integrity of the interface between the matrix and the reinforcement. $PMMA_{high}$ nanofibres with diameters ranging from 400-650 nm were used to investigate suitable processing conditions for preparing single polymer composites of PMMA. $PMMA_{low}$ was used as the matrix material.

Figure 6.1 shows the SEM images of the composites prepared at 140, 150 and 160 °C. The processing temperatures are well above the glass transition (T_g) of $PMMA_{low}$. The SEM images of the composites prepared at 140 and 150 °C show two phases. Thus, the composites have a layered structure consisting of outer film layers and a layer in-between, which is associated with the non-woven nanofibre mats plus the softened matrix that has diffused onto the non-woven fibre mat. Possible partial softening of the surface of the non-woven fibre mat

is present. This results in a good interface, which should translate into enhanced mechanical properties as a result of efficient stress transfer.

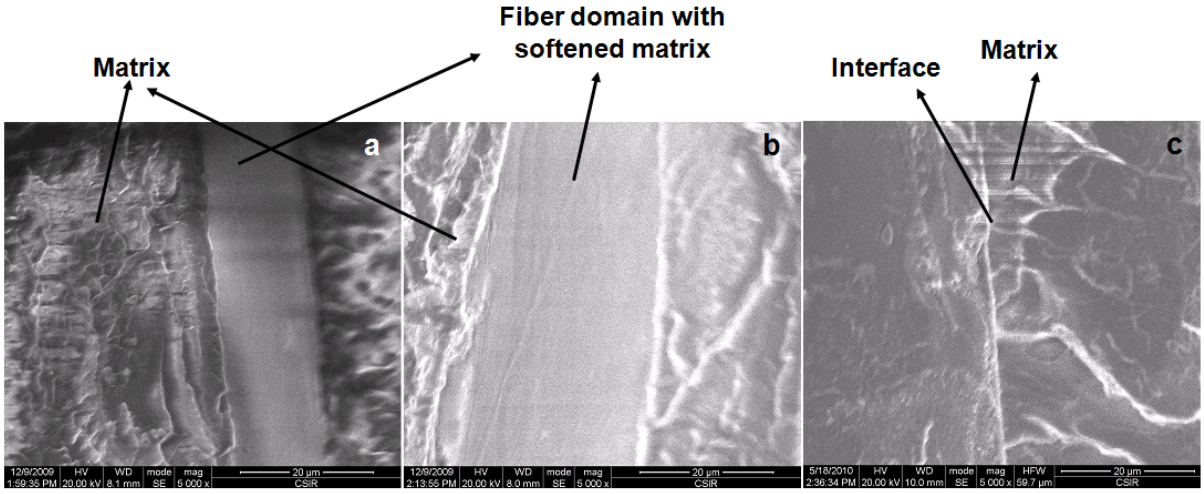

Figure 6.1 SEM images (scale bar: 20 μm) of PMMA single polymer composites prepared at (a) 140 °C, (b) 150 °C and (c) 160 °C.

The SEM images seem to be in agreement with the previous study of Capiati and Porter [1]. It is likely that the layered structure observed for the composites is due to a combination of two composite fabrication methods, namely film stacking and hot compaction. Hine et al. [2] demonstrated that such a combination of film stacking with hot compaction results in a better overall balance of mechanical properties and a wider temperature range for processing compared to a standard compaction procedure without a film. Furthermore, this combination gives rise to better wetting of the reinforcement compared to the traditional film stacking process, due to the partial softening of the entire fibre surface. This better wetting of the fibres results in good interfacial adhesion between the phases, which can be seen from the SEM images in Figure 6.1.

It must be pointed out that delamination between the different matrix layers for the composite prepared at 140 °C was observed. This was due to insufficient softening of the matrix material at a processing temperature of 140 °C. The SEM analysis of the composite samples prepared at 160 °C does not show two well-defined phases (Figure 6.1c). This suggests that the nanofibres could have also softened in addition to the matrix. Thus, processing temperatures of 140 and 160 °C does not seem to be suitable for the preparation of a good quality PMMA single polymer composite in this instance. The best composite with two

distinguishable physical phases and adequate melting of the matrix material was therefore obtained at a processing temperature of 150 °C.

The dimension of the layer related to the non-woven fibre mat, as observed from Figure 6.1, is around 10 to 15 μm. On the other hand, the diameter of the non-woven $PMMA_{high}$ fibres was found to be around 200-900 nm (Figure 4.1 and Table 4.1 in Chapter 4). Differences in the nanofibre dimensions and morphology, as visualised in Figures 4.1 and 6.1, are explained by Figure 6.2. Before compression moulding, non-woven $PMMA_{high}$ fibre mats are entangled among themselves (left hand side of Figure 6.2). For preparing a single polymer composite, $PMMA_{low}$ sheets are stacked above and below the non-woven fibre mat. Under pressure, the $PMMA_{low}$ matrix softens and fills the vacant spaces around the non-woven fibre mat. The SEM morphology of the peeled-off structure after compression moulding (right hand side of Figure 6.2) demonstrates the presence of the softened $PMMA_{low}$ matrix as well as the non-woven $PMMA_{high}$ fibre mat. However, these nanofibres are hidden when the cross-section morphology of the composites are taken. This is attributed to the absence of fibre pull-out from the matrix when fractured.

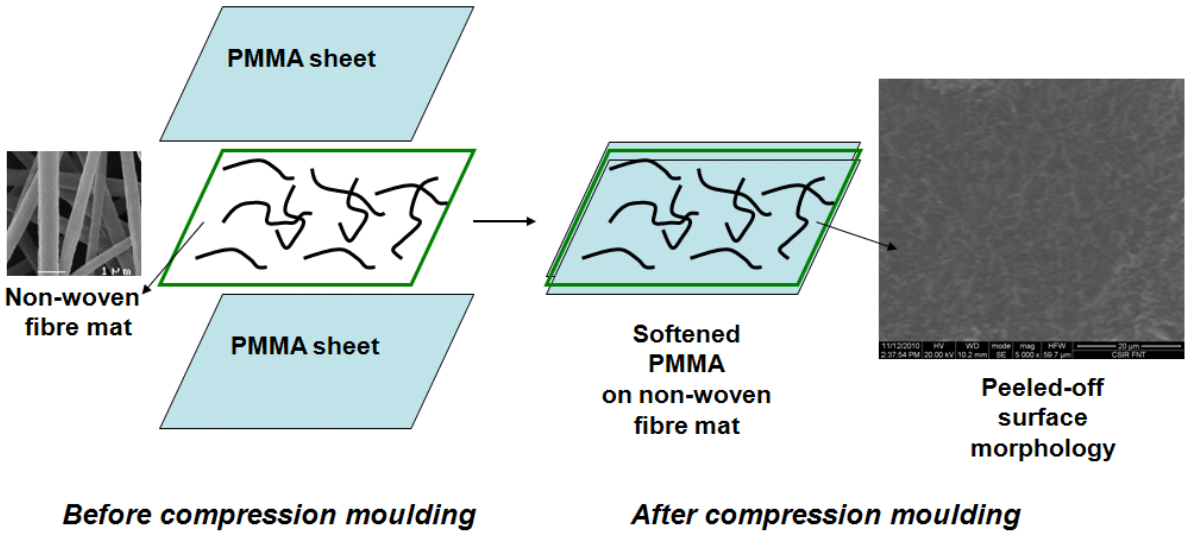

Figure 6.2 The appearance of the $PMMA_{high}$ nanofibre non-woven mat in the single polymer composite system after compression moulding. Scale bar for peeled-off picture is 20 μm.

6.2 Characterization of single polymer composites of PMMA

The effect of the nanofibre diameter and loading on the thermal properties (DMA and TGA) of PMMA single polymer composites prepared at 150 °C was investigated. The chosen processing temperature of 150 °C is based on the results obtained in Section 6.2.1. Furthermore, for comparison purposes composites were also prepared at 140 and 160 °C and their graphs are presented in the Appendix. The nanofibre reinforcements consisted of three different fibre diameter ranges at two different loadings. The nanofibres electrospun at 15 kV and 10 cm at the various concentrations were used to prepare the single polymer composites.

6.2.1 Dynamic mechanical analysis of PMMA single polymer composites processed at 150 °C

The effects of the nanofibre diameter and nanofibre loading on the dynamic mechanical properties of six different types of PMMA single polymer composites prepared at 150 °C were investigated. The designations for the six different types of composites are presented in Table 6.1.

Table 6.1 Designations of PMMA single polymer composites

Sample designation	**Matrix**	**Reinforcement by**	
		5 wt% of $PMMA_{high}$ nanofibres (nm)	**10 wt% of $PMMA_{high}$ nanofibres (nm)**
SPC01	$PMMA_{low}$ sheet	200-400	NA
SPC02		400-650	NA
SPC03		600-900	NA
SPC04		NA	200-400
SPC05		NA	400-650
SPC06		NA	600-900

6.2.1.1 Effect of nanofibre diameter on the dynamic mechanical properties of PMMA single polymer composites at 150 °C

The change in storage modulus and damping behaviour (tan δ) of the neat $PMMA_{low}$ matrix compared to the composites SPC01 to SPC03 with 5 wt% nanofibre loading are shown in Figure 6.3.

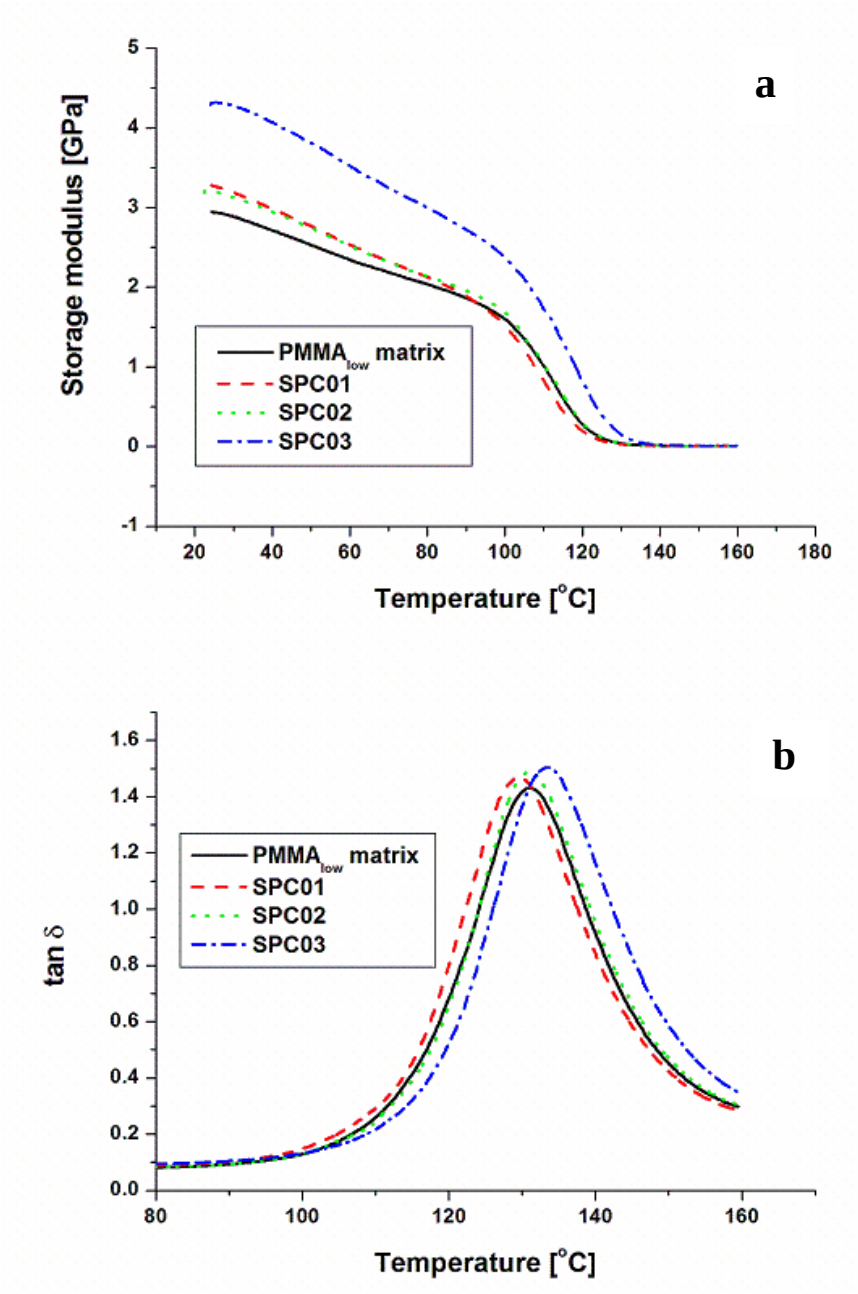

Figure 6.3 Effect of fibre diameter on the (a) storage modulus and (b) tan δ of PMMA composites at 5 wt% nanofibre loading and processing temperature of 150 °C.

A slightly higher stiffness was observed for SPC01 and SPC02 compared to the neat $PMMA_{low}$ matrix. A significantly higher reinforcing affect of the higher diameter fibres at a loading of 5 wt% was observed. Composite SPC03 showed an increase in stiffness of approximately 46% compared to the neat $PMMA_{low}$ matrix. A slight increase in the peak temperatures of the tan δ peaks of the composites compared to the neat $PMMA_{low}$ matrix was observed (Figure 6.3b). This increase is once again more noticeable in SPC03. This means that the inclusion of the nanofibres affected the mobility of the polymer chains to some degree. Furthermore, at a 5 wt% inclusion of the nanofibres, no significant shift in the peak temperature is observed for SPC01 and SPC02 compared to the neat $PMMA_{low}$ matrix. However, the peak temperature shifted marginally by about 4 °C in the case of SPC03 compared to the matrix. This means that there is stronger physical interaction between the larger diameter nanofibres and the neat PMMA matrix.

The storage modulus and damping behaviour (tan δ) of the neat $PMMA_{low}$ matrix compared to the composites SPC04 to SPC06 with 10 wt% nanofibre loading are shown in Figure 6.4. The stiffness of all the composites was higher than that of the neat $PMMA_{low}$ matrix. A maximum improvement in stiffness of 83% compared to the matrix was obtained. This is due to the reinforcing effect of the nanofibres. Different stiffness and damping behaviour was observed for the composites with 10 wt% nanofibre loading compared to the ones with a 5 wt% nanofibre loading. The composites (SPC04 and SPC05) reinforced with fibres of smaller diameters showed a larger improvement in stiffness compared to the one reinforced with the highest diameter fibres. This is contrary to what was observed for the composites with a 5 wt% nanofibre loading. This is probably the result of the higher fibre content and the larger surface area of the nanofibres with smaller diameters. In this case an increase in the stiffness of the composites is observed as the diameter of the reinforcement decreases. In addition, a less pronounced decrease in the stiffness of all the composites compared to the neat $PMMA_{low}$ matrix was observed. Figure 6.4b shows the damping behaviour of the neat $PMMA_{low}$ matrix compared to the composites reinforced with a 10 wt% nanofibre loading. Similar damping behaviour is observed for all the composites. The addition of a 10 wt% nanofibre loading had no significant effect on the maximum value of the tan δ peaks of the composites. Thus, the mobility of the polymer chains in the matrix and the composites are quite similar. Nevertheless, the position of the T_g of the composites shifted to higher temperatures as compared to the $PMMA_{low}$ matrix. This shift to higher temperatures is

attributed to the increase in the stiffness of the composites due to the reinforcement effect of the nanofibres.

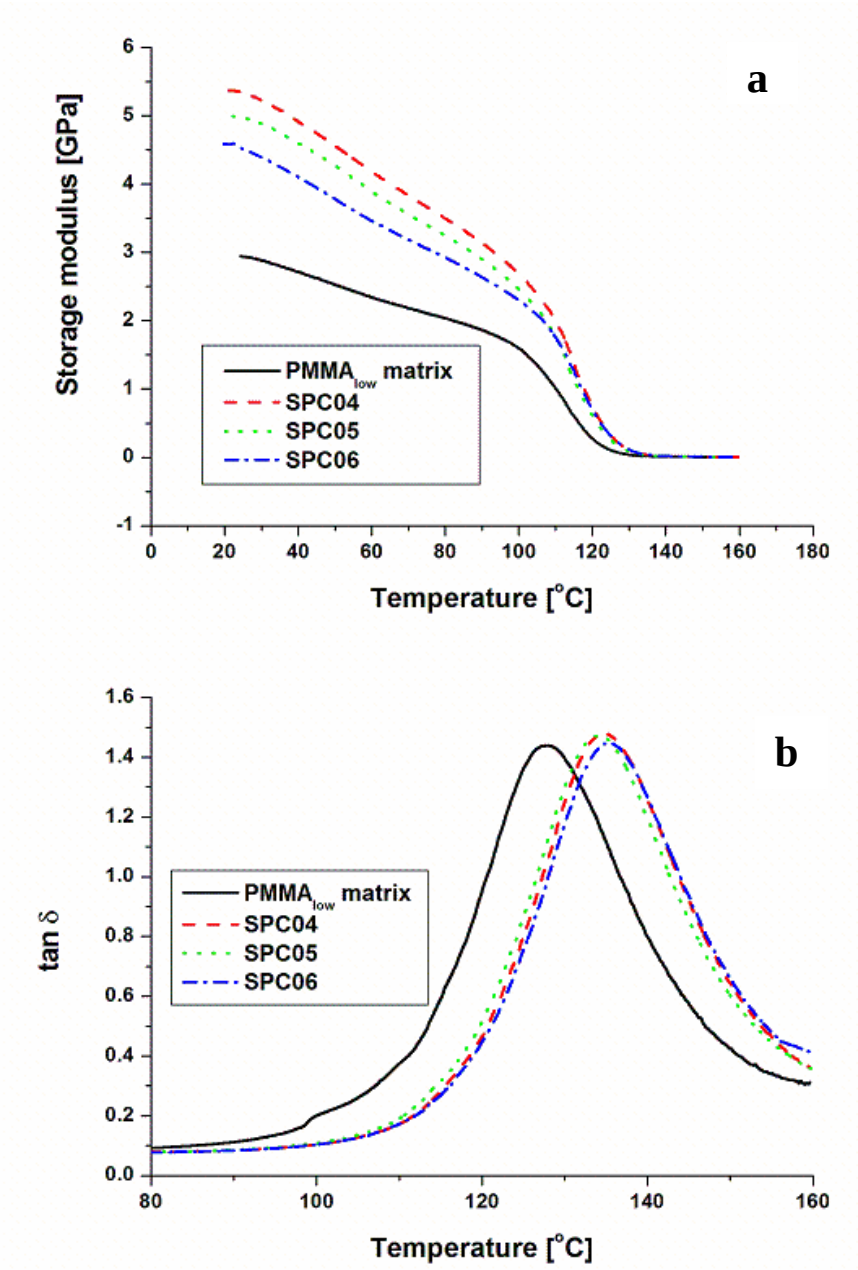

Figure 6.4 Effect of fibre diameter on the (a) storage modulus and (b) tan δ of PMMA composites at 10 wt% nanofibre loading and processing temperature of 150 °C.

The variation of loss modulus with temperature for the composites reinforced with different diameter fibres is shown in Figure 6.5. For the 5 wt% nanofibre loading [Figure 6.5 (a)], the loss modulus for SPC03 (composite with the 600-900 nm fibres) is higher, broadened and extended to a higher temperature as compared to the $PMMA_{low}$ matrix and the other

composites (SPC01 and SPC02). There is no noticeable change in the curve for SPC02 as compared to the $PMMA_{low}$ matrix. Furthermore, the SPC01 showed a decrease in the loss modulus and the curve shifted to a lower temperature as compared to the $PMMA_{low}$ matrix and the other composites.

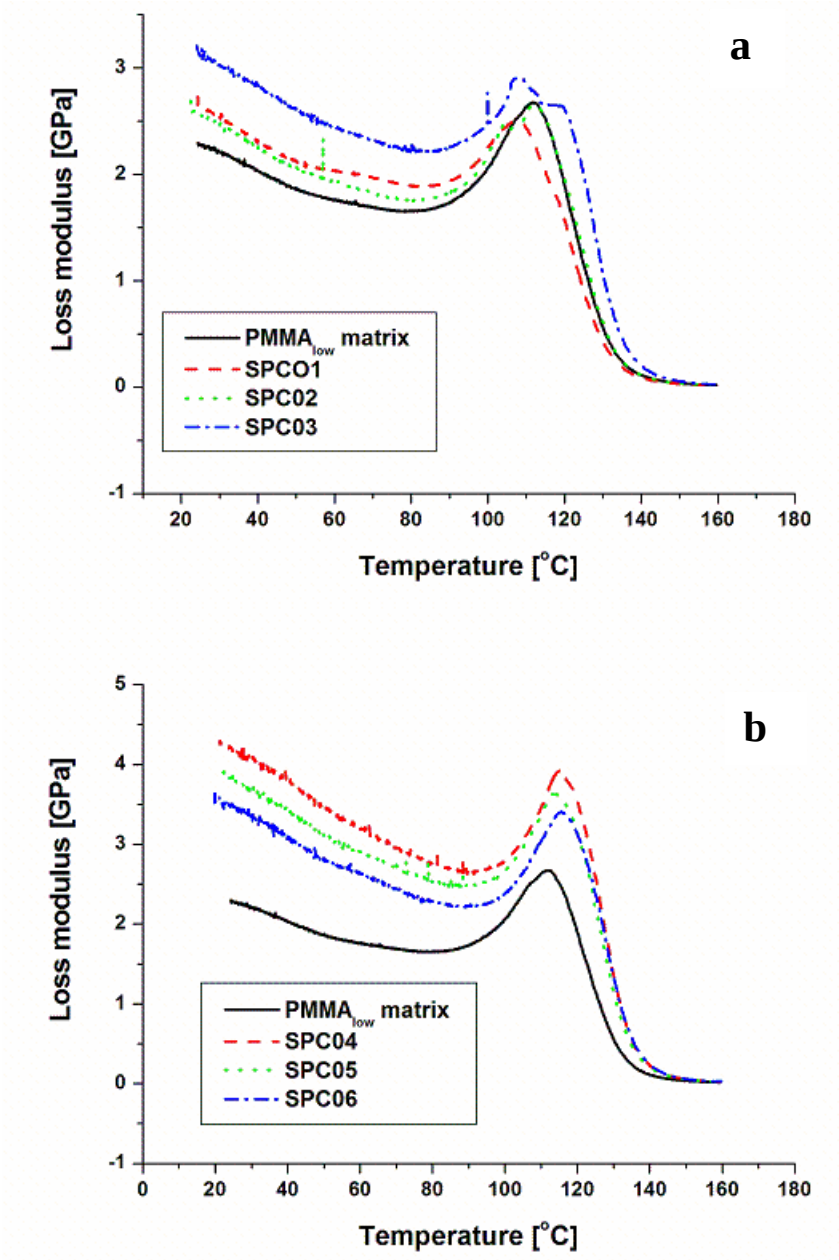

Figure 6.5 Effect of fibre diameter on the loss modulus for PMMA composites at (a) 5 wt% and (b) 10 wt% nanofibre loading and processing temperature of 150 °C.

As the loading increased to 10 wt% (Figure 6.5 (b)), the effect of the nanofibres became more prominent as the loss moduli of the composites are significantly higher than the $PMMA_{low}$ matrix. SPC04 (composite with smallest diameter fibre) showed higher loss modulus and had its curve slightly shifted to higher temperatures as compared to the SPC05 and SPC06. The higher loss modulus of the composites as compared to the matrix is probably the result of the improved energy absorption due to the introduction of the nanofibres.

6.2.1.2 Effect of nanofibre loading on the dynamic mechanical properties of PMMA single polymer composites at 150 °C

Storage modulus

The storage modulus as a function of temperature at a frequency of 1 Hz is shown in Figures 6.6 to 6.8. The results show the effect of fibre loading on the stiffness of the laminates prepared at 150 °C for each fibre diameter range (200-400 nm, 400-650 and 600-900 nm). It can be observed that the storage modulus increases with increasing nanofibre content at all temperatures when compared to the unreinforced $PMMA_{low}$ matrix. However, SPC01 showed a smaller storage modulus above the T_g (100 °C) as compared to the $PMMA_{low}$ matrix. It can be seen from Figure 6.6 that the storage modulus of the $PMMA_{low}$ matrix, SPC01 and SPC04 are respectively 3.00, 3.24 and 5.39 GPa at room temperature. The storage modulus improved from 8% for SPC01 (5 wt% fibre loading) to 80% for SPC04 (10 wt% loading) compared to the matrix. Figure 6.7 shows an initial storage modulus of 3.00, 3.21 and 4.99 GPa for the $PMMA_{low}$ matrix, SPC02 and SPC05. An improvement in the storage modulus from 7% to 66% for SPC02 and SPC05, respectively, was observed. Figure 6.8 shows an increase in the storage modulus of SPC03 and SPC06 compared to the $PMMA_{low}$ matrix. Initial storage moduli of 3.64 and 4.57 GPa are reported for SPC03 and SPC06, respectively. An improvement in the storage modulus from 21% (SPC03, 5 wt% fibre loading) to 52% (SPC06, 10 wt% fibre loading) as compared to the $PMMA_{low}$ matrix was obtained. The effect of the nanofibre loading on the storage modulus of the composites was therefore more pronounced in the case of the smallest fibre diameter range (200-400 nm). A tenfold improvement in the storage modulus of the composites was observed when the fibre loading was doubled. A similar result was obtained for the composites reinforced with the 400-650 nm fibres.

As expected, the storage modulus decreases linearly with increasing temperature. Above 100 °C the stiffness of the unreinforced $PMMA_{low}$ matrix and the corresponding composites drops significantly. The decrease in modulus is as a result of the softening of the matrix, the initiation of the relaxation processes and melting. However, in the case of the composites with a 10 wt% nanofibre loading, the decrease in stiffness with temperature was less pronounced. This is due to the closer packing of the nanofibres, which caused efficient stress transfer at the interface and the positive reinforcing effect of the $PMMA_{high}$ nanofibres [3]. Furthermore, the increased modulus above T_g (100 °C) where the materials are expected to be soft indicates the positive reinforcing effect of the $PMMA_{high}$ nanofibres.

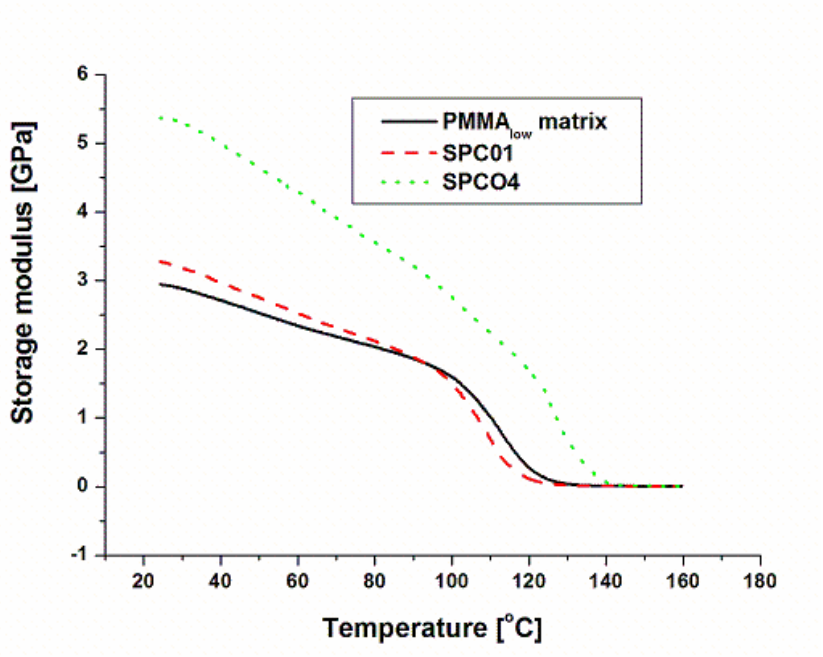

Figure 6.6 Effect of nanofibre loading on PMMA composites prepared at 150 °C. Nanofibre diameter: 200-400 nm.

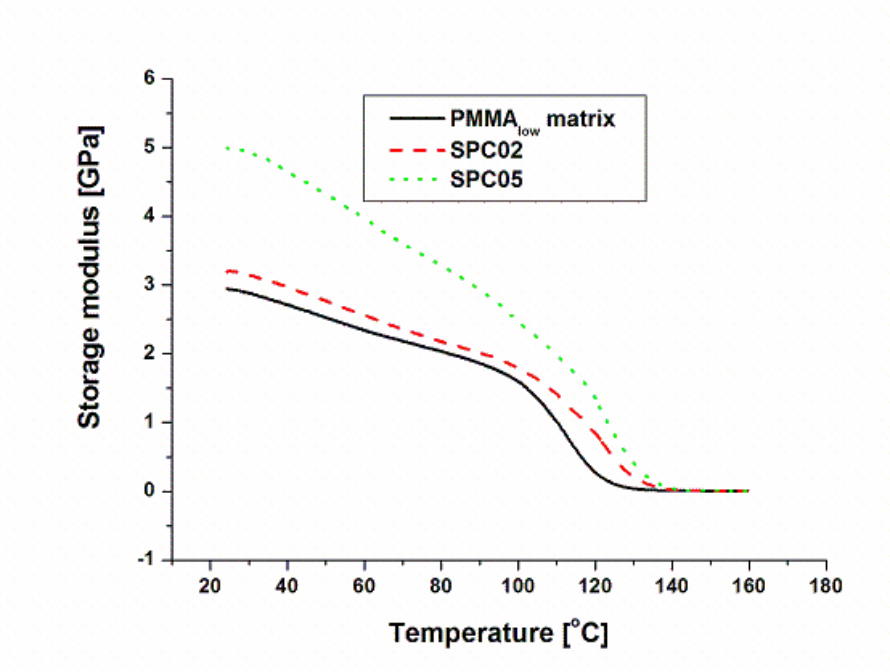

Figure 6.7 Effect of nanofibre loading on PMMA composites prepared at 150 °C. Nanofibre diameter: 400-650 nm.

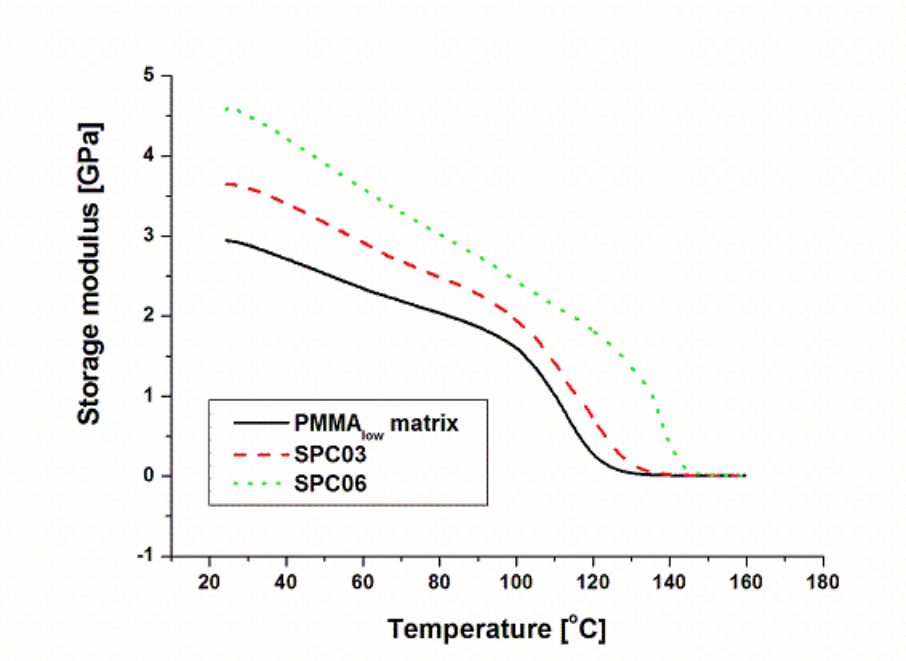

Figure 6.8 Effect of nanofibre loading on PMMA composites prepared at 150 °C. Nanofibre diameter: 600-900 nm.

Loss factor (tan δ)

Figures 6.9 to 6.11 represent the tan δ versus temperature curves of the $PMMA_{low}$ matrix and the corresponding composites at different fibre loadings. As shown in the graphs, the dominant relaxation peak is located at around 131 °C (β-relaxation) and this corresponds to the glass-rubber transition of the amorphous portions. Furthermore, the temperature of the tan δ maximum is assigned as the glass transition temperature (T_g) of the matrix. It can be seen that the increase in fibre loading shifts the T_g to higher temperatures. With the addition of the nanofibres at 5 wt% loading, the tan δ curve corresponding to SPC01 shifted to lower temperatures. As the loading increased to 10 wt %, the tan δ curve shifted to higher temperatures. The highest T_g (141.7 °C) was obtained for SPC04 as compared to the 130.6 °C for the $PMMA_{low}$ matrix.

In the case of the 400-650 and the 600-900 nm fibre reinforced PMMA composites, the position of the T_g also shifted to higher temperatures as the fibre content increased. Previous authors reported decreased tan δ values for the composites as compared to the matrix, suggesting a reduced damping behaviour of the composites due to the reinforcing effect [4], but in this instance the maximum tan δ values for all the composites are higher than that for the unreinforced PMMA matrix. Although the tan δ peak values of the composites are not reduced, the increase of the T_g would indicate a reduced mobility of the polymer chains leading to lower degrees of molecular motion and hence lower damping characteristics, but this is not observed in this instance. These findings support the fact that the nanofibres have a positive reinforcing effect on the $PMMA_{low}$ matrix.

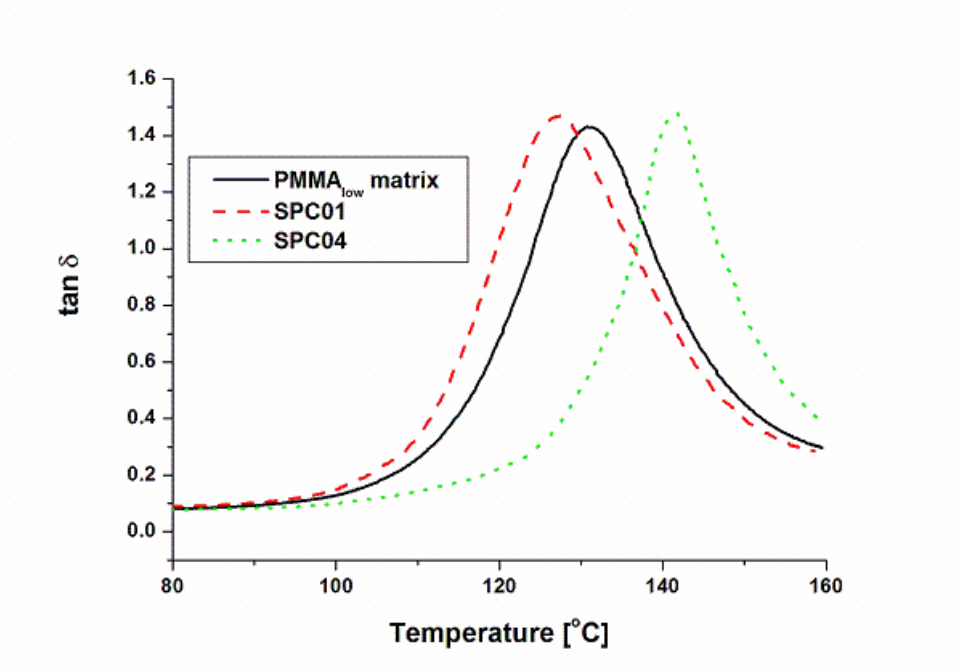

Figure 6.9 Effect of nanofibre loading on the tan δ of PMMA composites prepared at 150 °C. Nanofibre diameter: 200-400 nm

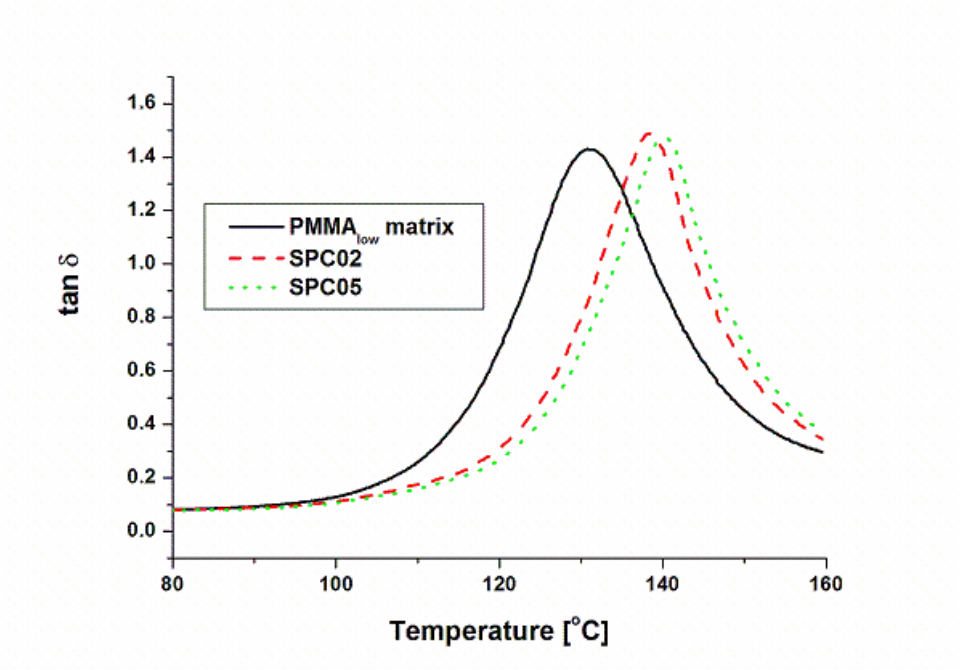

Figure 6.10 Effect of nanofibre loading on the tan δ of PMMA composites prepared at 150 °C. Nanofibre diameter: 400-650 nm.

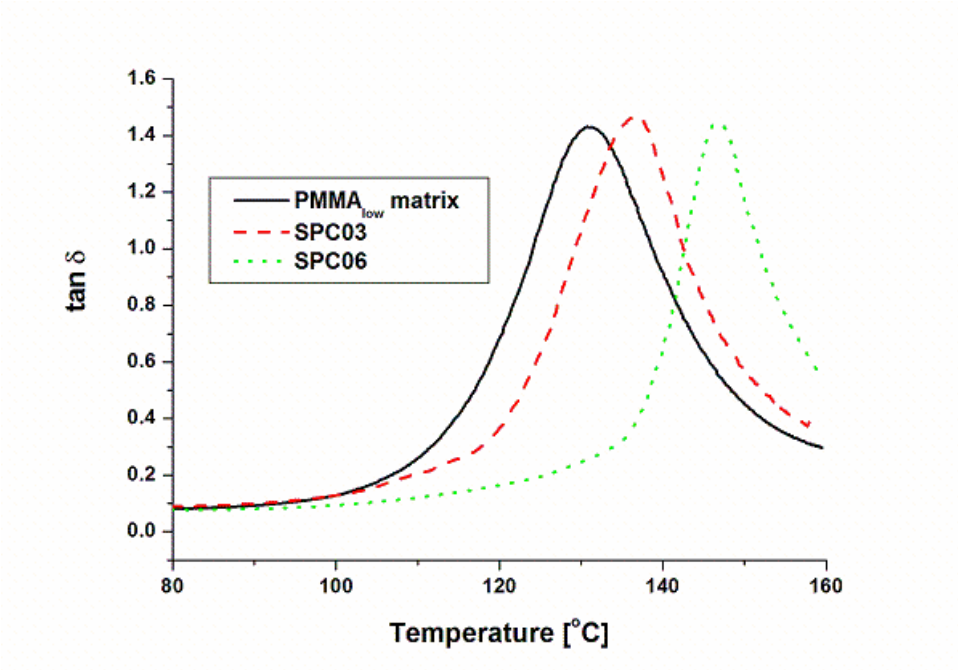

Figure 6.11 Effect of nanofibre loading on the tan δ of PMMA composites prepared at 150 °C. Nanofibre diameter: 600-900 nm.

Loss modulus

Figures 6.12 to 6.14 depict the loss modulus of the $PMMA_{low}$ matrix and the corresponding composites as a function of temperature at different fibre loadings. The composite materials were prepared at 150 °C. Loss modulus measures the viscous response of materials and is related to the amount of energy lost [4]. It is obvious that loss modulus increases with the increase in fibre loading. It has been reported that the maximum heat dissipation occurs at the temperature where the loss modulus is maximum indicating a relaxation phenomenon [4]. It can be seen from Figure 6.12 that the loss modulus curve for SPC01 flattened and extended toward lower temperatures. However, the curve for SPC03 broadened and shifted towards higher temperatures as compared to the $PMMA_{low}$ matrix. The same trend was observed for the 400-650 nm and 600-900 nm fibre reinforced composites whereby the addition of nanofibres caused a broadening and a shift towards higher temperatures. The increase in the loss modulus is a result of the increase in energy absorption caused by the addition of the fibres.

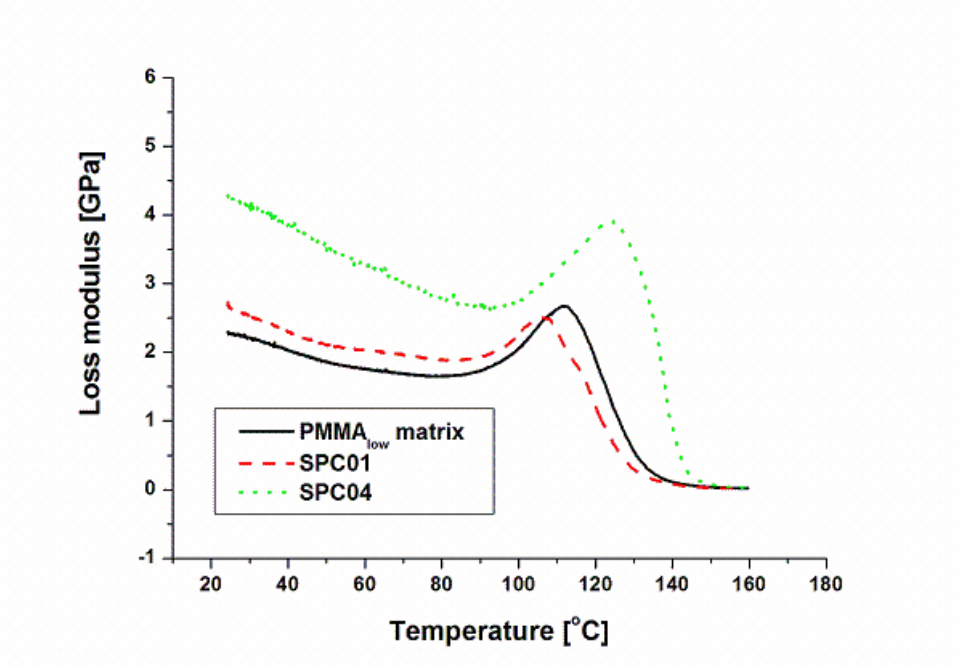

Figure 6.12 Effect of nanofibre loading on the loss modulus of PMMA composites prepared at 150 °C. Nanofibre dioameter: 200-400 nm

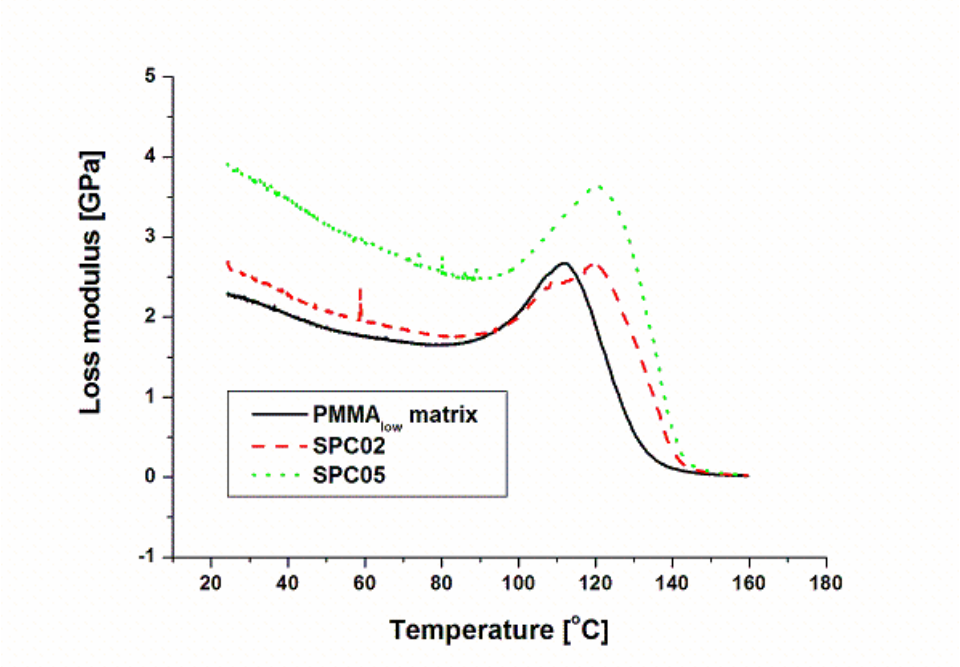

Figure 6.13 Effect of nanofibre loading on the loss modulus of PMMA composites prepared at 150 °C. Nanofibre diameter: 400-650 nm.

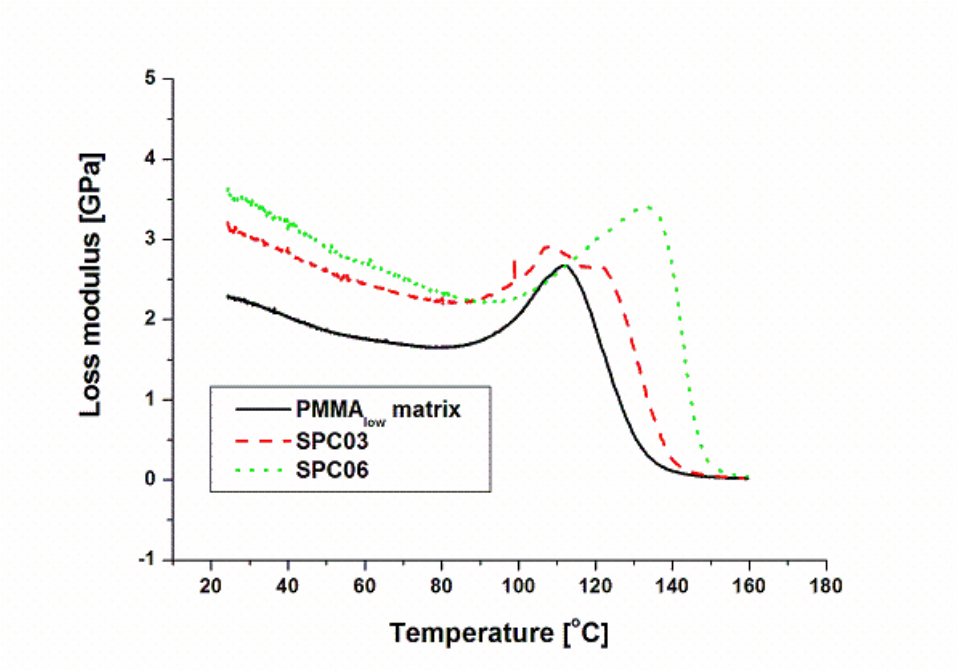

Figure 6.14 Effect of nanofibre loading on the loss modulus of PMMA composites prepared at 150 °C. Nanofibre diameter: 600-900 nm

6.2.2 Dynamic mechanical analysis of PMMA single polymer composites processed at 140 and 160 °C

6.2.2.1 Effect of fibre diameter at 140 °C with 5 and 10 wt% nanofibre loading

Figure 6.15(a) shows the storage modulus as a function of temperature for the composites with different fibre diameters (5 wt% fibre loading) at a frequency of 1 Hz. For the 5 wt% reinforced PMMA composites, the results show that all the composites have higher storage moduli as compared to the neat $PMMA_{low}$ matrix. However, slightly higher stiffness values were achieved by the composite with 400-650 nm fibres followed by 200-400 nm and 600-900 nm fibres, which showed similar stiffness. Above the T_g, the composite with 600-900 nm fibres seemed to be slightly stiffer than the 400-650 and 200-400 nm fibre reinforced PMMA composites.

There is no clear change in the T_g (tan δ) (Figure 6.15(b)) for the neat $PMMA_{low}$ and the 5 wt % composites with 200-400 and 400-650 nm fibres. However, the composite with 600-900 nm fibres showed a higher T_g.

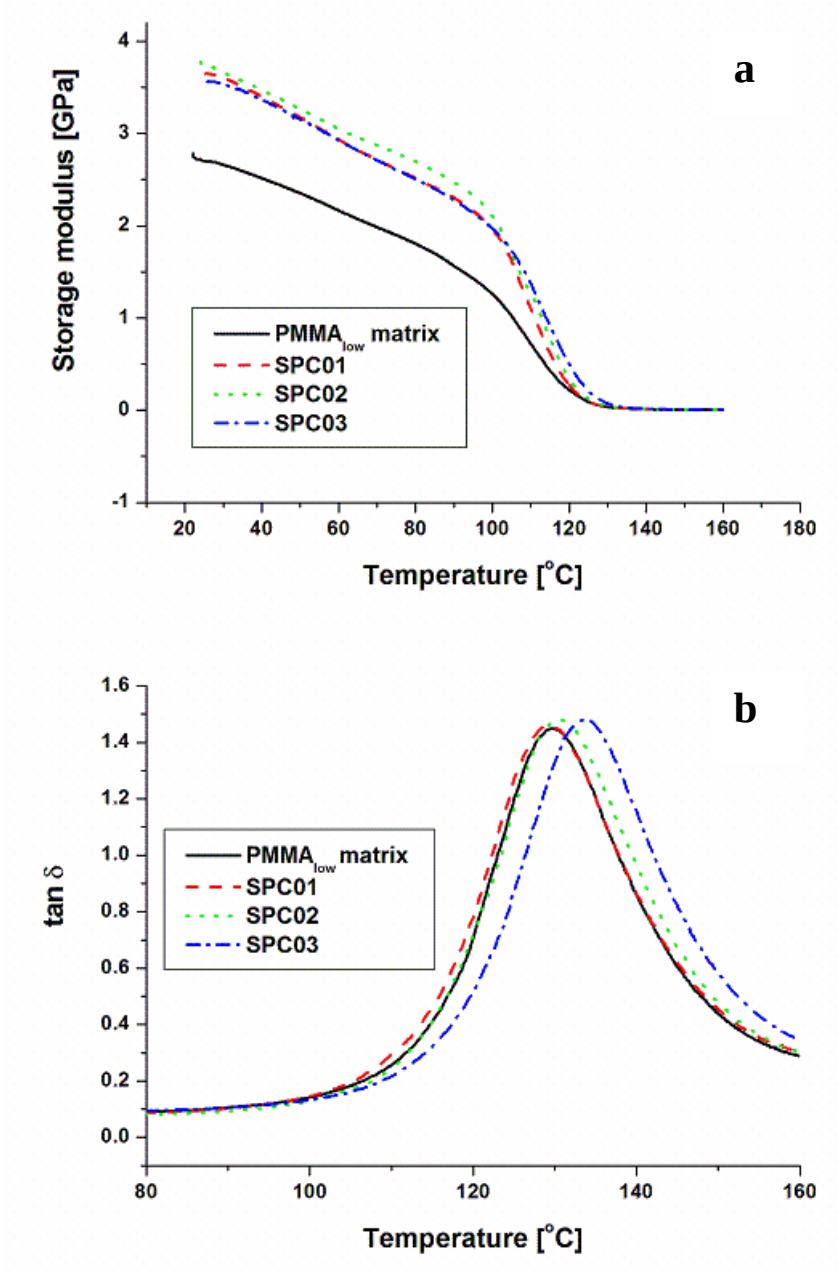

Figure 6.15 Effect of fibre diameter on the (a) storage modulus and (b) tan δ of PMMA composites prepared at 140 °C with 5 wt % nanofibre loading

The effect of fibre diameter on the stiffness became more prominent at 10 wt % loading (Figure 6.16(a)). All the composites showed higher storage moduli as compared to the neat $PMMA_{low}$ matrix. However, the higher storage modulus was achieved by the composite with 200-400 nm fibres followed by the 400-650 nm fibres. As the fibre loading increased to 10 wt%, the composites showed increased T_g (tan δ) (Figure 6.16(b)) as compared to the neat $PMMA_{low}$ matrix. Furthermore, the highest T_g was achieved with the composite with 200-400 nm fibres followed by the 400-650 and 600-900 nm fibres, which showed similar T_g values. Moreover, the peak values of tan δ are slightly higher for the composites as compared to the pure $PMMA_{low}$ matrix.

The loss modulus (Figure 6.17(a)) for the 5 wt % composites is higher than the neat $PMMA_{low}$ matrix. However, the loss modulus for the composites with the 600-900 and 400-650 nm fibres seemed to have shifted more to higher temperatures, more than the composite with the 200-400 nm fibres. The 10 wt% fibre loading (Figure 6.17(b)) resulted in higher loss modulus for the composite with 200-400 nm fibres followed by 400-650 and 600-900 nm fibres.

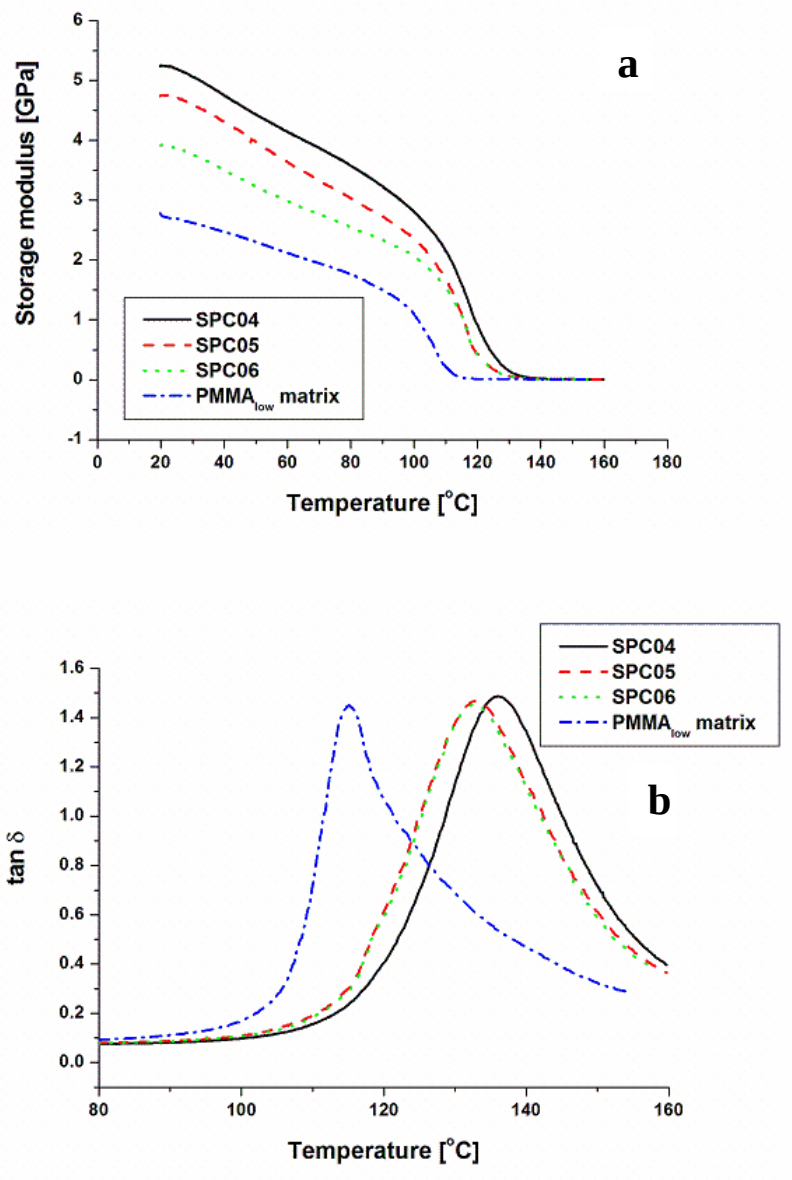

Figure 6.16 Effect of fibre diameter on the (a) storage modulus and (b) tan δ of PMMA composites prepared at 140 °C with 10 wt % nanofibre loading

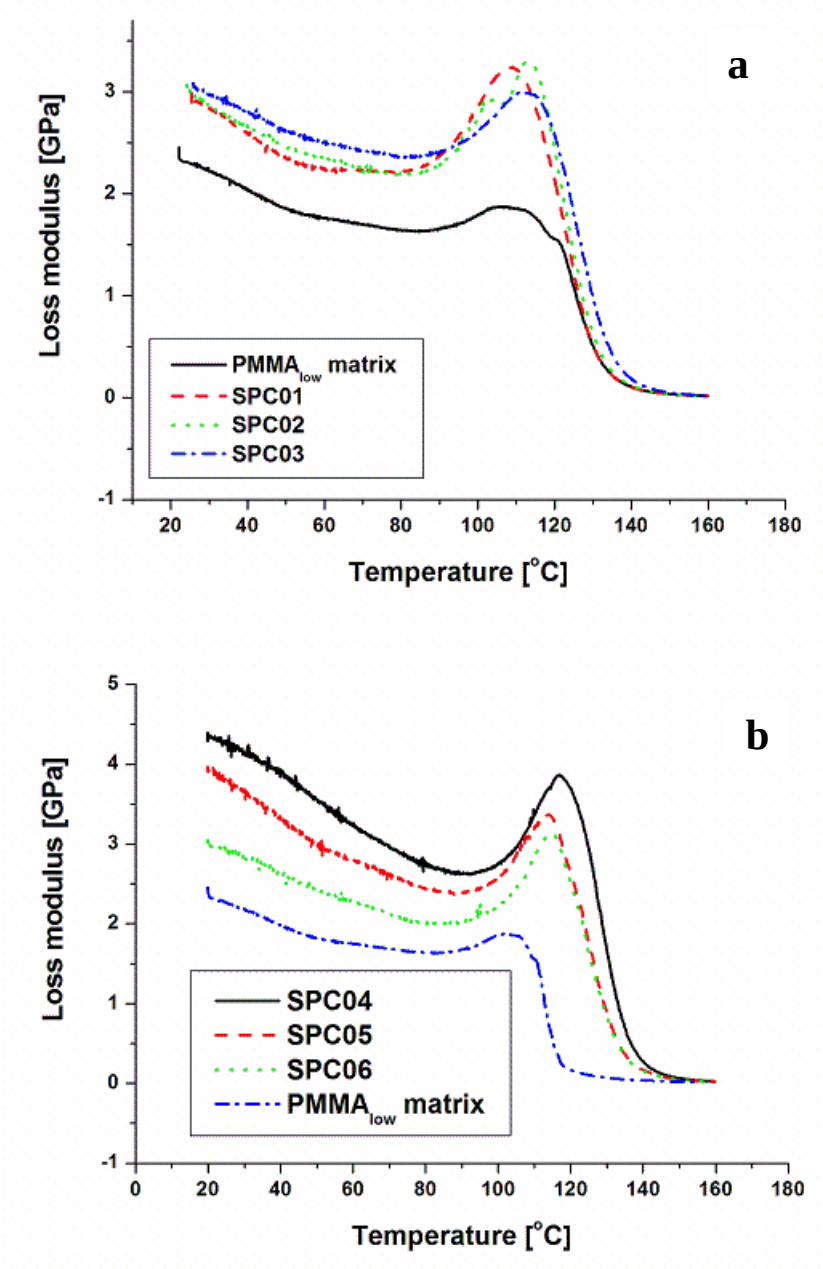

Figure 6.17 Effect of fibre diameter on the loss modulus of PMMA composites prepared at 140 °C with (a) 5 and (b) 10 wt % nanofibre loading

6.2.2.2 Effect of fibre diameter at 160 °C with 5 and 10 wt% nanofibre loading

It can be seen that the 5 wt% nanofibre reinforced composites (Figure 6.18(a)) show lower storage modulus as compared to the neat $PMMA_{low}$. This is probably the result of the melting of the nanofibres. There is no significant change in the T_g of the neat $PMMA_{low}$ matrix (Figure 6.18(b)) and the composites with the 5 wt% nanofibre loading. However, a slightly

higher T_g and peak value of the tan δ is observed for the composite with the 600-900 nm fibres (SPC03). Furthermore, the T_g for SPC01 shifted slightly towards lower temperatures as compared to the $PMMA_{low}$ matrix and the other composites.

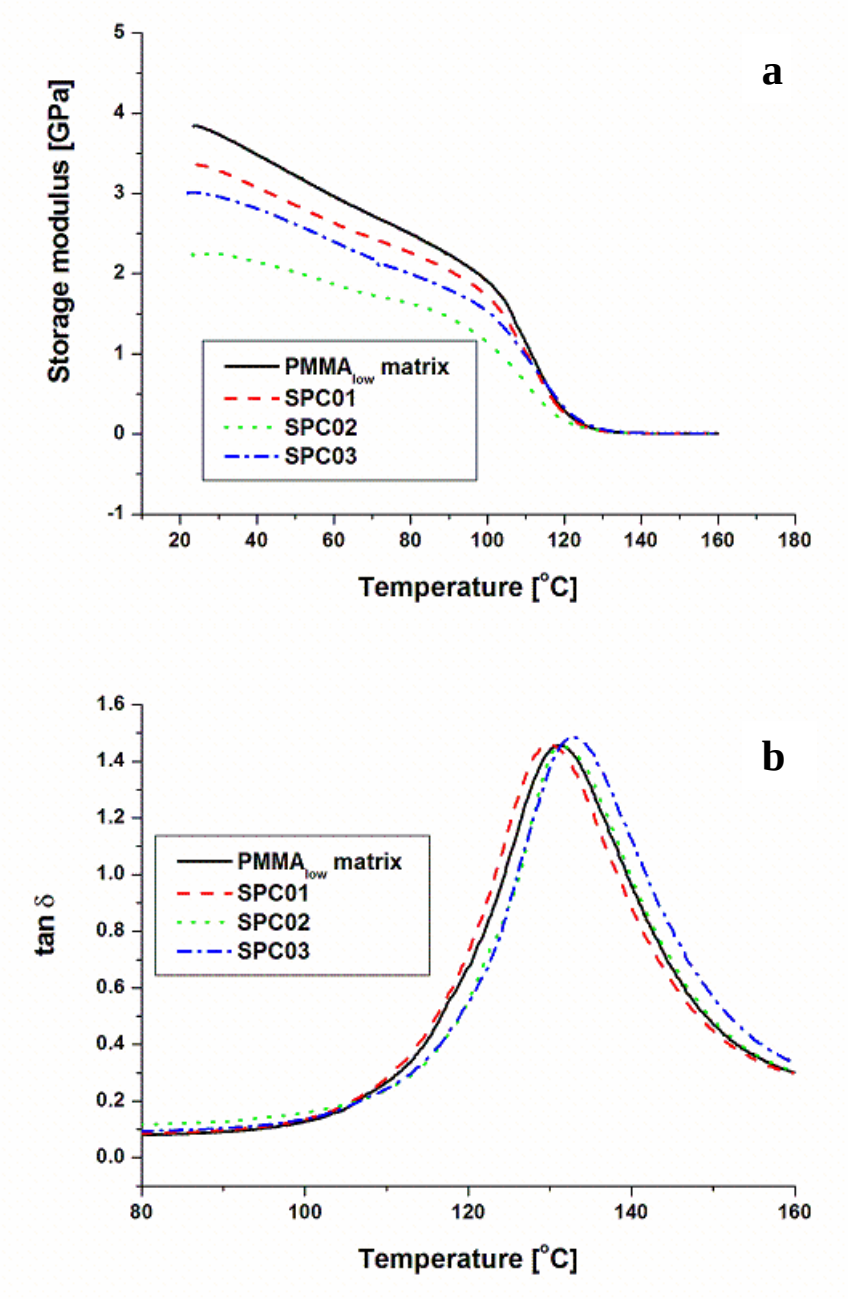

Figure 6.18 Effect of fibre diameter on the (a) storage modulus and (b) tan δ of PMMA composites prepared at 160 °C with 5 wt % nanofibre loading:

As the loading increased to 10 wt% (Figure 6.19(a)), the storage modulus for the composites increased significantly compared to the neat $PMMA_{low}$ matrix at all temperatures. SPC05 and SPC04 (composites with 400-650 and 200-400 nm fibres) seemed to be slightly stiffer than SPC06 (600-900 nm fibres). The effect is even more prominent above the T_g where the material is expected to be soft. The increase in the nanofibre loading to 10 wt% (Figure 6.19(b)) resulted in a significant change of the T_g of the composites as compared to the neat $PMMA_{low}$ matrix. The T_g of the composites shifted to higher temperatures as compared to the $PMMA_{low}$ matrix. This is an indication of the positive reinforcing effect of the nanofibres as it is suspected that not all of the nanofibres have melted in this instance.

The loss modulus for the composites with 5 wt% nanofibre loading (Figure 6.20(a)) is lower than that of the neat $PMMA_{low}$ matrix. As the fibre loading increased to 10 wt% (Figure 6.20(b)), the loss modulus for the composites increased and shifted to higher temperatures compared to the neat $PMMA_{low}$ matrix with the 200-400 and 400-650 nm fibre reinforced composites being slightly higher, though not significant, than the other composite.

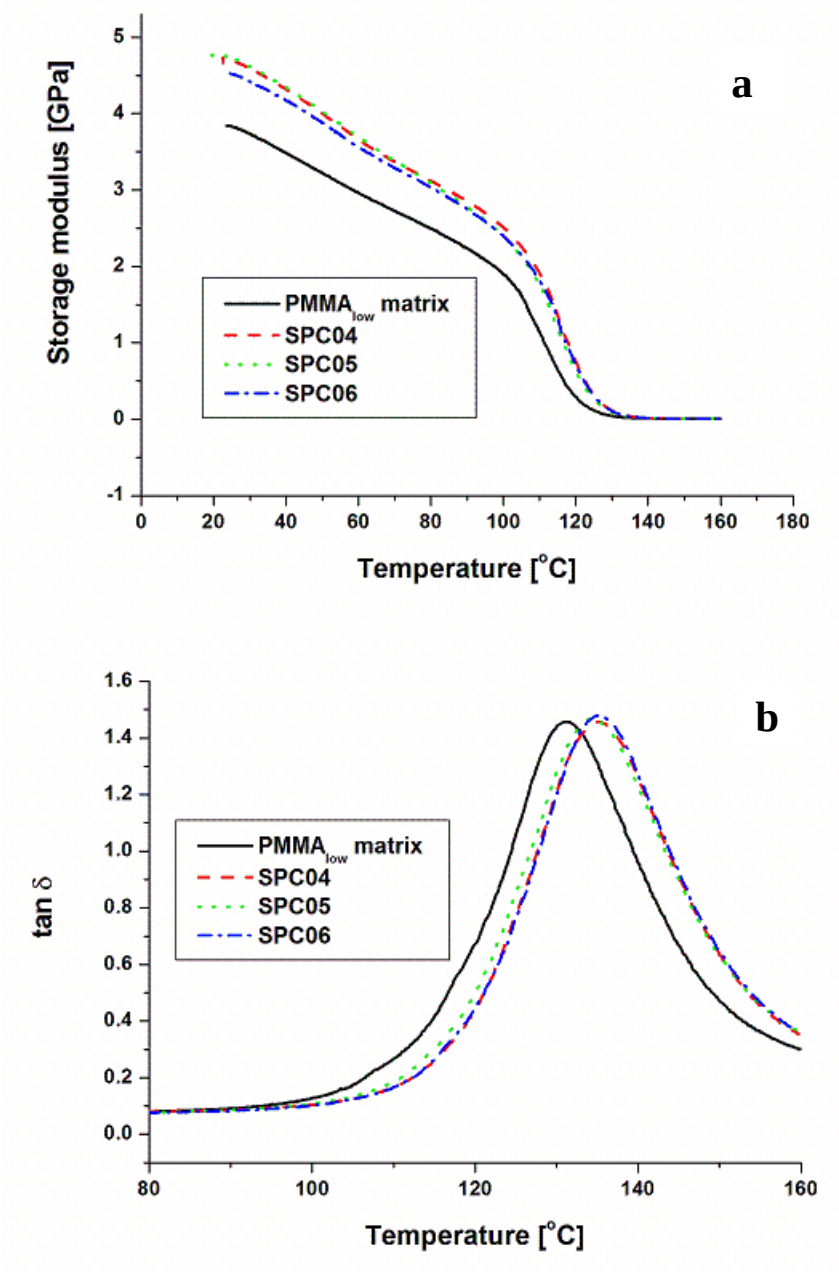

Figure 6.19 Effect of fibre diameter on the (a) storage modulus and (b) tan δ of PMMA composites prepared at 160 °C with 10 wt % nanofibre loading

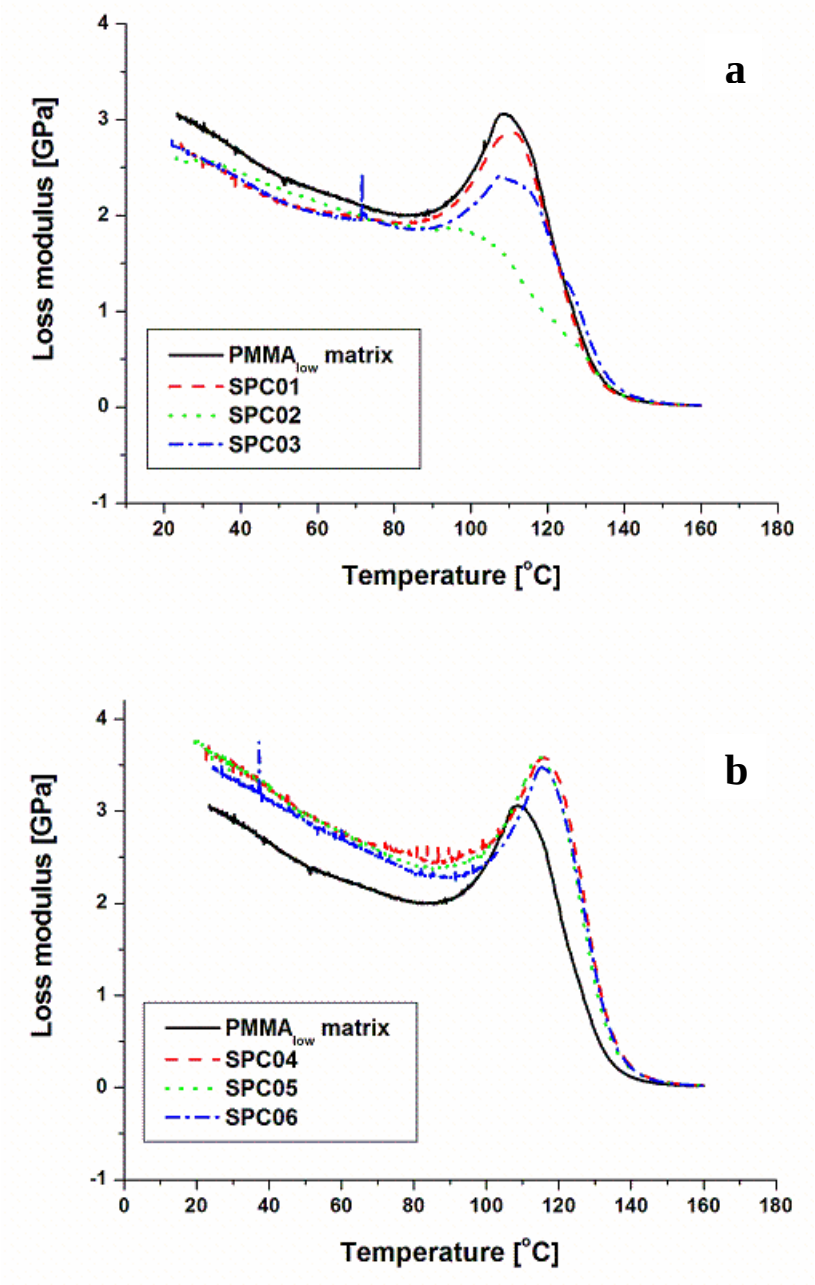

Figure 6.20 Effect of fibre diameter on the loss modulus of PMMA composites prepared at 160 °C with (a) 5 wt% and (b) 10 wt % nanofibre loading

6.2.3 Thermogravimetric analysis of PMMA single polymer composites processed at 150 °C

6.2.3.1 Effect of nanofibre diameter at 150 °C with 5 and 10 wt % loading

Figure 6.21 shows the TGA curves of the neat $PMMA_{low}$ matrix and composites with varying nanofibre diameters ranging from 200 to 900 nm. Figure 6.21(a) shows the composites prepared at 150 °C with 5 wt% nanofibre loading. SPC01, the composite reinforced with the smaller fibre diameter (200-400 nm), seemed to be more thermally stable as compared to the neat $PMMA_{low}$ matrix, SPC02 and SPC03. SPC02 and SPC03 exhibit the same thermal decomposition behaviour and is slightly less thermally stable than the neat $PMMA_{low}$ matrix. The TGA curves for the 10 wt% nanofibre reinforced PMMA composites are shown in Figure 6.21(b). It is apparent that the slope of mass loss (%) is the same for all the nanofibre diameter reinforced composites. However, the onset of degradation temperature for SPC03 and the neat $PMMA_{low}$ matrix are higher than that of SPC01 and SPC02, although not significantly so.

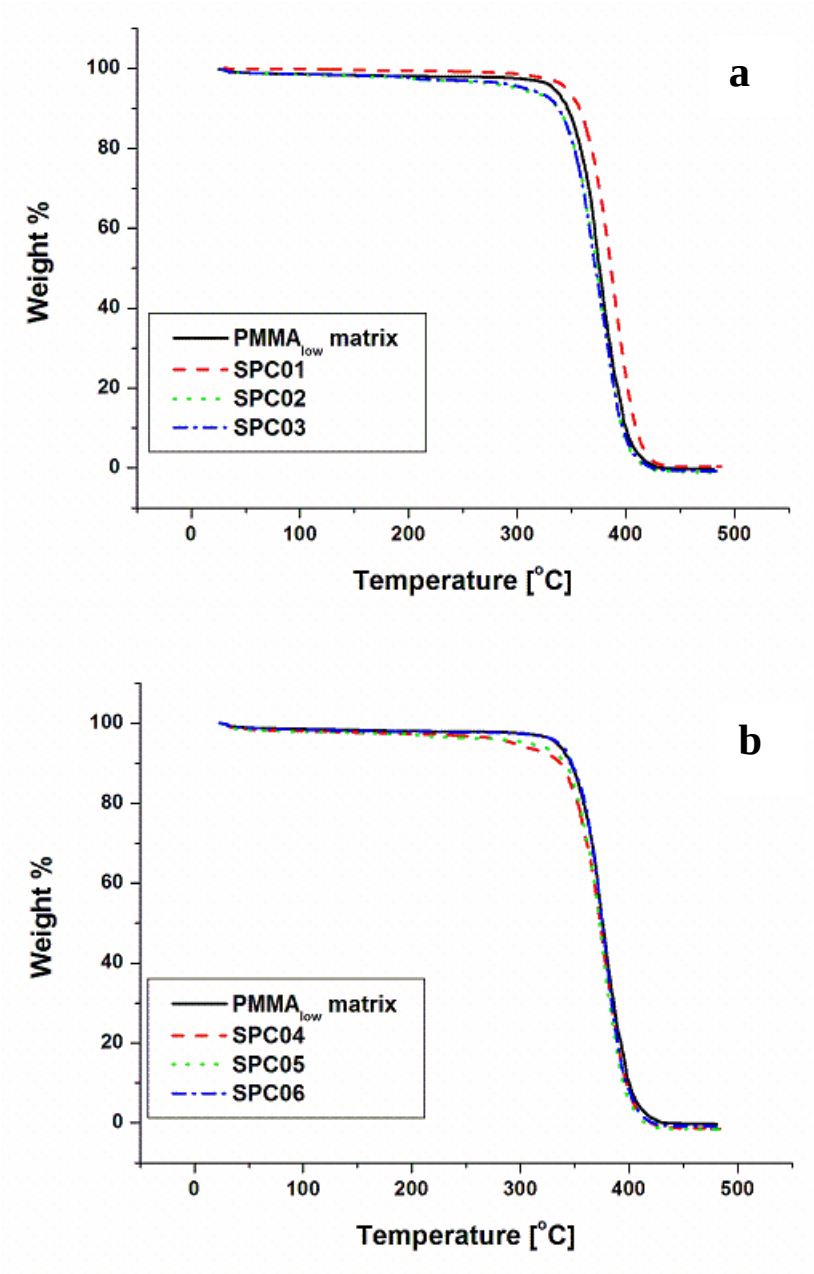

Figure 6.21 Effect of nanofibre diameter with (a) 5 wt% and (b) 10 wt % nanofibre loading for the composites processed at 150 °C.

6.2.3.2 Effect of nanofibre loading at 150 °C with 5 and 10 wt % loading

Figures 6.22 to 6.24 show the TGA curves for electrospun $PMMA_{high}$ nanofibres (with varying diameters), the $PMMA_{low}$ matrix and the different nanofibre reinforced PMMA single polymer composites. The TGA curves for the $PMMA_{high}$ nanofibres show three degradation steps. The first degradation between 56 and 124 °C is due to the decomposition

of relatively weak head-to-head linkages, impurities and trapped solvent. The second degradation between 217 and 334 °C is due to the degradation of the chain-ends of the PMMA and the third is due to the decomposition of the PMMA main chain (random scission of the polymer chains) [5]. $PMMA_{high}$ nanofibres exhibit lower thermal stability as compared to the $PMMA_{low}$ matrix and the corresponding composites. Evidently, the thermal degradation for the $PMMA_{low}$ matrix and the composites is the same. They all show a single degradation step indicating the main chain decomposition (random scission of the polymer chains). For the 200-400 nm fibre reinforced PMMA composites (Figure 6.22), the thermal stability of the $PMMA_{low}$ matrix decreased with increasing PMMA nanofibre loading (5 to 10 wt%). However, the 5 wt% nanofibre loading showed to be more thermally stable than the $PMMA_{low}$ matrix and the 10 wt% nanofibre loading. The decrease in thermal stability is probably the result of the lower thermal stability of the $PMMA_{high}$ nanofibres.

For the 400-650 nm fibre reinforced PMMA composites (Figure 6.23), the $PMMA_{low}$ matrix degrades at a higher temperature than the corresponding composites indicating that the thermal stability of the neat $PMMA_{low}$ is unaffected by the composites formation at different nanofibre loadings. Similarly, the thermal stability of the 600-900 nm reinforced PMMA composites (Figure 6.24) is also unaffected by the composites formation with different nanofibre loadings. Moreover, the 5 wt% nanofibre loading is thermally less stable as compared to the neat $PMMA_{low}$ and the 10 wt% nanofibre loading. This is contrary to what was observed for the 200-400 nm fibre reinforced composites. This behaviour is possibly the result of the higher nanofibre diameter. The decrease in thermal stability is probably the result of the lower thermal stability of the $PMMA_{high}$ nanofibres.

Therefore, it is obvious that the increase in PMMA nanofibre content from 5 to 10 wt% does not seem to increase the thermal stability of the composites. The PMMA nanofibres seem to enhance the degradation of the PMMA matrix. Another phenomenon might be that the nanofibres are not good insulators and mass-transport barriers to the volatile products generated during decomposition [6].

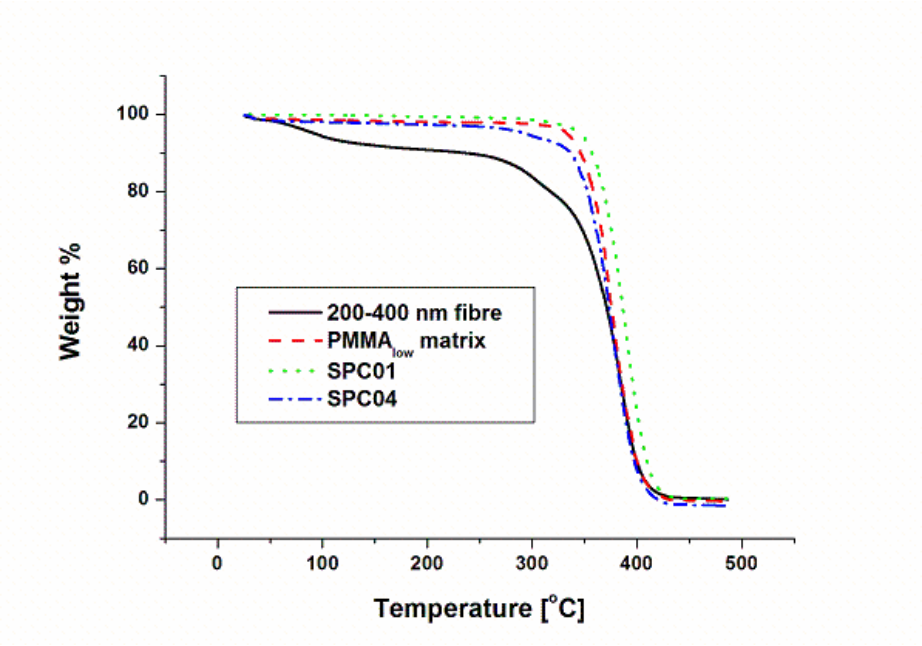

Figure 6.22 Effect of nanofibre loading on the mass loss of PMMA composites prepared at 150 °C. Nanofibre diameter: 200-400 nm.

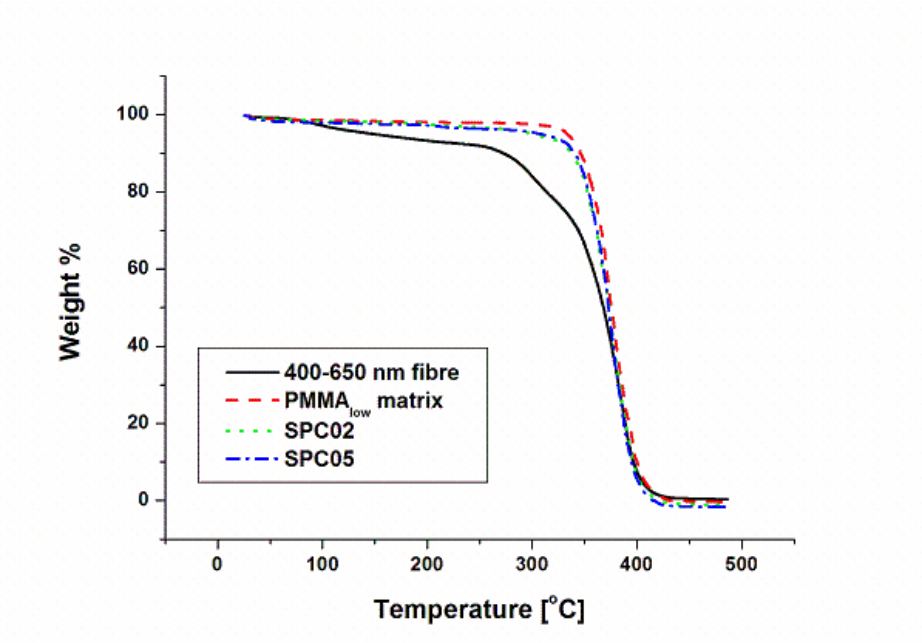

Figure 6.23 Effect of nanofibre loading on the mass loss of PMMA composites prepared at 150 °C. Nanofibre diameter: 400-650 nm.

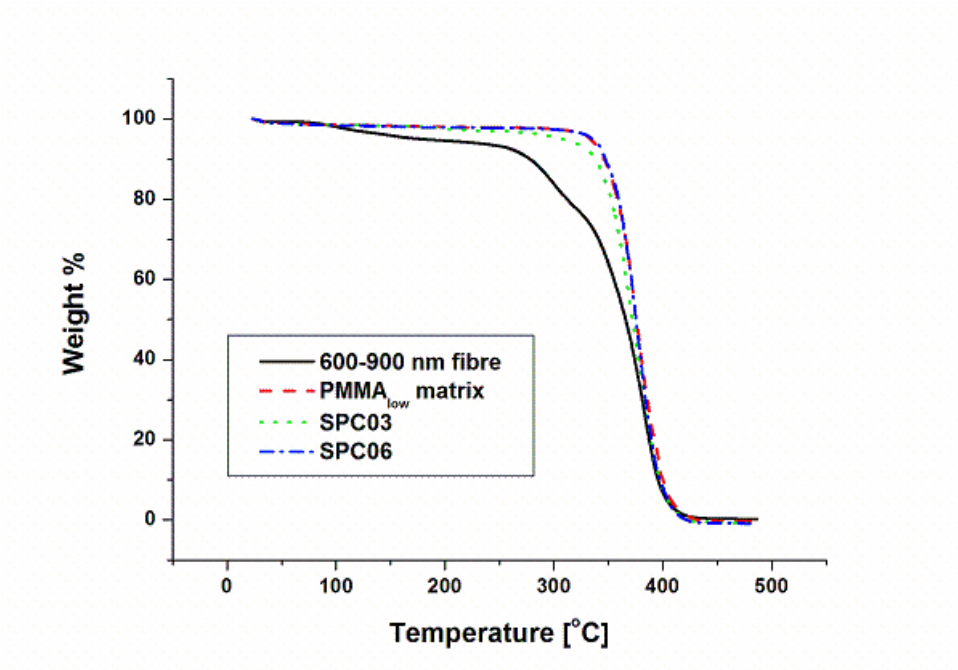

Figure 6.24 Effect of nanofibre loading on the mass loss of PMMA composites prepared at at 150 °C. Nanofibre diameter: 600-900 nm

6.2.4 Thermogravimetric analysis of PMMA single polymer composites processed at 140 and 160 °C

6.2.4.1 Effect of nanofibre diameter at 140 °C with 5 and 10 wt% loading

Figure 6.25 shows the TGA curves of the neat $PMMA_{low}$ matrix and the composites reinforced with different nanofibre diameters at 5 wt% and 10 wt% nanofibre loading. The composites were prepared at 140 °C with 5 and 10 wt % nanofibre loading (Figures 6.25(a) and 6.25(b)). The TGA curve for the composite with 5 wt% nanofibre loading shows that the neat $PMMA_{low}$ matrix is more thermally stable compared to the other nanofibre reinforced composites. However, the 200-400 nm reinforced composite exhibits a higher onset temperature of degradation than the 400-650 and the 600-900 nm reinforced composites, which appear to have similar onset of degradation temperatures. Figure 6.25(b) shows the TGA curve of the composite with the 10 wt% nanofibre loading. The neat $PMMA_{low}$ matrix also shows a higher onset of degradation temperature than the different nanofibre reinforced

composites. The onset of degradation temperatures of the composites seemed to be unaffected by the nanofibre diameters.

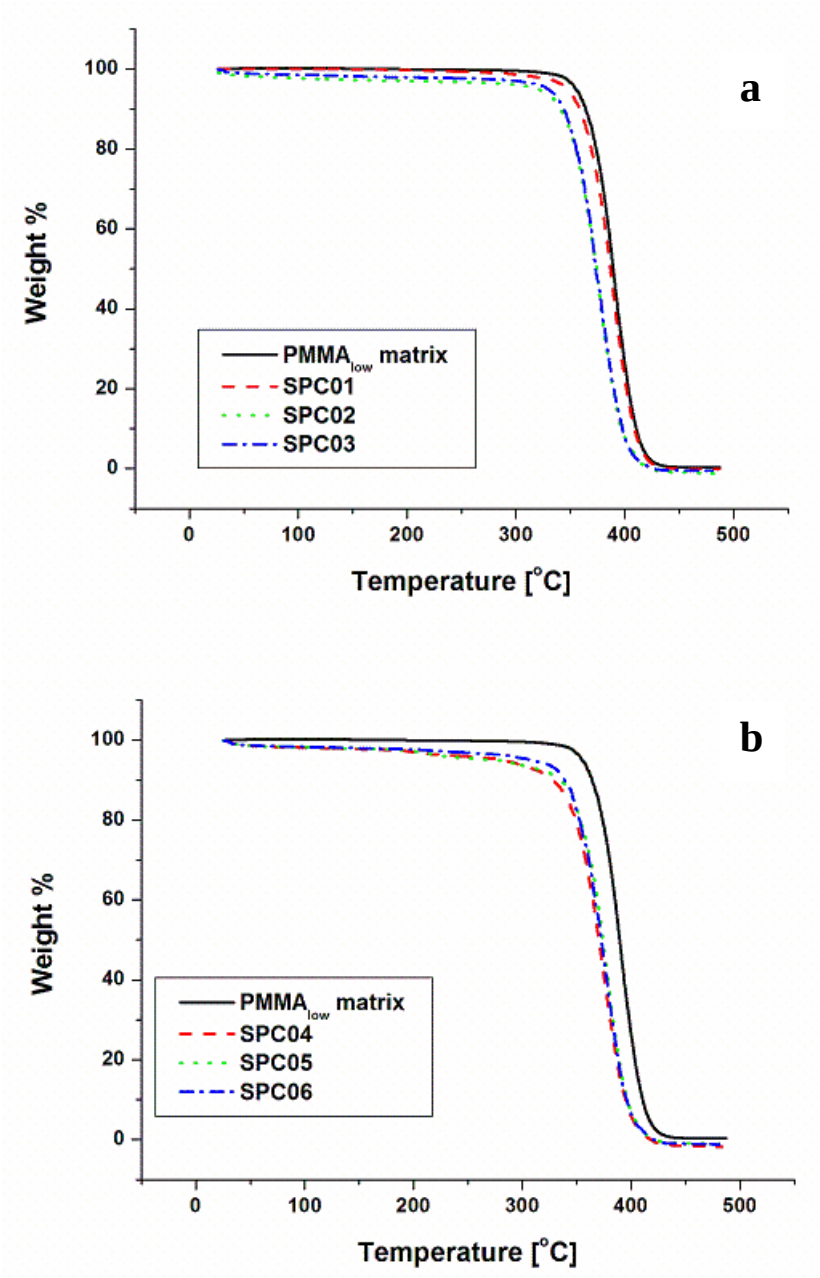

Figure 6.25 Effect of nanofibre diameter on the mass loss of PMMA composites prepared at 140 °C with (a) 5 wt% and (b) 10 wt % loading

6.2.4.2 Effect of nanofibre diameter at 160 °C with 5 and 10 wt% nanofibre loading

Figure 6.26 shows the TGA curves of the neat $PMMA_{low}$ matrix and the different nanofibre reinforced composites prepared at 160 °C with 5 and 10 wt% nanofibre loading. The TGA curve (Figure 6.26(a)) of the composites with the 5 wt% nanofibre loading shows that the 200-400 nm reinforced composites appear to be more thermally stable than all the composites and the neat $PMMA_{low}$ matrix. The neat $PMMA_{low}$ matrix and the 600-900 nm fibre reinforced composites display similar onset of degradation temperatures, which is higher than those of the 400-650 nm fibre reinforced composites. The 10 wt% nanofibre reinforced composites (Figure 6.26(b)) show higher onset of degradation temperatures for the neat $PMMA_{low}$ matrix and the 600-900 nm fibre reinforced composites as compared to those of the 200-400 and 400-650 nm fibre reinforced composites, which degrade at lower temperatures. However, their slope of mass loss (%) is the same. It is apparent that the nanofibre diameter has no influence on the thermal stability of the $PMMA_{low}$ matrix.

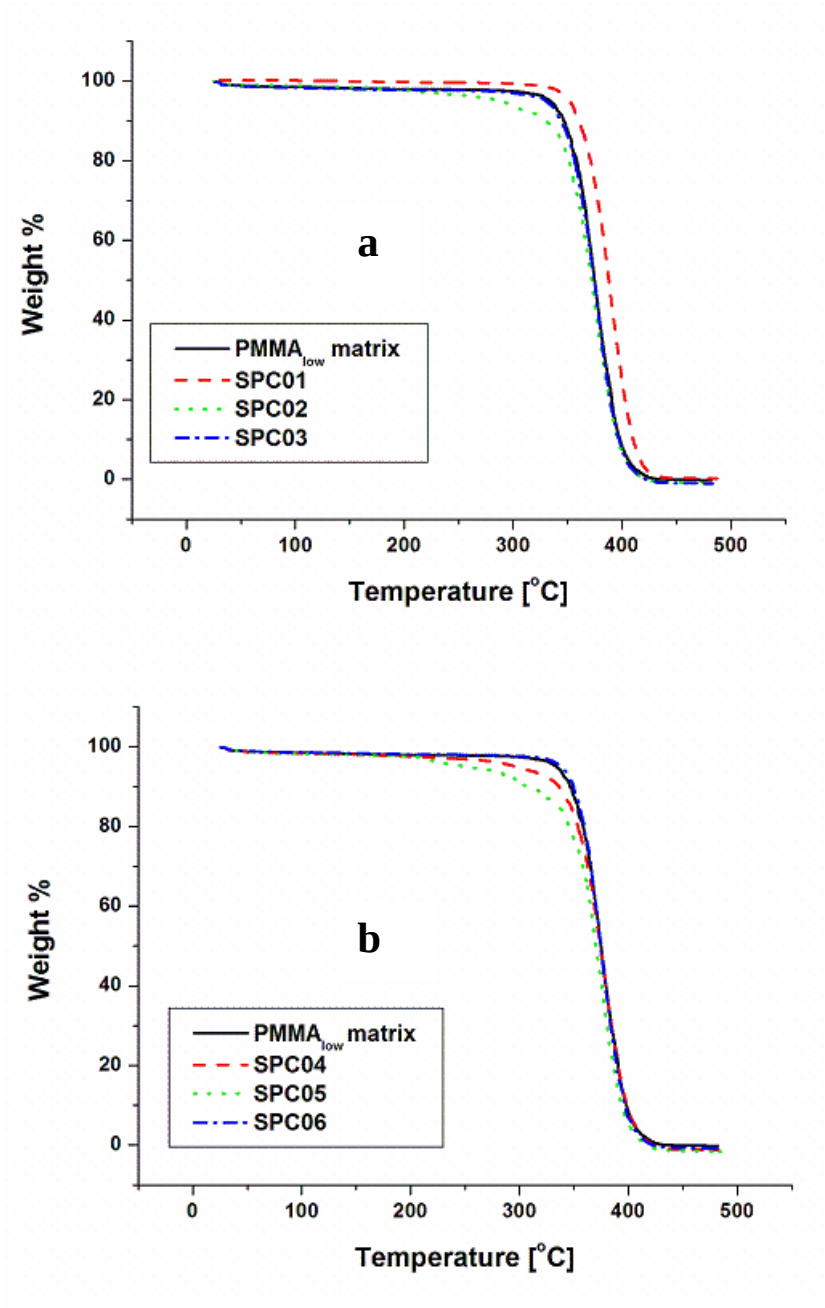

Figure 6.26 Effect of nanofibre diameter on the mass loss of PMMA composites prepared at 160 °C with (a) 5 wt% and (b) 10 wt % loading

6.3 Conclusions

The processing conditions for the preparation of single polymer composites of PMMA were investigated. It was determined that a processing temperature of 150 °C at the stipulated pressures (Chapter 4, Section 4.2.2) was adequate for the preparation of a good composite. A discernible layer of fibres and matrix were observed under these processing conditions. The composites generally showed an improvement in dynamic mechanical properties compared to the neat $PMMA_{low}$ matrix. The increases in the stiffness (up to 83%) and glass transition temperatures (up to 10 °C) of the composites were pronounced in the case of a 10 wt% nanofibre loading. The effect of fibre diameter on the thermal stability of the PMMA single polymer composites was also investigated. It was shown that, for the 5 wt% nanofibre loading, SPC01 (composite with smaller fibre diameter) was more thermally stable than the pure $PMMA_{low}$ matrix and the other composites (SPC02 and SPC03). As the fibre loading increased to 10 wt%, no significant change in the thermal stability was observed. Moreover, a decrease in thermal stability as the nanofibre loading increased was observed. This decrease was a result of the lower thermal stability of the nanofibres.

6.4 References

[1] N.J. Capiati, P.S. Porter. The concept of one polymer composites modelled with high density polyethylene. Journal of Materials Science 1975; 10:1671-1677. DOI: 10.1007/BF00554928

[2] P.J. Hine, R.H. Olley, I.M. Ward. The use of interleaved films for optimising the production and properties of hot compacted, self reinforced polymer composites. Composites science and Technology 2008; 68:1413-1421. DOI:10.1016/j.compscitech.2007.11.003

[3] S. Houshyar, R.A. Shanks, A. Hodzic. The effect of fibre concentration on mechanical and thermal properties of fibre-reinforced polypropylene composites. Journal of Applied Polymer Science 2005; 96:2260-2272. DOI:10.1002/app.20874

[4] M.J. John, R.D. Anandjiwala. Chemical modification of flax reinforced polypropylene composites. Composites Part A: Applied Science and Manufacturing 2009; 40:442-448.

DOI10.1016/j.compositesa.2009.01.007

[5] J.M. HWU, G.J. Jiang, Z.M. Gao, W. Xie, W.P. Pan. The characterization of organic modified clay and clay-filled PMMA nanocomposite. Journal of Applied Polymer Science 2002; 83:1702-1710.
DOI: 10.1002/app.10093

[6] N.P. Cele, S.S. Ray, S.K. Pillai, M. Ndwandwe, S. Nonjola, L. Sikhwivhilu, M.K. Mathe. Carbon nanutubes based nafion composite membranes for fuel cell applications. Fuel Cells 2010; 10:64-71.
DOI: 10.1002/fuce.200900056

Chapter 7

Mechanical properties of single polymer composites of poly(methyl methacrylate)

In this study, electrospun PMMA nanofibres of different diameters were produced by the electrospinning process (Chapter 5) and used as reinforcement. The composites were prepared by the film stacking technique applying a two component approach and the mechanical properties (flexural, tensile and impact) were determined with an Instron mechanical tester. The effect of the nanofibre diameter and loading at a processing temperature of 150 ^{o}C on the mechanical properties of the single polymer composites was investigated. In addition, for comparison purposes, composites were also prepared at 140 and 160 °C. The composite samples are as defined in Table 6.1.

7.1 Mechanical properties of PMMA single polymer composites processed at 150 °C

7.1.1 Flexural strength

Figures 7.1 and 7.2 show the effect of fibre diameter on the flexural strength of the PMMA single polymer composites with different fibre loadings. It can be seen from Figure 7.1 that the flexural strength is the highest for SPC01, while the neat PMMA matrix, SPC02 and SPC03 show similar results. An improvement in flexural strength of 14% as compared to the neat PMMA was observed. The highest strength of the SPC01 is probably the result of the larger surface area and the smaller diameter of the nanofibres. It can be seen from Figure 7.2 that in the case of a 10 wt% fibre loading the composites show higher flexural strengths than the neat PMMA. A maximum improvement in the flexural strength of 44% was obtained. SPC04 exhibited the highest flexural strength, followed by SPC05 (34%) and SPC06 (28%). Once again, the highest improvement in the flexural strength was obtained with the lowest fibre diameter range.

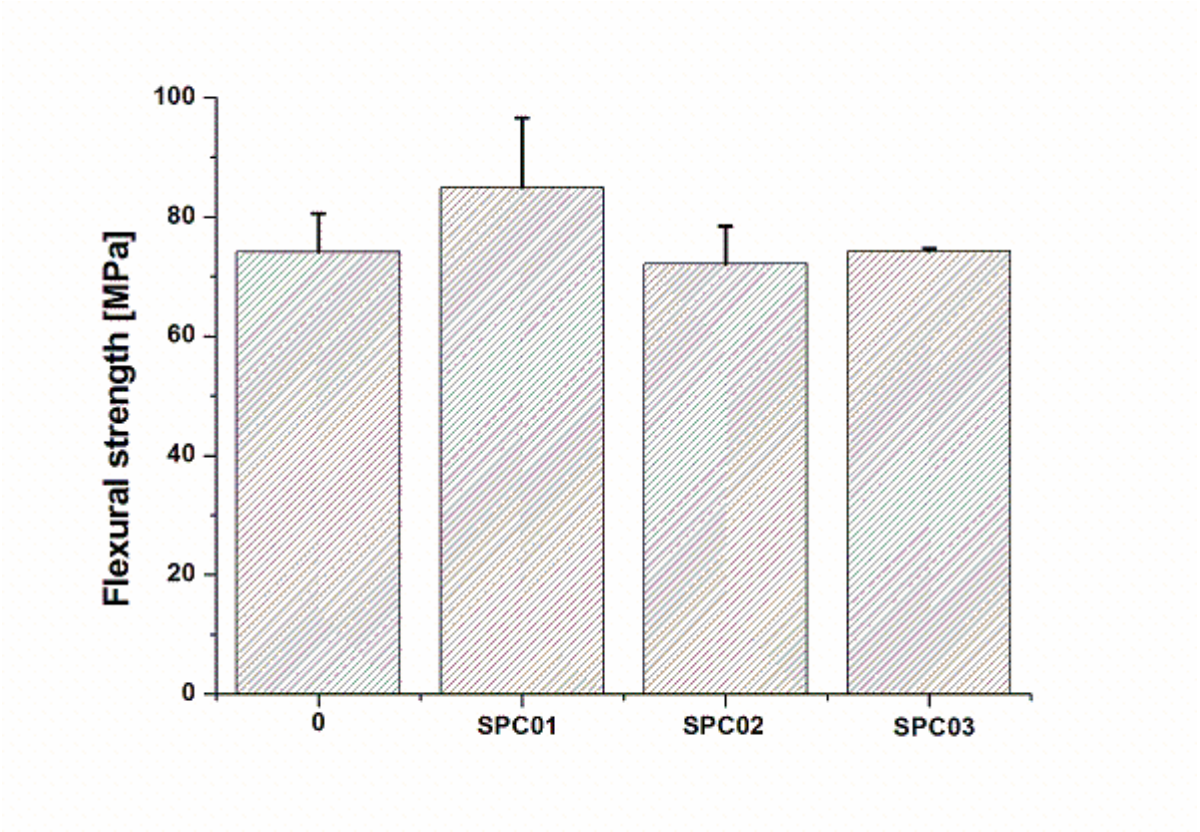

Figure 7.1 Effect of fibre diameter on the flexural strength of PMMA single polymer composites at 5wt % nanofibre loading

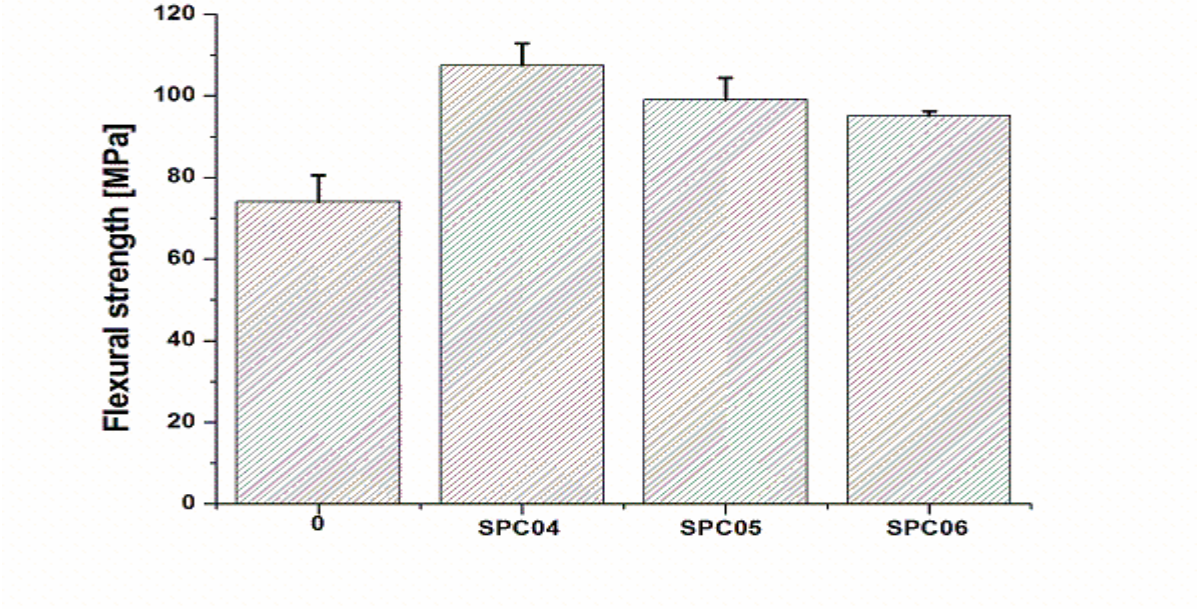

Figure 7.2 Effect of fibre diameter on the flexural strength of PMMA single polymer composites at 10 wt% nanofibre loading

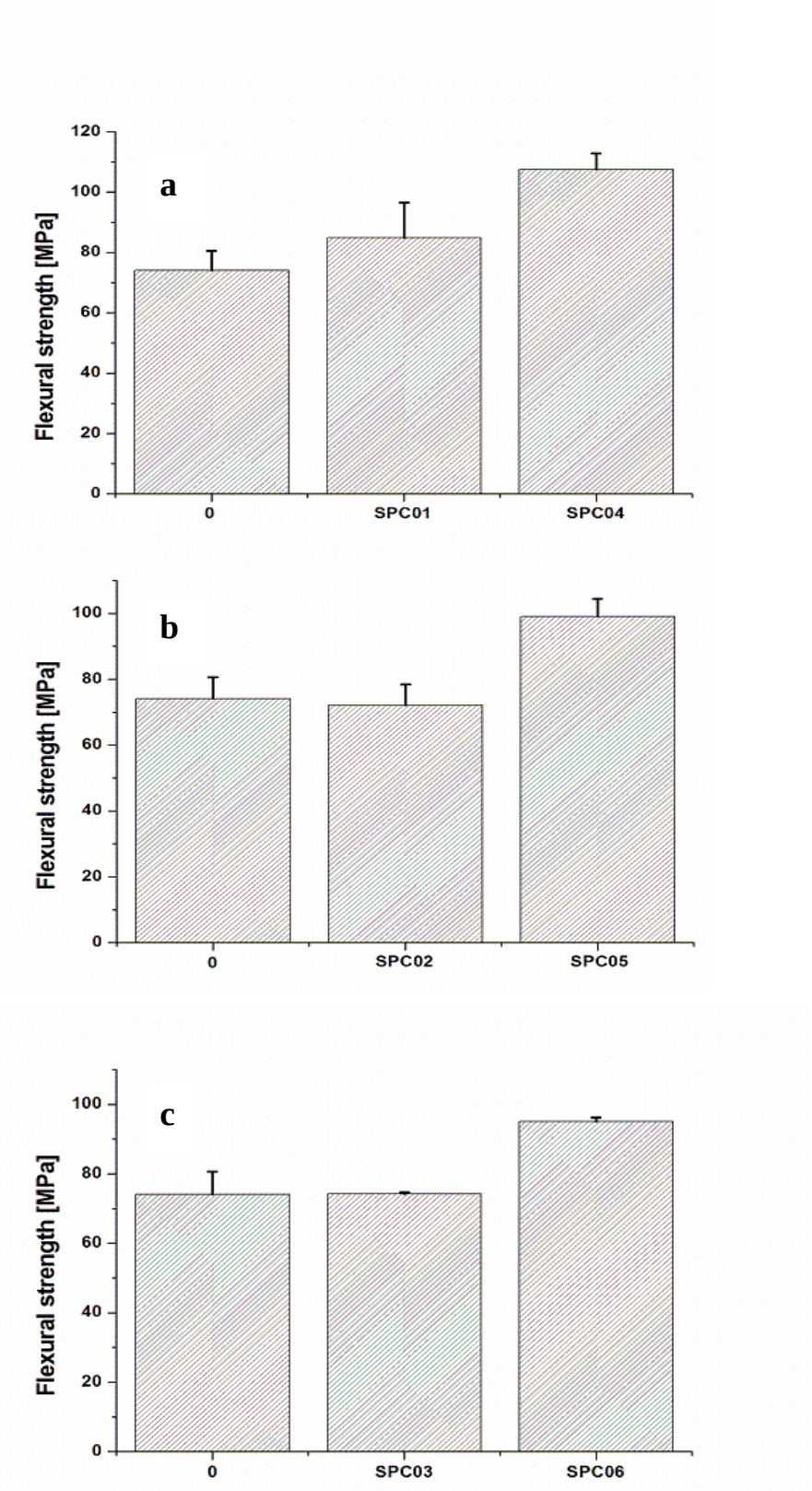

Figure 7.3 Effect of nanofibre loading on the flexural strength of PMMA single polymer composites. Nanofibre diameters: (a) 200-400 nm, (b) 400-650 nm and (c) 600-900 nm

The flexural strength of neat PMMA and nanofibre reinforced PMMA composites as a function of nanofibre loading of 5 and 10 wt% of electrospun PMMA nanofibres processed at 150 °C are presented in Figure 7.3. In all instances, the flexural strength is seen to increase with an increase in nanofibre loading. An improvement in flexural strength of 27% was obtained for SPC04 compared to SPC01. Similarly, SPC05 had 38% improvement in flexural strength compared to SPC02. Furthermore, a 28% improvement was obtained for SPC06 compared to SPC03. This increase in the flexural strength is primarily attributed to the nanofibres allowing efficient stress transfer from the matrix to the fibres. At low fibre loading, the matrix is not restrained by enough fibres and highly localised strains occur in the matrix at low stresses [1]. As the fibre loading is increased to 10 wt%, the stress was more evenly distributed and the composite strength increased.

7.1.2 Flexural modulus

The effect of fibre diameter on the flexural modulus of the PMMA composites with different fibre loadings are shown in Figures 7.4 and 7.5. The flexural moduli essentially remained unchanged for the composites (SPC01, SPC02 and SPC03) compared to the neat PMMA with an increase in nanofibre diameter at a loading of 5 wt%. In the case of the 10 wt% nanofibre loading, the moduli of the composites (SPC04, SPC05 and SPC06) also did not show a significant improvement compared to the neat PMMA. However, for SPC04, the composite reinforced with the lowest diameter nanofibres, a higher flexural modulus than SPC05 and SPC06 was observed.

In general, no meaningful change in the flexural moduli of the composites compared to the neat PMMA with an increase in nanofibre loading was observed (Figures 7.6 to 7.8). In the case of the composites reinforced with the nanofibres of the lowest diameter, SPC01 and SPC04, a slight increase (8%) in the flexural modulus was obtained with an increase in the nanofibre loading. As for SPC02 and SPC05, no considerable change in the flexural moduli was observed. They were, however, slightly higher than that for the neat PMMA. The same trend was observed for SPC03 and SPC06.

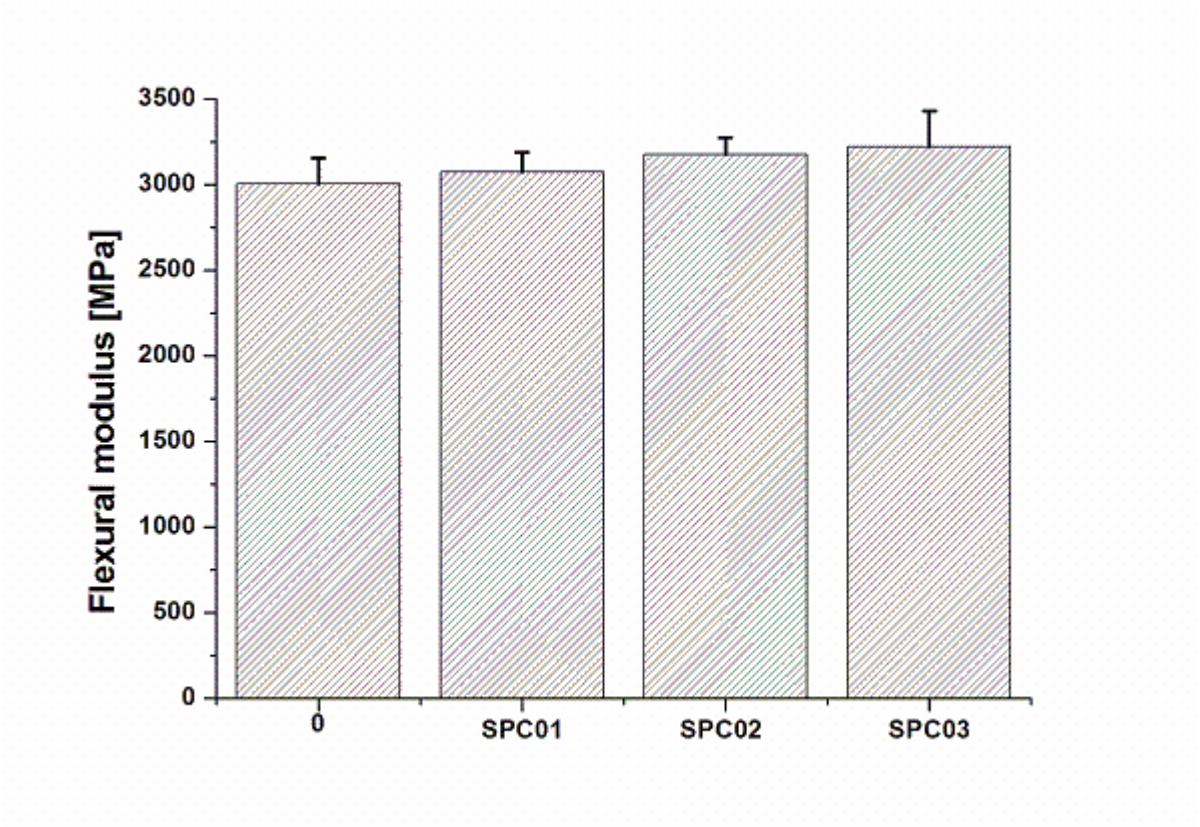

Figure 7.4 Effect of fibre diameter on the flexural modulus of PMMA single polymer composites at 5 wt% nanofibre loading

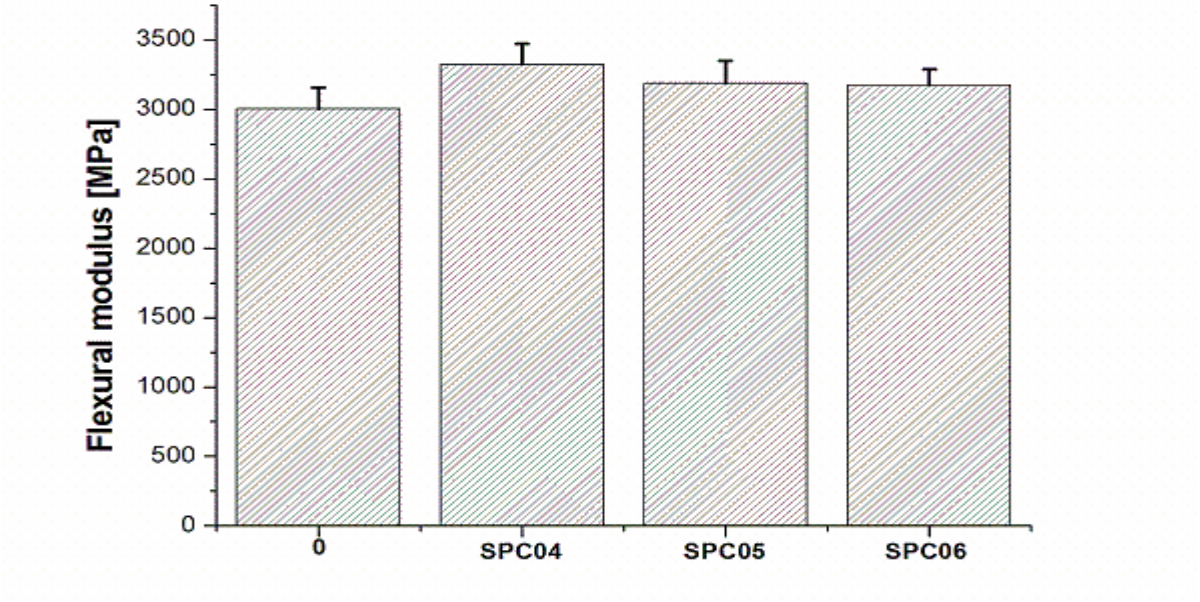

Figure 7.5 Effect of fibre diameter on the flexural modulus of PMMA single polymer composites at 10 wt% nanofibre loading

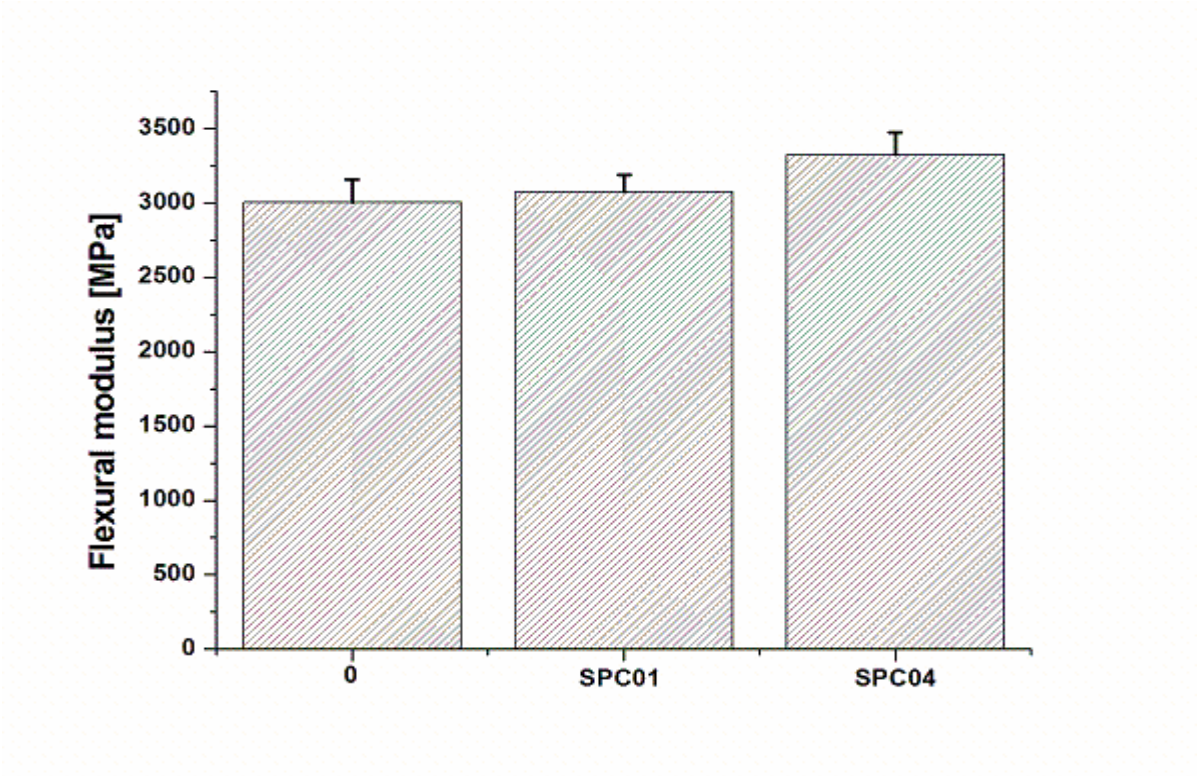

Figure 7.6 Effect of nanofibre loading on PMMA composites at 150 °C. Nanofibre diameter: 200-400 nm

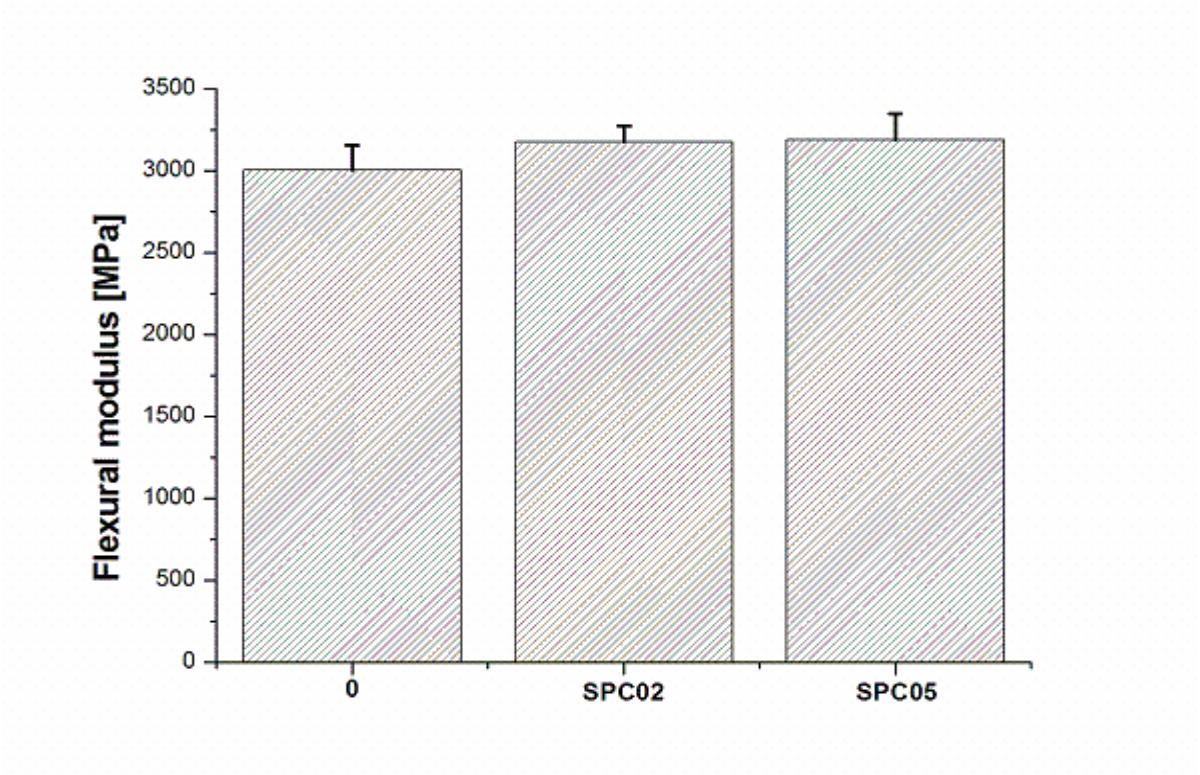

Figure 7.7 Effect of nanofibre loading on PMMA composites at 150 °C. Nanofibre diameter: 400-650 nm

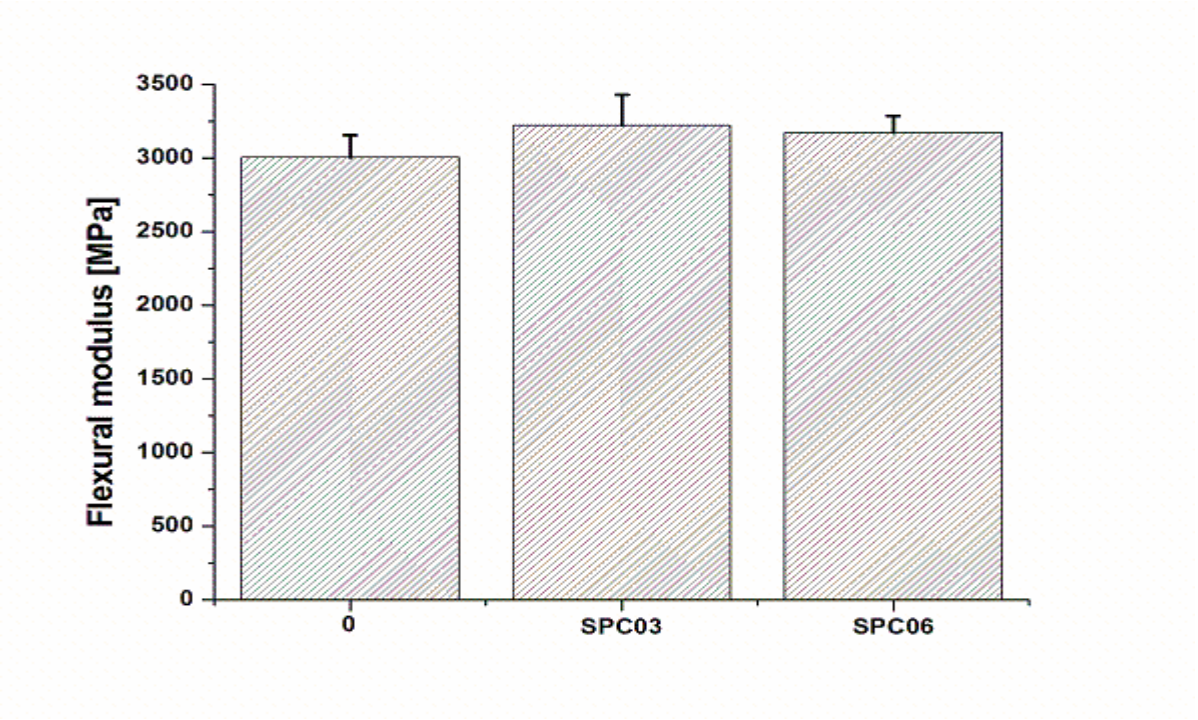

Figure 7.8 Effect of nanofibre loading on PMMA composites at 150 °C. Nanofibre diameter: 600-900 nm

7.1.3 Tensile strength

Figures 7.9 and 7.10 show the effect of nanofibre diameter on the tensile strength of the PMMA composites with different fibre loadings. An unexpected decrease in the tensile strength of the composites compared to that of the neat PMMA was observed as the fibre diameter increased. However, there is no considerable change in the tensile strength of SPC01 and SPC02 compared to that of the PMMA matrix. The tensile strength was the lowest for SPC03, which showed an 18% decrease in tensile strength compared to that of the PMMA matrix. The tensile strength essentially remained unchanged for the composites (SPC04, SPC05 and SPC06) compared to that of the neat PMMA with an increase in nanofibre diameter at a loading of 10 wt%. These results suggest that the investigated nanofibre diameters had no noticeable influence on the tensile strength of the composites prepared at 150 °C.

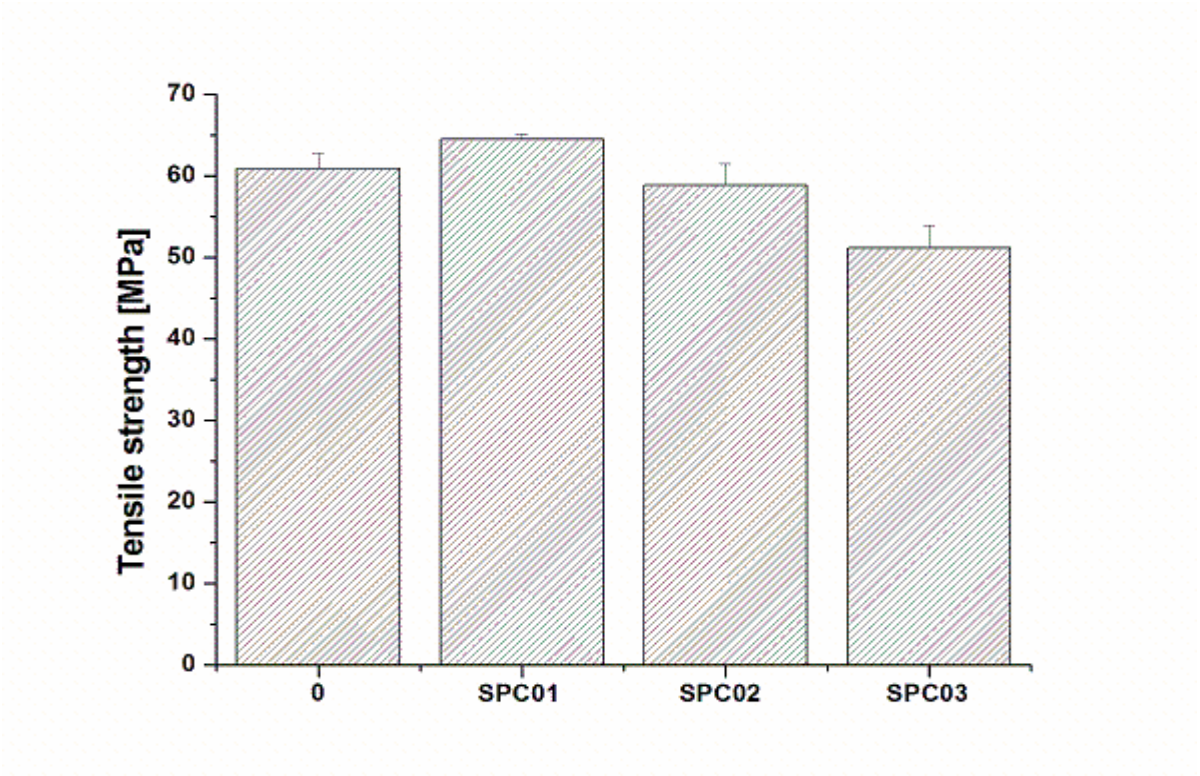

Figure 7.9 Effect of nanofibre diameter on the tensile strength of PMMA single polymer composites at 5 wt% nanofibre loading

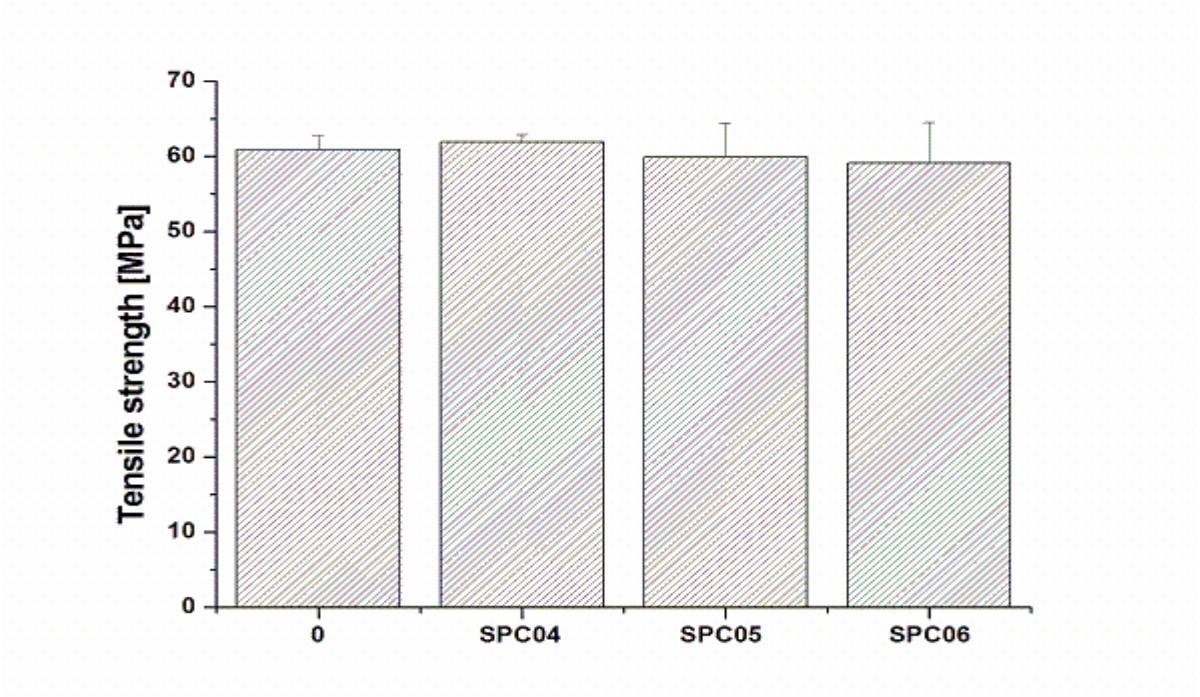

Figure 7.10 Effect of fibre diameter on the tensile strength of PMMA single polymer composites at 10 wt% nanofibre loading

The tensile strength of the neat PMMA and the composites as a function of nanofibre loading is shown in Figures 7.11 to 7.13. For the composites reinforced with the nanofibres of smallest diameters, SPC01 and SPC04, no significant change in the tensile strength was observed compared to that of the PMMA matrix. The same trend was observed for SPC02 and SPC05. In the case of the composites reinforced with the nanofibres of highest diameters, SPC03 and SPC06, no noticeable change in the tensile strength was observed. However, the SPC03 showed a much lower tensile strength.

In general, the tensile strength is not significantly influenced by the investigated nanofibre diameters and loadings. This phenomenon might have been caused by the non-woven character of the electrospun PMMA nanofibres, as they were not aligned in the tensile stress direction to carry most of the load. Another possible reason is that their tensile properties are lower than that of the pure PMMA matrix. The variation in the composites' tensile results is possibly as a result of the tensile testing samples being taken from different sections along the thickness of the moulded composites.

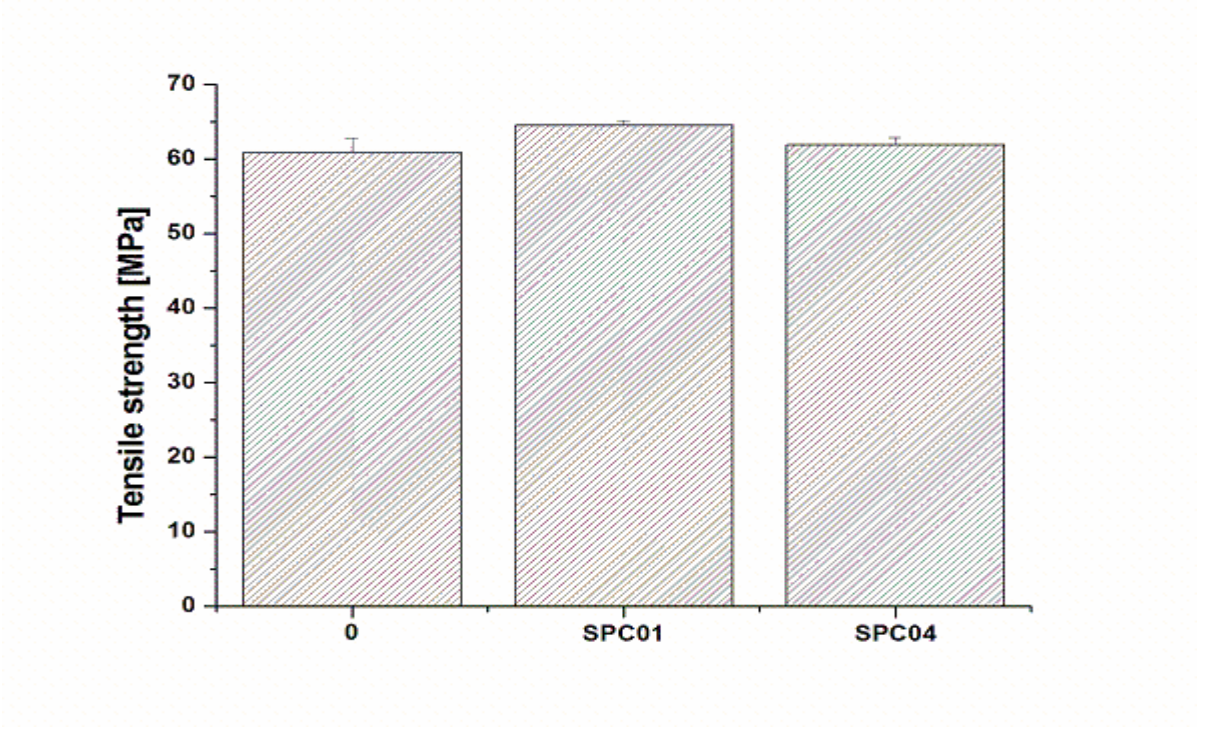

Figure 7.11 Effect of nanofibre loading on PMMA composites at 150 °C. Nanofibre diameter: 200-400 nm

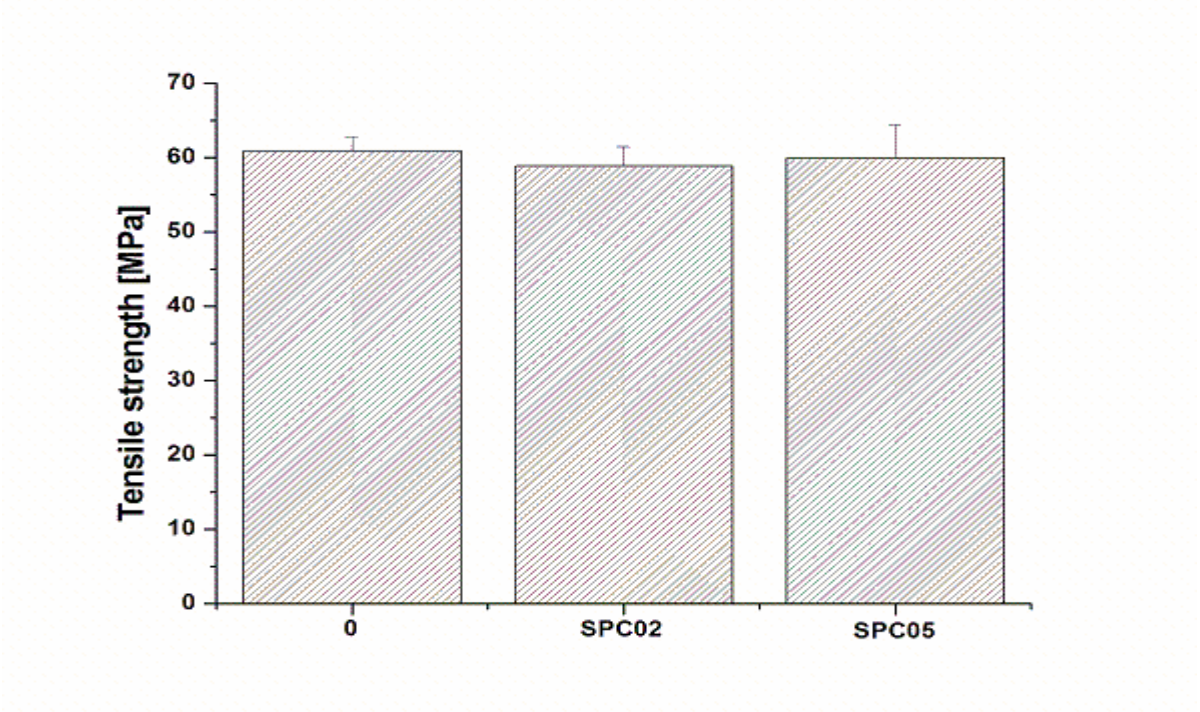

Figure 7.12 Effect of nanofibre loading on PMMA composites at 150 °C. Nanofibre diameter: 400-650 nm

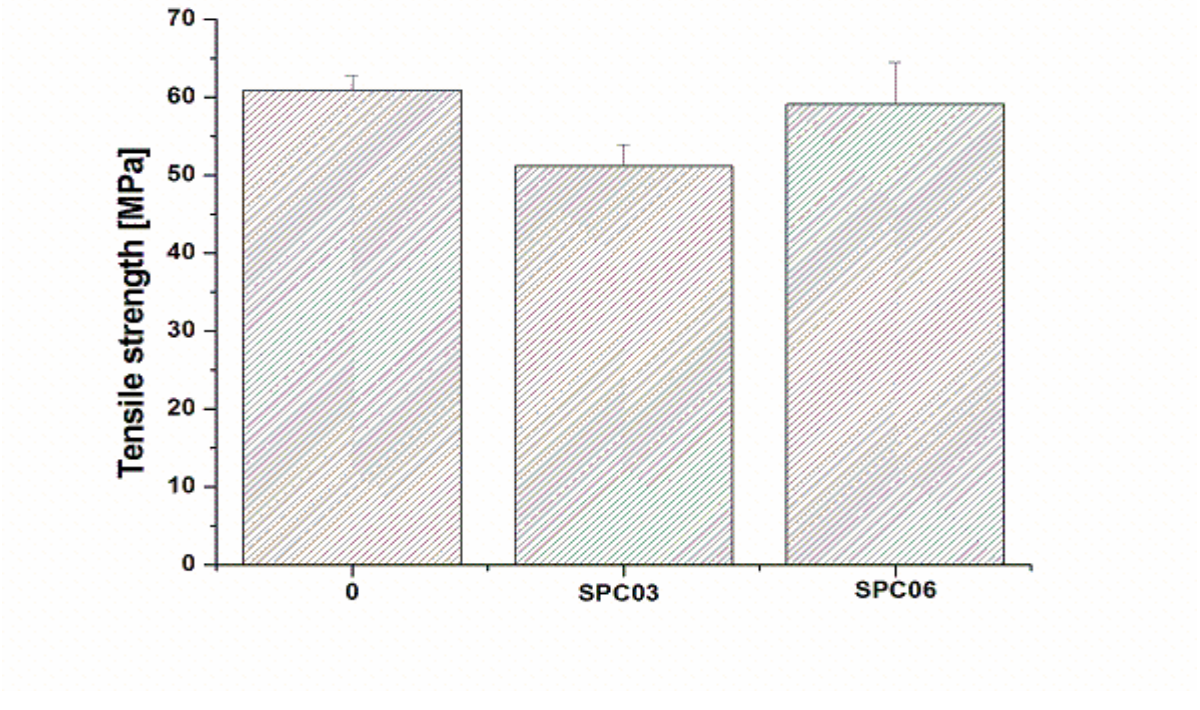

Figure 7.13 Effect of nanofibre loading on PMMA composites at 150 °C. Nanofibre diameter: 600-900 nm

7.1.4 Tensile modulus

Figures 7.14 and 7.15 show the effect of nanofibre diameter on the tensile modulus of the composites with different nanofibre loading. It is clear that there is no significant difference in the tensile moduli of the neat PMMA matrix and the composites at a 5 wt% nanofibre loading. Similarly, for the 10 wt% nanofibre loading, no significant change in the tensile moduli of the PMMA matrix and the nanofibre reinforced composites were observed. The results indicate that the nanofibre diameter does not influence the tensile modulus for the same reasons as mentioned above.

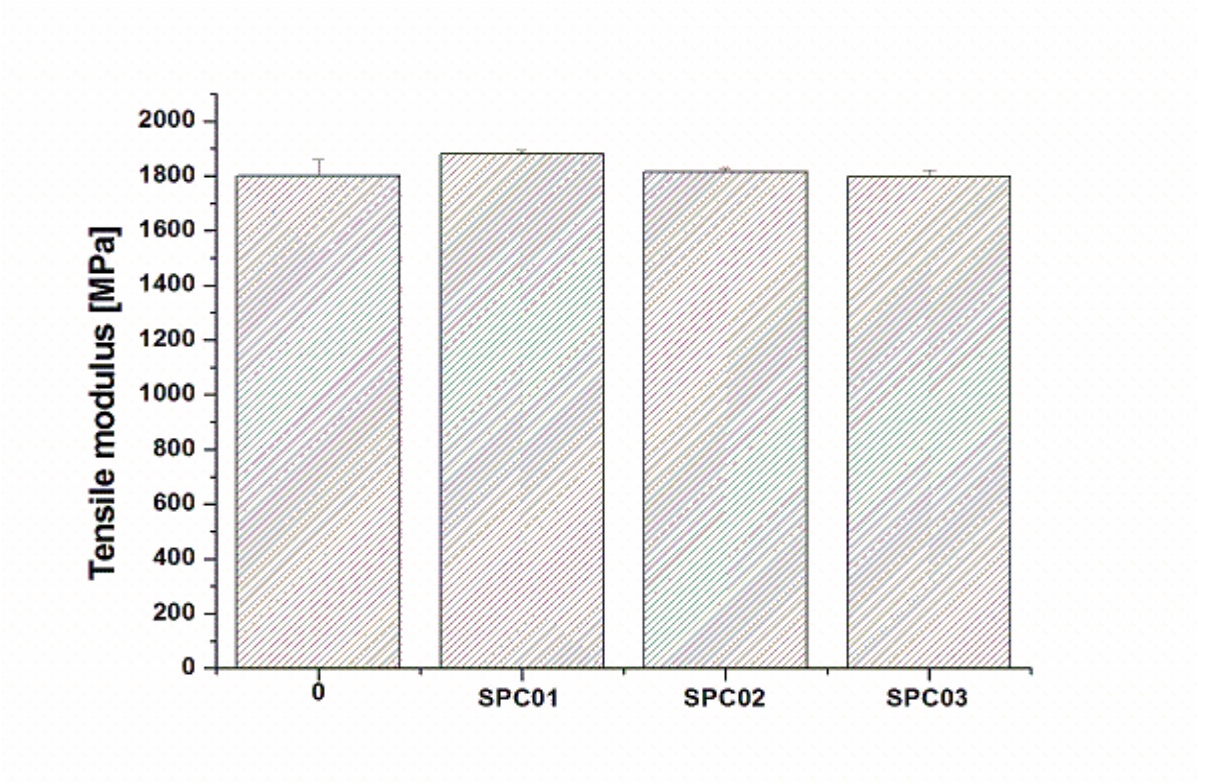

Figure 7.14 Effect of fibre diameter on the tensile modulus of PMMA single polymer composites at 5 wt% nanofibre loading

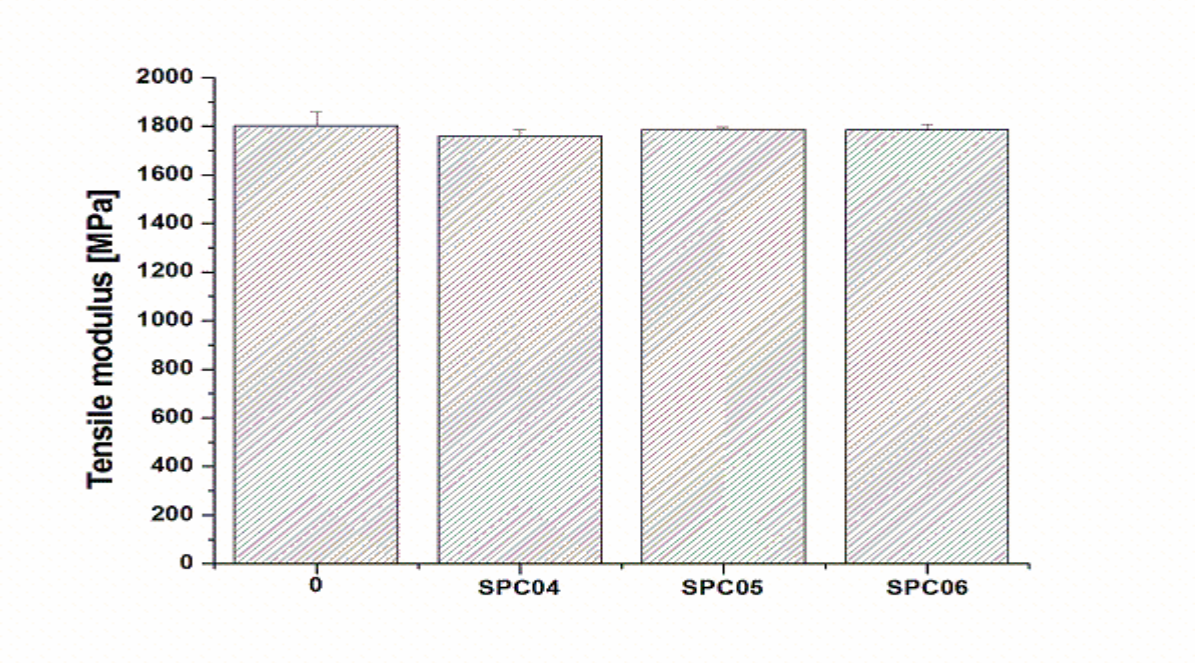

Figure 7.15 Effect of fibre diameter on the tensile modulus of PMMA single polymer composites at 10 wt % nanofibre loading

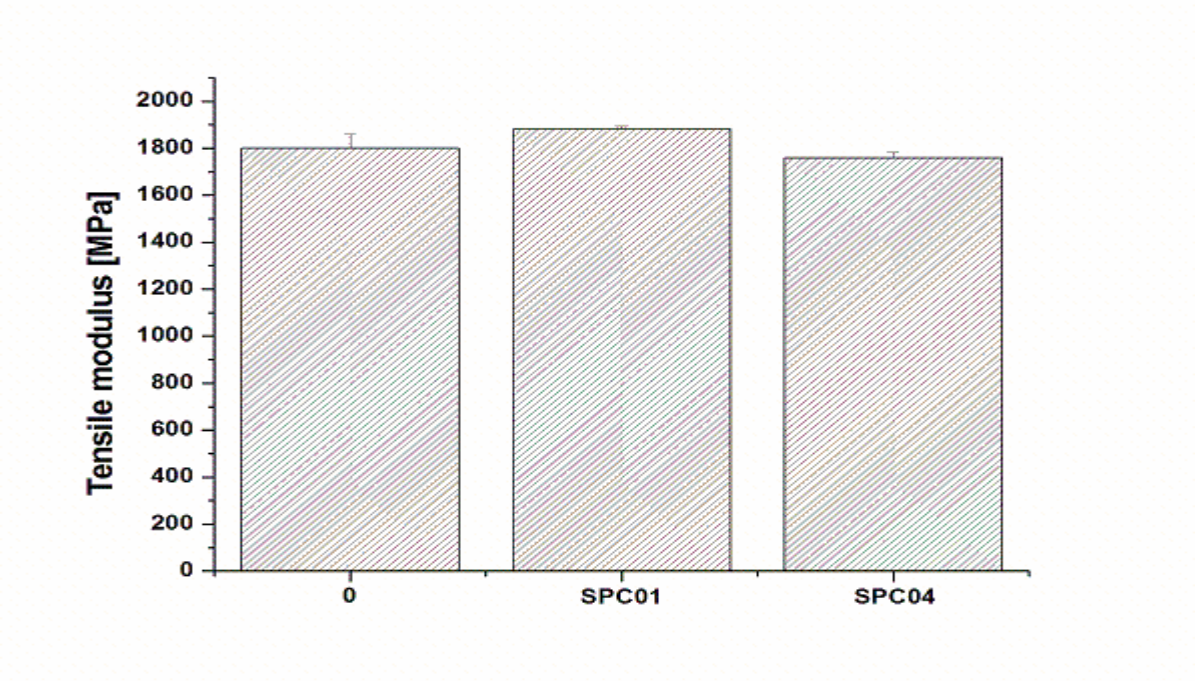

Figure 7.16 Effect of nanofibre loading on PMMA composites at 150 °C. Nanofibre diameter: 200-400 nm

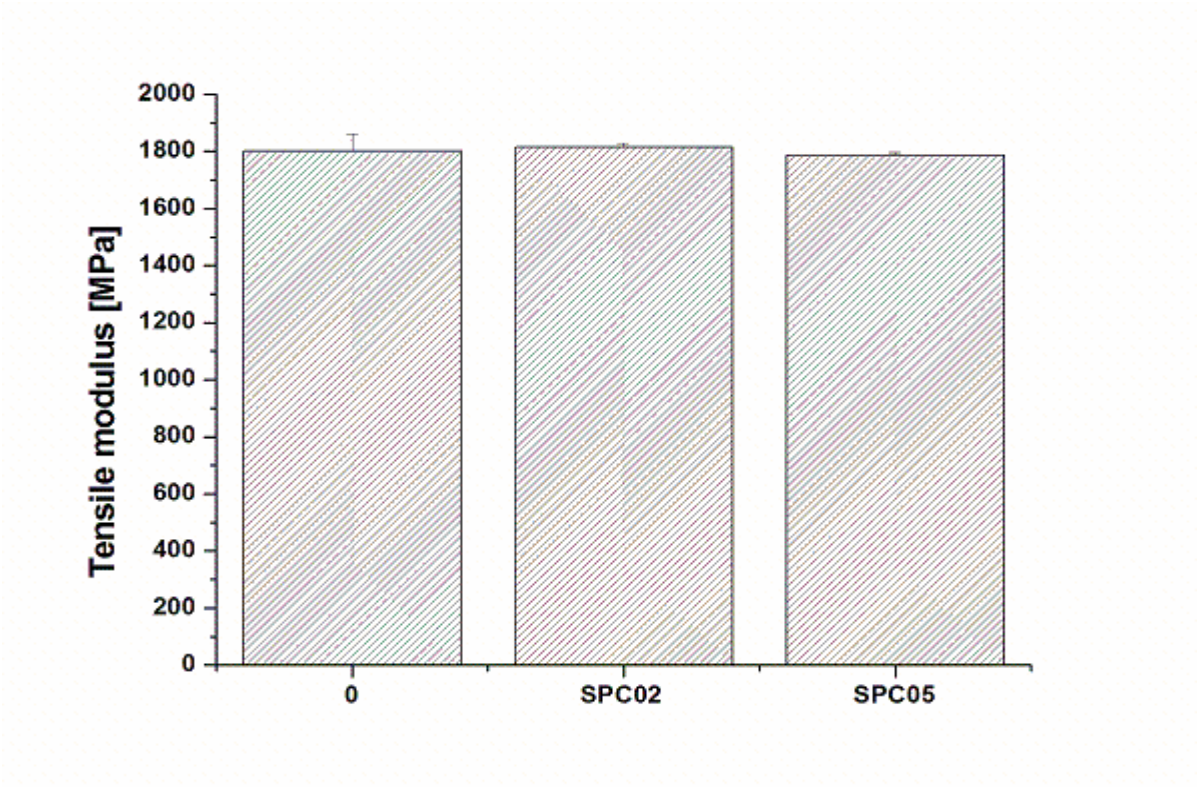

Figure 7.17 Effect of nanofibre loading on PMMA composites at 150 °C. Nanofibre diameter: 400-650 nm

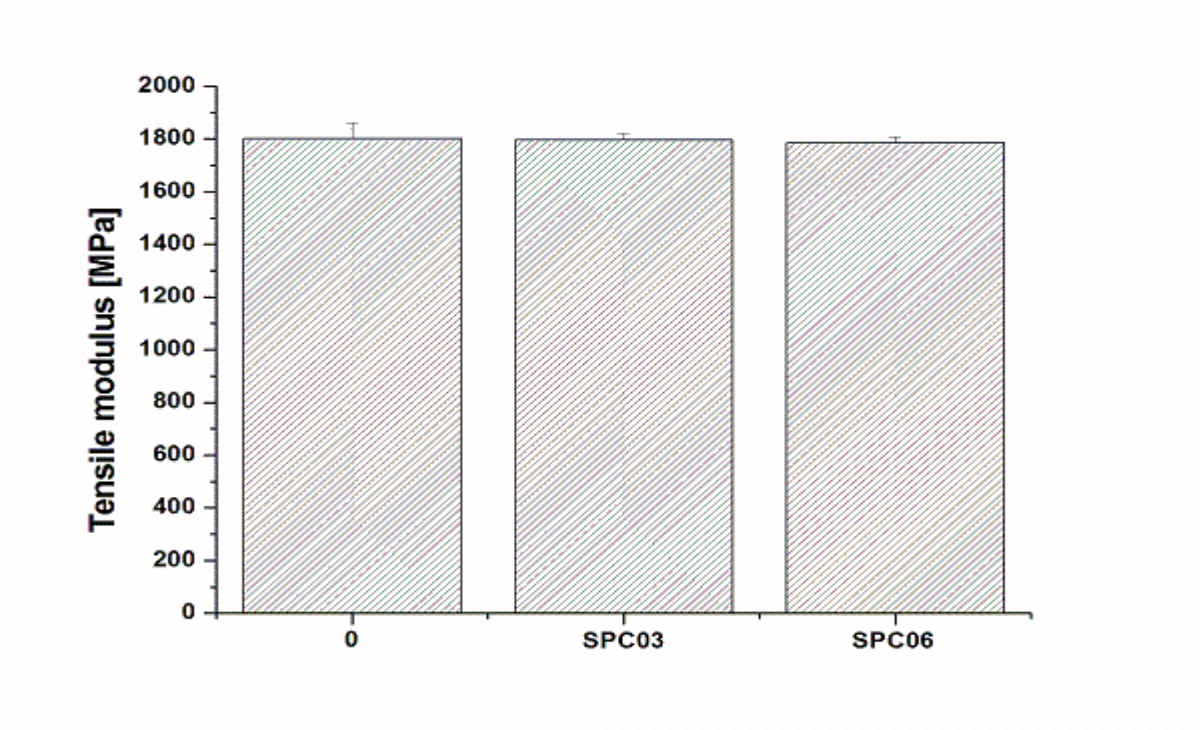

Figure 7.18 Effect of nanofibre loading on PMMA composites at 150 °C. Nanofibre diameter: 600-900 nm

Figures 7.16 to 7.18 show the tensile moduli of the neat PMMA and the composites as a function of nanofibre loading. There is no meaningful change in the tensile moduli of SPC01 and SPC04 compared to that of the neat PMMA. Simillarly, SPC02, SPC05, SPC03 and SPC06 showed no change in the tensile moduli.

It is obvious that the tensile modulus, which is an indication of the load bearing capacity [2], did not change upon incorporation of PMMA nanofibres. This suggests that the load was carried mainly by the matrix.

7.1.5 Impact strength

The variation of impact strength of the PMMA composites with different fibre loadings is presented in Figures 7.19 and 7.20. There is no significant change in the impact strength of SPC02 and SPC03 compared to that of the neat PMMA. However, SPC01 shows a 50% improvement in the impact strength compared to that of the neat PMMA. This is probably the result of the larger specific surface area of the nanofibres. In the case of the 10 wt% nanofibre loading, the impact strength of the composites (SPC04, SPC05 and SPC06) improved significantly. An improvement in impact strength of 76% was observed SPC04 compared to that of the neat PMMA. SPC05 and SPC06 achieved 54% and 69% improvement in impact strength, respectively. Again, the highest impact strength was obtained for the lowest fibre diameter range.

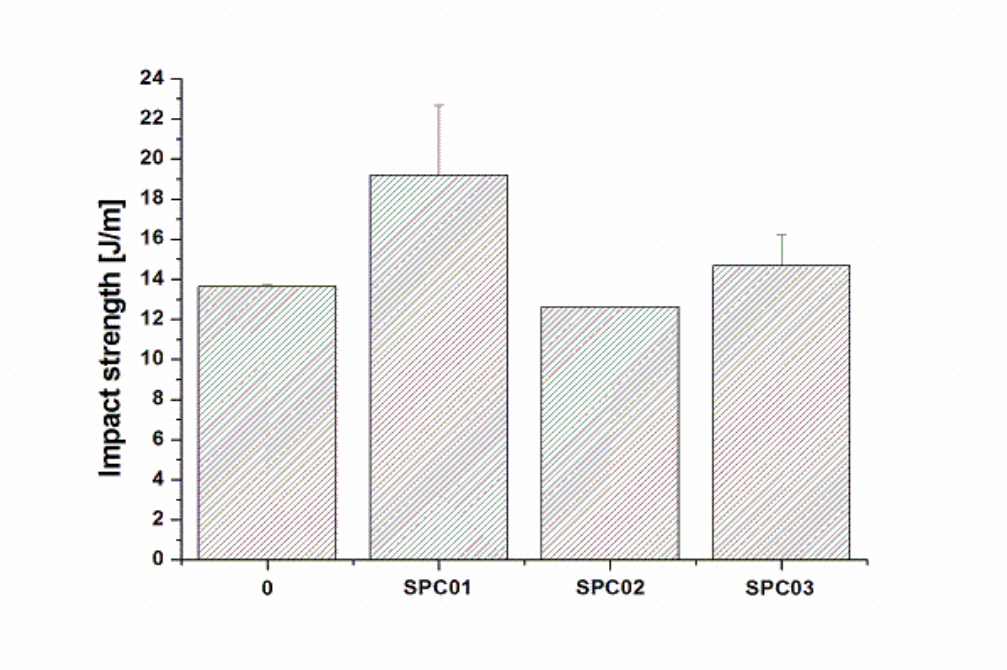

Figure 7.19 Effect of fibre diameter on the impact strength of PMMA single polymer composites at 5 wt % nanofibre loading

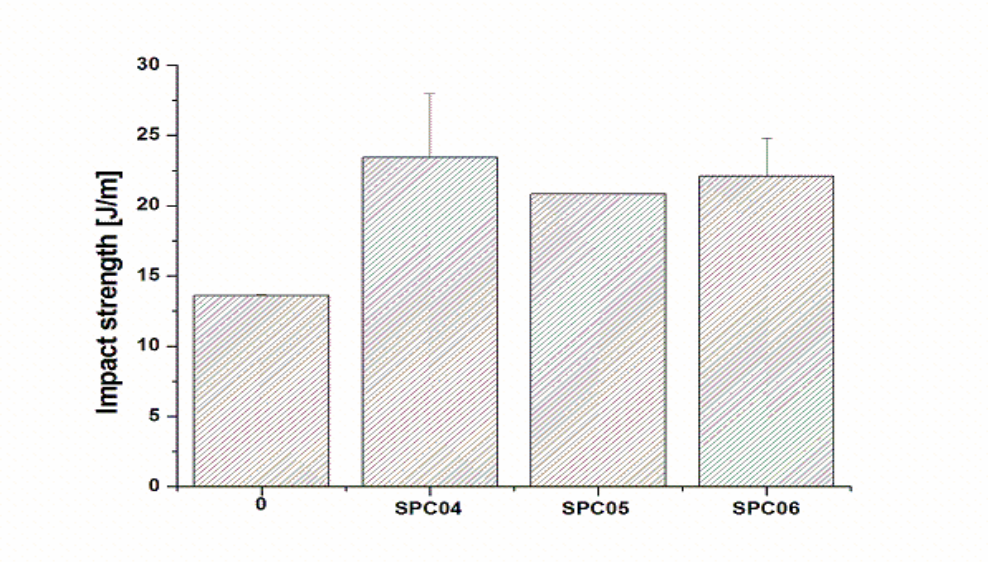

Figure 7.20 Effect of fibre diameter on the impact strength of PMMA single polymer composites at10 wt % nanofibre loading

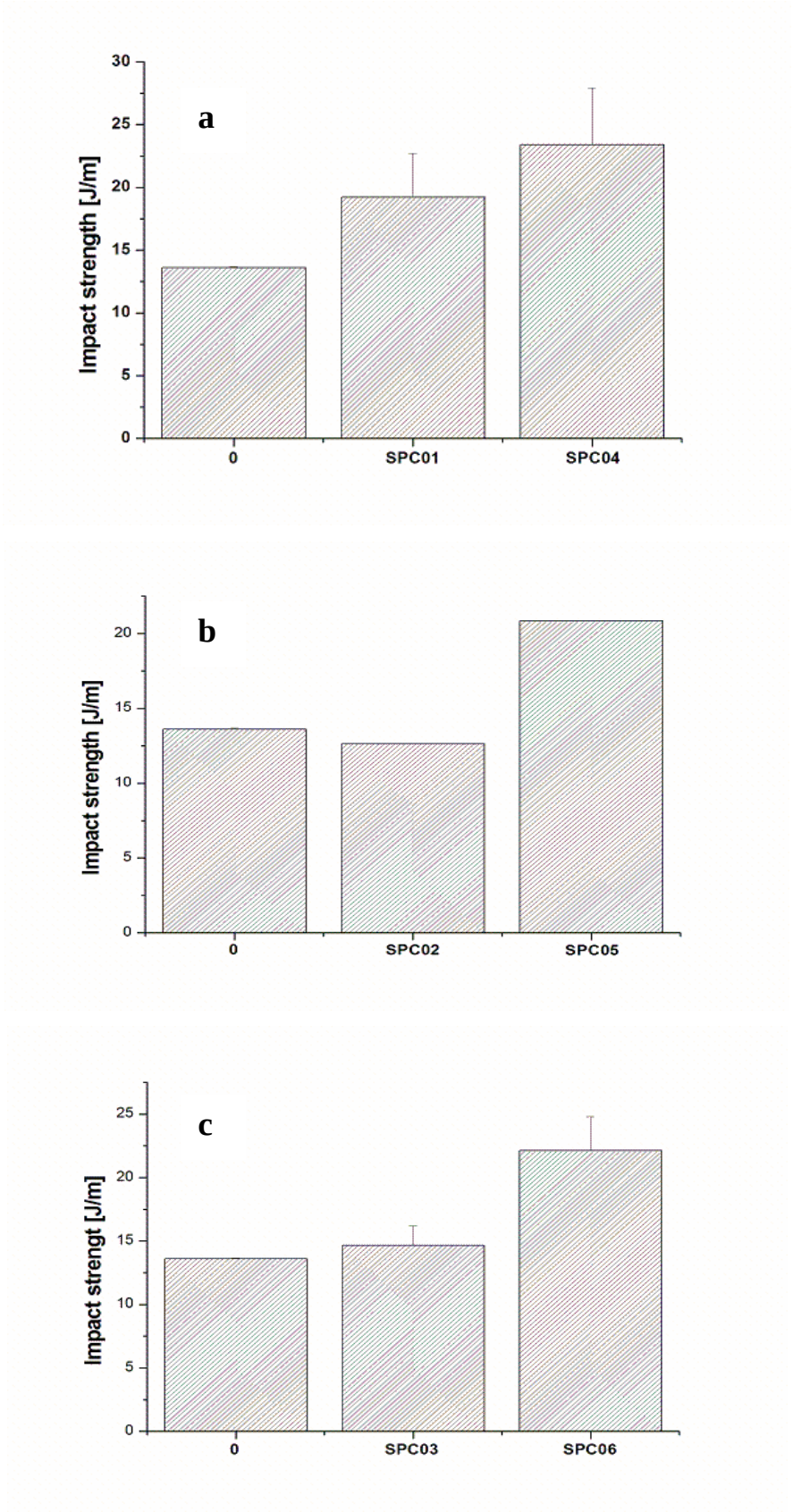

Figure 7.21 Effect of nanofibre loading on the impact strength of PMMA single polymer composites. Nanofibre diameter: (a) 200-400 nm, (b) 400-650 nm and (c) 600-900 nm

Figures 7.21 shows the charpy impact strength as a function of the nanofibre loading for the composites prepared at 150 °C. It can be seen that the impact strength of all the composites increases with an increase in nanofibre loading. SPC04 had a further 21% improvement compared to SPC01. SPC05 had a 60% improvement in impact strength compared to SPC02. SPC06 shows a 47% improvement in impact strength compared to SPC03. The increase is probably the result of the higher energy dissipation of the PMMA nanofibres. It has been reported that the energy dissipation mechanisms operating during impact fracture are matrix and fibre fracture, fibre-matrix debonding and fibre pull-out [2]. Matrix and fibre fracture dissipates lower energy as opposed to fibre-matrix debonding and fibre pull-out. In this study, the main failure mechanism is matrix and fibre fracture as there were no fibre pull-out and minimal fibre-matrix debonding due to the chemical similarity of the fibre and the matrix.

7.2 Mechanical properties of PMMA single polymer composites processed at 140 and 160 °C

It must be noted that the mechanical properties of the PMMA single polymer composites that were processed at 140 and 160 °C were merely performed for comparison and completeness reasons. Once again it must be pointed out that no high-quality composite was obtained at a processing temperature of 140 °C as insufficient bonding between the different matrix layers was noticeable. In the case of the composites processed at 160 °C, technically no composite was obtained as the nanofibres was suspected to have melted (refer to Figure 6.1 (c)). See the appendix for the graphs of the flexural, tensile and impact properties for these “composites”. Generally, as expected, no meaningful trend was observed, but some of the results for the samples that were processed at 160 °C are reported.

The flexural strength of the samples improved compared to that of the neat matrix for the samples with a 10 wt% nanofibre loading, but decreased with an increase in the nanofibre diameter (Figure 7.22). No meaningful variation in flexural strength was seen for the samples with a 5 wt% nanofibre loading. Likewise, the flexural modulus essentially remained unchanged for all the samples compared to that of the neat matrix. In the instance of the tensile strength and modulus, a slight improvement was observed for the samples compared to the neat matrix in some instances, but no obvious trend with a change in fibre diameter and loading was seen. The impact strength showed a general improvement across the fibre

diameters and loadings for the samples compared to the neat matrix, ignoring some inconsistent variations. This was particularly true for the samples with a 10 wt% nanofibre loading (Figure 7.23).

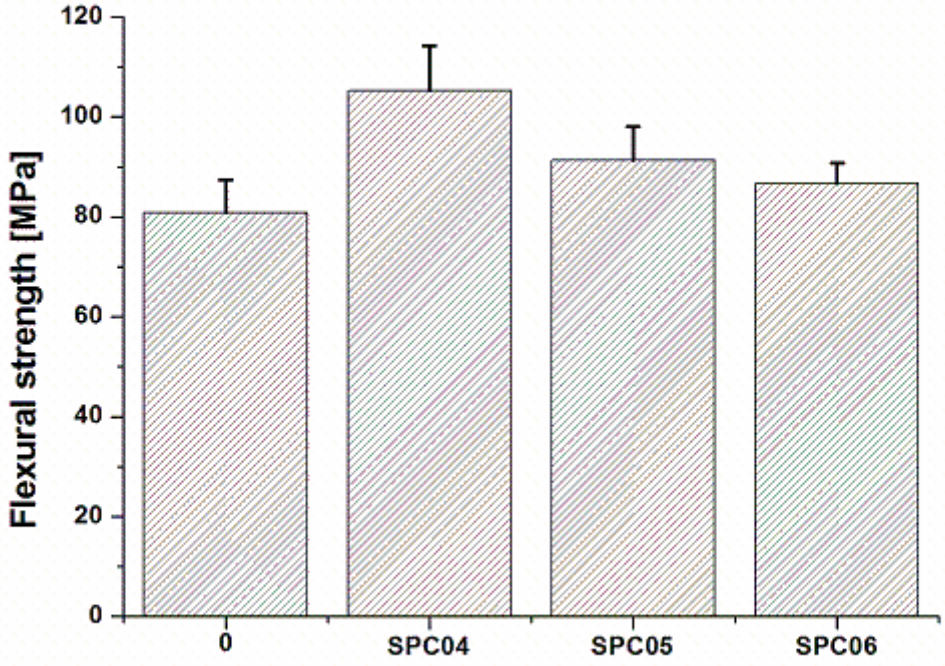

Figure 7.22 Effect of fibre diameter on the flexural strength of samples processed at 160 °C. Nanofibre loading: 10 wt%

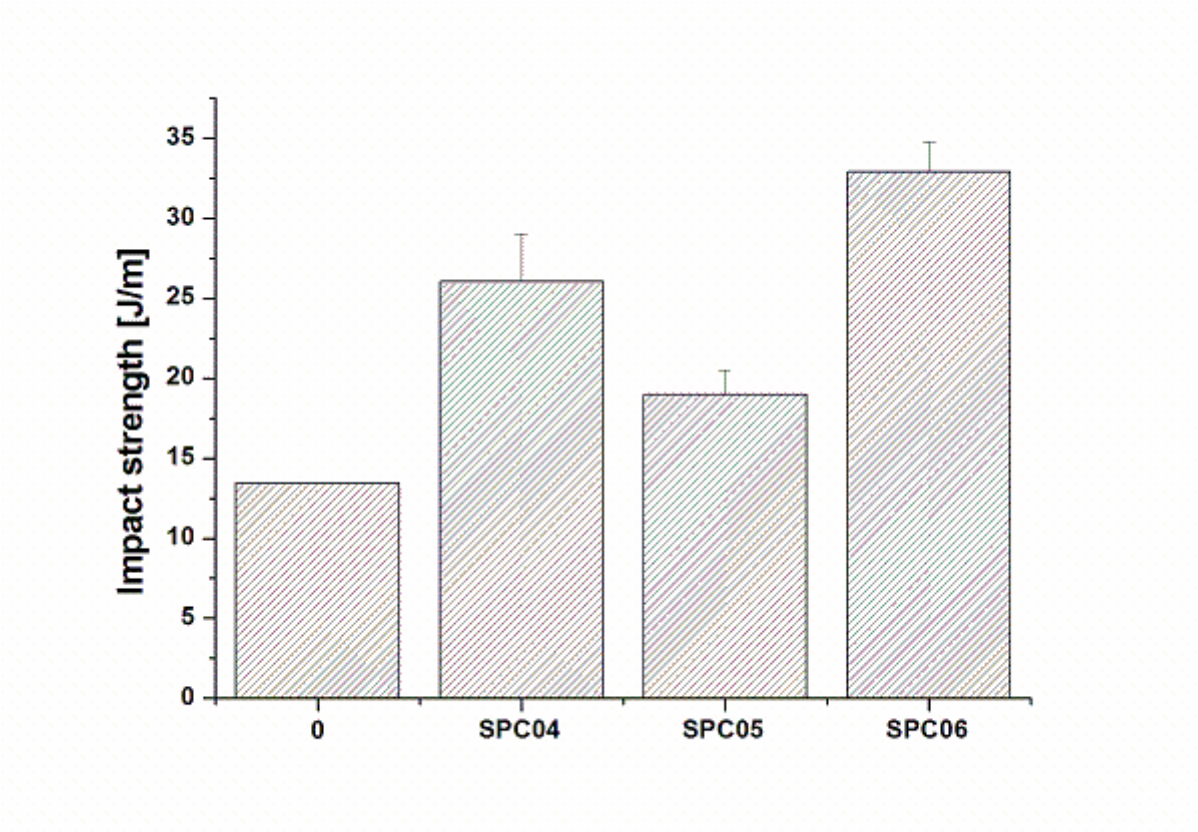

Figure 7.23 Effect of fibre diameter on the impact strength of samples processed at 160 °C. Nanofibre loading: 10 wt%

7.3 Conclusions

In this study, the influence of the nanofibre diameter and loading on the mechanical properties of the PMMA single polymer composites was investigated. A positive effect of the nanofibres on the flexural strength was observed as the different nanofibre diameter reinforced composites' strength was higher that that of the PMMA matrix, particularly the smaller diameter reinforced PMMA composites. An improvement in flexural strength of 44% was obtained. In addition, the flexural strength was seen to increase with an increase in nanofibre loading. However, there was no significant change in the flexural moduli of the composites compared to that of the neat PMMA. The nanofibres did not have an influence on the tensile strength and moduli of the composites compared to those of the PMMA matrix. This behaviour is probably a result of the lower stiffness of the nanofibres compared to the traditional fibres. The impact strength of the composites was higher than that of the PMMA matrix. A maximum improvement of 76% in impact strength was achieved. This

improvement, in certain instances, in the mechanical properties of the composites compared to the neat matrix confirms the positive reinforcing effect of the electrospun nanofibres.

7.4 References

[1] S. Houshyar, R.A. Shanks, A. Hodzic. The effect of fiber concentration on mechanical and thermal properties of fiber-reinforced polypropylene composites. Journal of Applied Polymer Science 2005; 96:2260-2272.
DOI:10.1002/app.20874

[2] M.J. John, R.D. Anandjiwala. Chemical modification of flax reinforced polypropylene composites. Composites Part A: Applied Science and Manufacturing 2009; 40:442-448.
DOI:10.1016/j.compositesa.2009.01.007

Chapter 8

Conclusions and Recommendations

8.1 Conclusions

The study investigated the processing and characterization of single polymer composites of poly(methyl methacrylate) (PMMA) using electrospun nanofibres as the reinforcement. The nanofibres were produced by the electrospinning process using DMF:THF (1:1) solutions. The effects of the electrospinning parameters (polymer solution concentration, applied voltage and spinning distance) on the morphology and diameters of the electrospun high molecular weight PMMA ($PMMA_{high}$) nanofibres were evaluated. Furthermore, suitable processing conditions for the PMMA single polymer composites were investigated and the thermo-mechanical, thermogravimetric and mechanical properties of the composites were analysed.

The electrospinning results have shown that the fibre diameter is seen to increase with an increase in polymer solution concentration. The larger nanofibre diameters at high concentrations were the result of the higher viscosity of the solution. From the SEM images of the fibres it was seen that the fibres had a smooth, regular and cylindrical morphology with no beads and junctions. The uniform morphology of the nanofibres had been ascribed to the very high molecular weight of the PMMA and sufficient entanglements of the polymer chains in the solution. The results also indicated that the applied voltage had no effect on the morphology of the $PMMA_{high}$ nanofibres. However, the changes in the applied voltage were reflected on the shape of the suspending droplet at the capillary tip and the velocity of the electrospinning jet. An increase in the applied voltage favoured the production of fibres with smaller diameters for the more concentrated $PMMA_{high}$ solution (6 wt% $PMMA_{high}$) at a shorter spinning distance (10 cm). No significant changes in the diameters of the less concentrated solutions were observed, but decreased fibre diameters were observed at higher voltages. The decrease in fibre diameters with an increase in spinning voltage became more noticeable at increased distance. This is a result of the increased electrostatic forces induced on the electrospining jet. Nanofibres with slightly reduced diameters were obtained with

increasing spinning distance. Moreover, the morphology of the nanofibres remained unchanged as the distance increased.

Thermal analysis (TGA & DSC) has shown that the nanofibres were thermally more stable than the as-received high molecular weight PMMA powder. The Raman spectra of the as-received $PMMA_{high}$ and electrospun $PMMA_{high}$ nanofibres were similar, which shows that no change in chain conformation occurred during the electrospinning process. It is therefore unclear at this stage what the reason is for the improved thermal stability of the electrospun nanofibres. It might just be a purely physical phenomenon of the powder particles versus the fibre strands.

The results for the effect of the processing temperature on the morphology of the composites have shown that a processing temperature of 150 °C yielded the best composites with two distinguishable physical phases and adequate melting of the matrix material. Delamination between the different matrix layers for the composites prepared at 140 °C were observed. This was due to insufficient softening of the matrix material at this processing temperature. The SEM analysis of the composite samples prepared at 160 °C did not show two well-defined phases. This suggests that the nanofibres could have also softened in addition to the matrix. Thus, processing temperatures of 140 and 160 °C does not seem to be suitable for the preparation of a good quality PMMA single polymer composite in this instance.

The study of the influence of nanofibre diameter and nanofibre loading on the thermo-mechanical properties of the PMMA single polymer composites at a processing temperature of 150 °C generally showed a significant improvement in the dynamic mechanical properties of the composites compared to the neat matrix. The increases in the stiffness (up to 83%) and glass transition temperature (T_g) (up to 10 °C) of the composites compared to the neat matrix were pronounced in the case of a 10 wt% nanofibre loading. The effect of the nanofibre loading on the storage modulus of the composites was more pronounced in the case of the smallest fibre diameter range (200-400 nm). A tenfold improvement in the storage modulus of the composites was observed when the fibre loading was doubled. The T_g of the composites shifted to higher temperatures at a 10 wt% nanofibre loading compared to the $PMMA_{low}$ matrix. Once again, the improvement in T_g was more pronounced in the case of the smallest fibre diameter range (200-400 nm). This behaviour is the result of the positive

reinforcing effect of the nanofibres. The thermogravimetric analysis of the PMMA single polymer composites showed that the thermal stability of the $PMMA_{low}$ matrix was not affected by the incorporation of the $PMMA_{high}$ nanofibres. The observed behaviour was attributed to the lower thermal stability of the $PMMA_{high}$ nanofibres compared to the $PMMA_{low}$ matrix.

The mechanical properties of the composites have also been investigated. It was found that the composites exhibited higher flexural strength compared to the neat $PMMA_{low}$ matrix, notably at increased nanofibre loading. SPC04 exhibited the highest flexural strength with a 44% improvement compared to the matrix. This was attributed to the ability of the nanofibres to allow efficient stress transfer from the matrix to the fibres. There were no significant changes in the flexural modulus of the composites compared to the $PMMA_{low}$ matrix. The incorporation of the nanofibres (5 and 10 wt% loading) did not have any effect on the tensile properties of the composites. This is probably the result of the electrospun $PMMA_{high}$ nanofibres not being aligned in the tensile stress direction to carry most of the load. Furthermore, the nanofibres are less stiff than the traditional fibres. The results for the impact strength were seen to increase upon composites formation. Significant improvements were seen in the impact strength in the case of SPC04, SPC05 and SPC06 compared to the unreinforced matrix. A maximum improvement in impact strength of 76% was achieved for SPC04. The increase in the impact strength is primarily the result of a higher energy absorption of the $PMMA_{high}$ nanofibres.

The improvement in the dynamic mechanical and mechanical properties of the composites is an indication that the electrospun nanofibres have a positive reinforcing effect when applied in the form of PMMA single polymer composites.

8.2 Recommendations

The following recommendations for further research are proposed:

- Characterization of the mechanical properties of the electrospun nanofibres;
- Investigation of the amount of orientation in the electrospun nanofibres and its effect on the processing window of the single polymer composites;

- Effect of annealing on the properties of the electrospun nanofibres and its subsequent effect on the properties of the single polymer composites;
- Production and characterization of aligned electrospun nanofibres and its resultant effect on the properties of the single polymer composites.

APPENDIX

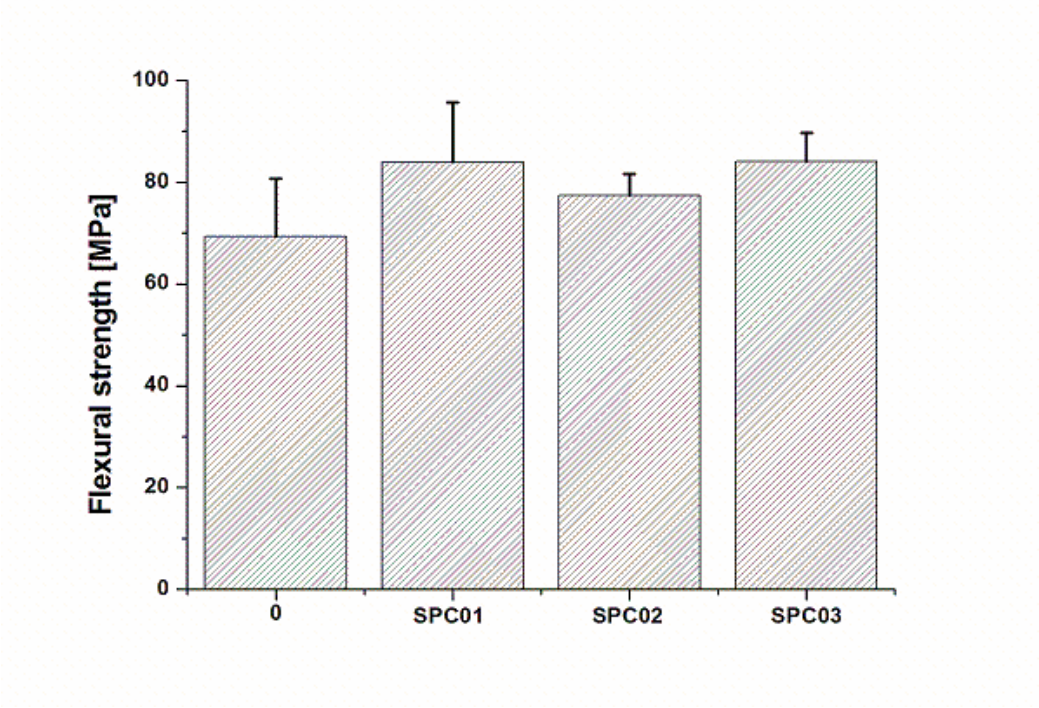

Figure A.1 Effect of fibre diameter on the flexural strength at 5wt % nanofibre loading at 140 °C

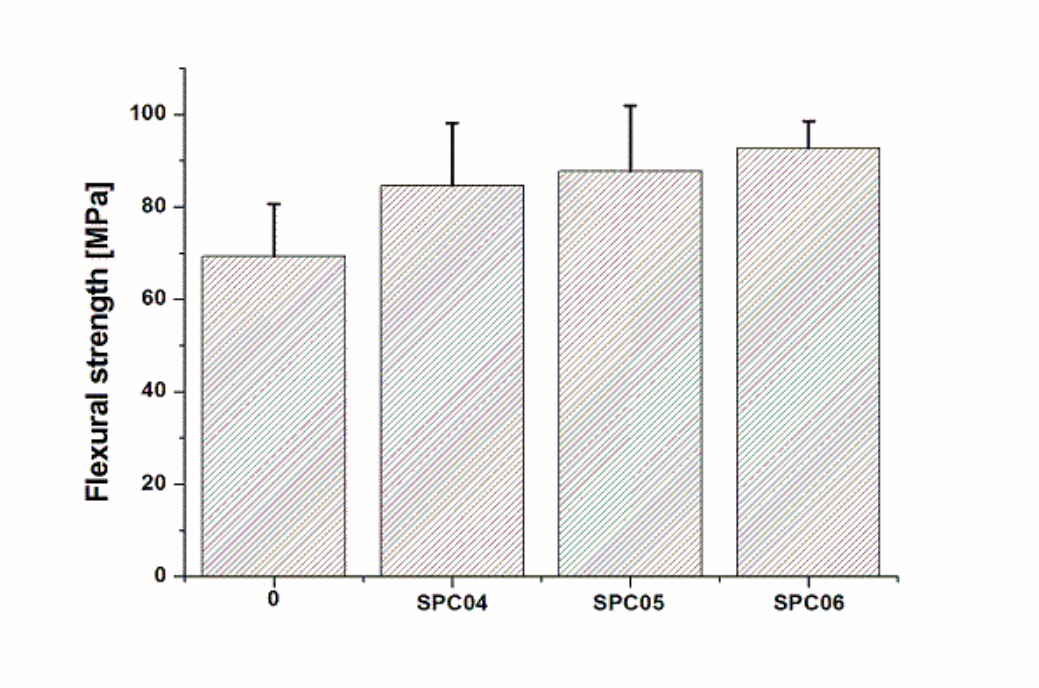

Figure A.2 Effect of fibre diameter on the flexural strength at 10 wt % nanofibre loading at 140 °C

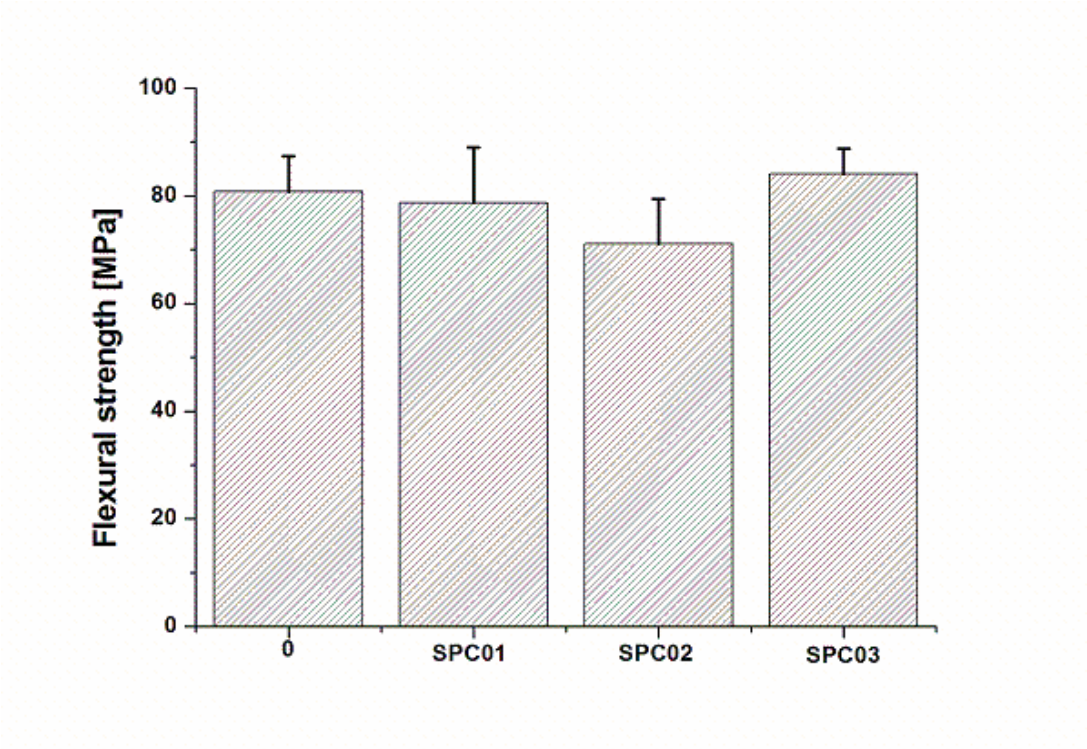

Figure A.3 Effect of fibre diameter on the flexural strength at 5wt % nanofibre loading at 160 °C

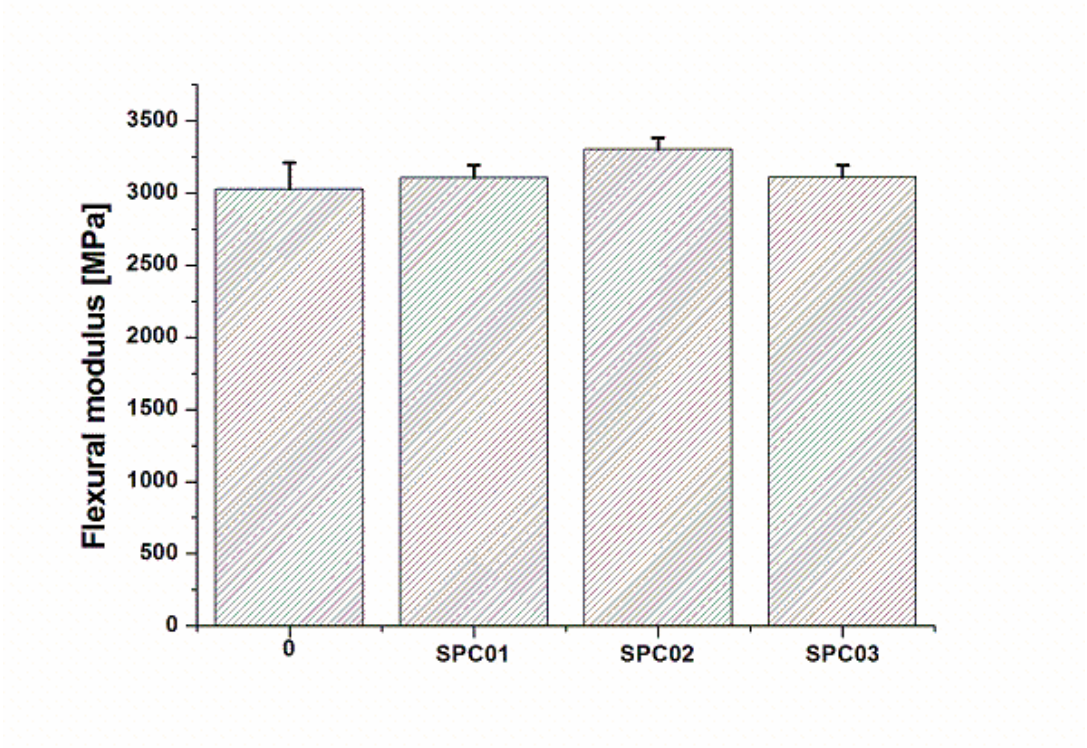

Figure A.4 Effect of fibre diameter on flexural modulus at 5wt % nanofibre loading at 140 °C

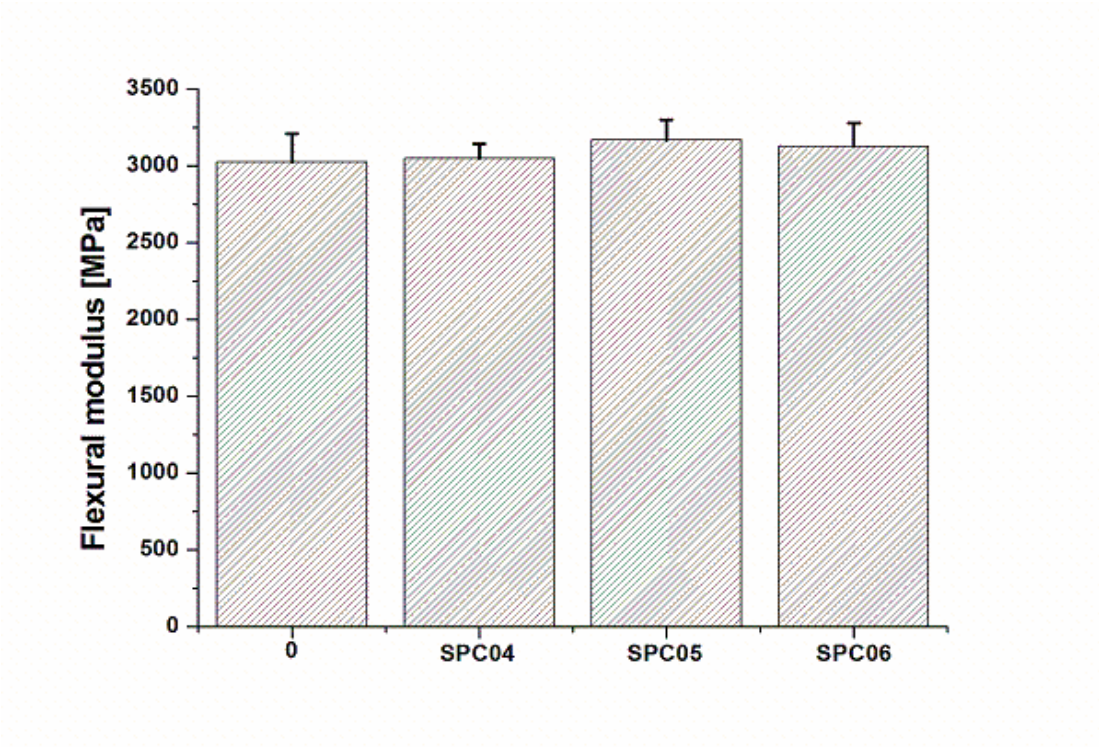

Figure A.5 Effect of fibre diameter on flexural modulus at 10 wt % nanofibre loading at 140 °C

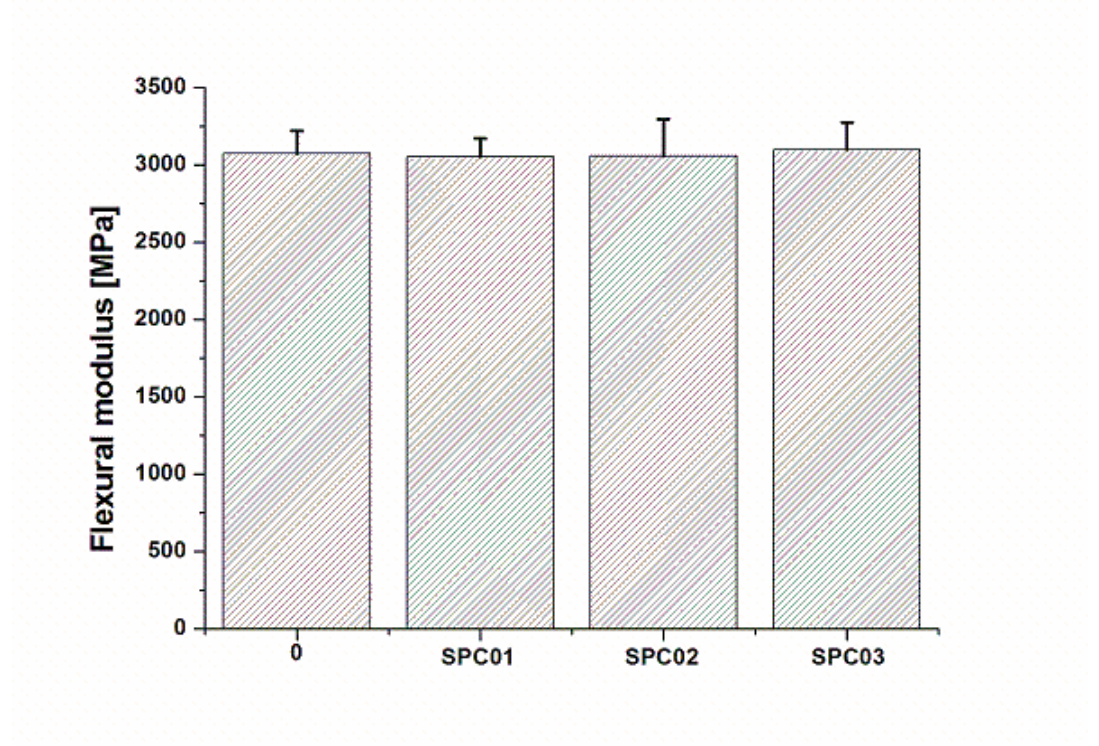

Figure A.6 Effect of fibre diameter on the flexural modulus at 5wt % nanofibre loading at 160 °C

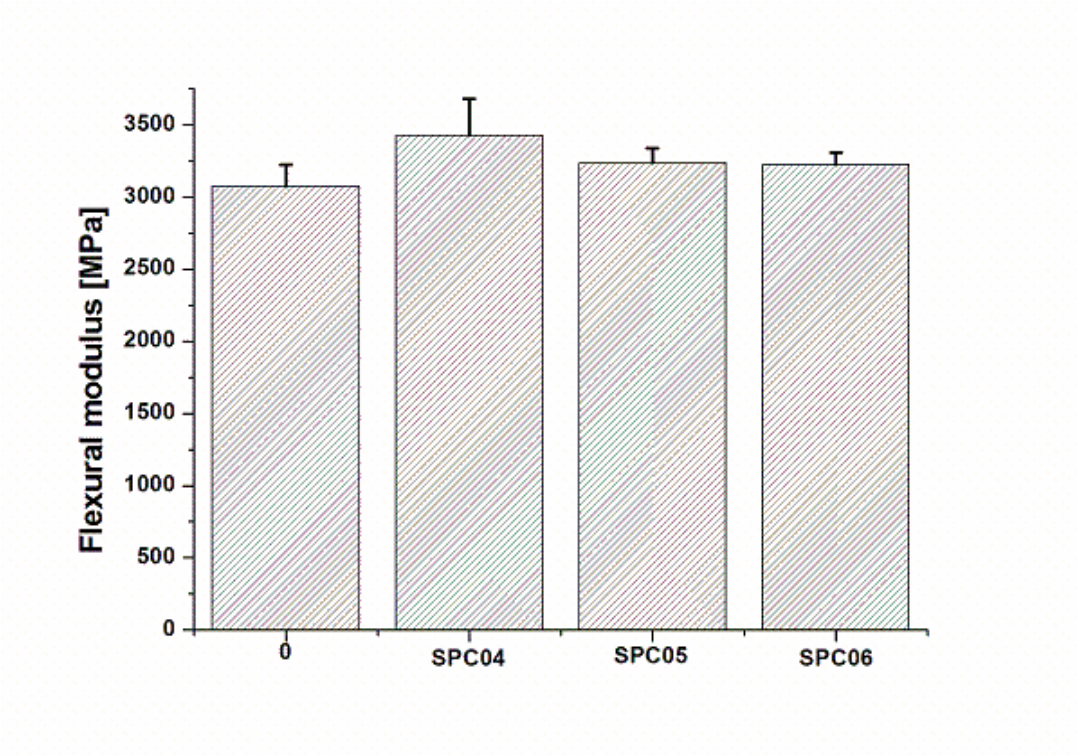

Figure A.7 Effect of fibre diameter on the flexural modulus at 10 wt % nanofibre loading at 160 °C

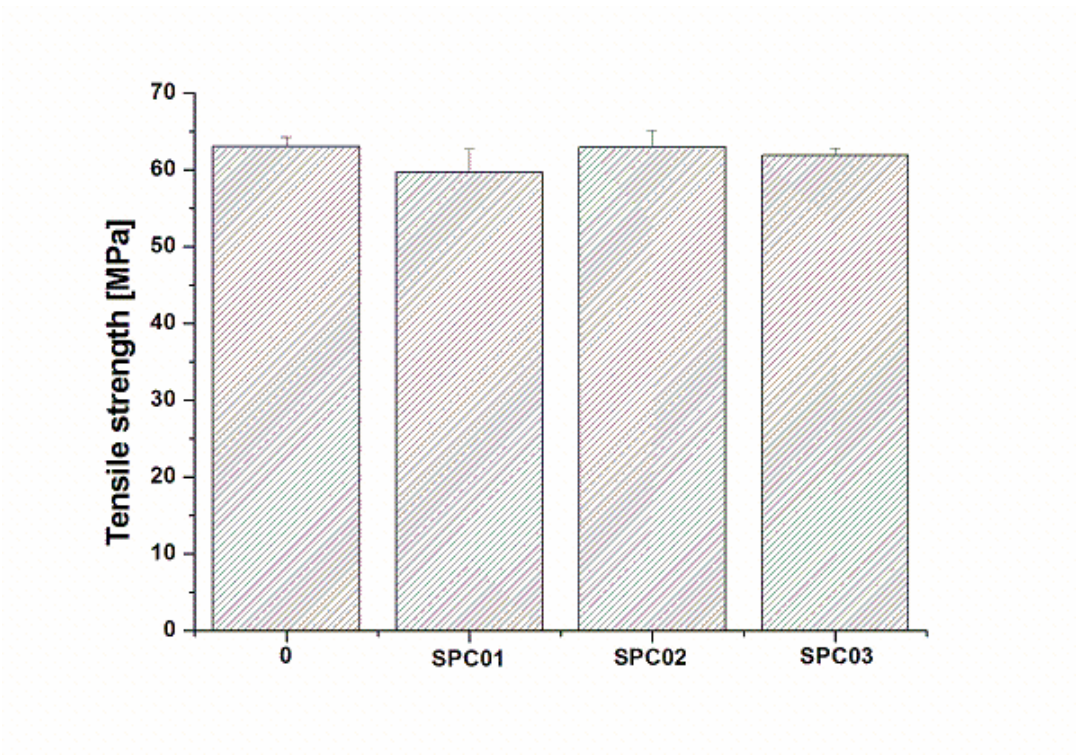

Figure A.8 Effect of fibre diameter on tensile strength at 5wt % nanofibre loading at 140 °C

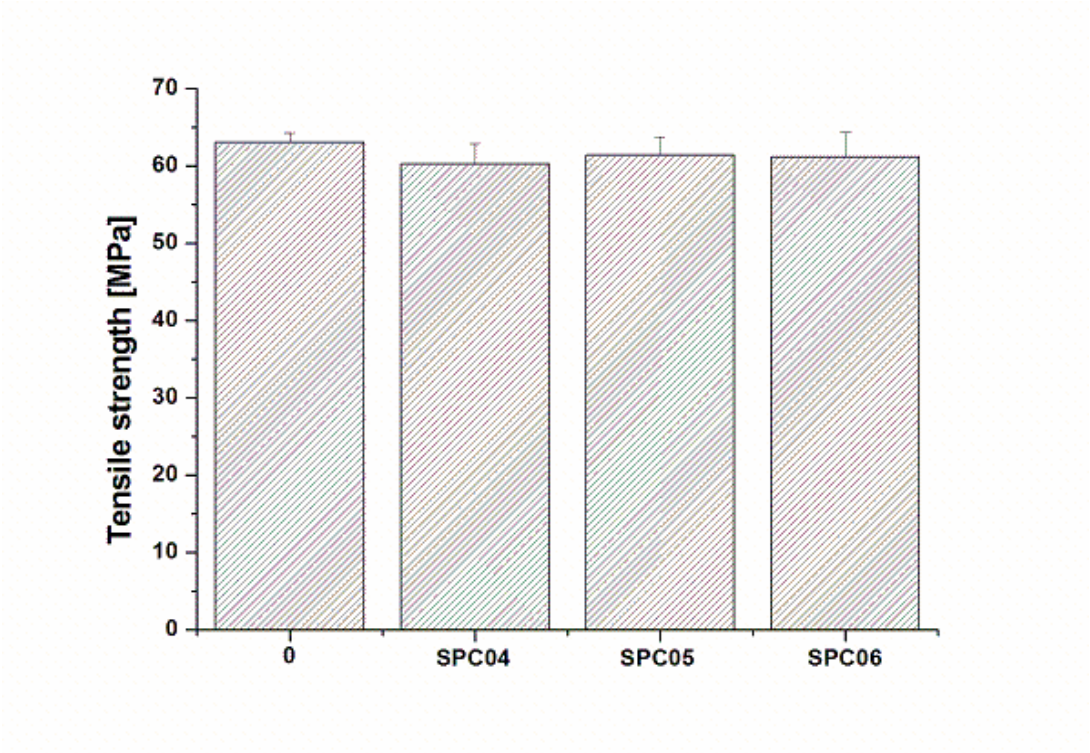

Figure A.9 Effect of fibre diameter on tensile strength at 10 wt % nanofibre loading at 140 °C

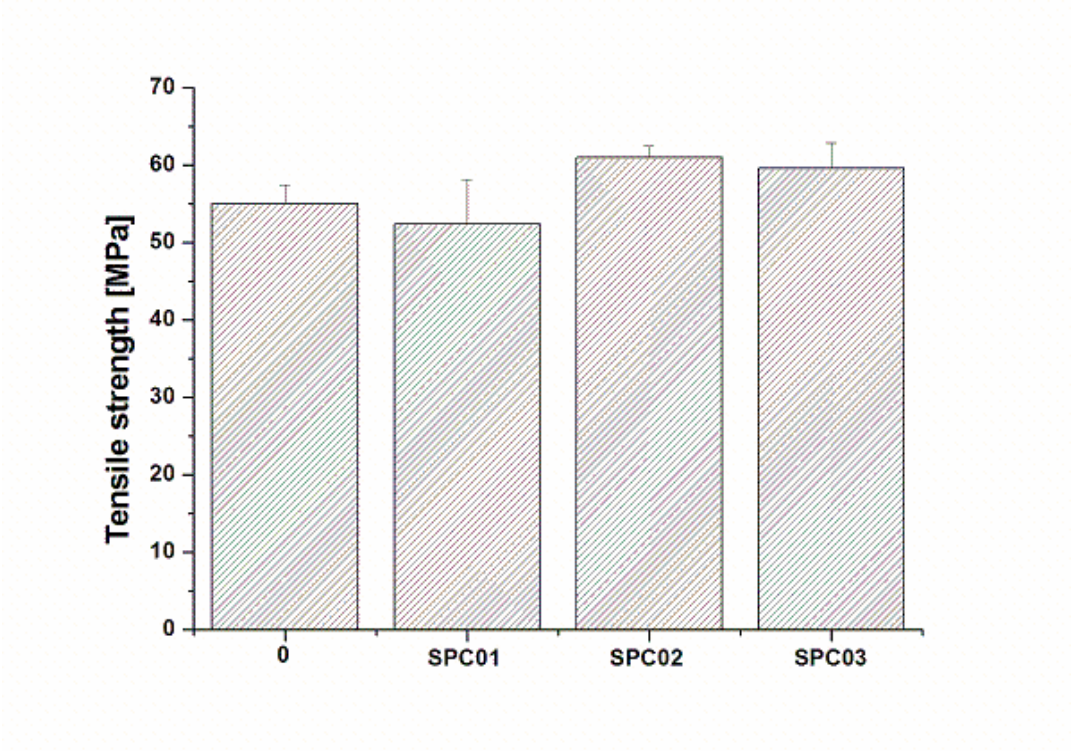

Figure A.10 Effect of fibre diameter on tensile strength at 5wt % nanofibre loading at 160 °C

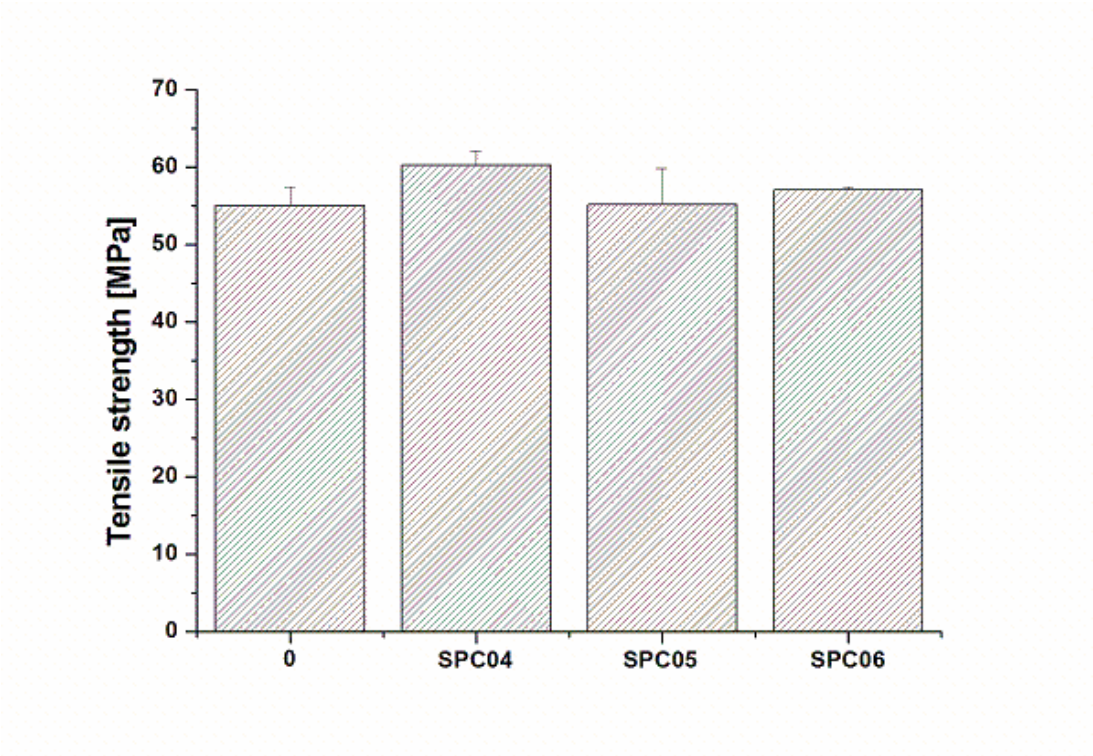

Figure A.11 Effect of fibre diameter on tensile strength at 10 wt % nanofibre loading at 160 °C

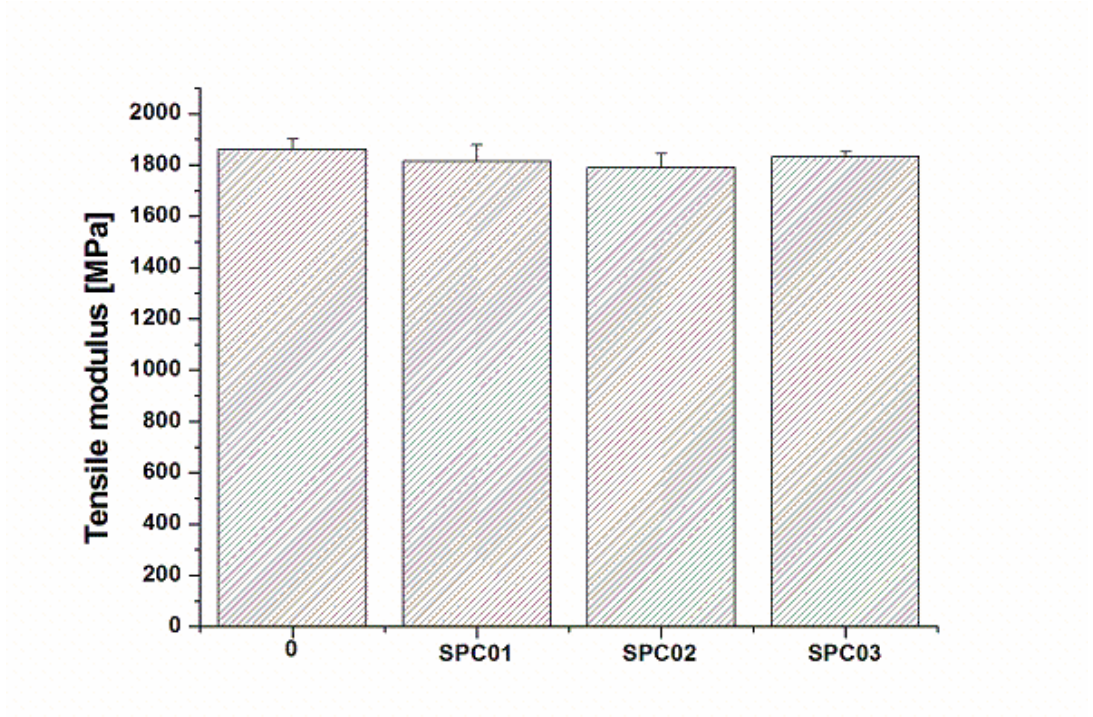

Figure A.12 Effect of fibre diameter on tensile modulus at 5wt % nanofibre loading at 140 °C

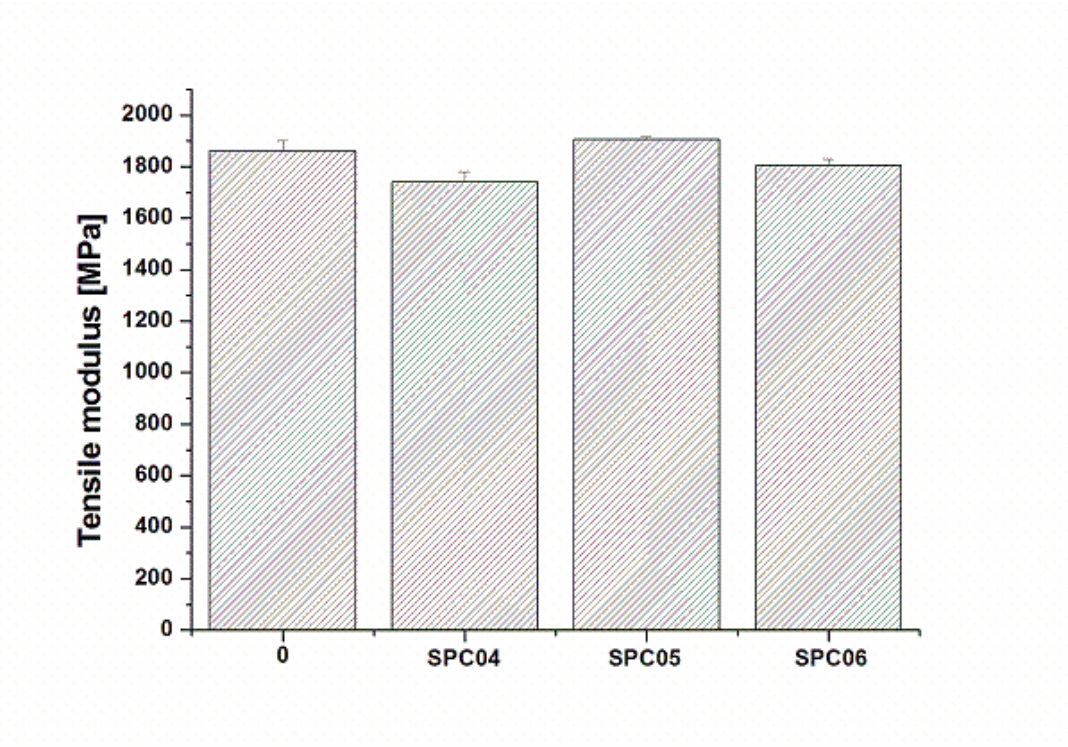

Figure A.13 Effect of fibre diameter on tensile modulus at 10 wt % nanofibre loading at 140 °C

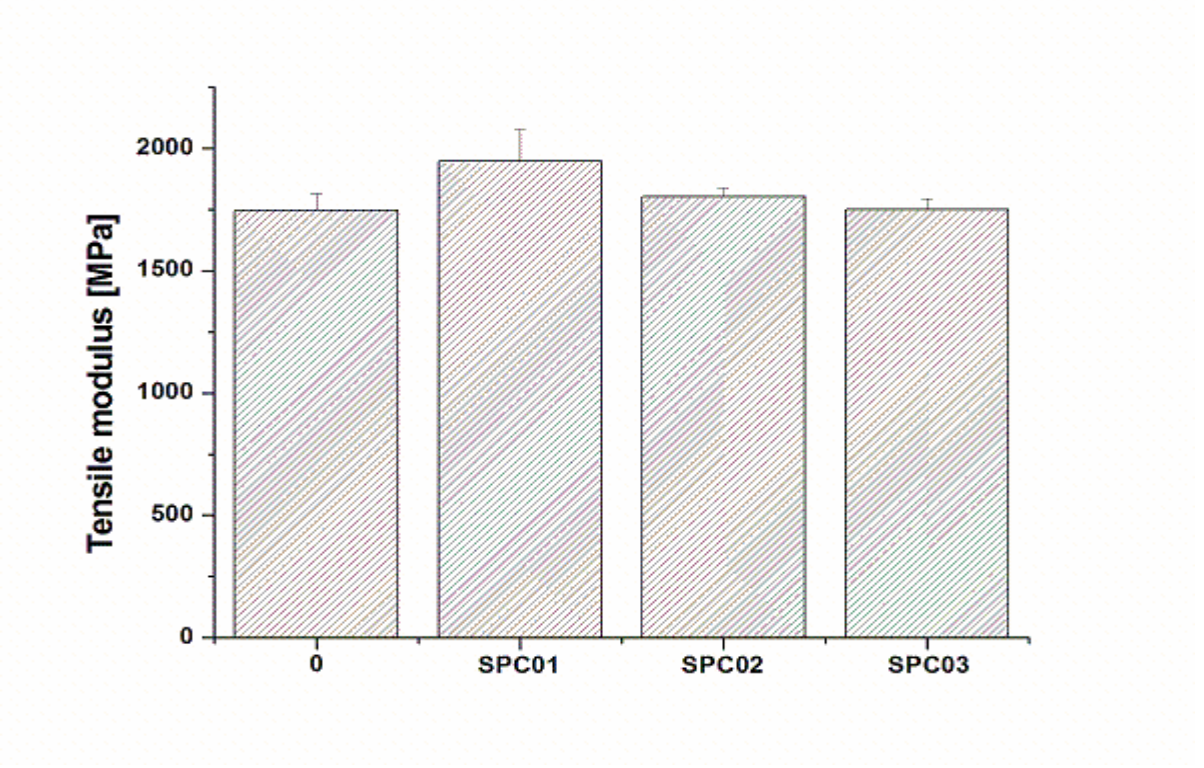

Figure A.14 Effect of fibre diameter on tensile modulus at 5wt % nanofibre loading at 160 °C

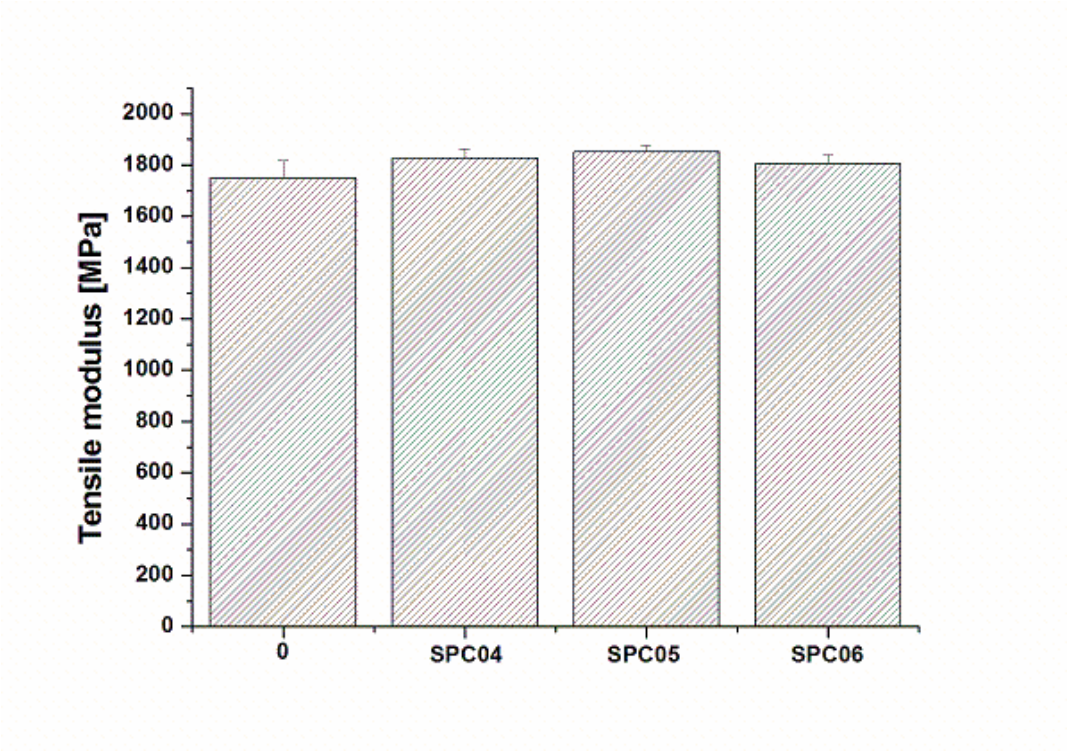

Figure A.15 Effect of fibre diameter on tensile modulus at 10 wt % nanofibre loading at 160 °C

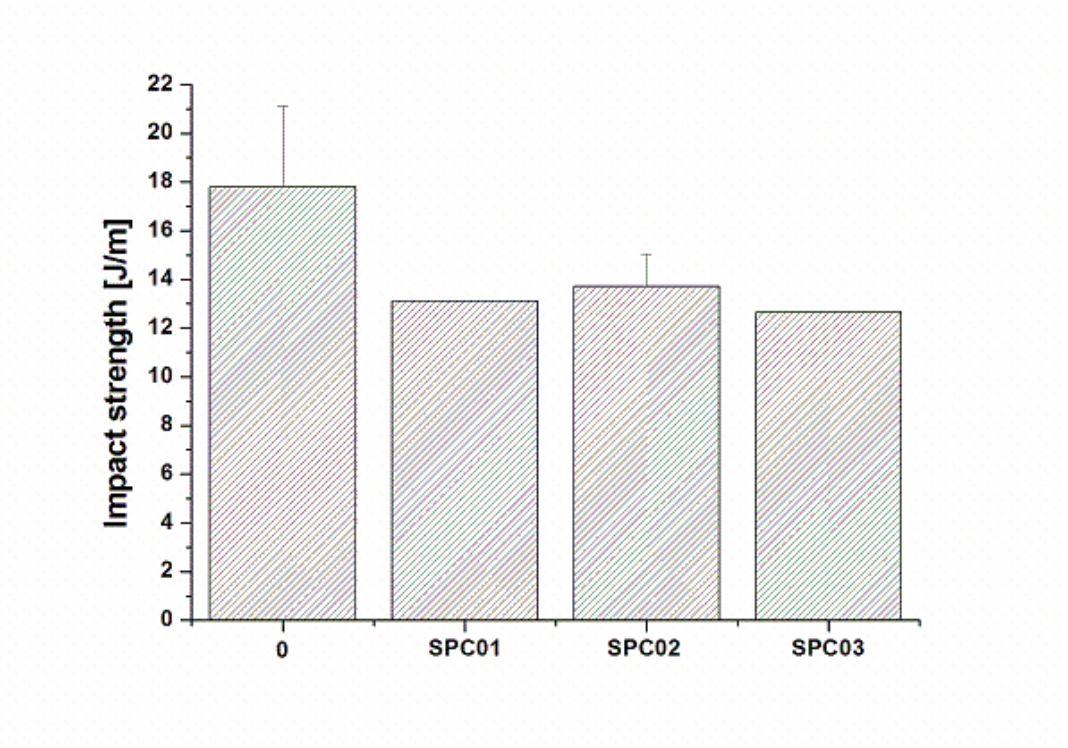

Figure A.16 Effect of fibre diameter on impact strength at 5wt % nanofibre loading at 140 °C

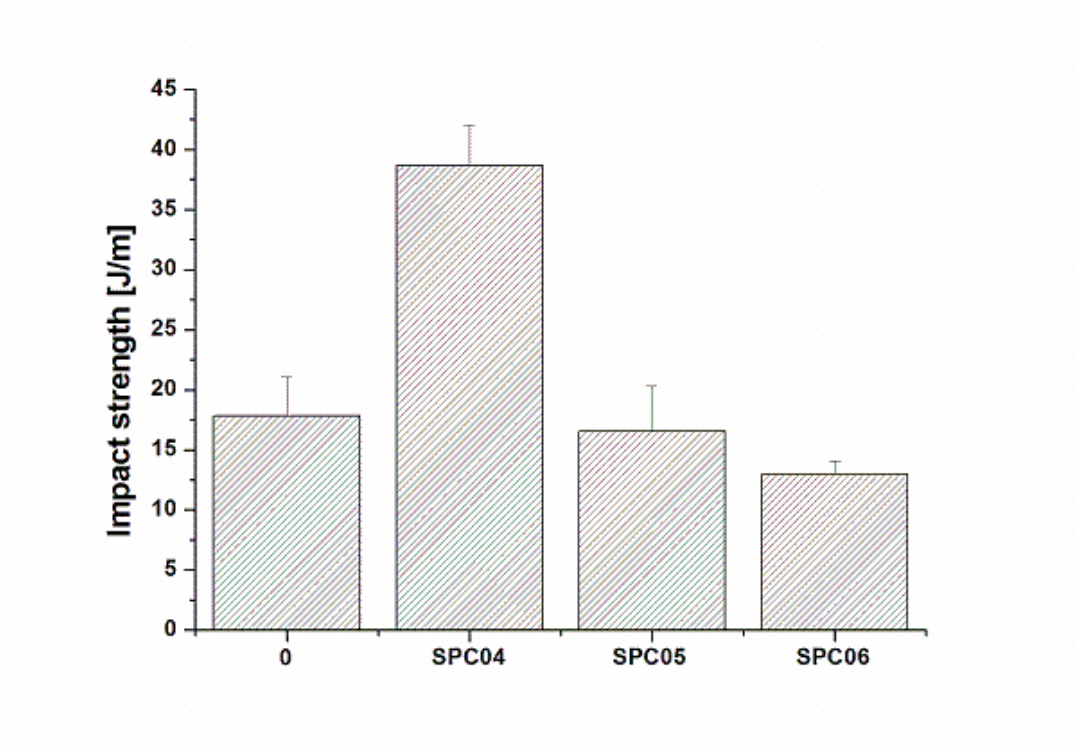

Figure A.17 Effect of fibre diameter on impact strength at 10 wt % nanofibre loading at 140 °C

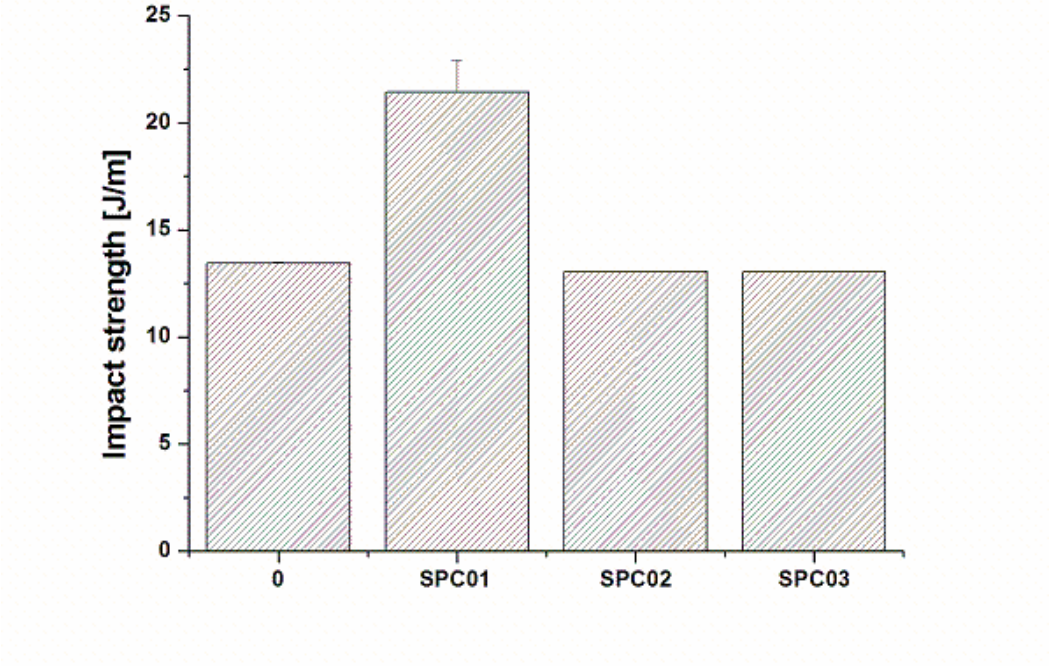

Figure A.18 Effect of fibre diameter on impact strength at 5wt % nanofibre loading at 160 °C